POLITECNICO DI TORINO

Scuola di Dottorato di Ricerca

TESI DI DOTTORATO DI RICERCA
IN INGEGNERIA CHIMICA
XVI Ciclo

DYNAMICS AND CONTROL OF FORCED
UNSTEADY-STATE CATALYTIC REACTORS

Davide Fissore

Advisor: Antonello A. Barresi

2004

Index

Summary

This research deals with the dynamics and control of forced unsteady-state catalytic reactors and it is focused on two topics:

1. auto-thermal after-treatment of lean VOC mixtures. Two reactor configurations have been taken into consideration: the reverse-flow reactor (RFR), where the flow direction is periodically changed, and the network of two or three reactors (RN), where the flow direction remains the same, but the feeding position is periodically changed, thus simulating a moving bed. This study (§3) has been organised as follows:

   - modelling of the two reactor configurations and study of the influence of the main operating parameters (§3.1 and §3.2). As the RFR shows higher stability with respect to disturbances in the feed a deeper investigation has been carried out on this device;

   - optimisation of the RFR. A simplified model has been used for this analysis in order to strongly reduce the computational effort which is required by detailed models. It has been pointed out that both heat capacity and thermal conductivity of the catalyst play a role, not less important than kinetic activity, strongly influencing the minimum inlet VOC concentration required for autothermal operation (§3.3);

   - experimental validation of the modelling results in a bench-scale RFR with reduced influence of the wall effects. This activity has been carried at the Departamento de Ingeniería Química y Tecnología del Medio Ambiente-Universidad de Oviedo (Spain) in the framework of

the Research Project "Azioni Integrate Italia-Spagna", granted by the Italian Ministry of Research (MIUR).

In addition to the intrinsecally dynamic behaviour of the RFR, one must deal with unexpected external perturbations (feed concentration, composition and temperature) which may lead to reactor extinction or catalyst overheating. In order to avoid these problems it is necessary to implement some closed-loop control strategy based on the measurement of the inlet concentration (and composition) and the outlet conversion. This study has been organised as follows:

- a model-based soft-sensor (observer) has been developed, in order to quickly and reliably estimate the feed composition from some temperature measurements in the reactor, thus avoiding expensive hardware sensors and time consuming on-line measurements. As deriving an observer from a detailed model is an overwhelming task, a simplified model has been developed and validated in a medium-size RFR. This research has been carried out in cooperation with prof. H. Hammoury and D. Schweich of the CPE-Lyon, France (§4.1);

- a Model Based control strategy has been proposed and tested to prevent reaction extinction and catalyst overheating (§4.2);

2. enhancement of conversion and selectivity in exothermic, equilibrium-limited reactions. Methanol synthesis and syngas prouction by partial oxidation of methane have been considered as test reactions. This section has been organised as follows:

- modelling of the two processes in the two reactor configurations previously described. The influence of the main operating conditions has been addressed with the aim to optimise the two processes. As the RN has shown higher conversion and selectivity with respect to the RFR, in the following the research will be focused on this device (§5);

- a simple open loop control policy, which can be useful for a safe start-up, has been also tested to study the response of the RN to disturbances on the input parameters, showing that a more robust

control strategy is needed for this application;

- if a tight control on the outlet product conversion is needed, a Model Predictive Control scheme (MPC) should be used, varying the switching time to maximise the conversion and the selectivity of the reactor. The on-line optimisation requires a simplified model and a Neural Network based model has been developed (§6).

IV

Chapter 1

Introduction

Many hydrocarbons are included in the VOC (Volatile Organic Compounds) category due to their high photochemical activity that leads to tropospheric ozone production, which is the origin of the well known photochemical smog contamination phenomenon. Many of them are even more dangerous due to their toxicity for the environment and humans. Although methane has a relatively low photochemical activity, its destruction from emissions to the atmosphere is also highly desirable because it is the leading contributor to greenhouse effect, after carbon dioxide. The combustion of methane, and hence its transformation to carbon dioxide is environmentally advantageous because the GWP (global warming potential) of methane is about 20 times higher than that of carbon dioxide. Moreover, methane is very adequate as test compound for catalytic destruction studies, because it has the highest ignition temperature among paraffinic and aromatic compounds, and as a consequence most pollutants will be destroyed at the temperature that allows for total methane combustion.

Among the existing end-of-pipe processes available, catalytic combustion is the most important technology for the abatement lean mixtures of gaseous hydrocarbons as a consequence of the energetic efficiency due to the decrease of the operation temperature, that leads also to lower NO_x emissions. Energy efficiency can be further increased using special process configurations, as in the case of recuperative (heat exchangers) and regenerative (heat regenerators) devices.

Among the regenerative processes, forced non-stationary reactors have received considerable attention in recent years as the integration of

regenerative heat exchange into the catalyst packing of a catalytic fixed bed could have specific advantages over a simple combination of an adiabatic reactor with a separate heat exchanger. Forced unsteady-state catalytic reactors have been proposed also both for endothermal and exothermal processes as well as for reversible and equilibrium reactions. Favourable temperature and composition distributions, which cannot be attained in any steady-state regime, can be reached by means of forced variations of inlet parameters.

The periodic reversal of the flow direction is a simple technical solution to obtain forced unsteady-state conditions. Extensive investigations about the reverse-flow reactor (RFR) have been performed in the past thirty years, pointing out that this device can be used for the combustion of lean and cold mixtures as the reversal of the flow keeps the heat of reaction inside the bed, which acts as a regenerative heat exchanger, thus reducing the need for auxiliary fuel, except for start-up.

An alternative reactor configuration is the ring reactor, or reactors network (RN), which consists of a sequence of two or more catalytic fixed bed reactors where a sustained dynamic behaviour is obtained through the periodical variation of the feed position. By this way, contrary to the reverse-flow reactor, the flow direction is maintained, thus ensuring a uniform catalyst exploitation and avoiding the emissions of unburned gas due to wash-out, in correspondence of each switch. Autothermal behaviour can be obtained in the RN, even at low VOC concentration, but safe operation is limited to a narrow range of switching times.

The aim of this work is a deep investigation of the dynamic of the RFR and of the RN, when the combustion of lean VOC mixture takes place, is carried out in order to ottimise these devices, pointing out the influence both of the kinetic parameters and of the physical properties of the catalyst on the thermal stability.

In unsteady-state catalytic reactors it is also possible to achieve a temperature distribution which is optimal for exothermic equilibrium-limited reactions, approaching the ideal profile corresponding to maximum product generation. In this work methanol synthesis and syngas production by partial oxidation of methane have been studied by means of numeric simulation and both RFR and RN have been demonstrated to give higher conversion in comparison to traditional steady-state technology, based on multi-bed adiabatic reactors.

In addition to the intrinsecally dynamic behaviour of the RFR and of the RN, one must deal with unexpected external perturbations (feed concentration, composition and temperature) which may lead to reactor extinction or catalyst overheating in the case of VOC after-treatment, and to decreasing in conversion and selectivity in methanol synthesis and syngas production. In order to avoid these problems it is necessary to implement some closed-loop control strategies.

The aim of this thesis is also to develop and test a Model Based control system for the two applications investigated, namely the combustion of lean methane mixtures in a RFR and methanol synthesis in the RN. In particular, in the case of the RFR the control system will be able to avoid both catalyst overheating (during periods of high inlet concentration) and reaction extinction (when the inlet concentration il too low to sustain the autothermal combustion): a soft-sensor (observer) will be developed to give on-line extimation of the inlet VOC concetration, thus allowing the proper control action. In the case of methanol synthesis in the RN the aim of the control system is to maximise methanol yield; as a consequence a Model Predictive Control (MPC) will be proposed and a simple Neural Network based model will be proposed to allow for the on-line optimisation.

Chapter 2

Forced unsteady-state catalytic reactors

Forced unsteady-state gas-solid catalytic reactors have been deeply investigated in the past, as dynamic operation can improve the conversion and selectivity of a number of chemical processes. When performing forced unsteady processes in a heterogeneous catalytic reactor, one can outline two major factors responsible for positive effects (Boreskov and Matros, 1983; Matros, 1985, 1990; Matros and Bunimovich, 1996):

1. *Dynamic properties of the catalyst*: unsteady conditions in the gas phase can give rise to such changes in state, composition and structure of the catalyst, which can induce an increase of the selectivity and/or activity if compared to steady-state operation.

2. *Dynamic characteristics of a whole reactor system*: forced variation of the inlet parameters is aimed at formation of optimum temperature and composition distributions in the reactor, which cannot be obtained in any steady-state regime.

The first effect is relevant only if the characteristic time of the kinetic or the absorption steps are comparable to the imposed cycle period and depends on the catalyst dynamics, while the second one is generally more important and is a consequence of the improved thermal efficiency and of the optimum concentration and temperature profile obtainable in unsteady-state

conditions. Unsteady-state conditions may thus be useful to achieve these results:

1. *increasing of the catalytic activity*;
2. *improvement of selectivity and conversion*;
3. *lower catalyst deactivation rate* (Chanchlani *et al.*, 1994);
4. *process identification* (Renken, 1990, 1993).

Initial investigation of dehydrogenation of ethanol to ethylene and diethyl ether carried out by Denis and Kabel (1970) gave rise to a series of experimental works which demonstrated improved performance for nearly all large-scale heterogeneous catalytic processes. The list of such processes includes sulphur dioxide oxidation over vanadium catalyst, ammonia synthesis over promoted iron catalyst, Fisher-Tropsch synthesis over ruthenium and cobalt catalyst, CO oxidation on different metallic and oxide catalyst, etc. Typically the experimental system is an isothermal fixed bed reactor exposed to periodic oscillations of the inlet gas mixture composition. For example, in the case of NH_3 synthesis, H_2 and N_2 are fed alternatively, leading to conversion 25% higher than in the traditional process (Rambeau and Amariglio, 1981); in the oxidation of SO_2 with air, in presence of water, on a V_2O_5 based catalyst, the conversion of SO_2 to H_2SO_4 may be increased up to the 50% if the feeding of H_2O is periodically stopped (Silveston and Forrissier, 1985).

Almost all the input parameters of the reactor may be periodically changed; in particular it has been studied the influence of:

1. *feeding flow rate*. The influence of this parameters has been studied mainly by means of numeric simulation;
2. *feeding composition*;
3. *feeding flow direction*;
4. *temperature*. The influence of changes of the inlet temperature have been poorly investigated, evidencing that the thermal inertia of the system may strongly reduce the effects of any changes in the feed temperature;
5. *wall temperature*. This parameter can be varied by means of the temperature of the heating or cooling fluid or by the furnace; as in the previous case a high thermal inertia may make difficult to obtain changes in the wall temperature.

Table 2.1 gives a short summary of the main processes which have been investigated with variable inlet flow rate or composition.

Table 2.1: Processes that have been studied in unsteady-state conditions.

Authors	Process	Input changes
CO oxidation	Abdul-Kareem *et al.* (1980)	Composition
	Cutlip (1979)	Composition
SO_2 oxidation	Haure *et al.* (1989)	Feed flow rate
	Briggs *et al.* (1977)	Composition
	Silveston and Hudgins (1981)	Composition
Ethylene oxidation	Renken *et al.* (1976)	Composition
Propylene oxidation	Saleh-Alhamed *et al.* (1992)	Composition
Hydrocarbon oxidation	Wandrey and Renken (1973)	Composition
Butadiene Hydrogenation	Al-Taie and Kershenbaum (1978)	Composition
Ethanol hydrogenation	Helmrich *et al.* (1974)	Composition
	Baiker and Richarz (1976)	Composition
Acethylene hydrogenation	Bilimoria and Bailey (1978)	Composition
Diethyl ether from ethanol	Denis and Kabel (1970)	Feed flow rate
	Lehr *et al.* (1968)	Feed flow rate
	Renken (1974)	Composition
Esterification	Lee *et al.* (1980)	Composition
Ethyl acetate from acetic acid and ethylene	Leupold and Renken (1977)	Composition
Meta-acroleine	Müller-Erlwein and Guba (1988)	Composition
Methanol synthesis	Nappi *et al.* (1985)	Composition
NH_3 synthesis	Jain *et al.* (1983)	Composition
	Wilson and Rinken (1982)	Composition
Styrene polimerisation	Crone and Renken (1979)	Composition
Fisher-Tropsch synthesis	Dautzenberg *et al.* (1977)	Composition
	Adesina *et al.* (1986)	Composition
Claus process	El-Masry (1985)	Composition

2.1 The reverse-flow reactor

Reverse-flow operation in a fixed-bed catalytic reactor is an example of forced unsteady-state conditions whose effect is due to the appropriate use of whole reactor dynamics (Matros and Bunimovich, 1996). The process improvement under unsteady-state conditions can still be achieved even in the case when the catalyst quickly adjusts to the changes of the temperature and reaction mixture composition, and a steady-state approach to the reaction kinetics is valid.

The basic mode of operation is very simple and does not include forced oscillations of the inlet gas temperature or composition: the fixed catalyst bed is pre-heated and the flow direction of the cold feed is periodically reversed. Figure 2.1 illustrates the concept: when the control valves 1 and 4 are opened the feed flows to the reactor from left to right (forward flow mode), while when the control valves 2 and 3 are opened the feed flows to the reactor from right to left (reverse-flow mode). The total cycle consists of these two operations and the term switching time is used to denote the time at which the flow is changed from forward flow to reverse flow (or viceversa). If the forward and reverse flow times are the same, the operation is called symmetric, while if the two flow modes have different times, the operation is defined asymmetric. The cycle duration is the sum of the times of forward and reverse flow.
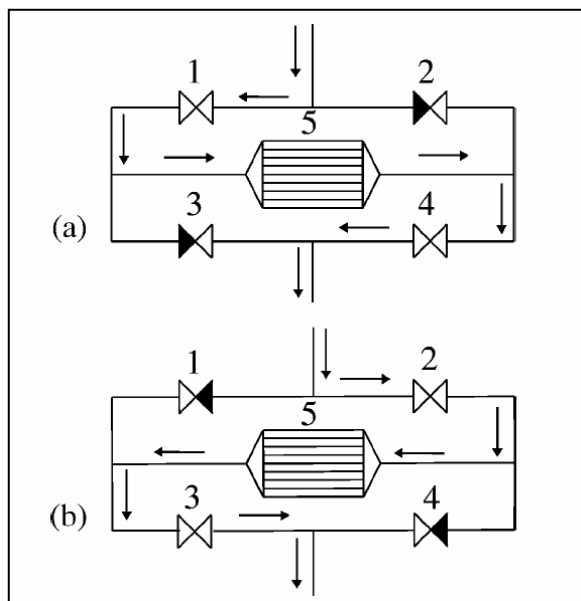

Figure 2.1: Illustration of the reverse-flow reactor concept.

During the last 30 years a number of papers have been devoted to studies and development of the reverse-flow reactor (RFR). Some of the papers only contain theoretical analysis on the basis of simple first-order reaction kinetics, others report attempts to simulate the real catalytic systems and to study them experimentally. The idea of the RFR appeared to be attractive for practical use and some companies tried to practice it on a pilot or commercial scale. The scope of possible applications includes:

1. *exothermic reversible processes*, such as SO_2 oxidation for H_2SO_4 production (Boreskov and Matros, 1983; Snyder and Subramanian, 1993; Xiao and Yuan, 1994), methanol synthesis (Froment, 1990; Neophydes and Froment, 1992; Vanden Bussche *et al.*, 1993), NH_3 synthesis (Matros, 1989; Gerasev and Matros, 1991);

2. *exothermic irreversible reactions*, such as catalytic combustion for purification of waste industrial gases from volatile organic compounds (VOC) (Eigenberger and Nieken, 1988; Haynes *et al.*, 1995; Cittadini *et al.*, 1999, Zufle and Turek, 1997a, b);
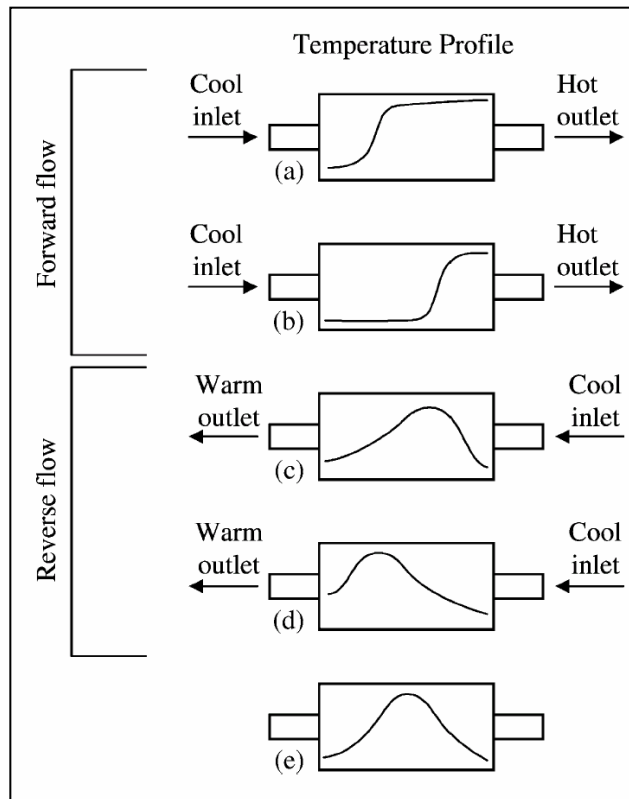

Figure 2.2: Illustration of the heat trap effect for reverse-flow operation.

3. endothermic processes, such as hydrocarbon dehydrogenation (Haynes *et al.*, 1992; Snyder and Subramanian, 1994), styrene synthesis (Kolios and Eigenberger, 1999), methane steam reforming and synthesis gas production (Blanks *et al.*, 1990; De Groote and Froment, 1996; Gosiewski *et al.*, 1999; Gosiewski, 2000).

For an exothermic reaction, the RFR exhibits a heat trap effect which can be used to achieve and maintain an enhanced reactor temperature compared to a single direction flow mode of operation; the principle of the heat trap effect is illustrated in Figure 2.2 (Salomons *et al.*, 2003). Fig. 2.2(a) illustrates a reactor temperature profile that might be observed in a standard unidirectional flow operation for a combustion reaction. The temperature initially rises slowly as the reaction commences, and then more sharply as the heat liberated in the reaction accelerates the rate owing to the exponential temperature dependence of the rate constant. The shape of the curve depends on the operating conditions, especially the inlet gas temperature. If the inlet temperature is lowered, the reaction rate will fall, and the temperature peak will tend to migrate towards the reactor exit. At a sufficiently low temperature, the reaction will effectively be extinguished and the reactor will lose most of its effectiveness as the leading edge of the "hot wave" (where most of the reaction occurs) migrates out of the reactor. If a temperature pattern shown in Fig. 2.2(a) or (b) is established, the reverse flow operation can then be used to take advantage of the high temperatures near the reactor exit to pre-heat the reactor feed. When the feed is switched to the "exit", the energy stored in the reactor during the previous reaction is then effectively used to pre-heat the feed. Because this stored energy is added to the feed stream, it is possible to achieve temperatures higher than the adiabatic temperature rise based on the fresh feed inlet temperature. Provided that the reactor is initially at a sufficiently high temperature (which may require some auxiliary heat source) and the cycle duration is carefully chosen, it is possible to achieve autothermal reactor operation at feed temperatures well below those required for auto-thermal operation with unidirectional flow. In such a case, a quasi-steady state operation may be achieved in which the reactor temperature profile has a maximum value near the centre of the reactor, which slowly oscillates as the feed is switched between the two ends of the reactor, as shown in Fig.2.2(c)–(e).
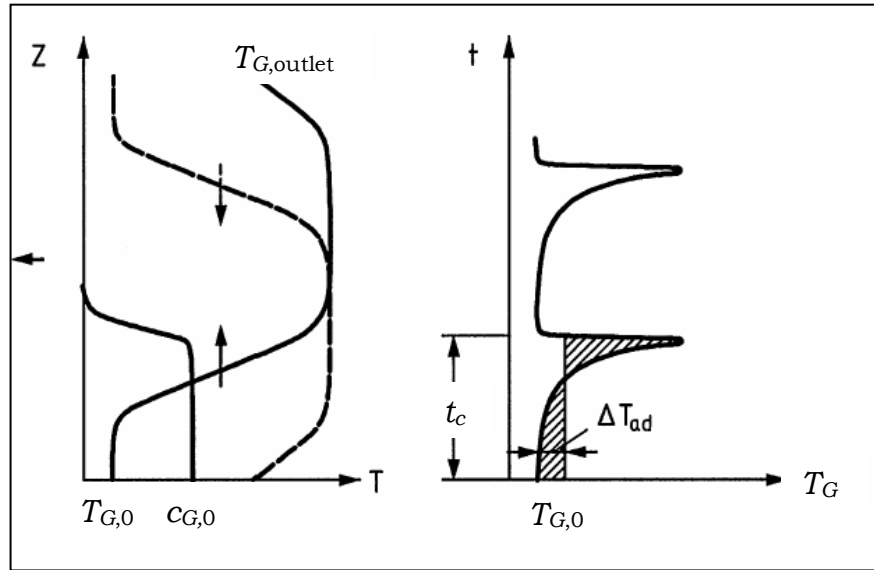
Figure 2.3: Temperature and concentration profiles in the periodic steady-state, feed values: $T_{G,0}$, $c_{G,0}$ (on the left); exit temperature $T_{G,outlet}$ vs. time (on the right).

Figure 2.3 shows the temperature and concentration profiles in the periodic steady state and the course of the reactor exit temperature $T_{G,outlet}$ with time t. In the periodic steady state the temperature (and conversion) profiles for two successive semi cycles are just mirror images of each other. It follows from an overall heat balance that the integral mean of the reactor exit temperature $T_{G,outlet}$ will exceed the feed temperature $T_{G,0}$ just by ΔT_{ad}.

Under periodic flow reversal both ends of the fixed bed are used as regenerative heat exchangers. Since regenerative heat exchange is generally considered simpler and more efficient than recuperative heat exchange, the RFR has found considerable industrial application primarily for the catalytic or homogenous combustion of organic pollutants in exhaust air, strongly reducing the need of auxiliary fuel to sustain the combustion, except during the start-up.

Beside this, the RFR allows for an approach toward optimum temperature distribution, which makes possible the creation of favourable thermodynamic conditions for exothermic equilibrium-limited reactions. Figure 2.4 shows the catalyst temperature and composition profiles in a RFR where methanol synthesis occurs: maximum solid temperature corresponds to a plateau in the concentration profile, due to the establishment of the chemical equilibrium, but the temperature decrease in the final part of the reactor allows for a further increase in the product conversion.
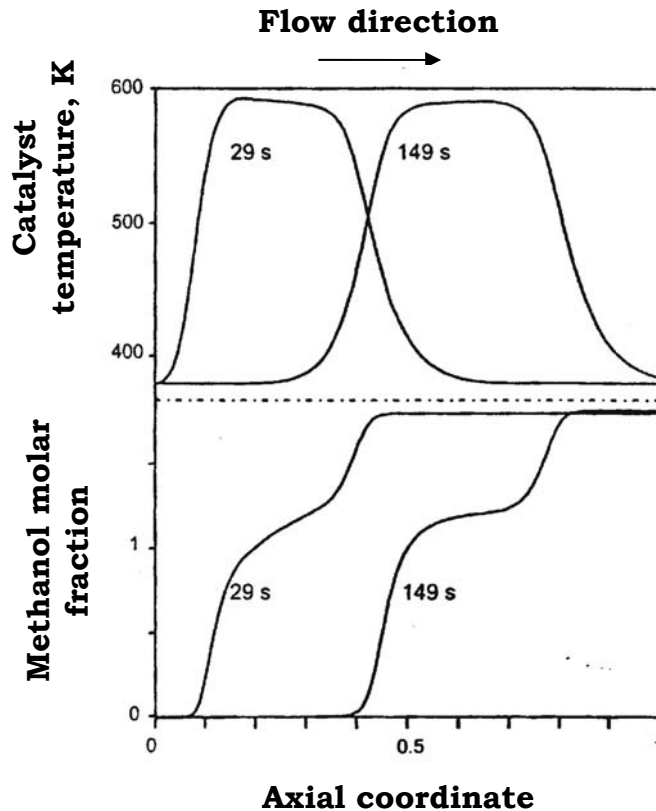
Figure 2.4: Temperature and methanol concentration profiles in a RFR when the steady-state has been reached (profiles are taken at the end of a semi cycle) for two different switching times.

2.2 The reactors network

The reverse flow reactor has found a number of industrial applications and continues to be a topic of investigation worldwide, but it is not the only way to achieve the above mentioned advantages. Vanden Bussche and Froment (1996) proposed the concept of STAR reactor, which can operate in a transient mode giving practically constant exit concentrations and higher conversion than the RFR. The reactors network (RN), which consists of a closed sequence of two or more catalytic fixed bed reactors, is another way to attain a sustained dynamic behaviour (Matros, 1985); this configuration, which has been also called "ring reactor", corresponds to a simulated moving bed: the unsteady-state condition is realised by periodically changing the order of reactors that form the network, varying the feed position. Figure 2.5 shows the working principle of a network made of three reactors: the system is fed through reactor number 1 and the order of the

reactors is 1-2-3. After a time period t_c, the feed position is shifted acting on a set of valves (not shown in Figure 2.5), so that the first reactor of the sequence becomes the third one, thus changing the order to 2-3-1. A further change of the feed position leads to the sequence of reactors 3-1-2. By this way it is possible to create a closed cycle, which prevents the heat front from leaving the system. Contrarily to the RFR, the flow direction is maintained, ensuring a uniform catalyst exploitation because temperature and concentration profiles migrates throughout the entire length of the system.
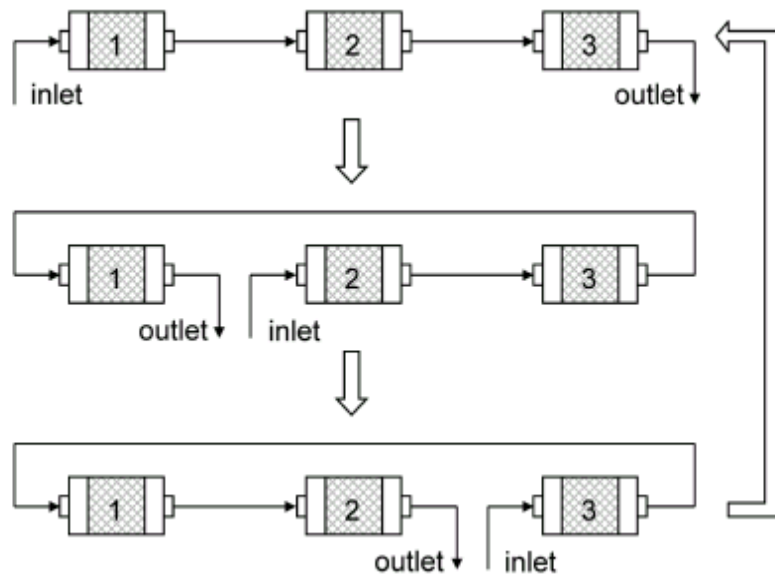
Figure 2.5: Working principle of a network of three catalytic fixed bed reactors in series.

Instead of feeding the second reactor of the sequence when the feeding position is changed, it is possible to feed the last reactor and to have the products leaving the system from the second; also this switching strategy allows maintaining constant the flow direction, but it has not been investigated in the literature.

The simulated moving bed reactor has received little attention up to now. Haynes and Caram (1994) presented some theoretical results concerning the operation of a two reactors network compared with reverse flow operation, showing the applicability to mildly exothermic processes, both for generic reversible and irreversible reactions. Auto-thermal behaviour with a nearly uniform catalyst utilisation are the main advantages of the network; it however presents a small range of switching times t_c which allow to reach and maintain a pseudo-steady state of operation.

The performance and behaviour of a network of three beds, applied to non-stationary catalytic destruction of volatile organic compounds (VOC), have been investigated by means of numerical simulations by Brinkmann *et al.* (1999). Each reactor presented a large inert section for heat exchange followed by the catalytic active part. The effect of transport parameters on conversion and maximum bed temperature has been studied as well as the influence of the design variables. Good conversion and auto-thermal behaviour can be obtained in certain conditions, even at low VOC concentration, but safe operation is related to a narrow range of switching times. This aspect has been investigated in detail and a more robust control policy than the open loop strategy, based on fixed switching time, has been proposed (Barresi *et al.* 1997, 1999a; Barresi and Vanni, 2002). Brinkmann *et al.* (1999) and Barresi *et al.* (1997) suggest that a network of catalytic fixed bed reactors can be a suitable alternative to reverse flow operation, because it can reduce the emissions of unburned gas related to the phenomenon of wash-out, i.e. the drop in combustion efficiency upon each flow reversal, due to the removal of unconverted gas immediately after the change of the inlet section (Cittadini *et al.*, 2002). Velardi and Barresi (2002) investigated application of the reactors network to methanol synthesis showing that this device allows for higher conversion than the RFR and it is not significantly affected by wash-out at the beginning of the cycle. Furthermore, a proper choice of the switching time allows for slight variation of the outlet gas temperature along the cycle, differently from the RFR, thus reducing potential disturbances of the equipment downward. Fissore *et. al.* (2002, 2004), Fissore and Barresi (2002) summarised the main characteristics and performances of the RN with respect both to the combustion of lean VOC mixtures and to exothermic equilibrium-limited reactions.

2.3 Mathematical modelling

Mathematical simulation of a forced unsteady-state reactor involves the solution of a system of mass and energy balances. Both one-dimensional and two-dimensional models can be used; concerning the description of the gas and solid phases both pseudo-homogeneous (Matros, 1989; Eigenberger and Nieken, 1988; Haynes *et al.*, 1992) and heterogeneous models have been proposed.

Purwono *et al.* (1994) used a pseudo-homogeneous model to simulate the behaviour of a catalytic reverse-flow after-burner, assuming steady state condition for the gas phase and an overall heat transfer coefficient to describe the heat transfer to the reactor wall. Eigenberger and Nieken (1988), for an analogous process, used a pseudo-homogeneous model with heat and mass axial dispersion in order to take into account deviation from a plug flow. Khinast *et al.* (1999) pointed out, by means of bifurcational analysis, that qualitatively different dynamic behaviour may arise in a RFR with external refrigeration when pseudo-homogeneous and heterogeneous models are used. Gawdzik and Rakowski (1988) compared the RFR and a tubular reactor, using a heterogeneous model without axial dispersion and gas phase accumulation. Vanden Bussche *et al.* (1993) simulated methanol synthesis by means of a heterogeneous model with plug flow in the gas phase and accumulation terms both in the gas and in the solid phase. Chaouki *et al.* (1994) obtained a good agreement between experimental data and simulations in the case of methane catalytic combustion, using a two-dimensional model taking into account heat losses at the wall, but neglecting axial heat and mass dispersion. Axial conduction in the solid phase may be neglected (Gupta and Bhatia, 1991) or not (Nieken *et al.*, 1995; Van de Beld and Westerterp, 1996, 1997).

Because of the higher thermal capacity of the solid with respect to the gas phase, temperature changes of the solid are slower than that of the gas; as a consequence the models can be simplified by assuming gas phase in steady-state (Matros *et al.*, 1993a; Young *et al.*, 1992; Zagoruiko *et al.*, 1992; Gosiewski and Sztaba, 1990; Gawdzik and Rakowski, 1988; Eigenberger and Nieken, 1988). This assumption may not be justified at high pressure (Vanden Bussche *et al.*, 1993) but also when operating at low pressure the dynamic in the gas phase may influence the performance of the system immediately after the inversion of the flow direction.

When bench scale units are considered, an additional energy balance for the reactor wall has been included to take into account radial heat losses from the bed to the wall and axial conduction at the wall: these effects are particularly relevant in reactors with small diameter, such as lab or bench scale units used for research purposes, or small industrial units, while large industrial reactors can be considered to operate adiabatically because of their high bed diameter/wall thickness ratio (Cittadini *et al.*, 1999).

When the switching time is very low, it can be comparable to the time scale of the catalytic reactions; as a consequence the solid operates in dynamic conditions and the kinetic model that have been obtained in steady-state conditions may not be adequate to describe the reaction. Bunimovich *et al.* (1995) used a nonstationary kinetic model to simulate the catalytic oxidation of SO_2, obtaining a good agreement with the experimental results.

From this discussion it follows that a model which has to be adequate to describe the dynamic of a forced unsteady-state reactor should be heterogeneous and dispersive (Reacek *et al.*, 1992; Snyder and Subramaniam, 1994; Grozev and Sapundzhiev, 1997; Khinast *et al.*, 1999).

Chapter 3

Abatement of gaseous pollutants using forced unsteady-state catalytic combustors

The treatment of gaseous emissions containing VOC mixtures can be accomplished by means of various processes, allowing for a recovery of the pollutant (in case of solvents and paints, for example) or for a complete removal.

Concerning the treatment of lean mixtures of waste gases, for which no recovering processes can compete economically with combustion, the RFR is a promising technology, as the reversal of the flow keeps the heat of reaction inside the bed, thus allowing autothermal operation even when cold and very lean mixtures are fed, reducing strongly (or even eliminating) the need for auxiliary fuel, except for the start-up and control purposes. After the transient period following the start-up, a pseudo-steady state (PSS), also called cyclic steady-state, is attained, in which the hot front shifts periodically in the central part of the reactor, while the external parts of the bed remain cold, allowing a very low heat loss in the outlet flow. For this reason the catalyst, in the external parts of the bed, can be substituted by inert material. Extensive investigations about the RFR, including both numerical simulations and experimental works, have been performed in the past thirty years and have been reviewed in § 2.1.

Flow reversal is not the only way to utilise the thermal storage capacity of the reactor to obtain an autothermal behaviour; a simulated moving bed,

made of different reactors connected in a closed sequence, with periodical variation of the feed position is an alternative configuration (§1.2). As the first part of each bed behaves mainly as a heat regenerator, while reaction occurs at the end, the system can operate with a large inert section and only a small catalytic part at the end of each bed. A set of valves enables the change of the feed position, thus varying the sequence of reactors, simulating the behaviour of a moving bed reactor. Contrary to the RFR, the flow direction is maintained in this way, ensuing a uniform catalyst exploitation.

In this chapter a network of two or three reactors in series is presented as an alternative to the well-investigated RFR for the treatment of the lean fugitive emissions from coke ovens. The composition of this mixture is very complex and variable cyclically with time, according to the operation, namely charging, pushing and door leaks. Pushing emissions are constituted by humid air with about 5% carbon dioxide and 200 ppmV carbon monoxide. Composition of charging and door emissions is similar, but taking into account the volume emitted, the most dangerous emissions are the ones produced during the charging of the coke ovens. Table 3.1 reports a typical composition for an industrial plant: methane is present in relatively high concentration; H_2O, H_2S, SO_2 and other compounds are also present in a lower concentration. Methane is also very adequate as test compound for catalytic destruction studies, because it has the highest ignition temperature among paraffinic and aromatic compounds, and as a consequence most pollutants will be destroyed at the temperature that allows for total methane combustion. Moreover the combustion of methane, and hence its transformation to carbon dioxide is environmentally advantageous because the GWP (global warming potential) of methane is about 20 times higher than that of carbon dioxide.

Table 3.1: Typical composition of the fugitive emissions from a coke oven.

Time, s	30	60	90	120	180
Pollutant, ppmV					
CO_2	27600	23000	13000	12000	450
CH_4	-	5500	3900	5500	-
H_2	-	7000	6600	7000	-
CO	-	6200	5200	6200	-
Velocity, m s^{-1}	0.17	0.17	0.15	0.12	0.08

A one-dimensional heterogeneous model has been used to simulate and to compare the behaviour of the RFR and of the RN and to point out the influence of the main operating parameters (§3.1). The results will show that the RFR is the best reactor configuration for this application, having as an objective the stability of the system, and thus this device has been optimised (§3.2). As the catalyst thermal properties (heat capacity and conductivity) will be demonstrated to play a role not less important than the kinetic activity, a simpler pseudo-homogeneous model has been used in order to optimise the catalyst (§3.3). Modelling results have been validated in a bench scale reactor with a special temperature control system based on a dynamic compensation of the thermal losses to get adiabatic behaviour (§3.4).

3.1 The model

A one-dimensional heterogeneous model has been considered in order to compare the RFR and the RN and to investigate the influence of the main operating parameters on the stability of the reactor; the details on the pseudo-homogeneous model will be given in (§ 3.3.1).

In the detailed model the pressure loss inside the system is neglected. Plug flow condition is assumed for the gas phase with dispersive transport of mass and energy; ideal gas law has been adopted. The transient term is taken into account in the gas phase equations and in the energy equation for the solid phase, while the solid catalytic surface is considered in pseudo-steady state condition. The effect of the intraparticle mass transport has been included in the model by estimation of the effectiveness factors, using the linearization method proposed by Gosiewski *et al*. (1999). Thus, the dynamics of the adiabatic process can be described by the following set of differential-algebraic equations (DAE):

- Continuity equation for the gas phase:

$$\frac{\partial c_G}{\partial t} + \frac{\partial}{\partial x} c_G v = \sum_{i=1}^{n_r} \frac{k_{G,i} a_v}{\varepsilon} (y_{S,i} - y_{G,i}) \tag{3.1}$$

- Continuity equation for component *j* in the gas phase:

$$\frac{\partial y_{G,j}}{\partial t} = D_{eff}\frac{\partial^2 y_{G,j}}{\partial x^2} - v\frac{\partial y_{G,j}}{\partial x} + \frac{k_{G,j}a_v}{c_G\varepsilon}\left(y_{S,j} - y_{G,j}\right) +$$

$$-y_{G,j}\sum_{i=1}^{n_r}\frac{k_{G,i}a_v}{c_G\varepsilon}\left(y_{S,i} - y_{G,i}\right) \quad \text{with} \qquad j = 1...(n_r - 1) \tag{3.2}$$

- Energy balance for the gas phase

$$\frac{\partial T_G}{\partial t} = \frac{k_{eff}}{\rho_G c_{p,G}}\frac{\partial^2 T_G}{\partial x^2} - v\frac{\partial T_G}{\partial x} + \frac{ha_v}{\rho_G c_{p,G}\varepsilon}(T_S - T_G) \tag{3.3}$$

- Mass balance for the solid phase:

$$k_{G,j}a_v\left(y_{S,j} - y_{G,j}\right) = [\rho_S(1-\varepsilon)]\sum_{k=1}^{N_R}\eta_k\nu_{j,k}R'_{k,j} \qquad \text{with} \quad j = 1...n_r \tag{3.4}$$

- Energy balance for the solid phase:

$$\frac{\partial T_S}{\partial t} = \frac{\lambda_S}{\rho_S c_{p,S}}\frac{\partial^2 T_S}{\partial x^2} - \frac{ha_v}{\rho_S c_{p,S}(1-\varepsilon)}(T_S - T_G) + \frac{1}{c_{p,S}}\sum_{i=1}^{n_r}\left(\sum_{k=1}^{N_R}\eta_k\nu_{i,k}R'_k\right)(-\Delta H_{f,i}) \tag{3.5}$$

For the catalytic part of the reactor, a first order rate equation is considered in the mass balance for the solid phase:

$$R'_{k,j} = k_r y_{S,j} = k_\infty \exp\left(-E_a/RT_S\right)y_{S,j} \tag{3.6}$$

$$k_\infty = k'_\infty\rho_S(1-\varepsilon)RT_G \tag{3.7}$$

while for the inert sections the reaction rate is set equal to zero. Similarly, the solid physical properties, namely density, specific heat and thermal conductivity, are set equal to the values either of the catalyst or of the inert, depending on the axial position in the reactor. If the physical and transport properties of the catalyst and of the inert are different, adequate boundary conditions (i.e. identity in the heat and mass fluxes) have to be specified in the boundary surface.

When small scale apparatus are considered a further equation is needed in order to take into account the effect of the reactor wall:

$$\frac{\partial T_W}{\partial t} = \frac{\lambda_W}{c_{p,W}\rho_W}\frac{\partial^2 T_W}{\partial x^2} + \frac{4}{c_{p,W}\rho_W\left(D_{R,e}^2 - D_{R,i}^2\right)}D_{R,i}h_i\left(T_G - T_W\right) \tag{3.8}$$

and the energy balance for the gas phase has to be modified accordingly:

$$\frac{\partial T_G}{\partial t} = \frac{k_{eff}}{\rho_G c_{p,G}}\frac{\partial^2 T_G}{\partial x^2} - v\frac{\partial T_G}{\partial x} + \frac{ha_v(T_S - T_G)}{\rho_G c_{p,G}\varepsilon} - \frac{4h_i}{\rho_G c_{p,G}D_{R,i}}(T_G - T_W) \tag{3.9}$$

When simulating the RFR conventional Danckwerts boundary conditions are assumed in $x=0$ and $x=L$; in the case of the RN Danckwerts boundary conditions are assumed for the gas phase in each reactor and the continuity of gas temperature and concentration profiles are imposed between the reactors of the network, i.e. in sections at $x = Kl$, with $K = 1,..., n_b\text{-}1$. In the following we refer to L as the total length of the reactors network, to n_b as the number of reactors in the sequence and to $l = L/n_b$ as the length of a single reactor of the sequence.

$$y_{G,j}\big|_{x=0^+} - \frac{D_{eff}}{v} \frac{\partial y_{G,j}}{\partial x}\bigg|_{x=0^+} = y_{j,0} \tag{3.10}$$

$$T_G\big|_{x=0^+} - \frac{k_{eff}}{\rho c_{p,G}} \frac{\partial T_G}{\partial x}\bigg|_{x=0^+} = T_{G,0} \tag{3.11}$$

$$\lambda_S \frac{\partial T_S}{\partial x}\bigg|_{x=0^+} = 0 \tag{3.12}$$

$$v\big|_{x=0^+} = v_0 \tag{3.13}$$

$$\frac{\partial y_{G,j}}{\partial x}\bigg|_{x=K\ell^-} = \frac{\partial T_G}{\partial x}\bigg|_{x=K\ell^-} = \frac{\partial T_S}{\partial x}\bigg|_{x=K\ell^-} = \frac{\partial y_{G,j}}{\partial x}\bigg|_{x=K\ell^+} = $$
$$= \frac{\partial T_G}{\partial x}\bigg|_{x=K\ell^+} = \frac{\partial T_S}{\partial x}\bigg|_{x=K\ell^+} = 0 \tag{3.14}$$

$$y_{G,j}\big|_{x=K\ell^-} = y_{G,j}\big|_{x=K\ell^+} \tag{3.15}$$

$$T_G\big|_{x=K\ell^-} = T_G\big|_{x=K\ell^+} \tag{3.16}$$

$$v\big|_{x=K\ell^-} = v\big|_{x=K\ell^+} \tag{3.17}$$

$$D_{eff} \frac{\partial y_{G,j}}{\partial x}\bigg|_{x=L} = 0 \tag{3.18}$$

$$k_{eff} \frac{\partial T_G}{\partial x}\bigg|_{x=L} = 0 \tag{3.19}$$

$$\lambda_S \frac{\partial T_S}{\partial x}\bigg|_{x=L} = 0 \tag{3.20}$$

Initially, gas phase temperature is considered constant along the reactors and equal to the inlet value and solid temperature is considered constant and equal to the pre-heating value; the initial reactants concentration is null:

$$t = 0, \quad \forall x \qquad y_{G,j}\big|_{t=0} = y_{G,0j}(x) \tag{3.21}$$

$$t = 0, \quad \forall x \qquad\qquad T_G\big|_{t=0} = T_{G,0} \tag{3.22}$$

$$t = 0, \quad \forall x \qquad\qquad T_S\big|_{t=0} = T_{ph} \tag{3.23}$$

The origin of the *x*-axis corresponds with the inlet section to the network; consequently it translates from the first reactor of the sequence to the second one when switching time is reached. At this point the boundary conditions are switched in order to simulate the variation of the inlet position:

$$x \in]i-1, i\ell] \qquad \begin{cases} y_{G,j}(x)\big|_{t^+} = y_{G,j}(x+\ell)\big|_{t^-} \\ T_G(x)\big|_{t^+} = T_G(x+\ell)\big|_{t^-} \qquad \text{for } i=1,..n_b \\ T_S(x)\big|_{t^+} = T_S(x+\ell)\big|_{t^-} \end{cases} \tag{3.24}$$

Transport and dispersion parameters have been evaluated according to previous works (van de Beld, 1995). Concerning the gas-solid heat transfer coefficient, the following correlation has been adopted:

$$\frac{h d_P}{\lambda_G} = 1.6\left(2 + F \cdot \text{Re}_P^{0.5} \, \text{Pr}^{1/3}\right) \tag{3.25}$$

with

$$F = 0.664\sqrt{1 + \left[\frac{0.0557 \cdot \text{Re}_P^{0,3} \, \text{Pr}^{2/3}}{1 + 2.44\left(\text{Pr}^{2/3} - 1\right)\text{Re}_P^{-0,1}}\right]^2} \tag{3.26}$$

and a similar correlation has been used to evaluate the mass transfer coefficient, according to Chilton-Colburn's analogy.

The prediction of the gas axial heat dispersion coefficient has been carried out adopting a correlation by Dixon and Cresswell (1979):

$$\frac{k_{eff}}{\rho v c_{p,G} d_P} = \frac{0.73 + \lambda_{st}/\lambda_G}{\text{Re}_P \, \text{Pr}} + \frac{0.5}{1 + 9.7/(\text{Re}_P \, \text{Pr})} \tag{3.27}$$

where the term λ_{st}/λ_G accounts for the stagnant zone contribution. According to Edwards and Richardson (1968) a correlation of the same form can be used for the prediction of mass dispersion:

$$\frac{D_{eff}}{v d_P} = \frac{0.73}{\text{Re}_P \, \text{Sc}} + \frac{0.5}{1 + 9.7/(\text{Re}_P \, \text{Sc})} \tag{3.28}$$

The influence of the temperature and composition on the density and the specific heat of the gas has also been taken into account.

Adiabatic operation has been considered, as this is the condition which closely approximates real-scale apparatus; the influence of non-adiabaticity

on the stability and the performance of the reactor, which can be important in small and lab scale apparatus, can be accounted for including a term for heat loss to the environment in the gas-phase energy balance if wall heat balance is neglected, otherwise to the wall, which exchanges heat with the exterior. The results available in literature both for the RN (Barresi *et al.*, 1999b) and for the RFR (Van de Beld, 1995) show that heat losses reduce the length of the hot zone, slightly modifying the temperature profile, and can be relevant during the start up.

The evaluation of the thermal properties of the porous solid is a complex task; for volume-proportional quantities, such as density or specific heat, a linear mixing law is valid, while for transport properties nonlinear mixing laws apply. The approach of Buntebarth and Schopper (1997) has been adopted in order to evaluate the thermal conductivity of the porous solid (λ_S^*) as a function of the solid matrix properties:

$$\lambda_S^* = \frac{\rho_S c_{p,S}}{\rho_{mtx} c_{p,mtx}} \frac{1}{1 + \alpha \varepsilon_c} \tag{3.29}$$

where α is a structural constant of the porous solid. The thermal conductivity of the catalyst bed (λ_S) can be evaluated taking into account the contribution of the solid phase and the heat dispersion in the gas phase; the static contribution is a function of the thermal conductivities of the solid and fluid phases, the void fraction, and, if radiation is important, the emissivity, mean temperature, and diameter of the solid particles. Heat transfer can be assumed to occur by the following mechanisms:

1. heat transfer through the fluid in the void space by conduction and by radiation between adjacent voids;
2. heat transfer through the contact surface of the solid particles and conduction trough the stagnant fluid near the contact surface;
3. radiation between surfaces of solid;
4. conduction through the solid phase.

According to Kunii and Smith (1960), except at low pressure, the term for heat transfer through the contact surfaces can be neglected; thus the thermal conductivity of the bed immersed in a stagnant fluid is given by

$$\frac{\lambda_S}{\lambda_G} = \varepsilon\left[1 + \beta\frac{h_{rv}d_P}{\lambda_G}\right] + \frac{\beta(1-\varepsilon)}{\dfrac{1}{\dfrac{1}{\phi} + \dfrac{h_{rs}d_P}{\lambda_G}} + \gamma\left(\dfrac{\lambda_G}{\lambda_S^*}\right)} \qquad (3.30)$$

To use equation (3.30) it is necessary to estimate the three quantities β, γ, ϕ, where β is the effective length between centres of two neighbouring solid particles in the direction of the heat flow, γ is the effective length of a solid particle for heat transfer and ϕ is the effective thickness of the fluid film adjacent to the surface of two solid particles. β, γ, ϕ have been evaluated according to Kunii and Smith (1960).

The domain of the spatial variable x has been discretised on a grid of equally spaced points; 101 points are sufficient to ensure a grid-independent solution. As a consequence, the Partial Differential Algebraic Equations (PDAE) system (3.1)-(3.9) is transformed into a Differential Algebraic Equations (DAE) problem. The integration in time of the differential part of the system has been performed implementing the Fortran routine LSODES, from the package ODEPACK (Hindmarsh, 1983). Both relative and absolute tolerance are set to the square root of the working machine precision.

After a transient period, the solution of the system evolves towards a pseudo-steady state (PSS): the behaviour of the reactor (temperature and concentration profiles) is the same within every cycle (every two or three switches, depending on the reactor configuration).

3.3 Comparison between the RFR and the RN

The behaviours of the RFR and of the RN have been compared for a constant total length of the reactors and the influence of the main operating conditions (inlet velocity, switching time, inlet concentration, inert fraction) and of the number of reactors on the performances of these devices has been pointed out (Fissore *et al.*, 2002, Fissore and Barresi, 2002). The physical properties and kinetic parameters adopted for the simulation refer to lean air-methane mixtures and are summarised in Table 3.2; physical properties correspond to values in a range of practical interest, while for the kinetic parameters the values used before by Barresi and Vanni (2002) have been considered.

The forced unsteady-state combustor can operate autothermally without external pre-heating of the gases, but the bed must be pre-heated above the

ignition temperature before start-up; a uniform temperature profile has been considered as initial condition, but it has been observed that the shape of the initial temperature profile does not influence the long term behaviour; on the contrary the length of the transient period which is needed to reach the pseudo-steady state depends both on the pre-heating temperature and the VOC concentration of the gases (that can be measured by the adiabatic temperature rise of the mixture).

Table 3.2: Main physical and kinetic parameters adopted in the simulations.

D_R	14	mm
L	0.3	m
d_P	0.7	mm
ρ_S	1000	kg m^{-3}
$c_{p,S}$	1000	J kg^{-1} K^{-1}
λ_S	0.18	W m^{-1} K^{-1}
ε	0.35	
A_v	10000	m^{-1}
k'_∞	46.5	mol kg^{-1}s^{-1}Pa^{-1}
E_a	91.244	kJ mol^{-1}
$-\Delta H_r$	802.5	kJ mol^{-1}
T_{ph}	600	K

Depending on the VOC load in the feed, either extinction or a state of periodical operation can be reached. If stable operation is possible, the maximum temperature reached by the gas (and by the catalyst, as the two temperatures are very close) in the centre of the reactor is higher than the ignition temperature of the hydrocarbon, and the conversion is always almost complete. This fact can be easily explained considering that, for lean mixtures, autothermal operation is possible only if almost all the methane is destroyed, otherwise the heat production is not sufficient to keep the internal temperature over the ignition point, and reaction extinguishes (Fissore *et al.*, 2001a; Barresi *et al.*, 2001a). An example of the evolution of the temperature profiles in the RFR and in the network of two and three reactors is shown in Figure 3.1, where the axial position is made dimensionless dividing by the total reactor length. Different switching periods have been considered for the various configurations as stable operation can be obtained in the network

only in a narrow range of t_c, that is also depending on the number of reactors, while the RFR has a much wider operating range as it will be shown later; for the comparison we have chosen the value of t_c where the methane conversion is higher. Even if the devices are different, the PSS temperature profile which is reached in the RFR and in the RN are similar, although in the second case they are not symmetric; both the maximum temperature on the solid and the number of switches which is required to reach the PSS are slightly higher in the network and they increase with the number of reactors in the network.
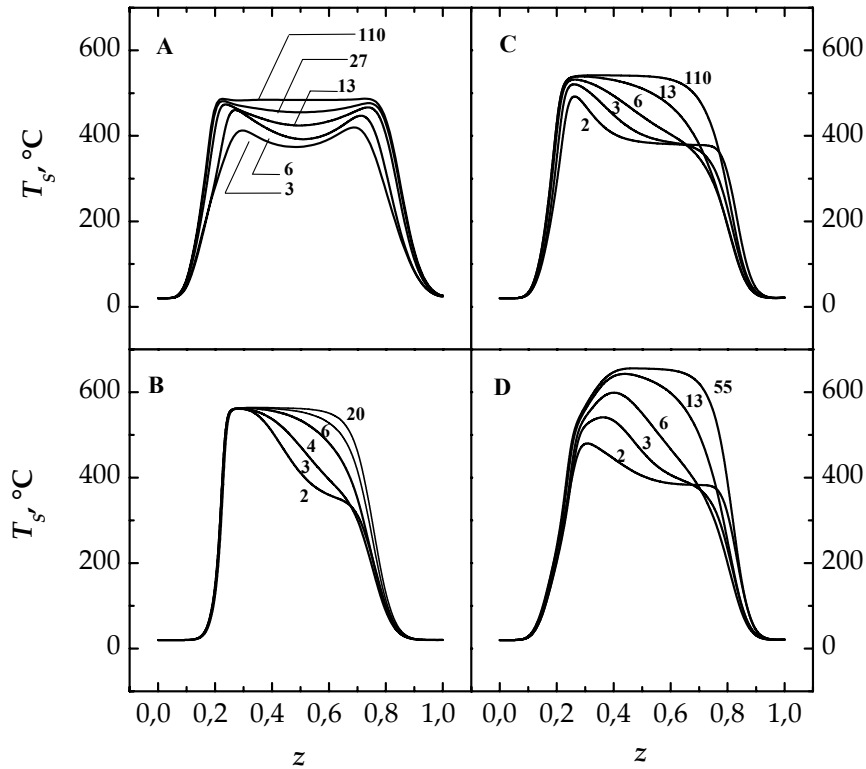

Figure 3.1: Development of the temperature profile in the RFR (graph A, t_c = 450 s), in the network of two reactors (graph B, t_c = 850 s), in the network of three reactors without inert (graph C, t_c = 450 s) and with 50 % of inert (graph D, t_c = 450 s), during the initial transient; $y_{G,0}$ = 5000 ppmV, u_0 = 0.1 m s^{-1}, adiabatic conditions. The profiles refer to the middle of the indicated semi-cycle.

The catalyst in the entrance and exit sections of the reactors, where the bed acts as heat regenerator, can be substituted by inert material. a large fraction (50%) in substituted in the example shown. It has been observed that the maximum temperature increases and the length of the hot zone is reduced similarly to what happens in the reverse flow reactor; Figure 3.1D shows the

behaviour of the three RN: it can be noted that the length of the transient period is decreased by the introduction of the inert.

The effect of the inlet VOC concentration on the pseudo-steady state temperature profile is shown in Figure 3.2 both for the two and three RN and for the RFR: the higher is the organic load, the wider is the hot zone, while the shape of the pseudo-steady state temperature profiles is only slightly affected by the inlet methane concentration; the maximum temperature in the reactor increases at higher methane inlet concentrations, and the variation is equal to the difference in the ΔT_{ad} of the feed.
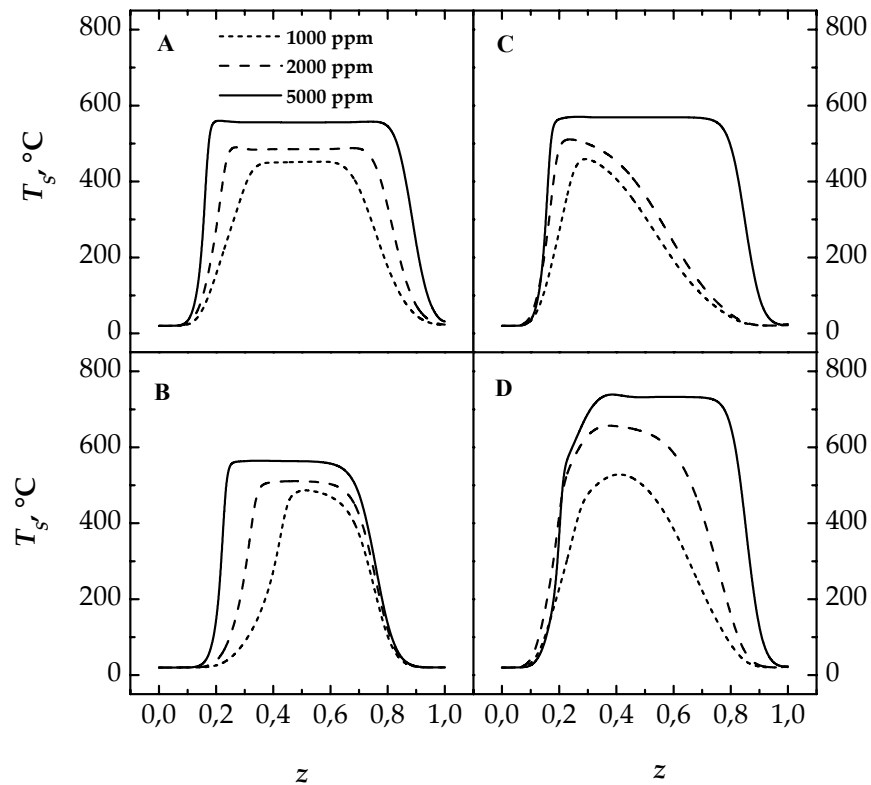

Figure 3.2: Dependence of the PSS temperature profile on the methane load in the RFR (graph A, t_c = 600 s), in the network of two reactors (graph B, t_c = 850 s), in the network of three reactors without inert (graph C, t_c = 600 s for $y_{G,0}$ = 5000 ppmV, t_c = 520 s for the other organic loads) and with 50 % of inert (graph D, t_c as in graph C).

Adiabatic conditions, u_0 = 0.1 m s^{-1}.

The temperature profiles in the RN become similar to those of the RFR for high methane load. Partial substitution of the catalyst pellets with inert material has also been considered in Fig. 3.2D: a strong increase of the maximum temperature and a different shape of the temperature profile have been observed. Different switching times have been considered, as before, as

a consequence of the different stability ranges.

The effect of the inlet surface velocity is shown in Figure 3.3 both for the network of two and three reactors and for the RFR: the higher the gas velocity the higher the solid temperature in the reactor. The length of the hot zone is slightly increased when the surface velocity increases in the FFR, while it is slightly reduced in the three RN; this effect is more relevant in the network of two reactors. The influence of the inert fraction is shown in Figure 3.3D: the maximum temperature of the solid increases slightly in the RFR and, if we increase the number of the reactors in the network, we obtain a larger increase of the temperature.
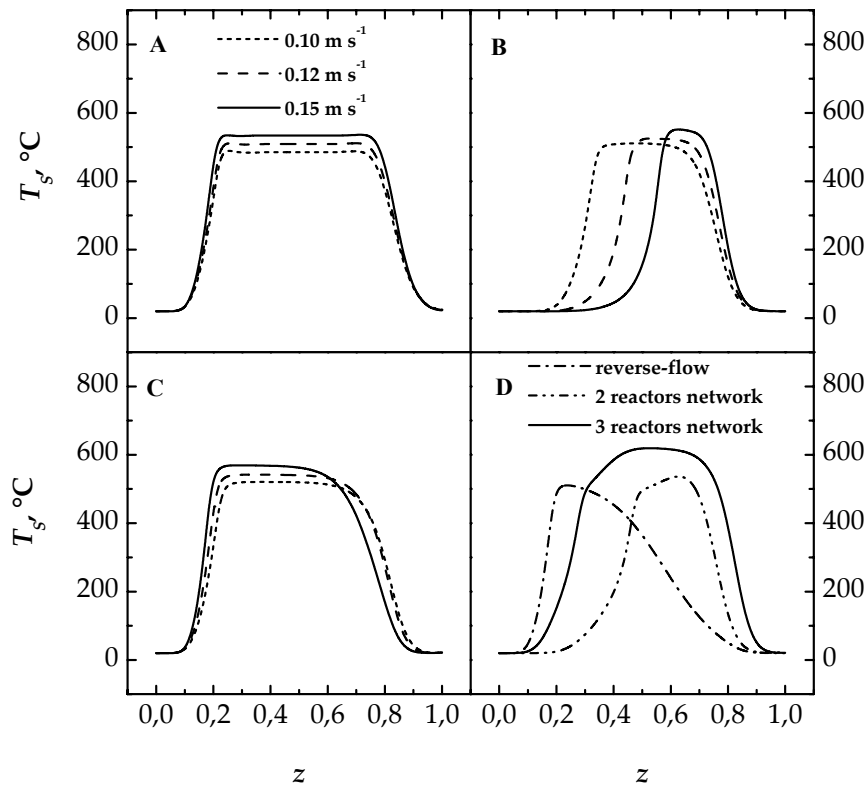

Figure 3.3: Dependence of the PSS temperature profile on the inlet surface velocity in the RFR (graph A, t_c = 600 s) in the two RN (graph B, t_c = 850 s for u_0 = 0.1 m s^{-1}, t_c = 730 s for u_0 = 0.12 m s^{-1} and t_c = 600 s for u_0 = 0.15 m s^{-1}) and in the three RN (graph C, t_c = 550 s for u_0 = 0.1 m s^{-1}, t_c = 450 s for u_0 = 0.12 m s^{-1} and t_c = 350 s for u_0 = 0.15 m s^{-1}) without inert. Graph D shows the effect of the inert (u_0 = 0.1 m s^{-1}, t_c = 600 s for the RFR, t_c = 850 s for the two RN and t_c = 550 s for the three reactors network), $y_{G,0}$ = 2000 ppmV, 50% of inert.

The effect of the switching period on the maximum temperature of the solid and on the stability limits is shown in Figure 3.4 for different inert fractions

in the case of the RFR and of the network of three reactors. We can observe that the switching time only influences slightly the maximum temperature in the reverse-flow reactor, except for very high inert fractions, as it has been shown also by Haynes and Caram (1994). For example in the case of 50% inert fraction the maximum temperature on the solid can overcome 1000°C for low t_c, but decreases strongly when the switching time is increased. In the case of the network of three reactors the effect of the switching time on the maximum temperature is observable also for low inert fractions, even if maximum variation is limited to about 50°C. The maximum temperature in the reactor is lower in the network than in the RFR, even with large inert fractions. The stability limits are not significantly influenced by an increase of the inert fraction, except for a slight reduction of the maximum value of t_c which allows autothermal operation.
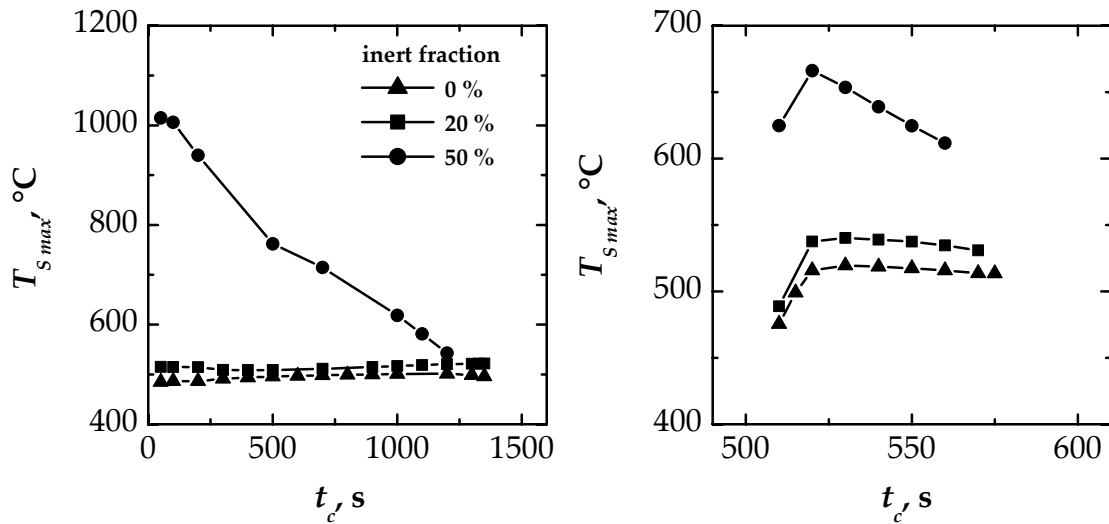

Figure 3.4: Dependence of the maximum solid temperature on the switching time, for different inert percentage, in the reverse flow reactor (on the left) and in the network of three reactors (on the right). Adiabatic conditions, $y_{G,0} = 2000$ ppmV, $u_0 = 0.1$ m s^{-1}. The whole range of t_c in which stable operation is obtained is shown.

As it can be seen from Figure 3.4, the stability limits of the RN are much narrower than in the case of the RFR: the methane conversion quickly decreases for t_c slightly lower or higher that the values which allows for autothermal behaviour with high conversion; the reason is that in the network of combustors the proper switching period is closely related to the velocity of the heat front: if the period is too long, the first section is cooled

too much, and the gases do not reach the catalyst at the required temperature, while if it is too short there is no time to accumulate enough heat in the second reactor before switching, and the system gradually extinguishes.
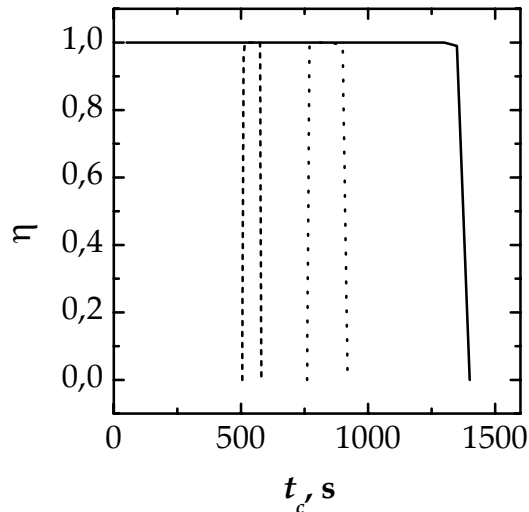

Figure 3.5: Methane conversion for the RFR (solid line) and for the network of two (dashed line) and three (dotted line) reactors. Adiabatic conditions, $y_{G,0}$ = 2000 ppmV, u_0 = 0.1 m s^{-1}.

This is evident also from Figure 3.5, where it appears that if the number of reactors is reduced, with constant total length, the stability limits become slightly wider. In the case of the RFR stable operation is possible even for very low switching periods, while, if the cycle time is too high, the heat front is removed from the reactor and no autothermal operation can be obtained.
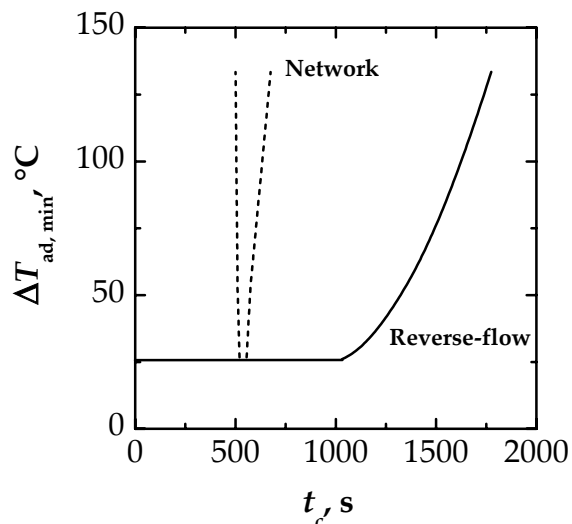

Figure 3.6: Dependence of the minimum inlet concentration that allows for stable autothermal combustion on the switching time for the RFR and the three RN. Adiabatic conditions, u_0 = 0.1 m s^{-1}.

Lean VOC concentrations have been considered until now, as the attention was focused on autothermal behaviour of lean mixtures, but the organic concentration strongly affects the behaviour of this system (Fissore *et al.*, 2004). The effect of the organic load on the stability limits of these devices is shown in Figure 3.6: both for the RFR and for the network of three reactors an increase of the adiabatic temperature rise of the mixture leads to a larger stability range, as the heat generation in the reactor is increased, but the effect is very limited for the network.
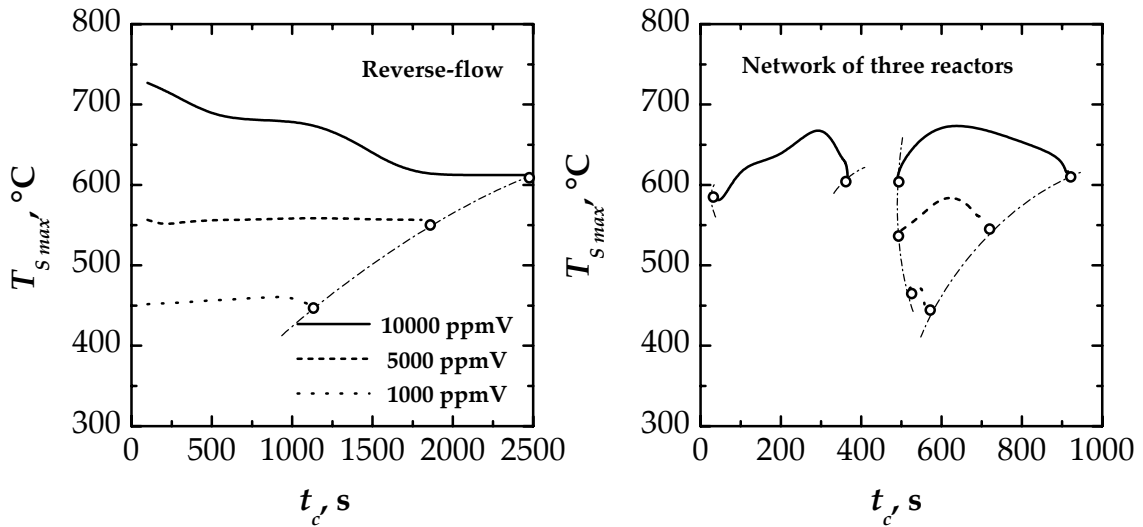

Figure 3.7: Comparison between the maximum temperature of the solid for the RFR and for the network of three reactors for different inlet concentrations and switching times.

The higher is the organic load, the higher is the maximum temperature of the solid as it is shown in Figure 3.7 for the RFR and the RN. The circles in Figure 3.7 delimit the stability range: the RN has a narrower stability range than the RFR as the VOC conversion quickly decreases for values of t_c slightly lower or higher than those leading to autothermal behaviour. Figure 3.7 also shows the effect of the switching period on the maximum temperature of the solid: t_c slightly influences the maximum temperature in the RFR, except for very high inlet concentration, where the higher the switching time, the lower the maximum temperature because the amount of heat which is kept inside the reactor decreases. In the ring reactor the influence of the switching time on the maximum temperature of the solid is more complex: a maximum value can be found inside the stability window and then it decreases when the stability limits are approached. If we increase the inlet concentration the maximum temperature increases both in the RFR and in the RN because of

the higher amount of heat released by the combustion reaction; as a consequence, the range of switching time which makes possible stable operation is enlarged and, in the case of the reactor network, a second stability range appears at high inlet VOC concentration.

The temperature profiles that are obtained in the different stability regions have different shapes, as it is shown in Figure 3.8.
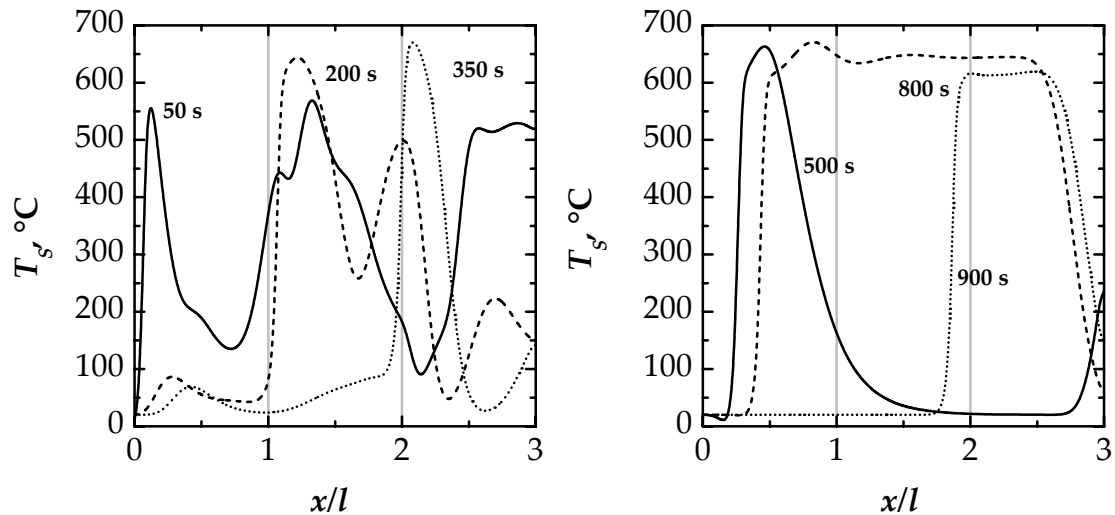

Figure 3.8: Solid temperature profiles in the network of three reactors with y_0 = 10000 ppmV in air for different switching times. The profiles are taken at the end of the semi-cycle, when the periodic-steady state has been reached.

When we are working in the region of high switching times (Figure 3.8, on the right) the temperature profiles are similar to those obtained in a RFR; the length of the central hot zone is reduced when we approach the extinction limits. When we are working at low switching times (Figure 3.8, on the left) the change of the feed position leads to the formation of temperature profiles that present a series of temperature drops, which are somewhat analogous to intermediate coolings.
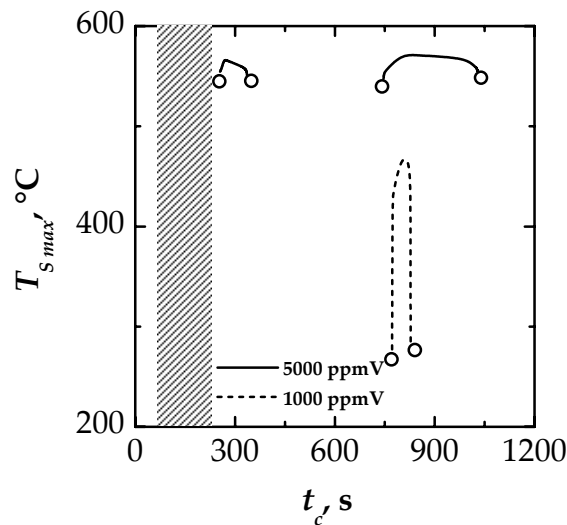
Figure 3.9: Maximum temperature of the solid in the network of two reactors for different inlet concentrations and switching times; the triangles refer to stable operation obtained with an inlet concentration of 5000 ppmV in air.

Figure 3.9 shows the analogous results for the network of two reactors: it appears that if we reduce the number of reactors, with constant total length, the stability limits become slightly wider, while no significant differences are observed in the maximum temperature if the same inlet concentration is considered. If we increase the organic load, a second stability window appears at 5000 ppmV, while in the three reactors network a higher concentration is required to obtain this second stability window.

Autothermal operation can be obtained for an inlet concentration of 5000 ppmV also in a third range of t_c: for some values of the switching time between 40 s and 210 s (the triangles plotted in the figure) complete methane conversion can be achieved without external heating. Stable operation can be obtained for these values of t_c (and inlet concentration) despite small changes in the feeding temperature and flow rate; on the contrary small changes in the switching time may lead to extinction of the reaction.

Figure 3.10 shows a comparison of the temperature profiles (taken at the end of the semicycle when the pseudo-steady state is reached) in the different stability regions, when the inlet concentration is equal to 5000 ppmV. The results that are obtained are similar to those presented for the network of three reactors: increasing the switching period the temperature profiles become similar to those of the reverse-flow reactor, while for low switching times the central hot temperature *plateau* disappears and is replaced by intermediate coolings.
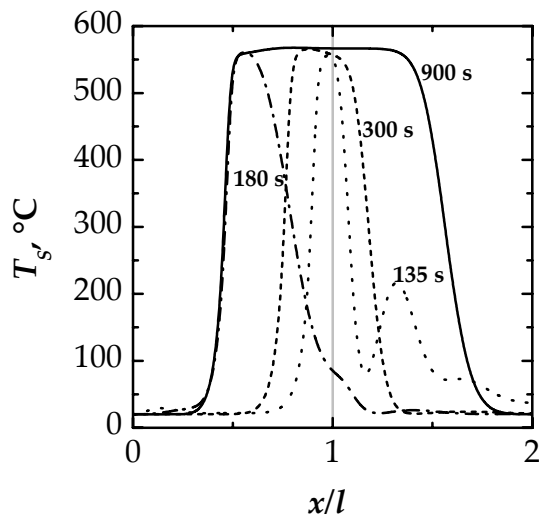
Figure 3.10: Solid temperature profiles in the network of two reactors with y_{in} = 5000 ppmV in air for different switching times. Switching times in the different stability windows are considered. The profiles are taken at the end of the semi-cycle, when the pseudo-steady state has been reached.

The dependence of the stability limits on the inlet surface velocity is shown in Figure 3.11: while stable autothermal operation is possible in the RFR also for high inlet velocity, this is not possible in the network of three reactors, which has narrower stability limits. For a fixed value of the inlet velocity the minimum inlet methane concentration that allows autothermal operation in the RFR is lower than that needed in the RN; in both devices if we decrease the surface velocity a higher $\Delta T_{ad\ min}$ is required to obtain stable operation.
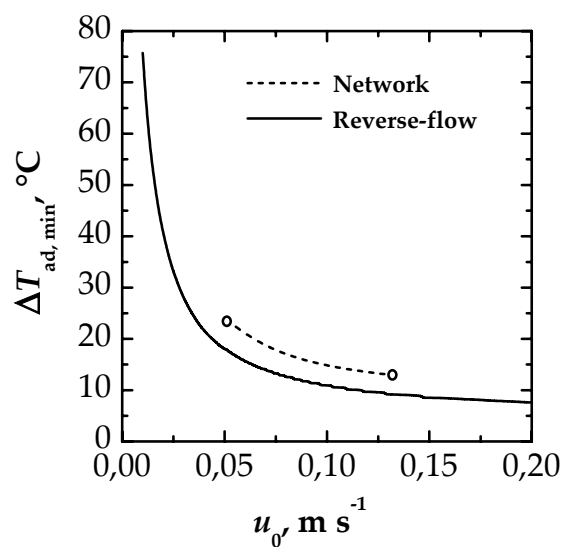

Figure 3.11: Dependence of the stability range on the inlet surface velocity for the reverse-flow reactor and for the three reactors network; adiabatic conditions.

34

From these analysis it follows that the behaviour of the RN is not very different from that of the RFR: the PSS temperature profile is very similar and the influence of the reactor length, the fraction of inert material, the inlet concentration, the flow rate on the profile itself are similar, too, even if the sensitivity toward the different parameters can be different. Nevertheless, there is an important difference concerning the influence of the switching time: the range of values that allows the autothermal operation is very narrow in the RN, and it is reduced if we increase the number of reactors; this optimal range of values changes slightly varying the feeding conditions (inlet concentration and flow rate). The maximum temperature on the solid is slightly influenced by the cycle time, and is increased by a large inert fraction; a similar behaviour can be observed in the RFR, where very high temperatures can be reached when a large fraction of inert and low switching times are used.

Heat losses at the wall reduce only slightly the maximum temperature reached in the reactor, if PSS is obtained: in fact, it is necessary that it is higher than the ignition temperature, as discussed before; but heat losses strongly modify the temperature profile in the reactor, influencing the region of stable operation: in particular, the minimum required adiabatic temperature rise of the mixture increases. Heat conduction in the reactor wall must be also taken into consideration, for small diameter equipment, as it hinders the development of the necessary temperature profile and the regenerative behaviour (Barresi *et al.*, 1997); as a consequence the frequency range for autothermal behaviour is modified. This can be understood considering that a minimum length of the hot zone, that assures complete combustion, is necessary for stable operation; it depends on the reactor length and cycle period. In a non-adiabatic combustor the length of the central hot zone is largely reduced (the system spontaneously evolves toward a situation that reduces thermal output), and in addition becomes weakly affected by the cycle period. As the maximum temperature is also reduced at high frequency, extinction can also occur at low cycle periods (differently from the adiabatic case).

It is interesting to point out that the RFR and the RN behave quite differently as concerns the level of emissions during the cycle. In both cases, at PSS, they have a periodic character, but the reverse flow combustor is affected by wash out: at each inversion of the flow direction, the VOCs not yet burned are emitted. The relevance of this effect depends on the switching

frequency and length of the reactor. Reducing the amount of inert in order to diminish this effect decreases maximum temperature and may impair the desired autothermal operation at constant catalyst mass. At the same time, the cycle time becomes much shorter than in the RN (Cittadini *et al.*, 1999).

The network of combustors does not suffer from the previous problem, and in this respect is superior to the RFR, even if the PSS conversion can be lower, due to a less effective usage of the catalyst. On the other hand the range of frequency for which the RN is stable is very small; as a consequence the network of unsteady burners can be considered very interesting only for processes with steady and controlled feeding conditions.

Another phenomenon that can occur in the RFR when part of the catalyst has been replaced by inert ceramic material, is the entrance of the hot front in the inert section if the cycle period is too long: autothermal behaviour can still be obtained, but high concentrations of unconverted VOC are emitted in the last part of each semi-cycle, with a reduction of the average conversion. This problem can be avoided by a proper choice of the cycle period; if t_c is not properly chosen, large emissions can occur also for small values of the inert fraction, especially if the system is almost adiabatic: in fact, heat losses reduce the length of the hot zone, confining it into a smaller internal zone.

3.3 Catalyst optimisation in reverse-flow combustors

Preliminary results about the RFR have evidenced that the stability of this device depends not only on the kinetic parameters of the reactions that take place, and thus on the catalytic activity, but also on the physical properties of the catalyst or the support. For example, increasing the thermal capacity of the bed, by mixing the catalyst with an inert material having higher thermal capacity, it is possible to reduce significantly the minimum inlet VOC concentration required for autothermal operation, notwithstanding the reduction of catalytic activity per unit volume due to dilution (Cittadini *et al.*, 2000).

The aim of this chapter is a detailed study of the influence of the physical properties of the catalyst (density, specific heat capacity and thermal conductivity) and of the catalytic activity on the stability of a RFR where the combustion of lean methane mixtures is carried out. A simplified pseudo-homogeneous model has been employed for the simulation of the reactor.

The final goal is the optimisation of the catalyst pellets, having as an objective the autothermal behaviour of the reactor (Fissore *et al.*, 2001a; Fissore and Barresi, 2003).

As it has been evidenced that the stability of small-diameter RFR can be strongly influenced also by heat capacity and heat conductivity of the wall, the problems related to the heat conduction and dispersion at the reactor wall, which can significantly alter the results of experiments carried out in bench or small pilot scale apparatus (Cittadini *et al.*, 2000; Hevia *et al.*, 2002, 2003a), masking the influence of the catalyst physical properties, will also be addressed.

3.3.1 *Simplified models*

The evaluation of the transient and PSS behaviour of the RFR, needed for the selection of optimum cycle time, bed size and initial catalyst temperature, is computationally very demanding, even if a simplified mono-dimensional model is adopted. A long simulation time is required, because about one hundred cycles are generally necessary before the PSS is reached; finding the limit conditions which cause extinction, in particular, requires very long simulations and a trial and error approach. As shown in previous works (Cittadini *et al.*, 1999, 2000), the use of a complete model permits to predict the behaviour in the period before the attainment of the PSS, during which large emissions can occur in certain conditions, and to evidence and understand the characteristics of the system, but it is very unpractical for routine design, sizing and optimisation of the bed. For the previous reasons, some authors have developed reduced models for the reverse-flow adiabatic reactors. A simplified high-switching frequency model has been proposed by Boreskov and Matros (1983), Matros *et al.* (1993b), Eigenberger and Nieken (1994), Nieken *et al.* (1994a, 1994b).

Matros and Bunimovich (1995) presented a model for high-frequency flow reversal, in which the system of partial differential equations is reduced to a system of ordinary differential equations, that, through further simplifications, can be solved analytically for the maximum temperature in the bed. Nieken *et al.* (1995) analysed the two limiting cases of very large switching period, for which the temperature profile approaches that of the stationary travelling reaction front, and of very short switching period; in the latter case, the cycle time is small when compared to the heat transfer process

time constant t_p

$$t_p = \frac{\rho_S c_{p,S} L}{u_0 \varepsilon \rho_G c_{p,G}}$$

(3.31)

due to the large thermal capacity of the solid: the solid temperature will not change, while the gas temperature switches between the two profiles below and above the solid temperature on every flow reversal. The behaviour of the reactor is similar to that of a countercurrent reactor, as it has been demonstrated by Haynes *et al.* (1995): instead of sending the mass flow during one period in one direction (Figure 3.12a) and during the next period in the opposite direction (Figure 3.12b), the same net result can be obtained by simultaneously sending half of it in each of the two direction (Figure 3.12c) and assuming that each of the two flows interacts with only one-half of the available catalyst. This means that the reactor and the catalyst are split into two halves with opposite flow directions: a countercurrent fixed-bed reactor arrangement results, with heat exchange over a catalytic wall that is ideally permeable for heat but impermeable for mass. The PSS temperature profile, developed after a large number of cycles, keeps a symmetric shape, with a nearly increase and decrease in the lateral sides and a high constant value in the middle zone. During the cycle period, the profile does not change in shape and values, only moving through the reactor bed. By simplification of the pseudo-homogeneous model it is possible to obtain simple quasi-analytical expressions for the most important parameters of the PSS temperature profile, namely T_{max} and dT/dx.

Haynes *et al.* (1995) demonstrated that the high switching frequency model can be derived from the full dynamic quasi-homogeneous model by expressing the process variables as a Taylor series in time, and compared its performances with those of the complete model. A different approach was proposed by Sun *et al.* (1996), who neglected axial conductivity in the bed, but allowed heat transfer between gas and solid, by considering different gas and solid temperatures. They succeeded in reducing the model to a simple system of ordinary differential equations, but finally a numerical solution is needed; a design procedure for the RFR was also given. Zufle and Turek (1997b) discussed the analogies between the RFR and two other apparatuses: the conventional adiabatic fixed bed reactor with external heat exchangers and the countercurrent reactor; they developed a model different from that of the previous authors, based on the partition of the bed in a cascade of

electrically heated elements and the subsequent discretisation of the variables. The solution is more complex, and an additional system parameter, the centre of gravity of the energy release caused by exothermic chemical reaction, is required; but, through an iterative procedure, it is possible to obtain again the main parameters of the PSS profiles.
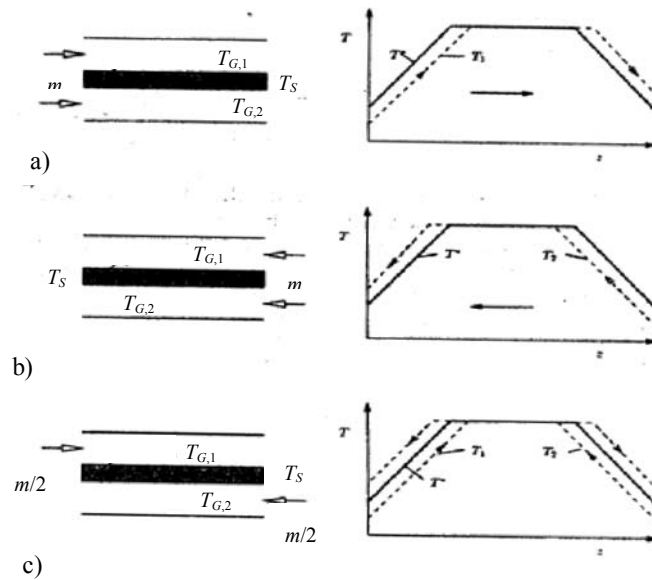

Figure 3.12: Reactor with simplified temperature profiles for rapid flow reversal (a, b) and a countercurrent fixed-bed reactor (c). Temperature in the solid phase (solid line); temperature in the gas phase (dashed line).

Design rules have been proposed in generalised form by Haynes *et al.* (1995): from given values of conversion, the bed length and the gas velocity can be calculated. It is important to note that in all the previous works the cycle period was not taken into consideration, while Thullie and Burghadt (1995) pointed out that the maximum cycle time is the most relevant parameter, because lower frequencies cause extinction of the reactor, and proposed a very simplified procedure to estimate it. Cittadini *et al.* (2001) developed a simple design procedure, pursuing further the approach proposed by Nieken *et al.* (1995); under simplifying assumptions, these results are exploited to predict the limiting operating conditions for autothermal operation: minimum bed length, maximum cycle period, minimum inlet concentration, minimum and maximum flow rate.

The complete model is reduced to only two ordinary differential equations, the energy balances having been lumped into a single quasi-homogeneous balance, in which only the temperature of the solid appears:

$$2\lambda_{eff}\frac{\mathrm{d}T_S}{\mathrm{d}x}-\frac{(-\Delta H)\rho_{G,0}u_0}{M}y_G=0 \tag{3.32}$$

$$\frac{\rho_{G,0}u_0}{M}\frac{\mathrm{d}y_G}{\mathrm{d}x}-\frac{\rho_G}{M}\frac{k_r k_G a_v}{k_G a_v+k_r}y_G=0 \tag{3.33}$$

The presence of a non stationary fluid has to be taken into account in order to evaluate the effective thermal conductivity of the system; the approach proposed by Nieken *et al.* (1995) has been followed:

$$\lambda_{eff}=\lambda_S+\frac{\left(\rho_{G,0}u_0 c_{p,G}\right)^2}{ha_v} \tag{3.34}$$

The expression for $\mathrm{d}T_S/\mathrm{d}y_G$, that can be obtained from eq. (3.32) and (3.33), is then integrated from the inlet to the outlet of the reactor, giving the following implicit expression for the maximum temperature (under the assumption that the reactant is completely consumed):

$$\frac{(-\Delta H)(\rho_{G,0}u_0)^2 y_{G,0}}{2M\lambda_{eff}}=\int_{T_{G,0}+(1/2)\Delta T_{ad}}^{T_{S,max}}\rho_G k_r\frac{k_G a_v}{k_G a_v+k_r}\mathrm{d}T_S \tag{3.35}$$

In order to evaluate the slope of the temperature profile in the zone of pre-heating (*ph*), the simplification $y_G=y_{G,0}$ can be considered, deriving the following analytical expression:

$$\left.\frac{\mathrm{d}T_S}{\mathrm{d}x}\right|_{ph}=\frac{(-\Delta H)\rho_{G,0}u_0}{2M\lambda_{eff}}y_{G,0} \tag{3.36}$$

Figure 3.13 illustrates that the temperature profile in the actual RFR can be approximated very well by a piecewise linear function, in terms of the simplified model parameters: in the first region of the reactor, the temperature is constant and equal to the inlet value; then, it increases with the slope $\mathrm{d}T_S/\mathrm{d}x$ given by Equation (3.36) till to the value of T_{max} predicted by Equation (3.35); then, it remains constant at this value along a portion of the reactor and finally drops to the inlet value with slope $\mathrm{d}T_S/\mathrm{d}x$. In addition, numerical simulations have shown that T_{max} and $\mathrm{d}T_S/\mathrm{d}x$ are almost independent from the cycle period, in agreement with the experimental results of Nieken *et al.* (1995) and van de Beld and Westerterp (1997). As a

consequence, through the following expression for the hot-front propagation velocity:

$$\omega = \frac{c_{p,G}\rho_{G,0}u_0}{c_{p,S}\rho_S(1-\varepsilon)}\left(1 - \frac{\Delta T_{ad}}{T_{S,max} - T_{G,0}}\right) \tag{3.37}$$

that was deduced by Wicke and Vortmayer (1959), a good approximation of the half-cycle temperature profile can be obtained for any cycle period. The construction of this profile is presented in Figure 3.14.
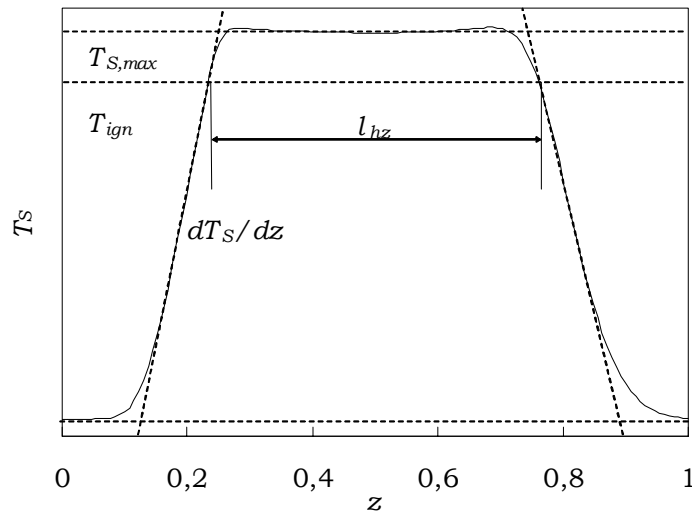

Figure 3.13: Comparison between the half semi-cycle temperature profile inside the RFR and the approximation by means of a piecewise linear function.

At the beginning of the cycle, the inlet of the reactor is supposed to be in a region of constant slope and the temperature is assumed to be $(T_{ign}-T_{G,0})/4$. Numerical simulations performed on the complete dynamic model have shown that such a value is actually a good approximation of the real figure, when the operation is close to extinction, which is the situation that has to be investigated in order to find the stability limits. Thus, the length of the first cold part of the reactor at half semi-cycle is given by the distance travelled by the hot front during the half cycle $(\omega t_c/2)$ minus $((T_{ign}-T_{G,0})/(4dT_S/dx))$. The transition from the heating part to the reactive part of the profile occurs when the gas temperature overcomes the ignition temperature. This construction leads to the following expression:

$$\frac{1}{2}L = \omega\frac{t_{csp}}{2} - \frac{T_{ign} - T_0}{4\,dT/dx|_{ph}} + \frac{T_{ign} - T_0}{dT/dx|_{ph}} + \frac{1}{2}l_{hz} \tag{3.38}$$

41

where l_{hz} is the length of the hot zone.

At this point, the aim of the work is to distinguish between the profiles that are possible in autothermal operation and the profiles that are not possible as the reaction extinguish before the PSS conditions are reached. The numerical simulations, as well as the works by Nieken *et al.* (1995) and by Zufle and Turek (1997b), have shown that PSS conversion is either higher than about 95% (ignited condition) or equal to 0% (extinguished condition).

This behaviour can be explained by considering that high inlet concentrations lead to high temperatures in the reactor, allowing total conversion of the pollutant, while, when the inlet concentration is only slightly larger than the minimum required for autothermal operation, conversion must be almost total, in order to get a sufficient thermal supply (otherwise the reaction extinguishes). The conversion can be very high only if the reactive hot part of the reactor is long enough.

The minimum length depends on the temperature of the hot zone and is given by the integration of eq. (3.33), where, in order to obtain a simple solution, the kinetics are computed at an average temperature:

$$T_a = \frac{T_{S,max} + T_{ign}}{2} \tag{3.39}$$

The final expression for the minimum length of the hot zone is:

$$l_{hz,min} = \frac{\rho_{G,0} u_0 (k_G a_v + k_r)}{\rho_G k_G a_v k_r} \ln\left(\frac{y_{G,0}}{y_{G,out}}\right) \tag{3.40}$$
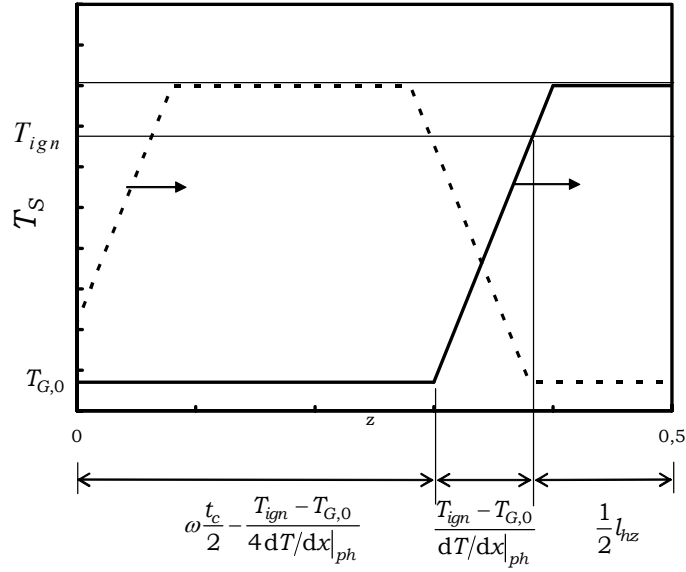
Figure 3.14: Construction of the simplified temperature profile at the half of a semi-period (solid line) and at the beginning of the cycle (dashed line).

Numerical simulations carried out with the full dynamic model indicate that the conversion that allows autothermal operation is about 0.93 for methane, corresponding to a ratio (y_0/y_{out}) of 15. The value of the maximum cycle period, over which the length of the hot zone is reduced below $l_{hz,min}$ and thus autothermal operation is not possible, is calculated by substituting l_{hz} in eq. (3.38) with the estimated value of $l_{hz,min}$, and obtaining:

$$t_{c,max} = \frac{1}{\omega}\left(L - \frac{3}{2}\frac{T_{ign} - T_{G0}}{dT_S/dx|_{ph}} - l_{hz,min} \right) \tag{3.41}$$

To evaluate the maximum cycle period it is necessary to know both $T_{S,max}$ and T_{ign}: the first one can be calculated from Eq. (3.35), as shown before; the ignition temperature depends on the catalyst and the components, but can be calculated if the kinetics is known or can be evaluated experimentally. The procedure suggested by van de Beld and Westerterp (1997) can be used:

$$T_{ign} = \frac{E_a}{R}\frac{1}{\ln\left(0.217 k'_\infty R T_{G,0} \frac{L}{u_0} \right)} \tag{3.42}$$

In order to find the $\Delta T_{ad\ min}$ that allows autothermal combustion in the reverse-flow reactor a trial-and-error procedure has been implemented: for a given value of inlet concentration the maximum temperature of the solid is evaluated and then the minimum length of the hot zone, according to the

43

procedure detailed above. The procedure is then repeated with different values of the inlet concentration until the minimum length of the hot zone equals the actual value.

Figure 3.15 shows the minimum inlet concentration (that can be measured by the adiabatic temperature rise of the mixture, ΔT_{ad}) required for stable autothermal behaviour as a function of the switching time. Different wall thickness are considered, showing that, even if the reactor is well insulated, the higher the thickness of the reactor wall, the higher the inlet concentration that allows stable operation, as a consequence of the heat conduction at the wall. The results of the simulations obtained by means of the complete and of the simplified model are compared in Figure 3.15, showing that when wall effects are negligible (i.e. the wall thickness is little in comparison to the reactor diameter, as it usually happens in an adiabatic large-size reactor) the complete and the simplified models give very close predictions if the switching time is significantly smaller than the thermal process time.
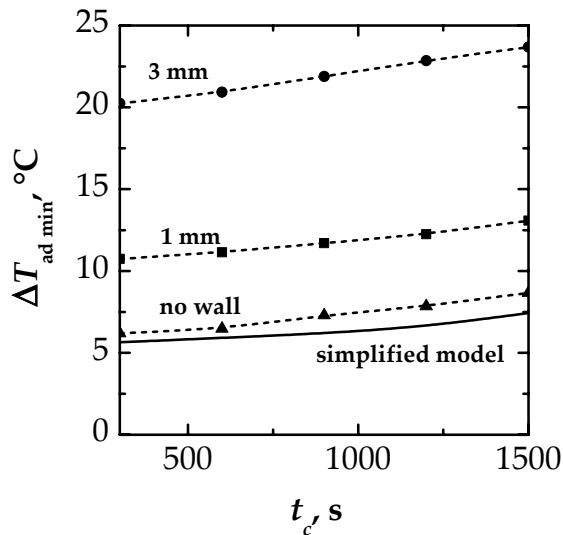

Figure 3.15: Comparison of $\Delta T_{ad\ min}$ required for autothermal operation predicted by the simplified model (solid line) and by the complete model with different wall thickness (dotted lines). ρ_S = 1500 kg m^{-3}, $c_{p,S}$ = 1200 J kg^{-1}K^{-1}, λ_S = 0.18 W m^{-1}K^{-1}, E_a = 90.16 kJ mol^{-1}, k_{∞}' = 9.86 mol s^{-1}kg^{-1}Pa^{-1}, quartz wall.

Obviously, not only the thickness but also the material of the reactor wall can strongly influence the stability of the RFR, even if adiabatic conditions are considered, because of axial conduction (Cittadini *et al.*, 1999). Hevia et al. (2002) showed for example that if stainless steel is used the stability of the device is strongly reduced in comparison with a quartz wall with the same

thickness, as a consequence of the higher thermal conductivity of the steel, and the maximum temperature of the catalyst can be reduced even of 50°C. Due to radial heat transfer also radial profiles are modified: initially the temperature increases toward the reactor wall and then decreases; however, wall conductivity and capacity smooth out the axial profiles near the wall. As a consequence the radial profiles on the ascending part of the temperature peak can show a minimum which affects local concentration of some extent, as it has been evidenced by Barresi *et al*. (1997); however these effects should not seriously affect the overall performance of the reactor.

3.3.2 *Influence of the catalyst physical properties on the stability of the RF*

A wide range of catalyst properties (apparent density, thermal capacity and conductivity) has been investigated. It is known that the switching frequency has a week effect on reactor conversion in the range in which stable operation can be obtained (Barresi and Vanni, 2002; Fissore and Barresi, 2002). Figure 3.16 shows how the range of allowable switching times changes as a function of the thermal properties of the catalyst (specific heat capacity on the left, thermal conductivity on the right). As it has been highlighted in the previous section, when the steady state is reached the conversion is either higher than about 95% or equal to 0%. Transition between the ignited and the extinguished condition occurs in a narrow range of t_c; as a consequence, in the followings, the influence of catalyst thermal properties and kinetics will be investigated at a fixed value of switching period (t_c=900 s).

The simplified model, less time consuming, will be employed as the aim of our work is the optimisation of the catalyst for industrial large-scale apparatus, where the assumptions of the simplified model are generally reasonable. Further simulations showed that the conclusions obtained for t_c = 900 s are still valid for higher and lower switching periods, as it can be seen in Figure 3.16 that the countercurrent model gives predictions similar to those of the detailed model up to more than 1200 s.
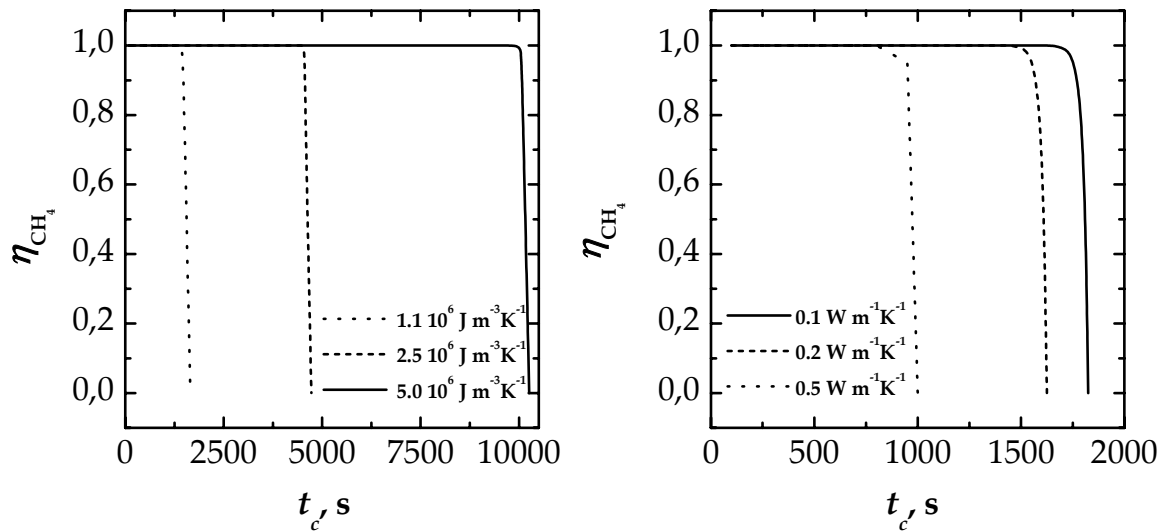
Figure 3.16: Methane conversion as a function of the switching time t_c for different heat capacity (on the left, $\lambda_s = 0.18$ W m^{-1}K^{-1}) and thermal conductivity (on the right, $\rho_s c_{p,s} = 1.1 \cdot 10^6$ J m^{-3}K^{-1}) of the catalyst. $k'_\infty = 9.86$ mol s^{-1}kg^{-1}Pa^{-1}, $E_a = 90.16$ kJ mol^{-1}, $y_{G,0} = 1000$ ppmV.

The influence of heat capacity and thermal conductivity of the catalyst has been investigated separately, varying only one parameter at a time. Figure 3.17 (on the left) shows the dependence on the heat capacity; the value of the term $\rho_s c_{p,s}$ has been varied in the model equation, but keeping ε_c and thus λ_s, constant. An increase of the frequency factor can lead to a reduction of the $\Delta T_{ad\ min}$ as a consequence of the higher reaction rate and subsequent higher heat generation; if the catalyst heat capacity is increased, lower values of inlet VOC concentration are required to sustain the combustion and the influence of the frequency factor (and so of the catalytic activity) is weaker.

The influence of the thermal conductivity is pointed out in Figure 3.17 (on the right), where we can see that the minimum inlet VOC concentration should be largely increased if we increase the thermal conductivity of the bed because of the higher heat dispersions. The influence of the activation energy is also shown: if E_a increases, higher values of $\Delta T_{ad\ min}$ are required because of the lower reaction rate.
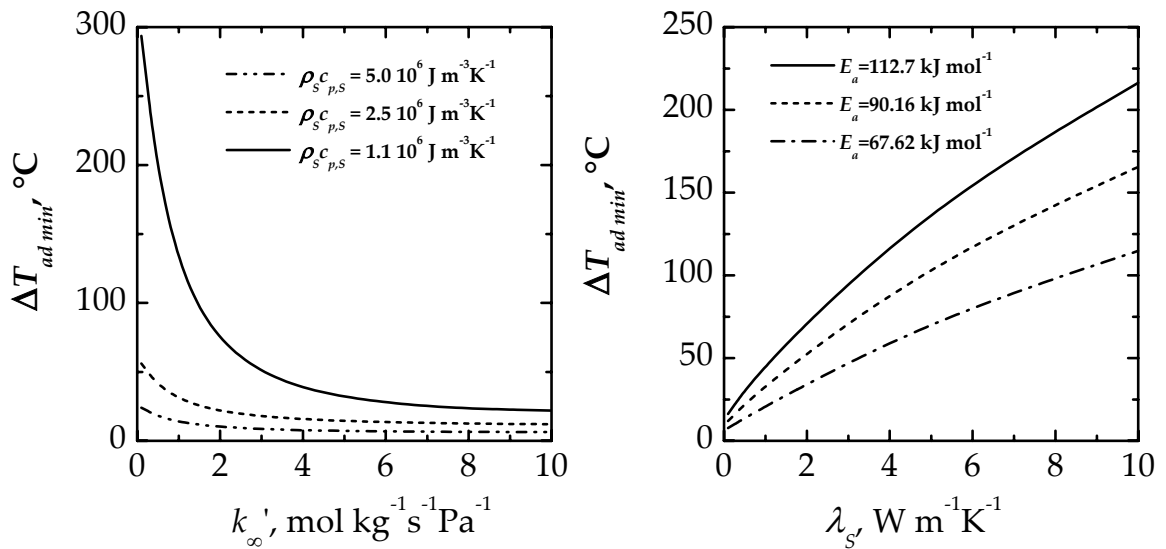
Figure 3.17: $\Delta T_{ad\,min}$ required for autothermal operation as a function of the frequency factor for different specific thermal capacities, E_a = 90.16 kJ mol⁻¹, λ_S = 0.18 W m⁻¹K⁻¹ (on the left). $\Delta T_{ad\,min}$ required for autothermal operation as a function of catalyst thermal conductivity for different activation energies. k'_∞ = 9.86 mol s⁻¹kg⁻¹Pa⁻¹, $\rho_S c_{p,S}$ = 1.1·10⁶ J m⁻³K⁻¹ (on the right).

Figure 3.18 (on the left) shows the simultaneous effect of thermal conductivity and heat capacity on the required $\Delta T_{ad\,min}$ (for a fixed value of the kinetic parameters). It is evident that when we use a catalyst with high thermal conductivity we have to feed a mixture with a higher value of $\Delta T_{ad\,min}$ to allow for autothermal behaviour, but the maximum temperature of the solid is reduced because of the higher heat dispersions as it is shown in Figure 3.18 (on the right) for a fixed value of inlet concentration; the maximum temperature of the solid decreases also when we increase the solid heat capacity.
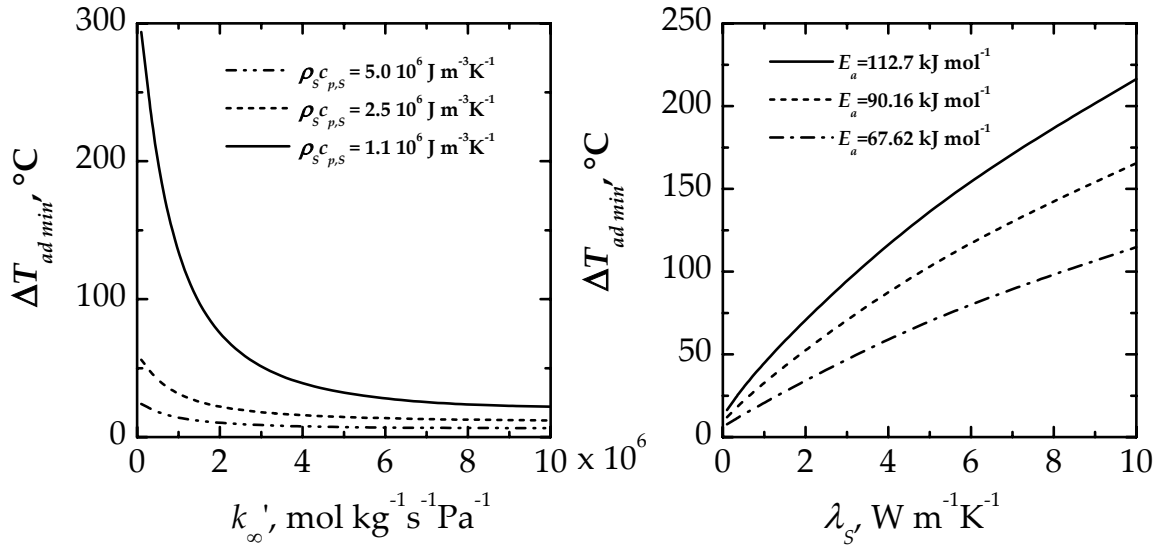
Figure 3.18: $\Delta T_{ad\ min}$ (on the left) and $T_{S,max}$ (on the right) for different thermal conductivities and thermal capacities of the catalyst support. E_a = 90.16 kJ mol^{-1}, k'_∞ = 9.28 mol kg^{-1}s^{-1}Pa^{-1}.

The performance of some of the most common catalyst supports has also been investigated as an example.

Table 3.3: Main physical properties of the catalysts considered in the simulations.

	Al_2O_3	SiO_2	ZrO_2/Y_2O_3	$La_{0.93}MnO_3$
ρ_{mtx} , kg m^{-3}	3900	2180	5900	6500
$c_{p,mtx}$, J K^{-1} kg^{-1}	850	750	450	1200
λ_{mtx} , W m^{-1} K^{-1}	25	1.3	2.5	0.33

Figure 3.19 shows that for all the catalysts considered an increase of the catalytic activity can lead to a reduction of the $\Delta T_{ad\ min}$, even if much more relevant can be the effect of the thermal conductivity and heat capacity. The results suggest that the influence of the thermal conductivity can be even more relevant than that of the thermal capacity: Al_2O_3, for example, has an higher heat capacity than ZrO_2/Y_2O_3, but the higher value of thermal conductivity requires higher $\Delta T_{ad\ min}$. The best results are obtained with the perovskites, which allow autothermal operation even feeding extremely lean mixtures to the reactor because of their high heat capacity and low thermal conductivity.

If the properties of the catalyst cannot be changed, the only way to increase the thermal capacity of the bed is to mix the catalyst with an inert

material having a higher thermal capacity. Cittadini *et al.* (2000) considered a mix of pellets made by catalyst and pellets made by inert material and showed that the replacement of part of the catalyst by inert material, with the same thermal capacity, causes a worsening of the performance of the reactor, for the reduction of activity, but if the thermal capacity of the inert material is high enough, the fall of activity can be compensated. The situation can be different if we consider the pellets made by an inert support coated by the catalyst because of the influence of the effectiveness factor (degree of exploitation of the catalyst): of course, the lower is the effectiveness, the higher is the improvement that can be obtained. Figure 3.20 shows the $\Delta T_{ad\,min}$ as a function of the ratio between the thermal capacity of inert material and that of the catalytic material, *r*, for a certain value of the catalyst mass fraction in the bed.
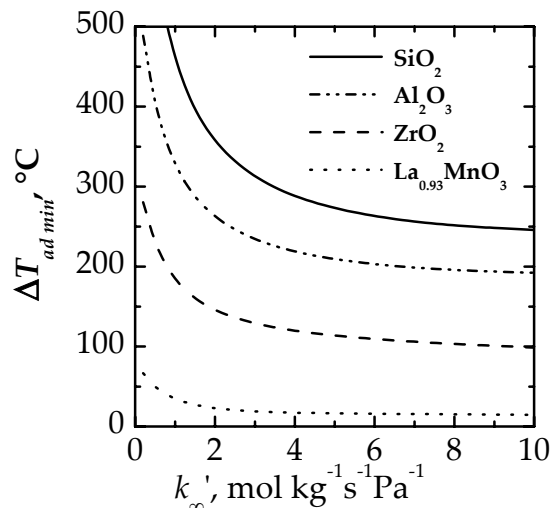

Figure 3.19: $\Delta T_{ad\,min}$ required for autothermal operation for different pre-exponential factors and catalyst supports. $E_a = 90.16$ kJ mol^{-1}.

In order to take into account wall effects which can significantly alter results obtained in bench-scale reactor the detailed model has to be solved, thus the investigation of the minimum adiabatic temperature rise that allows for autothermal combustion becomes more time consuming. Wall effects significantly increase inlet methane concentration needed to obtain autothermal behaviour, as it is shown in Figure 3.20 (on the right), as a consequence of the axial heat conduction that reduces the thermal efficiency of the reactor.
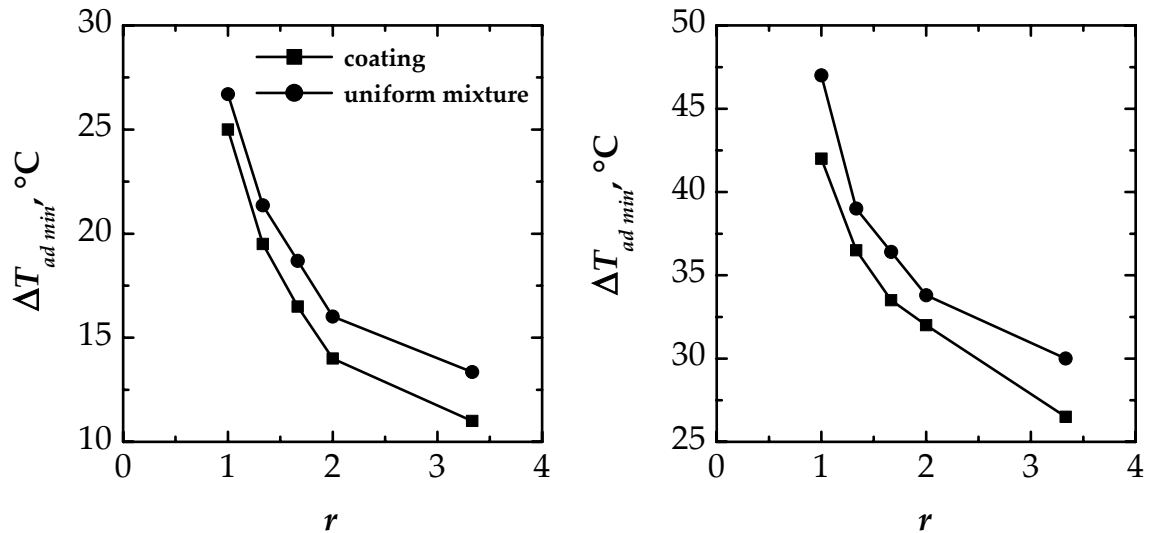
Figure 3.20: $\Delta T_{ad\,min}$ required for autothermal operation as a function of the ratio between the thermal capacity of inert material and that of the catalytic material without wall effects (on the left, simplified model) and with wall effects (on the right, quartz wall, detailed model). $\rho_s c_{p,s} = 1.5 \cdot 10^6$ J m^{-3}K^{-1}, $\lambda_s = 0.18$ W m^{-1}K^{-1}, $E_a = 90.16$ kJ mol^{-1}, $k'_\infty = 9.28$ mol kg^{-1}s^{-1}Pa^{-1}, catalyst mass fraction = 0.1, $t_c = 1800$ s.

3.4 Model validation

Modelling results concerning the RFR have been validated in a bench-scale reactor in the Universidad de Oviedo, Departamento de Ingeniería Química y Tecnología del Medio Ambiente. This device was designed by the Politecnico di Torino and built by the Universidad de Oviedo in the framework of a European Project (ENV4-CT97-0599). The main innovation in the design of this reactor is related to the way in which the adiabatic behaviour is reached: by means of a special temperature control system based on a dynamic compensation of the thermal losses. This system has been calibrated and experimental results have been compared to simulation, both in the transient and when the PSS is reached.

3.4.1 *The bench-scale reactor*

In §3.3 it has been pointed out that the regenerative performance of a RFR strongly depends on the physical properties of the packing (catalyst and

inert), namely density, specific heat and thermal conductivity, however, less attention has been paid to the influence of the reactor wall in the performance of the system (Van de Beld and Westerterp, 1996). The thermal efficiency of the RFR is strictly related to the capability to keep the heat of reaction in the central part of the bed, while the sides work as heat exchangers; as a consequence, the lower are axial heat dispersion (in the gas phase) and axial heat conduction (in the solid phase and in the wall), the higher is the thermal efficiency in the reactor. Reactor walls are usually made by metals (high thermal conductivity) and thus the contribution of the wall effect is very important if the reactor size is small. The values of the two ratios (external surface area/flow rate) and (wall section/flow rate) are proportional to ($1/D_R$); thus, if the reactor diameter is small (as in bench-scale reactors), radial heat losses and axial heat conduction at the wall affect more strongly the thermal balance of the plant than in the case of a large-scale industrial reactor. As a consequence, VOC concentration needed for autothermal operation is much higher and the results obtained by an experimental investigation can be different from the prediction of the performances of an industrial reactor. That is why wall effects must be evaluated, both in the design and in the evaluation of results obtained with lab or bench-scale reactors (Hevia *et al.*, 2002). From the modelling point of view it is sufficient to add the thermal balance at the reactor wall to the partial differential system that describes the dynamic evolution of the system.

The importance of the wall influence, depending of its physical properties, has been analysed, showing that wall effects increase when density, heat capacity and thermal conductivity of the reactor wall increase; as expected, wall effects increase also with wall thickness. Three different material have been considered, namely quartz, Inconel and stainless steel; Table 3.4 shows the values of the physical properties used in the simulations:

Table 3.4: *Values of the physical properties of the wall reactor materials*

	quartz	*Inconel*	*stainless steel*
ρ_w, kg m^{-3}	2200	8510	7800
$c_{p,\,w}$, J kg^{-1} K^{-1}	1037	450	510
λ_w, W m^{-1} K^{-1}	1.46	15.1	58

Figure 3.21 compares the solid PSS temperature profiles obtained in the same reactor, but with different wall materials; the physical properties of the wall strongly influence the temperature profile that is reached: when a stainless steel is used, for example, the high thermal conductivity, and subsequent heat dispersion, is responsible for lower maximum temperatures and for a reduction of the length of the hot zone.
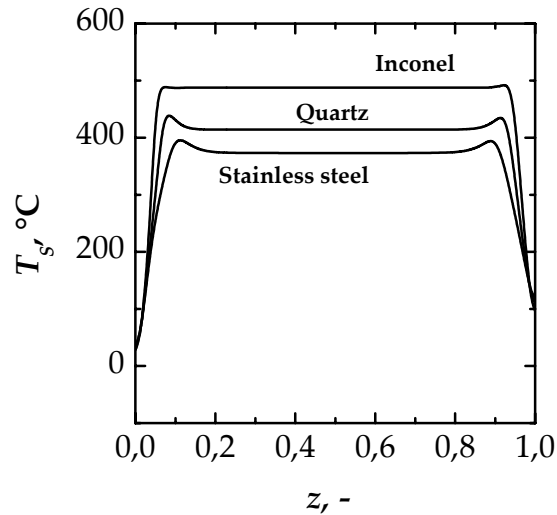

Figure 3.21: PSS solid temperature profiles (at the end of a semi-cycle) in the case of Inconel wall (left graph) and quartz wall (right graph). t_c = 1800 s, $D_{R,i}$ = 3 in, wall thickness = 3 mm, L = 0.5 m, $y_{CH4,0}$ = 3600 ppmV, u_0 = 0.1 m s^{-1}.

Also wall thickness may affect the temperature profiles, and thus reactor stability, as it is shown in Figure 3.22 for the Inconel wall (on the left) and for the quartz wall (on the right). As a consequence of the influence of wall on the thermal balance of the reactor, also the range of switching times which allows for autothermal operation is affected by wall material and thickness, as it is shown in Figure 3.23.
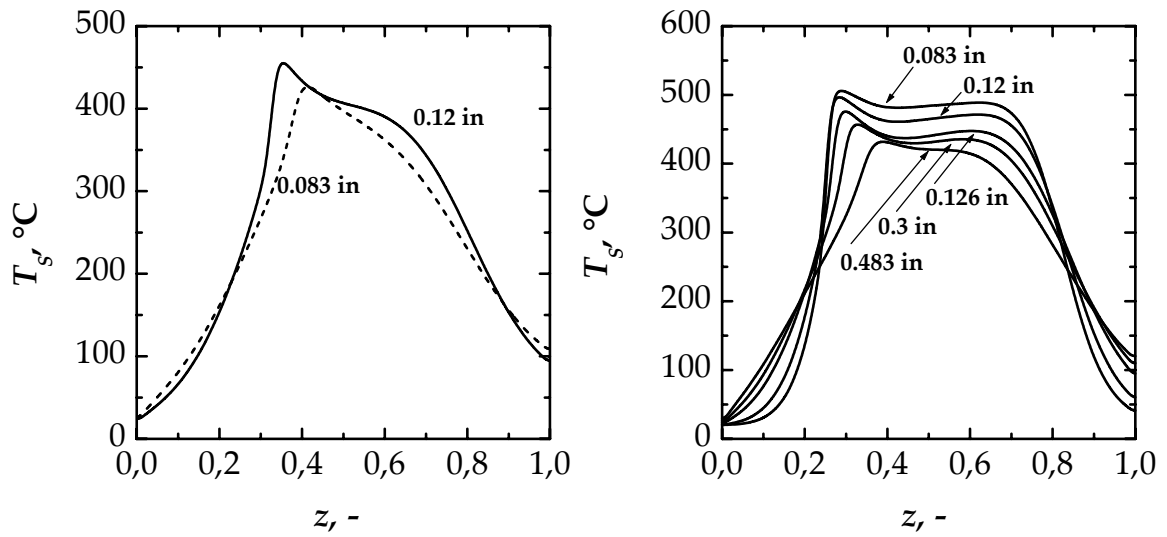
Figure 3.22: PSS solid temperature profiles (at the end of a semi-cycle) as a function of wall material. t_c = 200 s, $D_{R,i}$ = 6 in, L = 0.6 m, $y_{CH4,0}$ = 3600 ppmV, u_0 = 0.1 m s^{-1}.
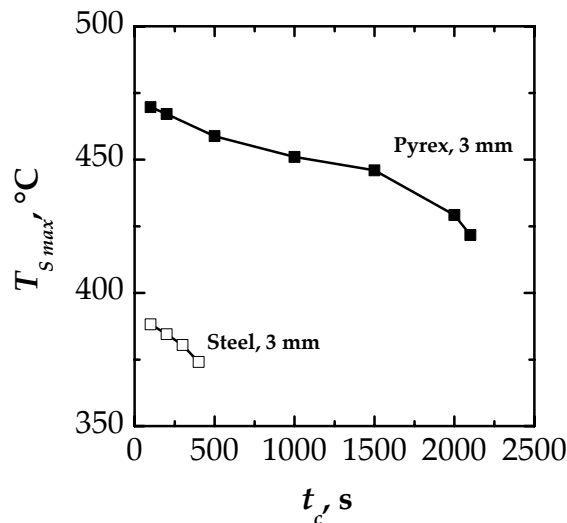

Figure 3.23: Influence of the switching time on the maximum solid temperature in the case of Pyrex and steel wall.

Thus, it can be concluded that the best materials to construct a bench-scale reactor in order to decrease the wall effect and to approximate the adiabatic behaviour are those with low thickness, density, heat capacity and thermal conductivity. Unfortunately, the materials which fit better with these requirements (Pyrex, quartz, ceramic materials) present low mechanical strength, and are prone to breaking. As a consequence a stainless steel tube has been considered with a system devoted to compensate the heat losses.

Different technical solution have been proposed in the past to face with this problem, namely standard insulation (Purwono *et al.*, 1994), evacuated jacket (Cunill *et al.*, 1997) or steady electrical thermal compensation. Nieken *et al.* (1994a) and Eigenberger and Nieken (1988) used a reactor insulated first with a layer of mineral fiber on which an electrical compensation heater was positioned along the central part. In order to prevent overcompensation, the temperature of the compensation heater was measured in the middle of the reactor and controlled to a value about 20 K below the value measured at the same axial position in the monolith. A reasonable but not perfect compensation of heat losses was achieved: a shallow dent in the middle of the temperature profile was not avoided. Zufle and Turek (1997a), in order to maintain adiabatic operation, provided the reactor with a homogeneous electrical heating on the wall; the total power (*P*) to be supplied was computed through a thermal balance of the bed (*P* = heat generation - outlet flow sensible heat). Nevertheless, this method does not allow to get a real adiabatic configuration: into the bed, the temperature changes quickly in time and space from 20°C to 500-600°C, so that a homogeneous steady heating does not stop completely the cooling of the hot zones and, at the same time, it heats actively the cold zones. Even if the two heat flows compensate each-other and the reactor is virtually adiabatic, the global effect is a by-pass of heat from the hot central part of the reactor to the cold ends, with the fall in the thermal efficiency that has been justified previously. About the problem of axial heat conduction at the wall, the only way proposed to reduce this effect is to adopt a thin wall (only 1.6 mm for the 14"-diameter van de Beld *et al.*'s reactor).

In order to avoid these problems a different approach has been used: the adiabatic behaviour is reached by means of a special temperature control system based on a dynamic compensation of the thermal losses. The reactor wall is surrounded by seven independent band heaters, whose temperatures are controlled by independent relays, so that everyone keeps constantly the same temperature of the part of the reactor that faces directly that heater (Figure 3.24).
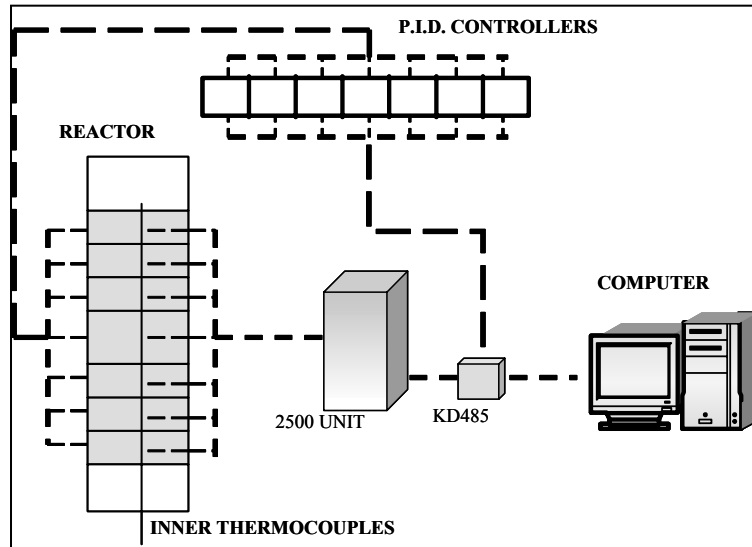
Figure 3.24: General scheme of the experimental apparatus.

Two thermocouples, one inside the heaters and one on the axis of the tube, positioned in correspondence of the heater, control the relays. The heater cooling is assured by an air flow on the outer surface that removes the heat in the band when the reactor is cooling.
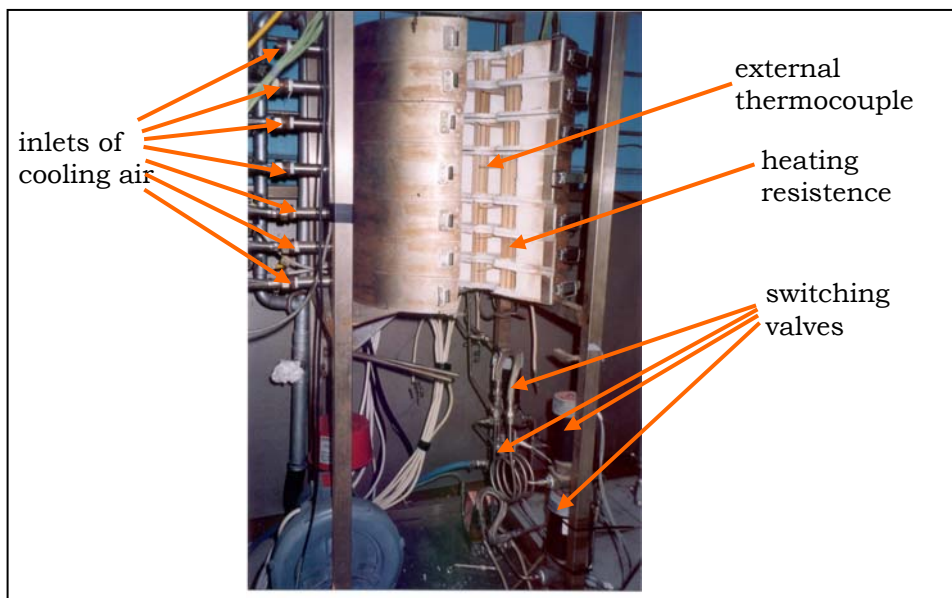

Figure 3.25: The bench-scale reactor.

The behaviour of the non-adiabatic reactor with the heat compensation system described above has been compared to a truly adiabatic reactor by means of simulation, showing that adiabatic conditions may be obtained (Figure 3.26).
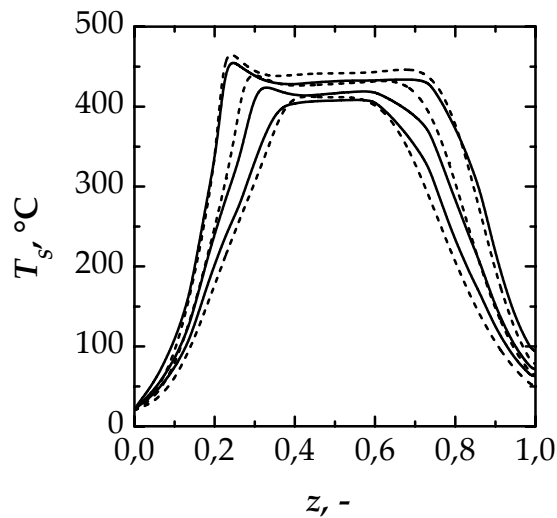
55

Figure 3.26: Temperature profiles for the adiabatic configuration and the band-heater configuration. ΔT_{ad}= 40°C, 60°C, 80°C

Such a result can not be obtained by a very thick standard insulation, or by an evacuated jacket, or by a steady electrical thermal compensation.

The flow of air and CH_4 pass through a pressure reducer and a flow meter and controller. Four solenoid valves, driven by the central computer, control the flow reversal. The power to be supplied to every heater is controlled by the central computer through a relay: when the difference between the inner temperature and the outer temperature exceeds a scheduled value, the relay is closed, while, when the outer temperature exceeds the inner one, the relay is opened. As the band heaters are surrounded by an insulating layer, a cooling air flow must be supplied on the outer surface, in order to let the elements to cool down with enough speed when the corresponding part of the bed is quickly cooling down. The cooling system is composed by a blower and two air distributors, that carry the air into the separated spaces between the band heaters and the outer insulation. An electric pre-heating device is placed in the upper part of the reactor: its function is to heat up the catalytic bed before running the reverse-flow process.

3.4.2 *Results*

In order to test the effectiveness of the temperature control system, preliminary runs without chemical reaction have been performed; Table 3.5

56

summarised the main characteristics of the reactor and of the catalyst. A Pd-based catalyst has been used in these runs; a first order kinetic is assumed for the methane combustion reaction. 25% of inert material (glass spheres having the same diameter of the catalyst pellets) are present at each ending section.

Table 3.5: Main catalyst and reactor parameters when a Pd-based catalyst is used.

Pre-heating temperature	670 K
Pellet diameter	2-4 mm
Catalyst density, ρ_s	2170 kg m^{-3}
Catalyst specific heat, $c_{p,s}$	848.1 J kg^{-1} K^{-1}
Catalyst porosity, ε_c	0.519
Catalyst tortuosity, τ	2
Catalyst thermal conductivity, λ_{eff}	0.472 W m^{-1} K^{-1}
Bed void fraction, ε	0.36
Frequency factor, k'_∞	1.0886$\cdot$10^5 mol kg^{-1} s^{-1} Pa^{-1}
Activation energy, E_{att}	1.12504$\cdot$10^5 J mol^{-1}
Inlet gas temperature	300 K
Gas velocity	0.115 m s^{-1}

A first series of experiments have been carried out to evaluate the adequateness of the temperature control system: the fixed bed is at ambient temperature and is fed with air; no methane is introduced into the system. The air is pre-heated by means of an electrical device positioned at the entrance of the reactor. Figure 3.27 shows a comparison between the prediction of the model (taking into account the presence of the wall and assuming adiabatic operation) and the experimental results obtained in non-adiabatic conditions but in presence of the temperature control system described above; the model prediction and measured values of the temperature in the middle of the seven sections in which the reactor has been considered to be divided are shown, demonstrating both the adequacy of the model to describe the dynamic of the system and the adequacy of the temperature control system to maintain adiabatic conditions.
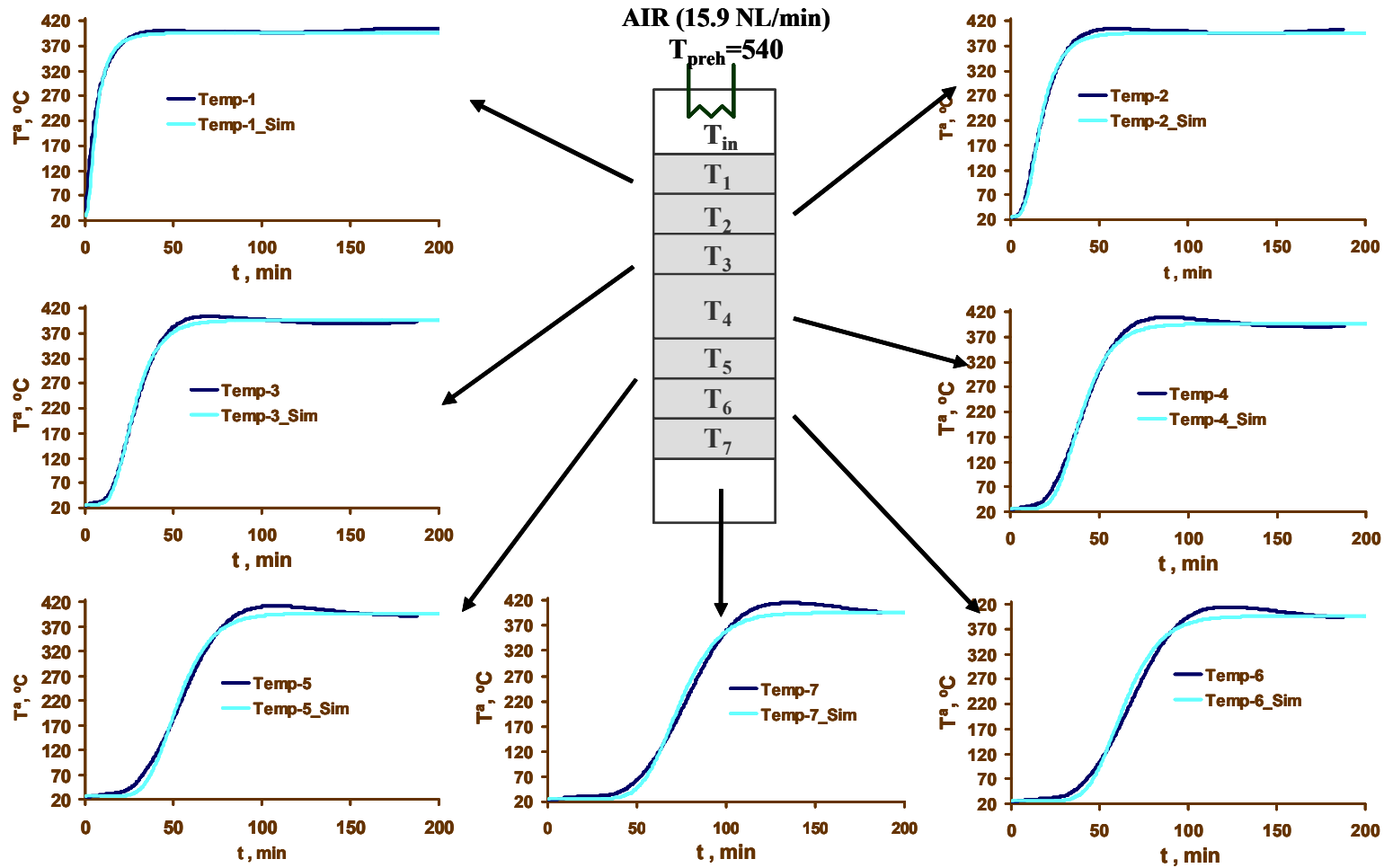
Figure 3.27: Comparison between the simulated and the experimental values of the solid temperature during the pre-heating phase. The values of the seven temperatures that are used by the heat compensation system are shown.
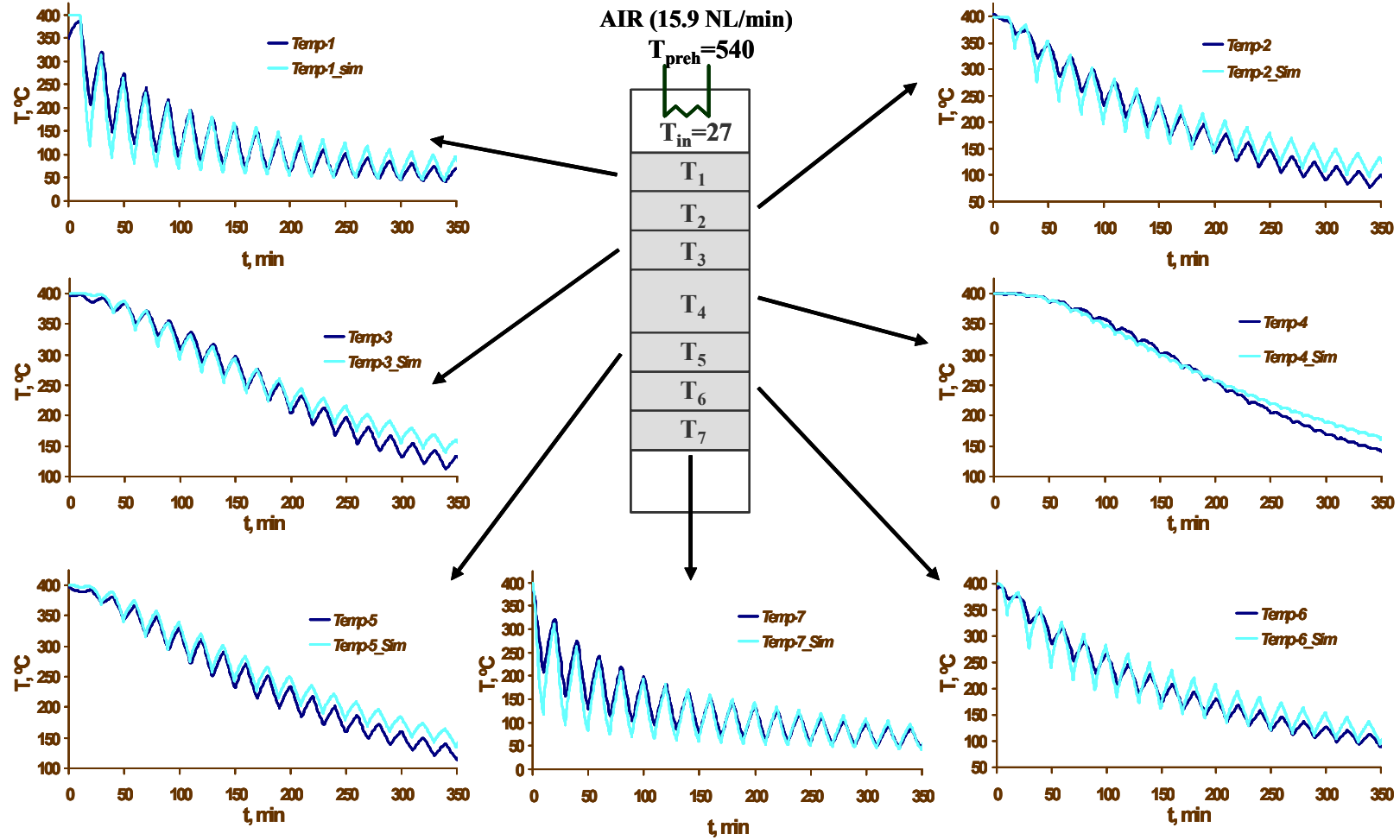
Figure 3.28: Comparison between the simulated and the experimental values of the solid temperature during the cooling down phase (t_c = 600 s). The values of the seven temperatures that are used by the heat compensation system are shown.

Modelling results are in good agreement with the experimental runs also during the cooling down of the system (Figure 3.28).
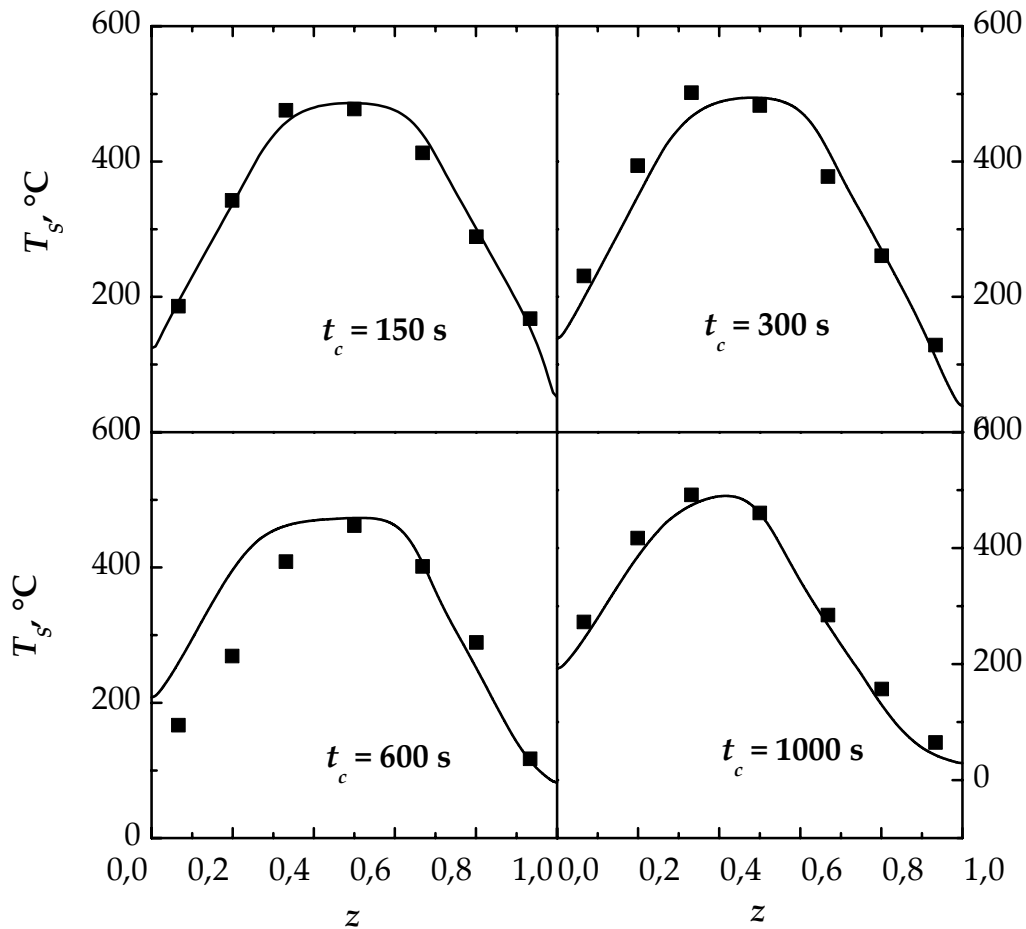
Figure 3.29: Comparison between the simulated (line) and the experimental (symbol) values of solid temperature; the profiles are taken at the end of the indicated semi-cycle, when the PSS has been reached. $y_{G,0} = 2500$ ppmV.

The results obtained when methane is fed to the reactor are in good agreement with the simulation of the adiabatic reactor both in the transient (Figure 3.29) and when the PSS has been reached (Figure 3.30), thus demonstrating that the heat supply system is effective in reaching adiabatic conditions. The catalytic activity of the Pd-based catalyst is particularly high (no methane concentration is detected in the outlet, even during the transient), but after few hours the catalytic activity decreased because of deactivation.
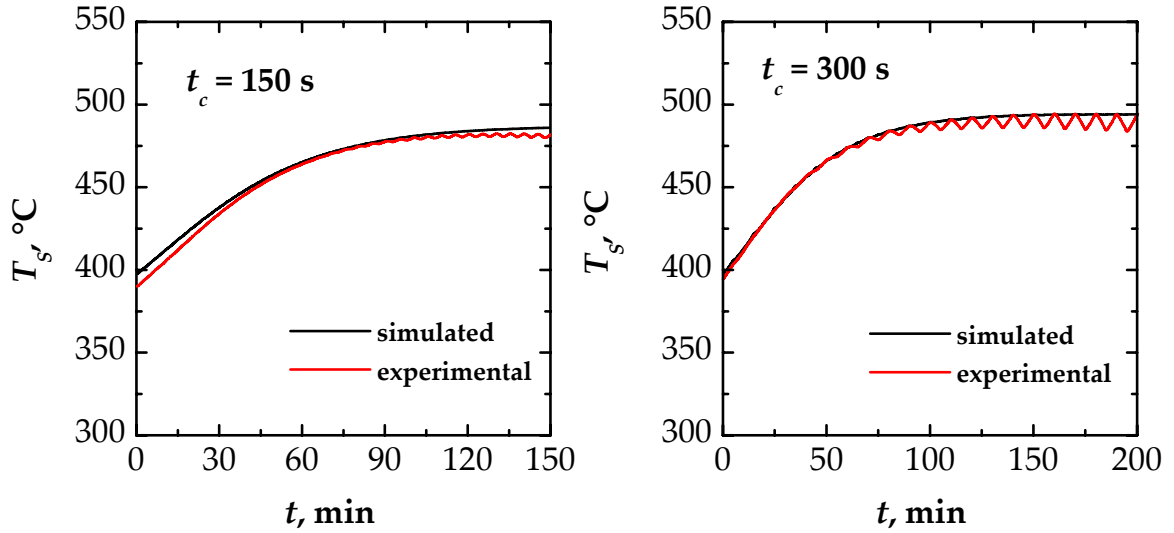
Figure 3.30: Comparison between the experimental and the simulated evolution of the solid temperature profiles in the middle of the RFR; t_c = 150 s (on the left), t_c = 300 s (on the right). $y_{G,0}$ = 3500 ppmV, Pd-based catalyst.

A second catalyst, based on metal oxide, has been tested in the bench-scale reactor; Table 3.6 shows the main parameters used for the simulations. Also in this case a good agreement between experiments and simulation has been obtained, both in the transient and when the PSS has been reached (Figure 3.31, on the left).

Table 3.6: Main catalyst and reactor parameters when a metal-oxide based catalyst is used.

|	
Pre-heating temperature	685 K
Pellet diameter	4 mm
Catalyst density, ρ_s	1541 kg m^{-3}
Catalyst specific heat, $c_{p,s}$	952.1 J kg^{-1} K^{-1}
Catalyst porosity, ε_c	0.45
Catalyst tortuosity, τ	2
Catalyst thermal conductivity, λ_{eff}	0.15 W m^{-1} K^{-1}
Bed void fraction, ε	0.36
Frequency factor, k_{∞}	1.084·10^3 mol kg^{-1} s^{-1} Pa^{-1}
Activation energy, E_{att}	1.223·10^5 J mol^{-1}
Gas velocity	0.1434 m s^{-1}
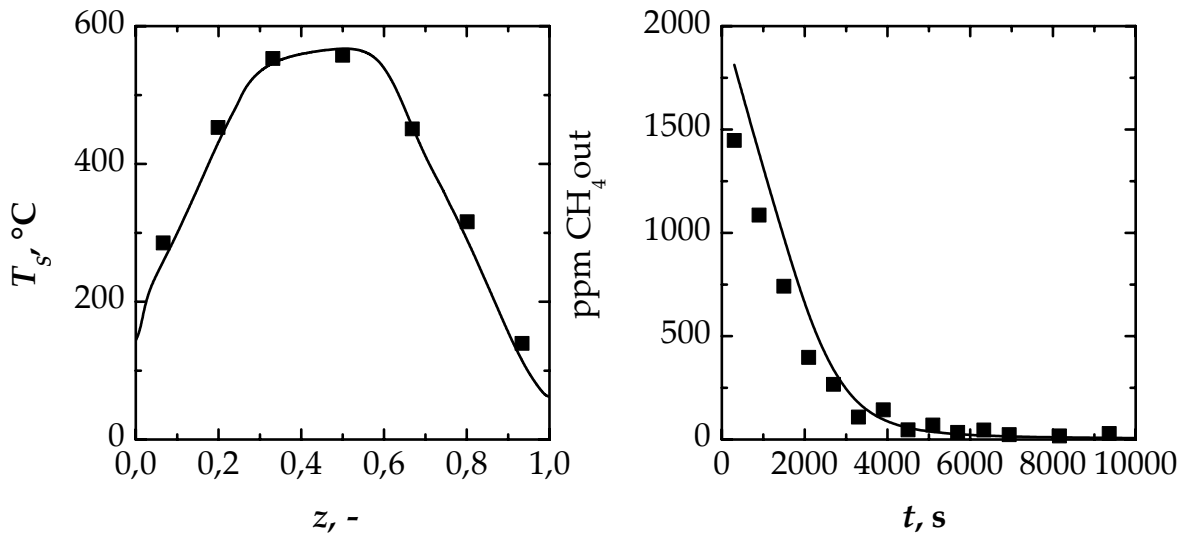
Figure 3.31: Comparison between the experimental (symbols) and the simulated values of the PSS solid temperature profiles at the end of a semi-cycle (on the left) and of the outlet methane concentration (on the right); $t_c = 600$ s, $y_{G,0} = 3500$ ppmV.

Contrary to the noble-metal based catalyst, outlet methane conversion increases during the transient, reaching the unit value when the PSS is reached; Figure 3.31 (on the right) shows a comparison between the prediction and the simulated values of the outlet methane molar fraction and also in this case a good agreement is obtained.

Figure 3.32: Comparison between the simulated and the experimental values of the solid temperature when methane (3500 ppmV) is fed to the reactor (t_c = 600 s, metal oxide-base catalyst). The values of the simulated and measured seven temperatures that are used by the heat compensation system are shown.
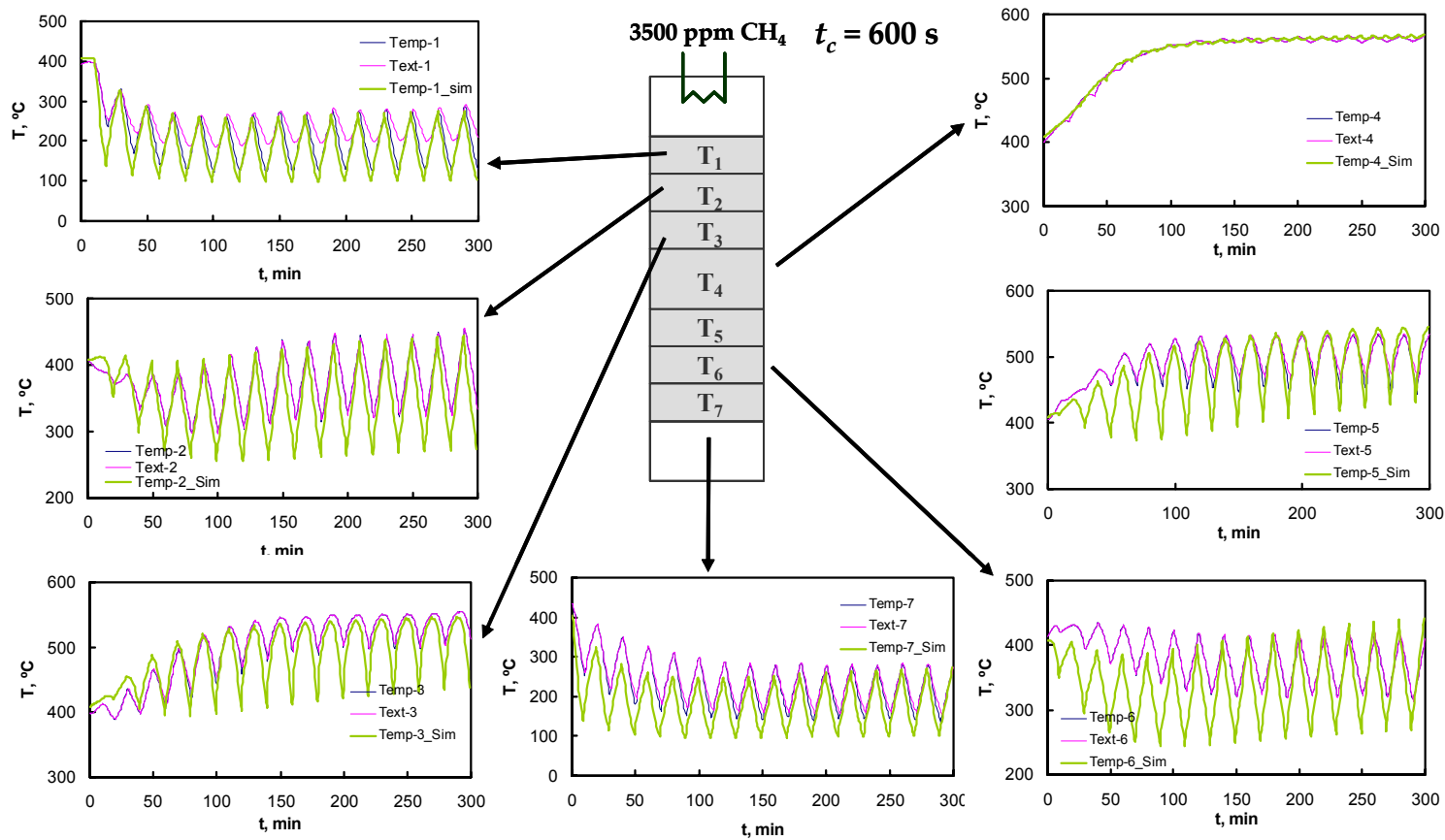
Figure 3.32 shows the comparison between the predicted and the measured values of the temperature in the middle of the seven sections of the reactor when chemical reaction occurs on the metal oxide-based catalyst. It is possible to see the good agreement between model prediction and experiments; the Figure shows also the external temperature in the seven sections: it is possible to see that the inner and the outlet temperature are almost the same, thus ensuring adiabatic operation.

Further experimental studies have been accomplished to investigate the influence of the main operating parameters on the performance of the reactors when the metal oxide-based catalyst is used. Figure 3.33 shows the influence of the switching time on the maximum temperature of the solid; both experimental and simulated values are shown.

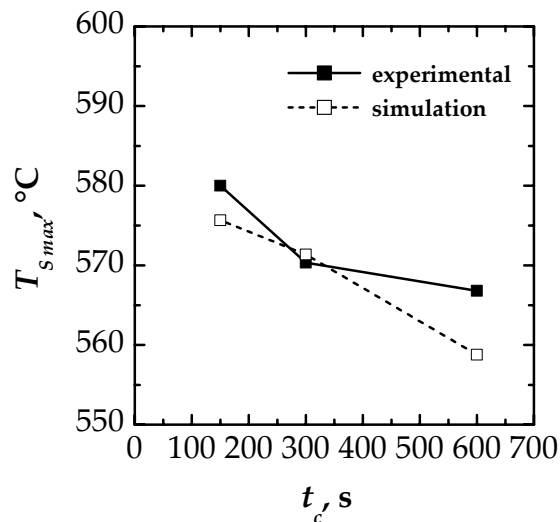Figure 3.33: Comparison between the experimental and the simulated values of solid maximum temperature vs. the switching time; u_G = 0.1434 m s^{-1}, $y_{G,0}$ = 3500 ppmV.

Figure 3.34 and Figure 3.35 shows the influence of the inlet concentration and of the inlet velocity on the maximum temperature of the solid; both experimental and simulated values are shown, evidencing the agreement which is obtained.
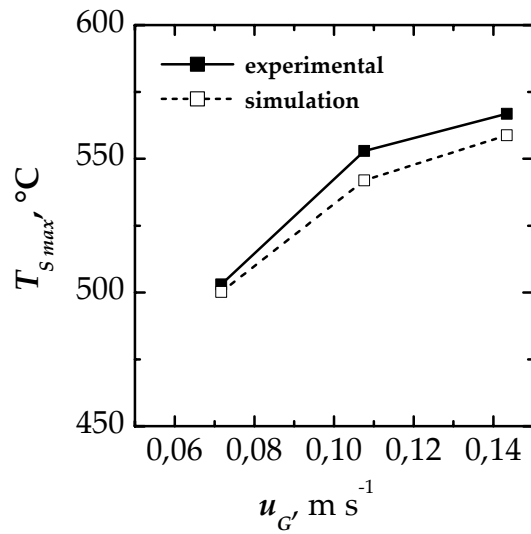
Figure 3.34: Comparison between the experimental and the simulated values of solid maximum temperature vs. the inlet surface velocity; t_c = 600 s, $y_{G,0}$ = 3500 ppmV.
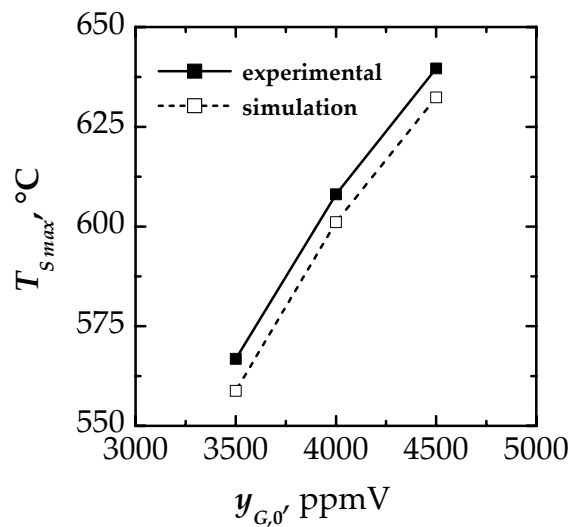
Figure 3.35: Comparison between the experimental and the simulated values of solid maximum temperature vs. the inlet surface velocity; t_c = 600 s, u_G = 0.1434 m s^{-1}.

A good agreement between predictions and experiments is obtained also as far as the PSS solid temperature profiles are concerned, as it is shown in Figure 3.36 for different values of the inlet velocity and in Figure 3.37 for different values of the inlet concentration.
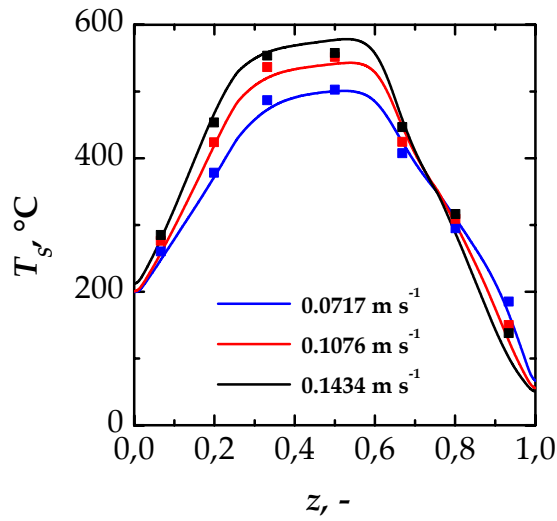
Figure 3.36: Comparison between the experimental (symbols) and the simulated values of the PSS solid temperature profiles at the end of a semi-cycle for the indicated values of inlet velocity. t_c = 600 s, $y_{G,0}$ = 3500 ppmV (metal oxide-based catalyst).
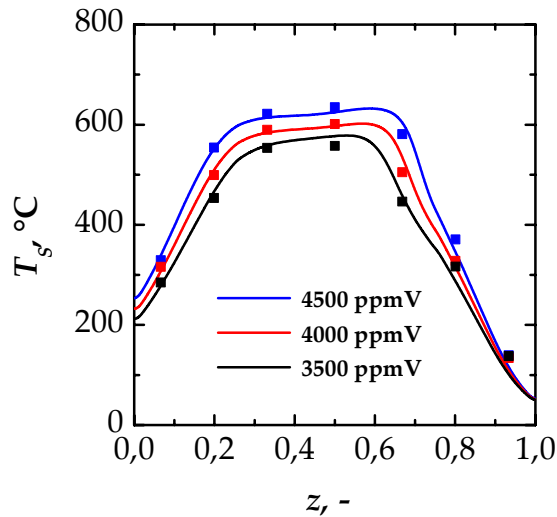
Figure 3.37: Comparison between the experimental (symbols) and the simulated values of the PSS solid temperature profiles at the end of a semi-cycle for the indicated values of inlet methane concentration. t_c = 600 s, u_G = 0.1434 m s^{-1} (metal oxide-based catalyst).

List of symbols

a_v	external particle surface area per unit volume of reactor, m^{-1}
c	molar concentration, mol m^{-3}
c_p	specific heat at constant pressure, J kg^{-1}K^{-1}
D_{eff}	effective mass dispersion coefficient, m^{2}s^{-1}

d_P	pellet diameter, m
D_R	reactor diameter, m
E_a	activation energy, J kmol^{-1}
ΔH_f	molar enthalpy of formation, J mol^{-1}
h	gas-solid heat transfer coefficient, J m^{-2}K^{-1}s^{-1}
h_{rs}	heat transfer coefficient for thermal radiation, solid surface to solid surface, W m^{-2}K^{-1}
h_{rv}	heat transfer coefficient for thermal radiation, void space to void space, W m^{-2}K^{-1}
k_∞	pre-exponential factor, s^{-1}
k'_∞	frequency factor, mol kg^{-1}s^{-1}Pa^{-1}
k_{eff}	effective heat dispersion coefficient, J m^{-1}K^{-1}s^{-1}
k_G	gas-solid mass transfer coefficient, mol m^{-2}s^{-1}
k_r	kinetic constant, s^{-1}
L	total reactor length, m
l	single reactor length in the RN, m
l_{hz}	length of the hot zone, m
M	molar mass, kg mol^{-1}
N_R	number of reactions
n_b	number catalytic fixed bed in the RN
n_r	number of components in the mixture
Pr	Prandtl number
r	ratio between the thermal capacity of inert material and that of the catalytic material
R	ideal gas constant, J K^{-1}mol^{-1}
Re$_P$	particle Reynolds number
Sc	Schmidt number
T	temperature, K
t	time, s
t_c	switching time, s
t_p	time constant of the heat transfer process, s
v	interstitial velocity, m s^{-1}
u	surface velocity, m s^{-1}
x	axial reactor coordinate, m
z	non-dimensional axial reactor coordinate
y	molar fraction

Greeks

α	structural constant of the porous solid
β, γ	parameters, eq. (2.31)
ε	void fraction of the catalytic bed
ε_c	void fraction of the catalyst
ϕ	parameter, eq. (2.31)
η	effectiveness factor
λ	thermal conductivity, J m^{-1}K^{-1}s^{-1}
λ_{s}^{*}	thermal conductivity of the porous solid, J m^{-1}K^{-1}s^{-1}
ν	stoichiometric coefficient
ρ	density (or apparent density for the solid), kg m^{-3}
τ	catalyst tortuosity
ω	hot front propagation velocity, m s^{-1}

Subscripts and superscripts

a	average value
G	gas phase
e	external value
i	internal value
ign	ignition value
max	maximum value
min	minimum value
mtx	solid matrix value
out	outlet value
ph	pre-heating value
S	solid phase or solid surface
st	stagnant
W	reactor wall
0	initial condition

Abbreviations

RFR	reverse-flow reactor
RN	reactors network
PSS	pseudo-steady state or periodic steady state

Chapter 4

Control of reverse-flow VOC after-burners

In addition to the intrinsecally dynamic behaviour of the RFR, one must deal with unexpected external perturbations (in the feed concentration, composition and temperature) which may lead to reactor extinction (and thus pollutants emissions) or catalyst overheating (and thus subsequent deactivation). In order to avoid these problems it is necessary to implement some closed-loop control strategies. Few papers have appeared in the literature concerning these topics. Van de Beld and Westerterp (1997) discussed different possible solutions to avoid pollutants emissions in a RFR:

a) *Increasing of the feed temperature*. In order to increase the bed temperature of a certain amount, it is necessary to increase the feed temperature by at least the same amount, whereas in most cases it must be larger. This requires a high energy input and is inefficient. For control purposes it is too slow, because the entire bed has to be heated by the hotter feed.

b) *Adding combustibles to the feed*. This seems the most logical methos to use, because it is simple to implement. However, a reactive combustible, when added to the feed, will react already in the inlet part of the catalyst bed and the increase of the maximum temperature in the centre of the bed is initially small. A component too difficult to oxidise will nor react at all or only with a very low conversion; obviously such a component is not the optimal additive. So it depends on the actual bed temperatures what is an

effective additive; moreover the ignition temperatures of the original pollutants and the supporting fuel must be almost equal, otherwise the reactor may establish the temperature profile corresponding to the component with the lower ignition temperature and will not be able to oxidise the component with the higher ignition temperature (Nieken *et al.*, 1994a, 1994b; Cittadini *et al.*, 2000).

c) *Adding combustibles in the central part of the reactor*. The heat of local combustion can be used as a source of energy. A combustible can be used which already reacts at low temperatures; the drawbacks given under points (a) and (b) are avoided, but now lack of good distribution of the contaminant over the entire cross-sectional area may cause difficulties.

d) *Installing an electrical heating device in the central part of the reactor*. As the need is to increase the temperature in the hottest zone of the bed in order to oxidise also a less refractive component, this might be achieved by an electrical heating device in the centre of the reactor. Such a device can increase the temperature very rapidly but the heat must be transferred from the heating device to the catalyst, thus introducing an additional heat transport resistence. Furthermore this device can be used for start-up purposes. Experimental results of Cunill *et al.* (1997) show that this device is effective as maximum temperature in the reactor is now a function of the electrical power and almost independent of the mixture components and composition; thus a mixture of contaminants with very different ignition temperatures can be burned completely, provided that the electrical power is sufficiently high. If a permanent heating support is required and electrical heating device is too expensive; in this case adding combustibles in the central part of the reactor is a better choice.

e) *Permanent adding of a component difficult to oxidise.* With such a component, fed in a concentration sufficient to ensure the ignition, the temperature level in the reactor will be high and all other more refractive contaminants are surely converted. The main drawback is that this is a rather energy consuming solution; furthermore, an increase in the inlet concentration may be difficult to handle, because the catalyst may become overheated.

f) *Supply of a hot gas in the centre of the reactor*. This also seems to be an inefficient way to increase the temperature, since the heat capacity of the gas is low in comparison to that of the bed.

g) *Change of the switching time.* Barresi and Vanni (2002) considered a one-point control strategy, with a temperature measurement located at either end of the active portion of the bed: flow direction is changed when temperature at the controller located close to the inlet drops below a certain set-point. Their simulations evidenced that at higher set-point also the maximum temperature is increased, but, at least for large portions of inert material, converison cannot be arbitrarly improved by this strategy; this is due to the shorter period at higher set-point, resulting in a stronger wash-out effect. With this configuration the cycle period decreases steeply in the first cycles, than slowly increases up to the final value.

Beside the problem of reaction extiction, the temperature in the reactor should not exceed the maximum allowable catalyst temperature; this may occur when the concentration of contaminants becomes too high during a significant period of time. A short peak of high concentration will not be a problem, since the heat capacity of the system is high and it will take time before the maximum temperature exceeds the limit. Furthermore a RFR exhibits some self-control with respect to the inlet concentration. For a low concentration, the reaction takes place in the central part of the reactor, so that part of the catalyst is used to store heat and to pre-heat the cold feed. If the inlet concentration is increased, the temperature and concentration profiles will move in the direction of the inlet and outlet of the reactor and a temperature plateau will develop. For higher inlet concentrations full conversion is already obtained in the first layers of the catalyst bed and the length of the "heat exchanger" equals that of the inert sections and remains constant. From this point on, the maximum temperature will increase very rapidly with the inlet concentration. Different technical solutions have been proposed in the literature (Eigenberger and Nieken, 1988):

a) *Dilution of the feed with additional air*. The effectiveness of this system has been discussed by Van de Beld and Westerterp (1997); the main drawback is that the total flow rate increases significantly, thus requiring additional energy costs to overcome the higher pressure drop. Moreover there is the

problem to obtain reliable and inexpensive on-line measurements of the inelt concentration.

b) *Increase of the switching time*. The influence of the switching time has been addressed in §2.3, pointing out that if the switching time is increased maximum temperature can be descreased, particularly when high inert fraction is used (Nieken *et al.*, 1994a; Cunill *et al.*, 1997).

c) *Heat recovery by internal heat exchange*. This possiblity has been discussed by Grozev and Sapundzhiev (1997) and by Nieken *et al.* (1994a, b) who pointed out that the switching period has to be increased such that the reaction front approaches the centre of the reactor before a noticeable influence upon the maximum temperature can be noticed; however no remarkable reduction of the maximum temperature is possible trough intermediate cooling, irrespective of the switching period used, although the energy recovery increases. Sapundziev *et al.* (1993) used an internal heat exchange to pre-heat the cold feed; by a proper choice of the operating parameters it is possible to operate the system with temperatures lower than a certain value depending on the catalyst used. External cooling restricts the region of operating variables that allows for autothermal behaviour as combustion can now be quenched if the coolant removes more heat than is generated (Purwono *et al.*, 1994). Budman *et al.* (1996) considered the application of a conventional PID controller with anti-windup: exit concentration is the controlled variable and it is used to infer the maximum temperature (as thermocouple locations in the bed are fixed, it may be extremely difficult to evaluate the maximum temperature, being the temperature profiles moving during the operation of the reaction). The same authors considered also a feedforward regulation of the exit concentration through knowledge of the inlet concentration. The idea behind this strategy is that if the inlet concentration is known, it is possible to evaluate the optimal combination of switching time and cooling rate to obtain full conversion and safe operation in the reactor. To this regard, a number of simulations have been performed to identify parameters region for safe operation.

d) *Cold gas injection*. A similar effect to intermediate cooling through heat exchange may be obtained by the injection of cold gas or water into the

middle of the packed bed. This may lead to a significant decrease of the temperature in the middle of the reactor, whereas the maximum temperature is more or less unaffected (Nieken *et al.*, 1994b).

e) *Hot gas withdrawal*. An alternative method for heat recovery is the withdrawal of part of the hot gas from the centre of the reactor; this allows for almost complete energy recovery, but again the maximum temperature cannot be lowered sufficiently; sidestream withdrawal just shifts the reaction zone towards the centre of the reactor, as it has been demonstrated by Nieken *et al.* (1994b).

f) *Structured fixed bed*. If the packed bed is composed of portions with high effective conductivity and of portions of low conductivity then it depends upon the position of the temperature fronts whether the maximum temperature is lowered or increased. If the fronts are always in the portion with high axial conductivity, the maximum temperature will be low and the efficiency of the heat recovery will be weak; if the fronts stay in the portion with low conductivity, the opposite is true. Since the position of the fronts can be shifted by the amount of the hot gas withdrawn, an interesting possibility exists to operate the reactor in either of the two regimes. To exploit this possibility a structured fixed bed is needed, where the packed bed is composed of three portions: an inner portion with high effective conductivity support and two outer portions with low conductivity support (Nieken *et al.*, 1994b).

In this work a model based control system will be described and proved to be effective in both controlling maximum temperature and reaction extinction; a model-based soft-sensor (observer) has been developed to give reliable estimations of the feed composition from some temperature measurements in the reactor, thus avoiding expensive hardware sensors and time consuming on-line measurements (§4.1). The information derived from the soft-sensor will be used to develop a model based control system (§4.2). The effectiveness of this method will be tested by means of simulations in presence of disturbances in the inlet concentration.

4.1 The RFR observer design

4.1.1 *Introduction and reactor modelling*

A soft-sensor combines the knowledge of the physical system (model) with experimental data (some on-line measures) to provide on-line estimates of the sought states and/or parameters. The system which has been taken into consideration is a medium-scale RFR as schematically shown in Figure 4.1 (Ramdani *et al.*, 2001), in the framework of a cooperation with the *Laboratoire de Genie des Procedé Catalytiques* (LGPC), CPE Lyon (France).
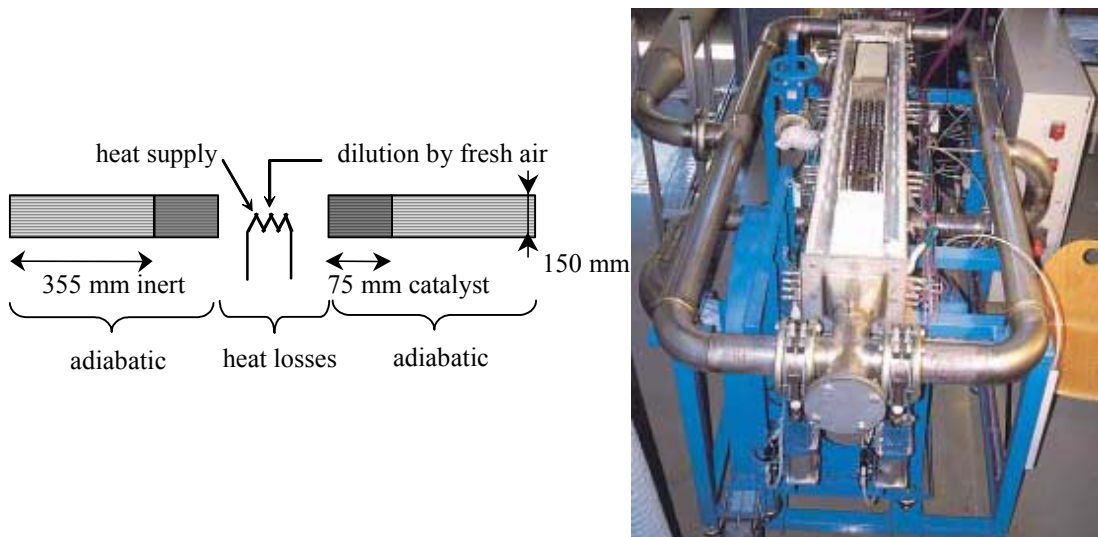

Figure 4.1: Main geometrical characteristics of the RFR.

The monoliths (cordierite) of square cross section are made of square channels 1x1 mm. Two inert monoliths are on both sides of the short catalytic monoliths. Several thermocouples are inserted in some channels to obtain temperature maps. An electrical heater is located in the core to start the process or for control purpose. A blower located downstream of the RFR keeps a constant underpressure, and ensures a flow rate up to 200 m^3 h^{-1} STP. The liquid pollutant (xylene, various pure esters or alcohols) is injected through a capillary tube into ambient air where it vaporizes upstream of the RFR. The combustion of xylene over a Pt/Al_2O_3 has been considered in this case; a first order reaction rate is used, according to Ramdani (2001). Owing to the small catalyst/inert ratio, the RFR is operated in the high-frequency domain (period from 10 to 20 s). The monoliths and the electrical heater are

in a thermally insulated rectangular box 1.8 m long. The lid of the box is not perfectly airtight, and a small amount of fresh air is aspirated into the core. Furthermore, the core being the hottest region, heat loss takes place. Because radial heat conductivity in a monolith is much less than in a packed bed, the monoliths are almost adiabatic. Table 4.1 summarise the main parameters used in the simulations.

Table 4.1: Main parameters used in the simulation of the medium scale RFR.

Solid density, ρ_S	2500 kg m^{-3}
Solid specific heat, $c_{p,S}$	900 J kg^{-1} K^{-1}
Axial solid thermal conductivity, λ_S	0.38 W m^{-1} K^{-1}
Monolith void fraction, ε	0.76
Frequency factor, k_∞	2400 s^{-1}
Activation energy, E_a	47750 J mol^{-1}
Inlet gas velocity, u_0	1.23 m s^{-1}

In order to simulate the behaviour of this device, a complete one-dimensional two-phase model has been used; PSS is assumed for the gas phase and the dynamic is exclusively governed by heat storage in the solid. Heat loss and dilution by fresh air are accounted for in the core region which is assumed to be well mixed. Thus, the balance equations for this device are:

- Energy balance in the solid phase:

$$(1-\varepsilon)\rho_S c_{p,S}\frac{\partial T_S}{\partial t} = \lambda_S \frac{\partial^2 T_S}{\partial x^2} + ha_v\left(T_G - T_S\right) + a_v\left(-\Delta H\right)r_S\left[T_S, c_S\right] \tag{4.1}$$

- Energy balance in the gas phase:

$$\rho_{G,0}u_0 c_{p,G}\frac{dT_G}{dx} + ha_v\left(T_G - T_S\right) = 0 \tag{4.2}$$

- Mass balance for the solid phase:

$$k_D\rho_G\left(\omega_G - \omega_S\right) + \upsilon M r_S = 0 \tag{4.3}$$

- Mass balance for the gas phase:

$$\rho_{G,0}u_0\frac{d\omega_G}{dx} + \rho_G k_D a_v\left(\omega_G - \omega_S\right) = 0 \tag{4.4}$$

- Boundary conditions:

$$T_{G,1}(x=0) = T_e = 293K$$

$$(1+N')\left[T_{G,2}\left(x=\frac{H}{2}\right)-T_e\right] = \alpha\left[T_{G,1}\left(x=\frac{H}{2}\right)-T_e\right] + \frac{Q_{res}}{\rho_G u_o c_{p,G} S}$$

(4.5)

The last boundary condition accounts for heat loss through the number of transfer units N', defined as:

$$N' = \frac{h_{loss} S_{loss}}{\rho_{G,0} u_0 c_{p,G} S}$$

(4.6)

and dilution by fresh air by α, which is defined as the ratio between the inlet and the outlet flow rate.

Simulation results are compared with experiments in Figure 4.2 which shows good agreement. Deviations between experimental and calculated temperatures may be essentially attributed to the exact location of the thermocouples.
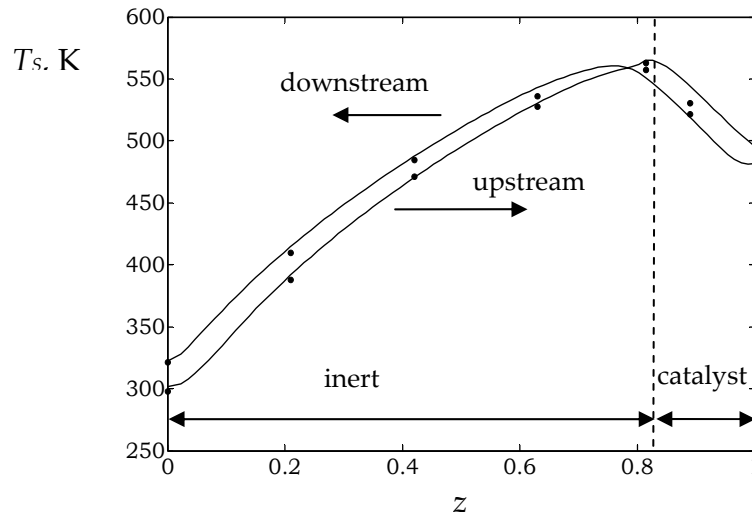

Figure 4.2: Experimental (symbols) and simulated (line) values of the temperature profiles in the monoliths at flow reversal. t_c = 16 s, ΔT_{ad} = 25 K.

Deriving an observer from a detailed model accounting for heat losses through the reactor wall, finite flow reversal frequency, reaction kinetics is an overwhelming task; as a consequence a simplified model has been developed. By taking advantage of the high frequency of flow reversal, the analogy with the countercurrent reactor has been considered (Nieken *et al.*, 1995). Figure 4.3 shows the countercurrent model:
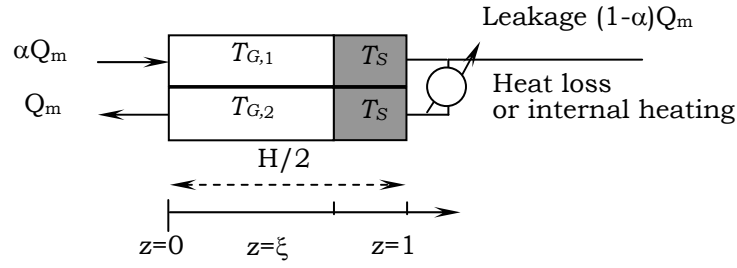
Figure 4.3: The countercurrent reactor model

The balance equations for the countercurrent model are:

- Energy balance for the solid phase:

$$\lambda_S \frac{\partial^2 T_S}{\partial x^2} + \frac{ha_v}{2}\left(T_{G,1} + T_{G,2} - 2T_S\right) + a_v\left(-\Delta H\right)\frac{r_{S,1} + r_{S,2}}{2} = (1-\varepsilon)\rho_S c_{p,S}\frac{\partial T_S}{\partial t} \qquad (4.7)$$

- Energy balance for the gas phase:

$$-\rho_{G,0}u_0 c_{p,G}\frac{\partial T_{G,2}}{\partial x} + ha_v\left(T_{G,2} - T_S\right) = 0 \qquad (4.8)$$

$$\alpha\rho_{G,0}u_0 c_{p,G}\frac{\partial T_{G,1}}{\partial x} + ha_v\left(T_{G,1} - T_S\right) = 0 \qquad (4.9)$$

- Mass balance for the gas phase:

$$-\rho_{G,0}u_0\frac{\partial \omega_{G,2}}{\partial x} + k_D a_v\rho_{G,2}\left(\omega_{G,2} - \omega_{S,2}\right) = 0 \qquad (4.10)$$

$$\alpha\rho_{G,0}u_0\frac{\partial \omega_{G,1}}{\partial x} + k_D a_v\rho_{G,1}\left(\omega_{G,1} - \omega_{S,1}\right) = 0 \qquad (4.11)$$

- Mass balance for the solid phase:

$$k_D\rho_{G,1}\left(\omega_{G,1} - \omega_{S,1}\right) = Mr_{S,1} \qquad (4.12)$$

$$k_D\rho_{G,2}\left(\omega_{G,2} - \omega_{S,2}\right) = Mr_{S,2} \qquad (4.13)$$

- Boundary conditions:

$$x = 0 \quad \begin{cases} \omega_{G,1} = \omega_{G,0} \\ T_{G,1} = T_0 \\ \partial T_S/\partial x = 0 \end{cases} \qquad (4.14)$$

$$x = \frac{H}{2} \begin{cases} \alpha\omega_{G,1} = \omega_{G,1} \\ \partial T_S / \partial x = 0 \\ (1+N')(T_{G,2} - T_{G,0}) = \alpha(T_{G,1} - T_{G,0}) + Q_{res}/\rho_{G,0}u_0 c_{p,G} S \end{cases} \tag{4.15}$$

If we consider to work with the reactor fully ignited, the reaction can be assumed instantaneous and under strong mass transfer limitation; $\omega_{S,1}$ and $\omega_{S,2}$ are thus negligible with respect to $\omega_{G,1}$ and $\omega_{G,2}$ respectively. This assumption implies that it will be impossible to predict the extinction phenomenon; conversely, the model is independent of any kinetic parameter. Normalising some variables and assuming that the Nusselt and Sherwood numbers on one hand and the Schmidt and Prandtl numbers on the other are equal, gives $h = k_D \rho_G c_{p,G}$ and:

$$\frac{1}{P_{ax}} \frac{\partial^2 T_S}{\partial z^2} + P \frac{T_{G,1} + T_{G,2} - 2T_S}{2} + P\Delta T_{ad} \frac{\omega_{G,1} + \omega_{G,2}}{2\omega_{G,0}} \varphi(z) = \tau \frac{\partial T_S}{\partial t} \tag{4.16}$$

$$\alpha \frac{\partial T_{G,1}}{\partial z} + P(T_{G,1} - T_S) = 0 \tag{4.17}$$

$$-\frac{\partial T_{G,2}}{\partial z} + P(T_{G,2} - T_S) = 0 \tag{4.18}$$

$$\alpha \frac{\partial \omega_{G,1}}{\partial z} + P\omega_{G,1} = 0 \tag{4.19}$$

$$-\frac{\partial \omega_{G,2}}{\partial z} + P\omega_{G,2} = 0 \tag{4.20}$$

where:

$$z = \frac{x}{H/2}, \quad P = \frac{ha_v H}{2\rho_G u_0 c_{p,G}}, \quad \frac{1}{P_{ax}} = \frac{2\lambda_S}{H\rho_G u_0 c_{p,G}}, \quad \tau = \frac{(1-\varepsilon)\rho_S c_{p,S} H}{2\rho_G u_0 c_{p,G}} \tag{4.21}$$

and $\phi(z)$ accounts for the type of monoliths: $\phi(z)=0$ in the inert monoliths ($z<\xi$) and $\phi(z)=1$ in the catalytic monoliths ($z>\xi$). Assuming P to be uniform over z, equations (4.19) and (4.20) yield:

$$\omega_{G,1} = \omega_{G,0} e^{-P\frac{z-\xi}{\alpha}} \quad (\text{for } z > \xi)$$

$$\omega_{G,1} = \omega_{G,0} \quad (\text{for } z < \xi) \tag{4.22}$$

$$\omega_{G,2} = \alpha\omega_{G,0}e^{-P\frac{1-\xi}{\alpha+1-z}} \quad (\text{for } z > \xi)$$

$$\omega_{G,2} = \alpha\omega_{G,0}e^{-P\frac{1-\xi}{\frac{z}{\alpha}+1}} \quad (\text{for } z < \xi) \tag{4.23}$$

In order to further simplify the reactor model, the two-phase equations are transformed into a pseudo-homogeneous system. The rigorous approach of Balakotaiah and Dommeti (1999) has been used and the gas temperature is written as a function of the solid temperature:

$$T_{G,1} = T_S + \sum_{k=1}^{\infty}\left(-\frac{\alpha}{P}\right)^k \frac{\partial^k T_S}{\partial z^k} \tag{4.24}$$

$$T_{G,2} = T_S + \sum_{k=1}^{\infty}\left(\frac{1}{P}\right)^k \frac{\partial^k T_S}{\partial z^k} \tag{4.25}$$

Since P is much greater than unity, convergence of the series is guaranteed and being $P \cong 80$ the series can be truncated, thus yielding to the following approximations:

$$T_{G,1} \cong T_S - \frac{\alpha}{P}\frac{\partial T_S}{\partial z} + \left(\frac{\alpha}{P}\right)^2 \frac{\partial^2 T_S}{\partial z^2} \tag{4.26}$$

$$T_{G,2} \cong T_S + \frac{1}{P}\frac{\partial T_S}{\partial z} + \left(\frac{1}{P}\right)^2 \frac{\partial^2 T_S}{\partial z^2} \tag{4.27}$$

The homogeneous model is thus described by a single heat balance equation:

$$\left(\frac{1}{P_{ax}} + \frac{1+\alpha^2}{2P}\right)\frac{\partial^2 T_S}{\partial z^2} + \frac{1-\alpha}{2}\frac{\partial T_S}{\partial z} + P\Delta T_{ad}\Psi(z) = \tau\frac{\partial T_S}{\partial t} \tag{4.28}$$

with

$$\Psi(x) = \varphi(x)\frac{\omega_{G,1} + \omega_{G,2}}{2\omega_{G,0}} \tag{4.29}$$

The first term of equation (4.28) involves an effective axial heat conductivity given by:

$$\frac{1}{P_{ax}} + \frac{1+\alpha^2}{2P} = \frac{\lambda_{eff}}{\rho_{G,0}u_0c_{p,G}H/2}, \quad \lambda_{eff} = \lambda_S + \frac{1+\alpha^2}{2}\frac{\left(\rho_{G,0}u_0c_{p,G}\right)^2}{ha_v} \tag{4.30}$$

When $\alpha=1$ (no dilution), λ_{eff} reduces to the well-known estimate of Vortmeyer and Schafer (1974) as used by Nieken *et al.* (1995). Boundary conditions for the pseudo-homogeneous model are the followings:

$$z = 0 \quad T_S - \frac{\alpha}{P}\frac{\partial T_S}{\partial z} = T_{G,0} \tag{4.31}$$

$$z = 1 \quad (1+N')\left(T_S + \frac{1}{P}\frac{\partial T_S}{\partial z} - T_{G,0}\right) = \alpha\left(T_S - \frac{\alpha}{P}\frac{\partial T_S}{\partial z} - T_{G,0}\right) + \frac{Q_{res}}{\rho_{G,0} u_0 c_{,G} S} \tag{4.32}$$

Figure 4.4 shows a comparison between the temperature profiles in the RFR as predicted by the pseudo-homogeneous model and the measured values:
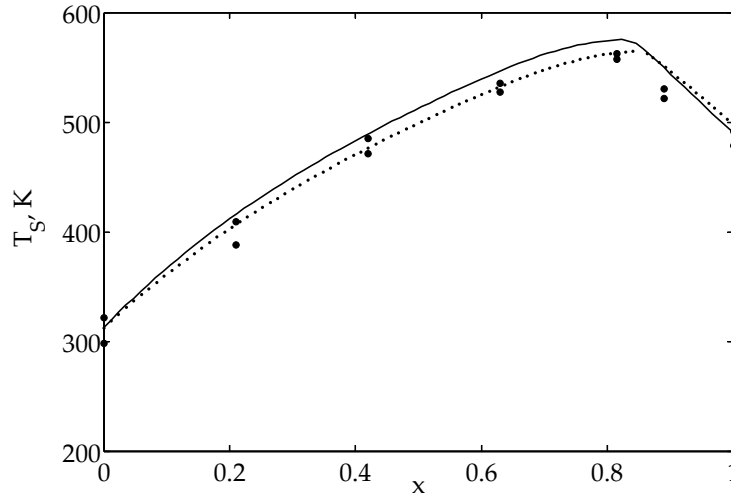

Figure 4.4: Comparison between the experimental values (symbols) and the simulated one of the temperature profile. The pseudo-homogeneous countercurrent reactor model has been used with (dotted line) and without (solid line) correction for the finite switching frequency. $t_c = 16$ s, $P = 73.9$, $\Delta T_{ad} = 25$ K, $\tau = 143$ s, $\xi = 0.826$.

The finite frequency in the RFR is responsible for a deviation with respect to the prediction based on the countercurrent model; no simple method is available to account for the finite frequency except using a detailed and time-consuming model. The approach of Edouard *et al.* (2003), which is based on physical arguments has been used. During a period t_c, the solid temperature profile moves back and forth; it is almost symmetrical except where the reaction takes place close to $z=\xi$. At that location, the temperature profile can be relatively flat in the downstream monolith or it can exhibit a temperature overshoot of ΔT_{ad} at most in the upstream monolith where the (instantaneous) reaction takes place. Knowing that the temperature rise from $z=0$ to $z=1$ (adiabatic system, no dilution, i.e., $N'=0$ and $\alpha=1$) is of the order $P\Delta T_{ad} \gg \Delta T_{ad}$, it is reasonable to assume that the solid temperature follows an oscillating and rather symmetrical profile within less than $\pm\Delta T_{ad}/2$. The

smaller the period, the more accurate the approximation would be. Figure 4.5 (left) illustrates this symmetry; the profiles were obtained with a detailed model as those described in (§ 3.2).
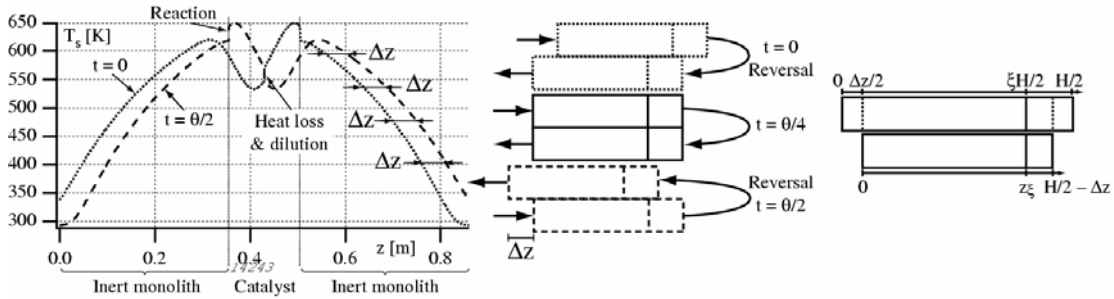

Figure 4.5: Left : almost symmetric temperature profiles just before flow reversal. Middle: sliding countercurrent monoliths that superimpose the solid temperature profiles. Right: truncated non-sliding "equivalent" monoliths.

In the countercurrent model, the solid temperature profile is identical in the upstream and downstream monoliths by definition. To obtain this identity in the RFR at finite frequency, one must shift one monolith with respect to the other (Figure 4.5, middle). On a first approximation, one may thus consider that the RFR at finite frequency behaves as a "sliding countercurrent reactor". At flow reversal, the monoliths are shifted over a distance $\Delta z = v_t t_c/2$, where v_t is the velocity of propagation of the temperature wave ($=H/2\tau$). On a time average basis over half a period, two parts of length $\Delta z/2$ on both sides of the upstream monolith are not in contact with the downstream monolith. If we assume that these parts do not contribute to the heat storage process, then the system behaves as a countercurrent reactor with non-sliding truncated monoliths of length equal to the average length of the parts in contact (see Figure 4.5, right). The real size $H/2$ is thus reduced by $\Delta z/2$ on both sides. This means that the corrected P and ξ are given by:

$$P^* = P\left(1 - \frac{t_c}{2\tau}\right) \tag{4.33}$$

$$\frac{1}{P_{ax}^*} = \frac{1}{P_{ax}} \frac{1}{1 - \frac{t_c}{2\tau}} \tag{4.34}$$

$$\xi^* = \frac{\xi - t_c/4\tau}{1 - t_c/2\tau}$$

(4.35)

These simple estimates hold provided that $0 < \xi t_c < 1$, i.e., $t_c/4\,\tau < Max(\xi, 1 - \xi)$. In Figure 4.4 the experimental results are compared also to the simulated values with the homogeneous countercurrent reactor model with correction for the finite flow reversal frequency, showing that an excellent agreement can be obtained, particularly with respect to the maximum temperature in the reactor. As a consequence the pseudo-homogeneous countercurrent reactor model with correction for the finite flow reversal frequency will be used to develop the soft sensor.

List of symbols

a_v	external particle surface area per unit volume of reactor, m^{-1}
c	molar concentration, $mol\ m^{-3}$
c_p	specific heat at constant pressure, $J\ kg^{-1}K^{-1}$
$-\Delta H$	heat of reaction, $j\ mol^{-1}$
E_a	activation energy, $Jkmol^{-1}$
h	gas-solid heat transfer coefficient, $J\ m^{-2}K^{-1}s^{-1}$
k_∞	pre-exponential factor, s^{-1}
k_{eff}	effective heat dispersion coefficient, $J\ m^{-1}K^{-1}s^{-1}$
k_D	gas-solid mass transfer coefficient, $mol\ m^{-2}s^{-1}$
H	total length of the monolith, m
M	molar mass, $kg\ mol^{-1}$
N'	number of transfer units for heat loss
P	Peclet number for solid-gas heat transfer
P^*	Peclet number for solid-gas heat transfer with correction for the finite flow reversal frequency
P_{ax}	axial Peclet number for heat conduction
P_{ax}^*	axial Peclet number for heat conduction with correction for the finite flow reversal frequency
Q_{res}	power supply, W
r_S	reaction rate, $mol\ m^{-2}s^{-1}$
S	cross section of the monolith, m^2

S_{loss} external area where heat loss to the exterior take place, m^2

T temperature, K

t time, s

t_c switching time, s

u surface velocity, $m\,s^{-1}$

x axial reactor coordinate, m

z non-dimensional axial reactor coordinate

Greeks

α ratio between the inlet and the outlet flow rate

ε void fraction of the catalytic bed

λ thermal conductivity, $J\,m^{-1}K^{-1}s^{-1}$

λ_{eff} effective axial heat conductivity, $J\,m^{-1}K^{-1}s^{-1}$

ν stoichiometric coefficient

ρ density, $kg\,m^{-3}$

τ heat storage time constant, s

ω mass fraction

ξ reduced abscissa of the boundary between the inert and the catalytic section

Subscripts and superscripts

G gas phase

e external value

S solid phase or solid surface

0 initial condition

Abbreviations

RFR   reverse-flow reactor

PSS   pseudo-steady state

4.1.2 *Fundamentals on observer design*

A model-based control or supervision strategy requires the knowledge of the state of the process; this may be achieved by using physical sensors. In many cases, due to cost consideration and physical constraints, the number and type of sensors could be very limited. An observer combines *a priori* knowledge about the physical system (model) with experimental data (on-line measurements) to provide an on-line estimation of states and/or parameters.

An observer for a dynamic system $S(x, y, u)$ with state x, output y and input u is another dynamic system $\hat{S}(\hat{x}, y, u)$ having the property that the state $\hat{x}$ of the observer converges to the state x of the process, independent of the input or the state. If a linear, continuous-time dynamic system is considered:

$$\dot{x} = Ax + Bu, \quad y = Cx \tag{4.36}$$

a full-order observer has the generic form

$$\dot{\hat{x}} = A\hat{x} + Ky + Hu \tag{4.37}$$

and the dimension of the state $\hat{x}$ is equal to the dimension of the process state x. The matrices appearing in Equation (4.37) must be chosen to conform with the required property that the observer state must converge to the process state independent by the state and the input. To determine these matrices, let

$$e = x - \hat{x} \tag{4.38}$$

be the estimation error. It follows that:

$$\dot{e} = \hat{A}e + \left(-\hat{A} + A - KC\right)x + (B - H)u \tag{4.39}$$

From equation (4.39) it is seen that for the error to converge to zero, independent of x and u, the following conditions must be satisfied:

$$\hat{A} = A - KC, \quad H = B \tag{4.40}$$

When these conditions are satisfied, the dynamic of the estimation error is governed by

$$\dot{e} = \hat{A}e \tag{4.41}$$

which converges to zero if $\hat{A}$ is a *stability matrix*. When $\hat{A}$ is constant, this means that its eigenvalues must lie in the (open) left half-plane. Since the

matrices A, B and C are defined by the plant, the only freedom in the design of the observer is the selection of the gain matrix K. To emphasize the role of the observer gain matrix, the observer can be written as

$$\dot{\hat{x}} = A\hat{x} + Bu + K\left(y - C\hat{x}\right) \tag{4.42}$$

Thus the observer comprises the model of the process and an added input, the so called "residual", which takes into account the difference between the actual measured state and the value of the state predicted by the model. A proper choice of the observer matrix K drives the residual to zero.

There is a considerable flexibility in the selection of the observer gain matrix; two methods are standard: optimisation and pole placement. In the first method the gain matrix is chosen as a Kalman filter gain matrix, thus involving the solution of the dynamic matrix Riccati equation; the second method involves numerical algorithms to find the matrix $\hat{A}$ with specified poles.

The concept of an observer carries over to nonlinear systems; however, in this case, the structure is not nearly as obvious as it is for a linear system. An observer for a plant, consisting of a dynamic system

$$\dot{x} = f\left(x,u\right) \tag{4.43}$$

with observations given by

$$y = g\left(x,u\right) \tag{4.44}$$

is another dynamic system, the state of which is denoted by $\hat{x}$, having the property that the error (4.38) converges to zero in steady-state. One way of obtaining an observer is to imitate the procedure used in a linear system, namely to construct a model of the original system and force it with the "residual":

$$r = y - \hat{y} = y - g\left(\hat{x},u\right) \tag{4.45}$$

The equation of the observer thus become

$$\dot{\hat{x}} = f\left(\hat{x},u\right) + \kappa\left(y - g\left(\hat{x},u\right)\right) \tag{4.46}$$

where $\kappa(\ )$ is a suitable chosen nonlinear function. The differential equation for the error e can thus be used to study its behaviour. This equation is given by

$$\dot{e} = x - \hat{x} = f\left(x,u\right) - f\left(x-e,u\right) - \kappa\left(g\left(x,u\right) - g\left(x-e,u\right)\right) \tag{4.47}$$

Suppose that by the proper choice of $\kappa(\ )$ the eq. (4.47) can be made asymptotically stable, so that an equilibrium state is reached for which

$$\dot{e} = 0 \tag{4.48}$$

Then, in equilibrium, eq. (4.47) becomes

$$0 = f(x,u) - f(-e,u) + \kappa\big(g(x-e,u) - g(x,u)\big) \tag{4.49}$$

Since the right-hand side of eq. (4.49) becomes zero when $e = 0$, independent of x and u, it is apparent that $e = 0$ is an equilibrium state of eq. (4.48). This implies that if $\kappa(\ )$ can be chosen to achieve asymptotic stability, the estimation error converges to zero.

The techniques used for selecting the gain for a linear observer can typically be adapted for a nonlinear observer. Pole placement is one method; another it to make the observer an extended Kalman filter.

In order to avoid numerical difficulties involved in the design of Kalman filter based observers, which render the on-line estimation very time-consuming, a different approach has been used in this thesis, deriving the observer from the high gain techniques (Bestele and Zeitz, 1981; Bonard and Hammouri, 1991; Deza *et al.*, 1992; Farza *et al.*, 1998; Gauthier *et al.*, 1992; Gauthier and Kupka, 1994). The calculation of the proposed observer gain does not require the resolution of any differential equation and its calibration, based on a canonical form, is very simple. In order to design a full order linear observer for a dynamic system, the canonical form has the following structure:

$$\begin{cases} \dot{z}^1 = a_1(t)A^1 z^1 + G_1\big(z^1,t\big) + d^1(t) \\ \dot{z}^2 = a_2(t)A^2 z^2 + G_2\big(z^1,z^2,t\big) + d^2(t) \\ \vdots \\ \dot{z}^q = a_q(t)A^q z^q + G_q\big(z^1,...,z^q,t\big) + d^q(t) \end{cases} \tag{4.50}$$

$$y = \big(y_1,y_2,...,y_q\big)^T = \big(z_1^1,z_1^2,...,z_1^q\big)^T \tag{4.51}$$

Here the state of the system is z_i with $z_i = \big(z_1^i,z_2^i,...,z_{n_i}^i\big)^T \in \mathbb{R}^{n_i}$ for $1 \le i \le q$ and $n_i \in \mathbb{N}$; the output measurements are given by y_i, i.e. the first component of the z_i. The matrices A_i have the form:

$$
A_i(t) = \begin{pmatrix} 0 & a_1(t) & 0 & \cdots & 0 \\ \vdots & \ddots & \ddots & \ddots & \vdots \\ \vdots & \ddots & \ddots & \ddots & 0 \\ \vdots & \ddots & \ddots & \ddots & a_{n_i-1}(t) \\ 0 & \cdots & \cdots & \cdots & 0 \end{pmatrix}
\tag{4.52}
$$

The $a_i(t)$ are known bounded signals which nowhere vanish and with bounded derivatives and $a_i(t) \geq \beta_i$ for some constant $\beta_i \geq 0$.

The nonlinear terms $G_i = \left(G_1^i, G_2^i, ..., G_{n_i}^i \right)^T$ have the following triangular structure:

$$
\begin{aligned}
G_j^1(z,t) &= G_j^1\left(z_1^1, ..., z_j^1, t, y \right) \text{ for } 1 \leq j \leq n_i \\
G_j^i(z,t) &= G_j^i\left(z^1, ..., z^{i-1}, z_1^i, ..., z_j^i, t, y \right) \text{ for } 2 \leq i \leq q, i \leq j \leq n_i
\end{aligned}
\tag{4.53}
$$

Finally the d^i denote the unknown disturbances affecting the system. To construct the gain of the observer the following notations are needed:

- for a given parameter $\Omega > 0$ and for $1 \leq i \leq q$, $\Delta_{i,\Omega}$ is an $n_i \times n_i$ diagonal matrix:

$$
\Delta_{i,\Omega} = \begin{pmatrix} \Omega & 0 & \cdots & 0 \\ 0 & \Omega^2 & \ddots & \vdots \\ \vdots & \ddots & \ddots & 0 \\ 0 & \cdots & 0 & \Omega^{n_i} \end{pmatrix}
\tag{4.54}
$$

- for $1 \leq i \leq q$ $K^i = \left(k_1^i, ..., k_{n_i}^i \right)^T$ is a constant array such that all the eigenvalues λ of the matrix

$$
\begin{pmatrix} k_1^i & 1 & \cdots & 0 & 0 \\ k_2^i & 0 & \ddots & 0 & 0 \\ \vdots & \vdots & \cdots & \vdots & \vdots \\ k_{n_i-1}^i & 0 & \cdots & 0 & 1 \\ k_{n_i}^i & 0 & \cdots & 0 & 0 \end{pmatrix}
\tag{4.55}
$$

are such that $\mathrm{Re}(\lambda) < 0$

- for $1 \leq i \leq q$ Λ_i is the $n_i \times n_i$ diagonal matrix defined by:

$$\begin{pmatrix} 1 & 0 & 0 & \cdots & 0 \\ 0 & a_1^i(t) & 0 & \ddots & 0 \\ 0 & 0 & a_1^i(t)\cdot a_2^i(t) & \ddots & 0 \\ \vdots & \vdots & \vdots & \ddots & \vdots \\ 0 & 0 & 0 & \cdots & a_1^i(t)\cdot a_2^i(t)\cdot\ldots\cdot a_{n_i-1}^i(t) \end{pmatrix} \tag{4.56}$$

The candidate observer is given by the following dynamical system:

$$\begin{cases} \dot{\hat{z}}^1 = a_1(t)A^1(t)\hat{z}^1 + G^1\left(\hat{z}^1,t\right) - a_1(t)\Lambda_1^{-1}(t)\Delta_{1,\Omega}K^1\left(\hat{z}^1 - y_1\right) \\ \dot{\hat{z}}^2 = a_2(t)A^2(t)\hat{z}^2 + G^2\left(\hat{z}^1,\hat{z}^2,t\right) - a_2(t)\Lambda_2^{-1}(t)\Delta_{2,\Omega}K^2\left(\hat{z}^2 - y_2\right) \\ \vdots \\ \dot{\hat{z}}^q = a_q(t)A^q(t)\hat{z}^q + G^q\left(\hat{z}^1,..,\hat{z}^q,t\right) - a_q(t)\Lambda_q^{-1}(t)\Delta_{q,\Omega}K^q\left(\hat{z}^q - y_q\right) \end{cases} \tag{4.57}$$

If the G^i are global Lipschitz functions (which is the case for almost every physical processes, as the state of the system is bounded), it is possible to demonstrate (Edouard *et al.*, 2003) that it exists $\Omega_0 > 0$, such that, for every $\Omega_0 > 0$

- in the absence of disturbances ($d_i = 0, 1 \leq i \leq q$):

$$\|\hat{z}(t) - z(t)\| \leq \mu e^{-vt}\|\hat{z}(0) - z(0)\|$$

- if the d_i does not vanish:

$$\|\hat{z}(t) - z(t)\| \leq \mu e^{-vt}\|\hat{z}(0) - z(0)\| + \delta$$

where $\delta > 0$ is a constant which depends only on the upper bounds of the $\|d_i\|$. In particular δ is small for small disturbances.

A crucial question when attempting to design an observer for a system is whether it is at all possible to estimate the state. Consider a linear, continuous-time dynamic system having the structure (4.36). Observability of a system is, loosely speaking, the property that the state can be uniquely determined from the input and output signals. Let y_u^0 and y_u^1 the out signals generated by applying the input signal u with initial conditions $x(0) = x^0$ and $x(0) = x^1$ respectively. The x^0 and x^1 are said to be indistinguishable if

$$y_u^0 \equiv y_u^1 \quad t \geq 0 \tag{4.58}$$

for all input signals u and otherwise they are distinguishable. The system (4.36) is said to be observable at x^0 if x^0 is distinguishable from all x. In order to verify if a system is observable the criterion of Kalman can be used:

the system (4.36) is said to be observable if the rank of the observability matrix

$$\begin{pmatrix} C & CA & CA^2 & \cdots & CA^{n-1} \end{pmatrix}^T \tag{4.59}$$

is equal to the dimension of the state-space.

Consider a non-linear system having the structure (4.43) - (4.44). Let y_u^0 and y_u^1 the out signals generated by applying the input signal u with initial conditions $x(0) = x^0$ and $x(0) = x^1$ respectively. The system is said to be observable at x^0 if x^0 is distinguishable from all x. It is easy to verify that the observability of a nonlinear system is a function of the input u considered. If the system (4.43)-(4.44) is observable for all the possible input u, it is said to be uniformly observable.

In the following sections a linear observer will be designed to estimate the temperature profile and the unknown pollutant concentration in a RFR. This observer will be shown not to be able to estimate the inlet concentration when the system approaches the extinction or when the kinetic parameters are not well known; in this case a non-linear observer will be considered.

4.1.3 *Linear observer design for a RFR*

To apply the observer described above, the balance equation (4.28) has been discretised and re-ordered to obtain the canonical form. The model has been discretised over 200 points: the same numbers of points has been considered both in the inert and in the catalytic monoliths, leading to different space discretisation:

- for $1 \leq i \leq 100$ and $102 \leq i \leq 200$:

$$\left. \frac{\partial T_S(x,t)}{\partial x} \right|_i = \frac{T_S(x_i,t) - T_S(x_{i-1},t)}{\Delta x_k}$$

$$\left. \frac{\partial^2 T_S(x,t)}{\partial x^2} \right|_i = \frac{T_S(x_{i+1},t) - 2T_S(x_i,t) + T_S(x_{i-1},t)}{\Delta x_k^2} \tag{4.60}$$

- for $i = 101$:

$$\frac{\partial T_S(x_{101},t)}{\partial x} = \frac{T_S(x_{101},t) - T_S(x_{100},t)}{\Delta x_1}$$

$$\frac{\partial^2 T_S(x_{101},t)}{\partial x^2} = \frac{T_S(x_{102},t)}{\Delta x_2^2} - \frac{(\Delta x_1 + \Delta x_2) T_S(x_{101},t)}{\Delta x_2^2 \Delta x_1} + \frac{T_S(x_{100},t)}{\Delta x_2 \Delta x_1} \tag{4.61}$$

where $\Delta x_k = x_i - x_{i-1}$. The temperatures in the points x_0 and x_{201} are given by the discretisation of the boundary conditions.

The discretised temperature profile will be denoted by:

$$X(t) = \left(X_1(t), X_2(t), ..., X_{200}(t)\right)^T \tag{4.62}$$

where

$$X_i(t) = T_S(x_i, t) \tag{4.63}$$

$\left(T_S(x_1,t), ..., T_S(x_{100},t)\right)^T$ corresponds to the non reactive monolith compartment ($\Delta x_k = \Delta x_1$) and $\left(T_S(x_{101},t), ..., T_S(x_{200},t)\right)^T$ corresponds to the reactive monolith compartment ($\Delta x_k = \Delta x_2$).

The discretisation of the eq. (4.28) yields to the linear system:

$$\dot{X}(t) = A(\alpha(t))X(t) + B(\alpha(t))U(t) \tag{4.64}$$

where

$$U(t) = \left(T_{G,0}, Q_{ext}(t), \Delta T_{ad}(t)\right)^T \tag{4.65}$$

$$A(\alpha(t)) = \begin{pmatrix} a_4(t) & a_1(t) & 0 & \cdots & \cdots & \cdots & 0 \\ a_3(t) & a_2(t) & a_1(t) & \cdots & \cdots & \cdots & 0 \\ 0 & \ddots & \ddots & \ddots & \cdots & \cdots & 0 \\ \vdots & \ddots & a_{3c}(t) & a_{2c}(t) & a_1(t) & 0 & \vdots \\ \vdots & \ddots & 0 & \ddots & \ddots & \ddots & 0 \\ 0 & \ddots & \ddots & 0 & a_3(t) & a_2(t) & a_1(t) \\ 0 & \cdots & \cdots & \cdots & 0 & a_3(t) & a_5(t) \end{pmatrix} \tag{4.66}$$

$$B(\alpha(t)) = \begin{pmatrix} b_1(t) & 0 & 0 \\ 0 & 0 & 0 \\ \vdots & \vdots & \vdots \\ 0 & 0 & 0 \\ 0 & 0 & \dfrac{P^*\psi(x_{101})}{\tau} \\ \vdots & \vdots & \vdots \\ 0 & 0 & \dfrac{P^*\psi(x_{199})}{\tau} \\ b_2(t) & b_3(t) & \dfrac{P^*\psi(x_{200})}{\tau} \end{pmatrix} \tag{4.67}$$

The coefficients a_i and b_i are given by:

$$a_1(t) = \frac{\lambda_{eff1}}{\Delta x_k^2} \, , \, a_2(t) = -2\frac{\lambda_{eff1}}{\Delta x_k^2} + \frac{D(t)}{\Delta x_k} \, , \, a_3(t) = \frac{\lambda_{eff1}}{\Delta x_k^2} - \frac{D(t)}{\Delta x_k}$$

$$a_4(t) = a_2(t) + a_3(t)\frac{\alpha(t)}{P^*\Delta x_1}\frac{1}{1 + \dfrac{\alpha(t)}{P^*\Delta x_1}}$$

$$a_5(t) = a_2(t) + a_1(t)\frac{1 + N' + \alpha^2(t)}{P^*\Delta x_2}\frac{1}{\left(1 + N'\right)\left(1 + \dfrac{1}{P^*\Delta x_2}\right) + \dfrac{\alpha^2(t)}{P^*\Delta x_2} - \alpha(t)}$$

$$a_{2c} = \left(\Delta x_1 + \Delta x_2\right)\frac{\lambda_{eff1}}{\Delta x_1 \Delta x_2^2} + \frac{D(t)}{\Delta x_1}$$

$$a_{3c} = \frac{\lambda_{eff1}}{\Delta x_1 \Delta x_2} - \frac{D(t)}{\Delta x_1}$$

$$b_1(t) = a_1(t)\frac{1}{1 + \dfrac{\alpha(t)}{P^*\Delta x_1}}$$

$$b_2(t) = a_1(t)\frac{1 + N' - \alpha(t)}{\left(1 + N'\right)\left(1 + \dfrac{1}{P^*\Delta x_2}\right) + \dfrac{\alpha^2(t)}{P^*\Delta x_2} - \alpha(t)}$$

$$b_3(t) = a_1(t)\frac{1}{\rho_{G,0}u_0 c_{p,G}S}\frac{1}{\left(1 + N'\right)\left(1 + \dfrac{1}{P^*\Delta x_2}\right) + \dfrac{\alpha^2(t)}{P^*\Delta x_2} - \alpha(t)}$$

with $D(t) = \dfrac{1 - \alpha(t)}{2\tau}$, $\lambda_{eff1} = \dfrac{1}{\tau P_{ax}^*} + \dfrac{1 + \alpha^2(t)}{2P^*\tau}$.

The state measurements that are used to estimate the state of the system are:

$$\begin{cases} y_1(t) = X_1(t) = T_S(x_1, t) \\ y_2(t) = X_{101}(t) = T_S(x_{101}, t) \\ y_3(t) = X_{200}(t) = T_S(x_{200}, t) \end{cases} \tag{4.68}$$

i.e. the temperature at the inlet of the non-reactive monolith, the temperature at the inlet of the reactive monolith and the temperature at the outlet of the upstream reactive monolith.

The inlet concentrations perturbation is random and can show steep changes over a large interval of values; as the dynamic of ΔT_{ad} is unknown, we assume:

$$\Delta \dot{T}_{ad} = \zeta(t)$$
$$\dot{\zeta}(t) = 0$$

(4.69)

where $\zeta(t)$ is an unknown and bounded function. As a consequence of these assumption, the observer will be based on the following model:

$$\begin{cases} \dot{X}(t) = A(\alpha(t))X(t) + B(\alpha(t))U(t) \\ \Delta \dot{T}_{ad} = \zeta(t) \\ \dot{\zeta}(t) = 0 \\ y_1(t) = X_1(t) = T_S(x_1, t) \\ y_2(t) = X_{101}(t) = T_S(x_{101}, t) \\ y_3(t) = X_{200}(t) = T_S(x_{200}, t) \end{cases}$$

(4.70)

To obtain the canonical form the following notations are used:

$$z^1(t) = \left(z_1^1(t), ..., z_{100}^1(t)\right)^T = \left(X_1(t), ..., X_{100}(t)\right)^T$$

(4.71)

$$z^2(t) = \left(z_1^2(t), z_2^2(t), z_3^2(t)\right)^T = \left(X_{101}(t), \Delta T_{ad}(t), \zeta(t)\right)^T$$

(4.72)

$$z^3(t) = \left(z_1^3(t), ..., z_{99}^3(t)\right)^T = \left(X_{200}(t), ..., X_{102}(t)\right)^T$$

(4.73)

With these notations, the system (4.70) can be rewritten as:

$$\begin{cases} \dot{z}^1 = a_1(t) A^1 z^1(t) + G^1\left(T_{G,0}, \alpha(t), y_2(t), z^1(t)\right) \\ \dot{z}^2 = A^2 z^2(t) + G^{2,*}\left(\alpha(t), y_2(t), z_{100}^1(t), z_{99}^3(t), z^2(t)\right) \\ \dot{z}^3 = A^3 z^3(t) + G^3\left(\alpha(t), y_2(t), z^2(t), z^3(t), T_{G,0}, Q_{ext}\right) \\ y_1(t) = z_1^1(t) = T_S(x_1, t) \\ y_2(t) = z_1^2(t) = T_S(x_{101}, t) \\ y_3(t) = z_1^3(t) = T_S(x_{200}, t) \end{cases}$$

(4.74)

A^1 and A^3 are 100x100 and 99x99 matrices of the form $\begin{pmatrix} 0 & 1 & \cdots & 0 & 0 \\ 0 & 0 & \ddots & 0 & 0 \\ \vdots & \vdots & \ddots & 1 & 0 \\ \vdots & \vdots & \ddots & 0 & 1 \\ 0 & 0 & \cdots & 0 & 0 \end{pmatrix}$;

A^2 is a 3x3 matrix defined by $\begin{pmatrix} 0 & \dfrac{P^*\psi(x_{101})}{\tau} & 0 \\ 0 & 0 & 1 \\ 0 & 0 & 0 \end{pmatrix}$.

The arrays G are given by:

$$G^1(z,t) = \begin{pmatrix} G_1^1(z,t) \\ G_2^1(z,t) \\ \vdots \\ G_{100}^1(z,t) \end{pmatrix} = \begin{pmatrix} a_4(t)z_1^1 + b_1 T_{G,0} \\ a_3(t)z_1^1 + a_2(t)z_2^1 \\ \vdots \\ a_3(t)z_{99}^1 + a_2(t)z_{100}^1 + a_1(t)y_2 \end{pmatrix}$$

$$G^{2,*}(z,t) = \begin{pmatrix} G_1^2(z,t) \\ G_2^2(z,t) \\ G_3^2(z,t) \end{pmatrix} = \begin{pmatrix} a_{3c}(t)z_{100}^1 + a_{2c}(t)z_1^2 + a_1(t)z_{99}^3 \\ 0 \\ 0 \end{pmatrix}$$

$$G^3(z,t) = \begin{pmatrix} G_1^3(z,t) \\ G_2^3(z,t) \\ \vdots \\ G_{99}^3(z,t) \end{pmatrix} = \begin{pmatrix} a_5(t) + b_2(t)T_{G,0} + b_3(t)Q_{ext} \\ a_1(t)z_1^3 + a_2(t)z_2^3 \\ \vdots \\ a_1(t)z_{97}^3 + a_2(t)z_{98}^3 \\ a_1(t)z_{98}^3 + a_2(t)z_{99}^3 + a_3(t)y_2 \end{pmatrix} + \begin{pmatrix} \dfrac{P^*\psi(x_{200})}{\tau}z_2^2 \\ \dfrac{P^*\psi(x_{199})}{\tau}z_2^2 \\ \vdots \\ \dfrac{P^*\psi(x_{103})}{\tau}z_2^2 \\ \dfrac{P^*\psi(x_{102})}{\tau}z_2^2 \end{pmatrix}$$

G^1 and G^2 have the desired structure stated in (4.53); $G^{2,*}$ has to be transformed into the canonical structure (4.50). It is possible to write:

$$G^{2,*} = d^2(t) + G^2(z,t) \tag{4.75}$$

where

$$d^2(t) = \begin{pmatrix} a_1(t)\left(z_{99}^3(t) - z_1^2(t)\right) \\ 0 \\ 0 \end{pmatrix} \qquad G^2(z,t) = \begin{pmatrix} a_{3c}(t)z_{100}^1(t) + \left(a_1(t) + a_{2c}(t)\right)z_1^2(t) \\ 0 \\ 0 \end{pmatrix}.$$

The observer for the system (4.74) takes the form:

$$\begin{cases} \dot{\hat{z}}^1(t) = a_1(t) A^1 \hat{z}^1 + G^1(\hat{z},t) - a_1(t) \Delta_{1\Omega} K^1\left(\hat{z}_1^1 - y_1(t)\right) \\ \dot{\hat{z}}^2(t) = A^2 \hat{z}^2 + G^2(\hat{z},t) - \Lambda_2^{-1} \Delta_{2\Omega} K^2\left(\hat{z}_1^2 - y_2(t)\right) \\ \dot{\hat{z}}^3(t) = a_3(t) A^3 \hat{z}^3 + G^3(\hat{z},t) - a_3(t) \Delta_{3\Omega} K^3\left(\hat{z}_1^3 - y_3(t)\right) \\ y_1(t) = z_1^1(t) = T_S(x_1,t) \\ y_2(t) = z_1^2(t) = T_S(x_{101},t) \\ y_3(t) = z_1^3(t) = T_S(x_{200},t) \end{cases}$$

(4.76)

where $\Lambda_2(t) = \begin{pmatrix} 1 & 0 & 0 \\ 0 & \dfrac{P^*\psi(x_{101})}{\tau} & 0 \\ 0 & 0 & \dfrac{P^*\psi(x_{101})}{\tau} \end{pmatrix}$.

The gains of the observer (K^1, K^2, K^3 and Ω) are obtained as follows:

- for each i = 1, 2, 3 a set of complex numbers $E = \left\{\lambda_1^i,...,\lambda_{n_i}^i\right\}$ is set, such that $\mathrm{Re}\left(\lambda_j^i\right) < 0$ and for every $\lambda_i \in E$ its conjugate $\bar{\lambda}_i \in E$;

- the gain's coefficients $\left(k_1^i,...,k_{n_i}^i\right)$ are calculated such that $\left(\lambda_1^i,...,\lambda_{n_i}^i\right)$ coincide with the eigenvalues of the matrix
$$\begin{pmatrix} k_1^i & 1 & \cdots & 0 & 0 \\ k_2^i & 0 & \ddots & 0 & 0 \\ \vdots & \vdots & \cdots & \vdots & \vdots \\ k_{n_i-1}^i & 0 & \cdots & 0 & 1 \\ k_{n_i}^i & 0 & \cdots & 0 & 0 \end{pmatrix}$$. The Ackermann's formula has been used;

- the choice of Ω is obtained from simulation. Indeed, many values of Ω have been tested as this values influences the dynamic of the estimated variables. Good results are obtained with $\Omega = 1$.

4.1.4 *Experimental validation of the linear observer*

The observer has been validated on-line under the following conditions:

- the reactor is ignited and $Q_{ext} = 0$;
- the external temperature is $T_{G,0} = 293K$;
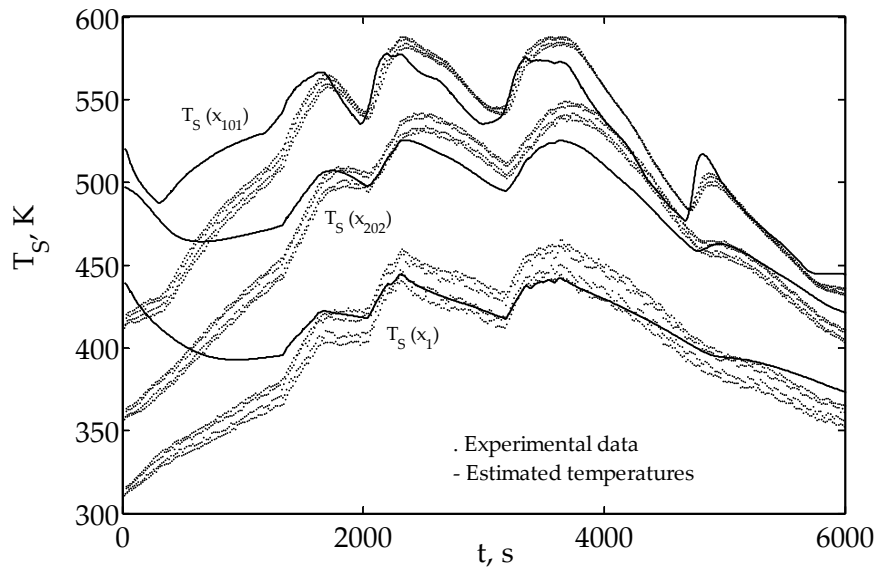- the inlet concentration perturbation is randomly varied.

Figure 4.6: Comparison between the measured and the estimated values of the temperatures at the inlet of the non-reactive monolith, at the inlet of the reactive monolith and at the outlet of the upstream monolith.

The measured temperatures at the inlet of the non-reactive monolith, at the inlet of the reactive monolith and at the outlet of the upstream monolith, together with their on-line estimation are plotted in Figure 4.6. Good agreement between estimation and measurements is obtained; moreover the observer play the role of a filter (the high frequencies are eliminated) and the estimated temperatures are smooth.

Figure 4.7 shows the comparison between the estimated values of the inlet concentration and the measured one; also in this case good agreement is obtained, even when steep variations are considered.
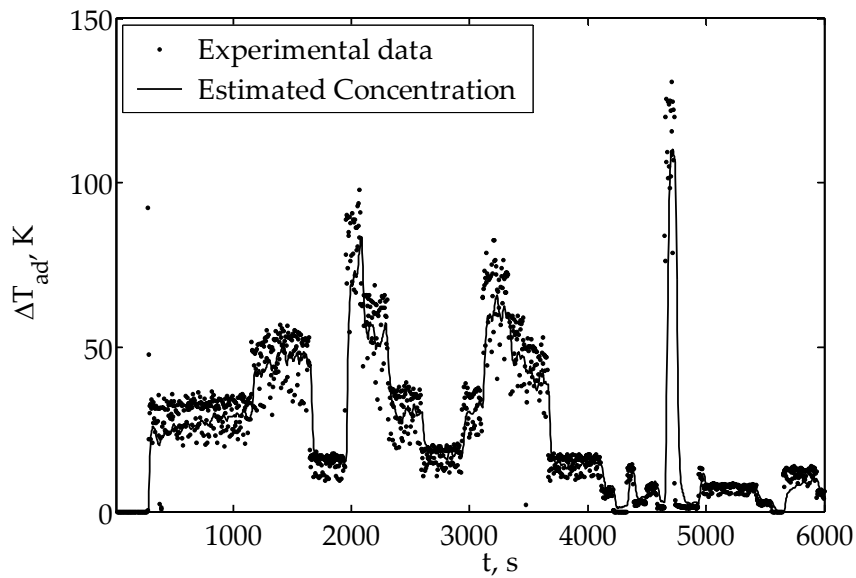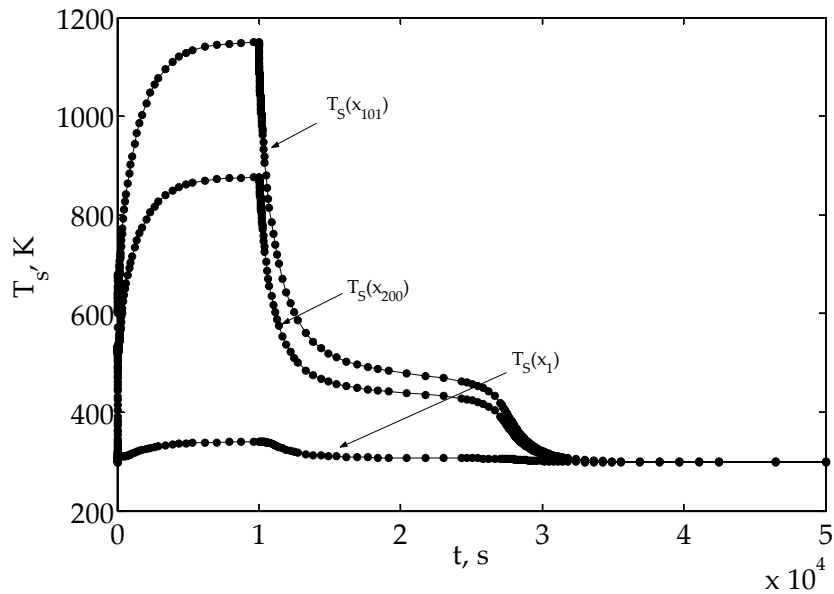
Figure 4.7: Comparison between the measured and the estimated values of the inlet concentration.

The linear observer design was based on the pseudo-homogeneous model of a countercurrent reactor with the correction for the finite flow reversal frequency; the main assumption of the model is that the reaction is instantaneous and under mass transfer control. This assumption implies that it will be impossible to predict the extinction phenomenon. Conversely, the model is independent of any chemical kinetic data.

Figure 4.8 compares the prediction of the observer and the simulated values of inlet concentration when extinction is considered, pointing out that when extinction takes place the observer estimate an inlet concentration equal to zero. In any case the observer is able to give correct prediction of the temperature evolution both in the inert and in the catalytic sections of the monolith (Figure 4.9).
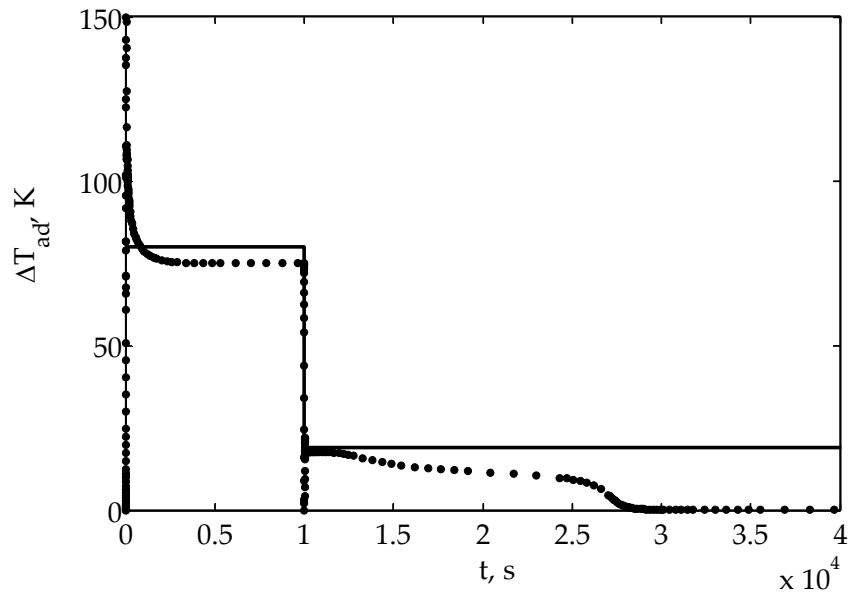
Figure 4.8: Comparison between the measured and the simulated values of the inlet concentration when extinction takes place.

Figure 4.9: Comparison between the simulated and the estimated values of the temperatures at the inlet of the non-reactive monolith, at the inlet of the reactive monolith and at the outlet of the upstream monolith.

4.1.5 *Non-linear observer design for a RFR*

In order to derive an observer able to estimate the inlet concentration also when extinction takes place and when kinetic data are important or unknown (for example when the pollutants fed to the reactor changes or

when the catalyst is deactivating), the model equations (4.28) has to be changed, taking into account the reaction rate (which is no longer under mass transfer control), leading to:

$$\left(\frac{1}{P_{ax}}+\frac{1+\alpha^2}{2P}\right)\frac{\partial^2 T_S}{\partial z^2}+\frac{1-\alpha}{2}\frac{\partial T_S}{\partial z}+\frac{a_c(-\Delta H)H/2}{\rho_{G,0}u_0 c_{p,G}}\frac{r_{S,1}}{2}=\tau\frac{\partial T_S}{\partial t} \tag{4.77}$$

with the assumption that the contribution of the second monolith to the reaction rate is negligible.

The discretisation of the equation (4.77) leads to a system analogous to (4.64); the only difference is due to the third column of $B(\alpha(t))$, where the

terms $\dfrac{P^*\psi(x_i)}{\tau}$ are now replaced by $\dfrac{P^*\Delta T_{ad}}{2\tau}\dfrac{k_0}{k_D}e^{-\frac{E_a}{RT_S(x_i)}}M(x_i)$, thus giving rise

to non-linearity as $M(x_i)=\displaystyle\prod_{k=1}^{i}\Lambda(x_k)\cdot\prod_{k=1}^{i-1}K(x_k)$, $K(x_i)=1+\dfrac{k_0}{k_D}e^{-\frac{E_a}{RT_S(x_i)}}$,

$$\Lambda(x_i)=\frac{\alpha}{\left\{1+\dfrac{k_0}{k_D}e^{-\frac{E_a}{RT_S(x_i)}}\right\}\{\alpha+P\Delta x_2\}-P\Delta x}.$$

As in the previous case, the system has to be written in a canonical structure (Hammouri and Farza, 2003):

$$\begin{cases}\dot{z}^1=a_1(t)A^1 z^1(t)+G^1\left(T_{G,0},\alpha(t),y_2(t),z^1(t)\right)\\\dot{z}^2=A^2 z^2(t)+G^{2,*}\left(\alpha(t),y_2(t),z^1_{100}(t),z^3_{99}(t),z^2(t)\right)\\\dot{z}^3=A^3 z^3(t)+G^3\left(\alpha(t),y_2(t),z^2(t),z^3(t),T_{G,0},Q_{ext}\right)\\y_1(t)=z^1_1(t)=T_S(x_1,t)\\y_2(t)=z^2_1(t)=T_S(x_{101},t)\\y_3(t)=z^3_1(t)=T_S(x_{200},t)\end{cases} \tag{4.78}$$

where now

$$z^2(t)=\left(z^2_1(t),z^2_2(t),z^2_3(t),z^2_4(t)\right)^T=\left(X_{101}(t),\Delta T_{ad}(t),\zeta(t),\frac{k_0}{k_D}\right)^T \tag{4.79}$$

A^1 and A^3 are 100x100 and 99x99 matrices of the form $\begin{pmatrix} 0 & 1 & \cdots & 0 & 0 \\ 0 & 0 & \ddots & 0 & 0 \\ \vdots & \vdots & \ddots & 1 & 0 \\ \vdots & \vdots & \ddots & 0 & 1 \\ 0 & 0 & \cdots & 0 & 0 \end{pmatrix}$;

A^2 is a 4x4 matrix defined by $\begin{pmatrix} 0 & 0 & 0 & 0 \\ 0 & 0 & 1 & 0 \\ 0 & 0 & 0 & 0 \\ 0 & 0 & 0 & 0 \end{pmatrix}$.

The arrays G are given by:

$$G^1(z,t) = \begin{pmatrix} G_1^1(z,t) \\ G_2^1(z,t) \\ \vdots \\ G_{100}^1(z,t) \end{pmatrix} = \begin{pmatrix} a_4(t)z_1^1 + b_1 T_{G,0} \\ a_3(t)z_1^1 + a_2(t)z_2^1 \\ \vdots \\ a_3(t)z_{99}^1 + a_2(t)z_{100}^1 + a_1(t)y_2 \end{pmatrix}$$

$$G^{2,*}(z,t) = \begin{pmatrix} G_1^2(z,t) \\ G_2^2(z,t) \\ G_3^2(z,t) \\ G_4^2(z,t) \end{pmatrix} = \begin{pmatrix} a_{3c}(t)z_{100}^1 + a_{2c}(t)z_1^2 + a_1(t)z_{99}^3 + \Lambda(z_1^2) \\ 0 \\ 0 \\ 0 \end{pmatrix}$$

$$G^3(z,t) = \begin{pmatrix} G_1^3(z,t) \\ G_2^3(z,t) \\ \vdots \\ G_{99}^3(z,t) \end{pmatrix} = \begin{pmatrix} a_5(t) + b_2(t)T_{G,0} + b_3(t)Q_{ext} \\ a_1(t)z_1^3 + a_2(t)z_2^3 \\ \vdots \\ a_1(t)z_{97}^3 + a_2(t)z_{98}^3 \\ a_1(t)z_{98}^3 + a_2(t)z_{99}^3 + a_3(t)y_2 \end{pmatrix} + \begin{pmatrix} M(x_{200}) \\ M(x_{199}) \\ \vdots \\ M(x_{103}) \\ M(x_{102}) \end{pmatrix}$$

The observer's gain for the state z^1 and z^3 have the same form previously stated, while for the state z^2 it results (Hammouri and Farza, 2003):

$$\dot{\hat{z}}^2(t) = A^2 \hat{z}^2 + G^2(\hat{z},t) - \Lambda \Delta_{2\Omega} K^2 (\hat{z}_1^2 - y_2(t)) \tag{4.80}$$

with $\Delta_{2\Omega} = \begin{pmatrix} \Omega & 0 & 0 & 0 \\ 0 & \Omega & 0 & 0 \\ 0 & 0 & \Omega^2 & 0 \\ 0 & 0 & 0 & \Omega^2 \end{pmatrix}$, $\Lambda = \left[\left(\dfrac{\partial \psi}{\partial z^2}\right)^T \left(\dfrac{\partial \psi}{\partial z^2}\right) \right]^{-1} \left(\dfrac{\partial \psi}{\partial z^2}\right)^T$, $\psi = \begin{pmatrix} z_1^2 \\ G_1^2(z^2) \\ \dfrac{\partial G_1^2}{\partial z_2^2} z_3^2 \end{pmatrix}$.

When the estimated conversion is equal to 1 the reaction is under diffusive control and the system is linear and the linear observer is used. When the estimated conversion starts decreasing the reaction becomes under kinetic

control and the non-linear observer is implemented in order to evaluate the inlet concentration and the kinetic parameters.

4.1.6 *Validation of the non-linear observer*

The proposed observer has been validated by means of simulations (Fissore *et al.*, 2003c); the complete model has been considered as a source of experimental data. Figure 4.10 shows a comparison between the prediction of the observer and the simulated values of inlet concentration and outlet conversion in the case of xylene combustion; fast and accurate reponse without overshoot are obtained for both variables even when steep changes are considered. The predictions are reliable both when the conversion is equal to 1 and when the reaction is extinguishing; it is important to point out that when the reaction is extinguished the temperatures quickly moves down to the ambient value and the system is no longer observable. The same accuracy is obtained when different pollutants (with different concentration and unknown kinetic parameters) are considered to be fed to the reactor as it is shown in Figure 4.11.
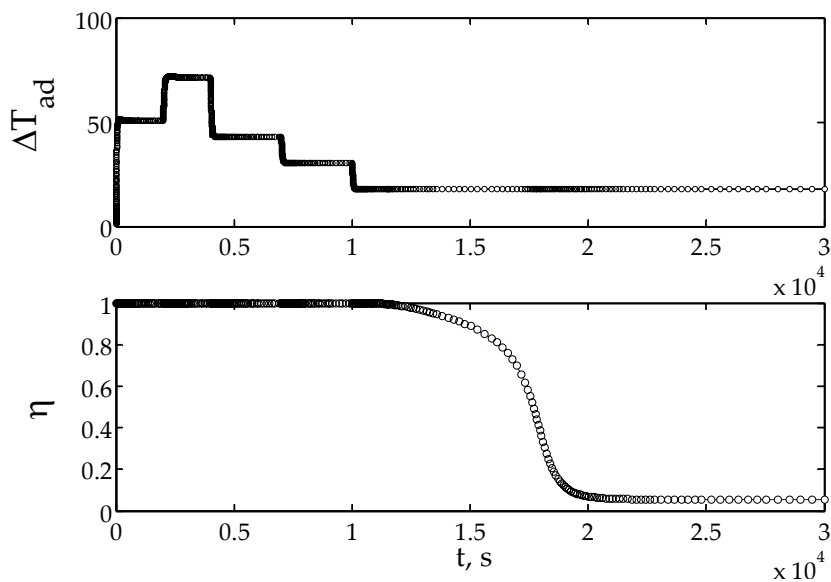
Figure 4.10: Comparison between the prediction of the observer (circle) and the simulated values (line) of the inlet concentration and outlet conversion when xylene combustion takes place.
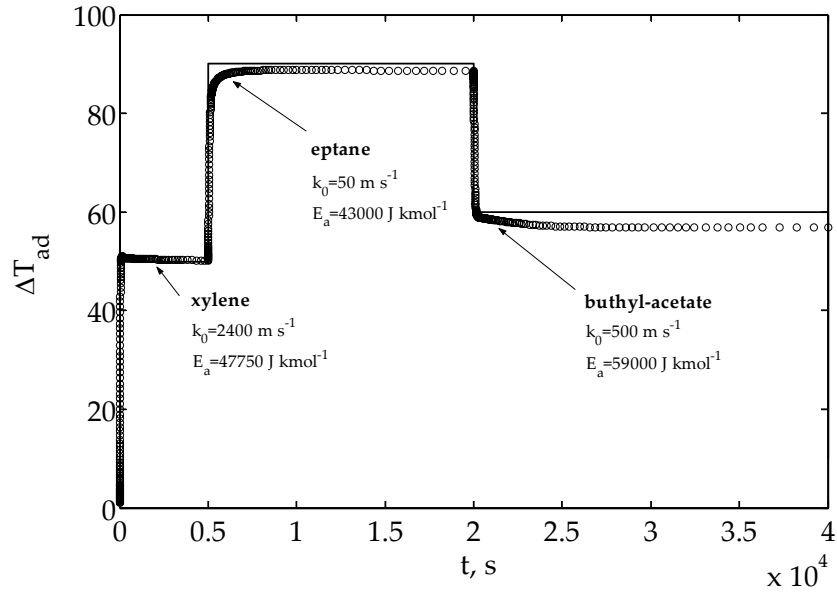
Figure 4.11: Comparison between the prediction of the observer (circle) and the simulated values (line) of the inlet concentration and outlet conversion when different compounds are fed to the reactor (kinetic parameters are taken from Ramdani, 2001).

A further test has been accomplished considering random changes in the frequency factor, activation energy and inlet composition of the reactor feed; this may simulate the change of the kinetic parameter due to catalyst fouling or deactivation. Also in this situation the estimations of the observer are close to the correct values (Figure 4.12).
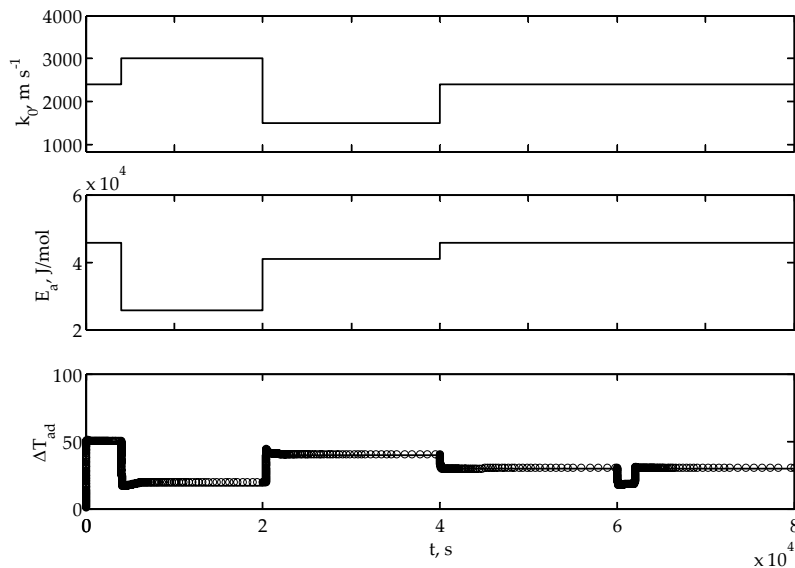
Figure 4.12: Comparison between the prediction of the observer and the simulated values of inlet concentration (lower graph) when the kinetic parameters of the pollutant changes (upper graphs).

4.2 The control system

Among the various applications for the observers, perhaps the most important is for the implementation of closed-loop control algorithms designed by state-space methods (Figure 4.13). The control algorithm is designed in two parts: a "full-state feedback" part based on the assumption that all the state variables can be measured, and an observer to estimate the state of the process based upon the measured output. The concept of separating the feedback control design into these two parts is known as the *separation principle*, which has rigorous validity in linear systems and in a limited class of nonlinear systems. Even when its validity cannot be rigorously established, the separation principle us often a practical solution to many design problems (Friedland, 1996).

In this work an approach similar to that of Purwono *et al*. (1994) has been used (Fissore *et al.*, 2003b). By means of numerical simulation a stability map of the reactor can be obtained (Figure 4.14) for a particular value of the inlet flow rate; similar diagrams can be obtained for other values of the flow rate (in the range of feasible values), thus leading to the definition of regions where maximum temperature (or conversion) is higher or lower than a certain value. Because of process constraints on outlet conversion and maximum temperature on the solid, a well defined operating region is obtained; in Figure 4.13 the region corresponding to conversion higher than 99.95 % and maximum solid temperatures lower than 650 °C is evidenced. In the definition of the operating region it is also possible to take into account modelling error by defining a percentage uncertainty over these curves.
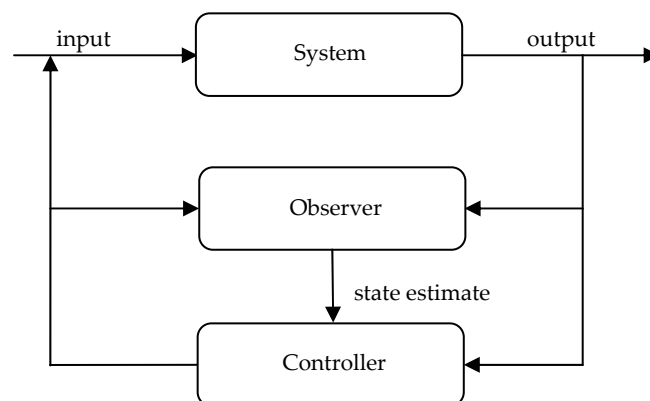

Figure 4.13: An observer in a control loop.

Until the point corresponding to the operating conditions (inlet concentration and switching period) is in the optimal region no control action is taken; if the inlet concentration increases too much, the control system has two possibilities: it may increase the switching time (as the maximum temperature slightly decreases when the switching time is increased) or, if this is not sufficient, it may dilute the feed. If the inlet concentration decreases too much a control action is taken just when the outlet conversion starts decreasing (because of the thermal inertia of the system, the reactor is able to sustain periods of low inlet concentration, with no decrease in the outlet conversion): either the switching time is reduced, if this can increase the conversion, or auxiliary fuel is added when the inlet concentration is lower than the minimum value that allows adiabatic operation.
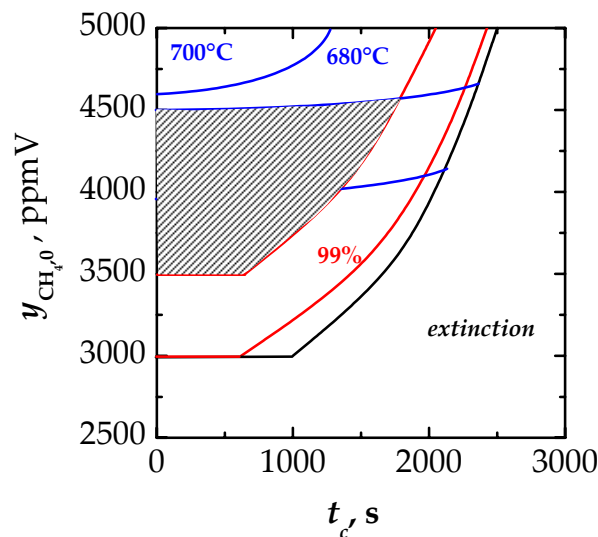
Figure 4.14: Example of stability map of a RFR (inlet gas velocity 0.14 m s^{-1}): the black line separates the region where extinction occurs from the region where stable operation can be obtained; red lines separate the regions where conversion is larger (upper part) or lower than the specified value; blue lines separate the regions where maximum solid temperature is higher (upper part) or lower than the specified value ($u_0 = 0.14$ m s^{-1}).

In the example of Figure 4.15 no changes in the switching time (as it can easily understood by looking at Figure 4.16) may be useful to avoid higher solid temperatures and low conversion; as a consequence dilution and injection of auxiliary fuel are needed.

In example of Figure 4.17 a reduction of the switching time is sufficient to avoid any conversion decrease (see Figure 4.18). The subsequent increase in

the inlet concentration doesn't require any control action as the system remains in the optimal region.
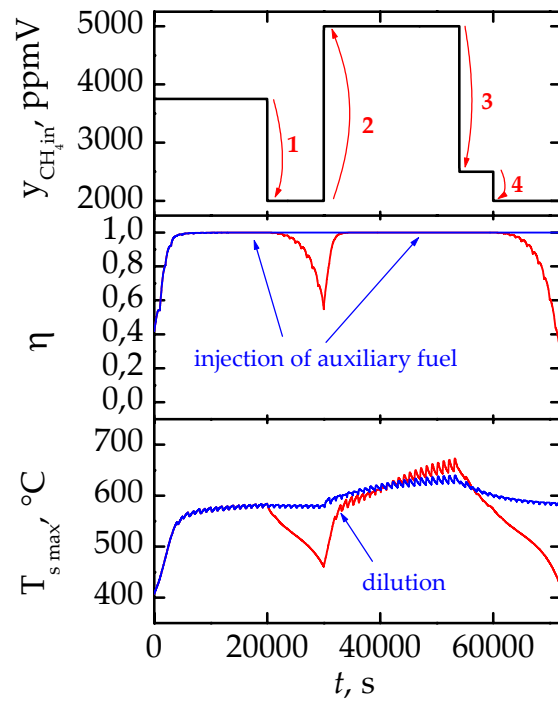

Figure 4.15: Maximum solid temperature and outlet conversion in a RFR with the inlet concentration is varied according to the upper graph. Dilution and injection of auxiliary fuel are evaluated in order to carry the inlet conditions in the optimal operating region. The behaviour with (blue line) and without (red line) control system is compared.
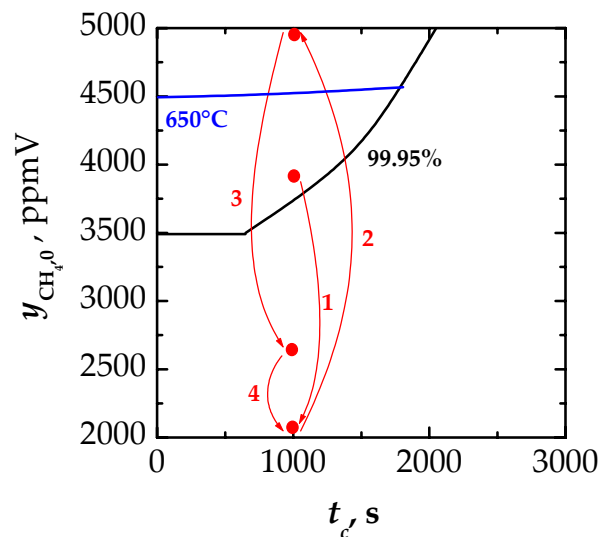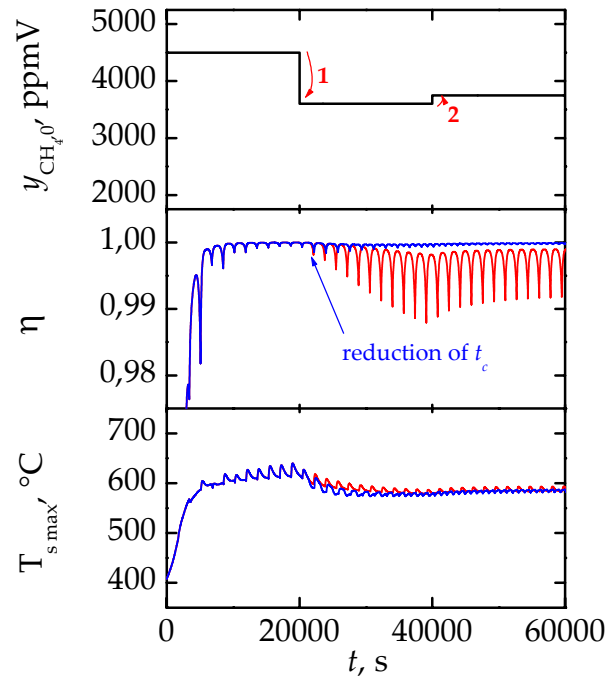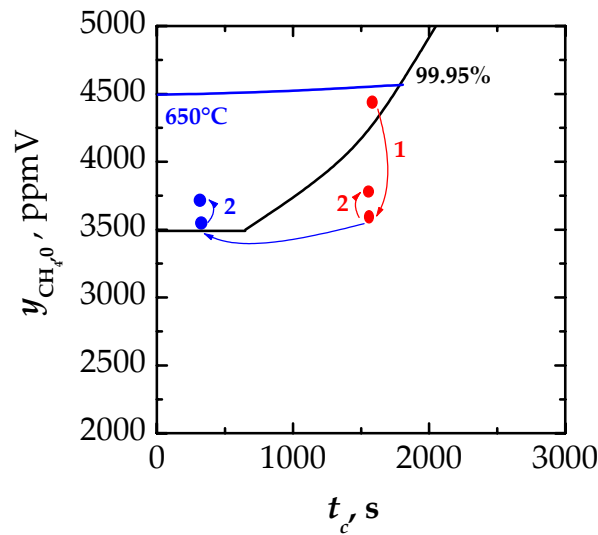

Figure 4.16: Changes in the inlet concentration considered in Figure 4.15.

Figure 4.17: Maximum solid temperature and outlet conversion in a RFR with the inlet concentration is varied according to the upper graph. Dilution and injection of auxiliary fuel are evaluated in order to carry the inlet conditions in the optimal operating region. The behaviour with (blue line) and without (red line) control system is compared.

Figure 4.18: Changes in the inlet concentration considered in Figure 4.17.

This simple control strategy is able to avoid any control action when this is useless, even if the inlet flow rate and concentration changes; moreover is able to lower the maximum temperature below the limit value of the catalyst and to maintain unitary conversion. When acting on the switching time is not

sufficient, maximum temperature is decreased by dilution of the feed, which has been proven to be the simplest and more effective control action to achieve the desired result and unitary conversion is guaranteed by injection of auxiliary fuel.

In order to apply this control strategy we need to know both the inlet flow rate (and this is easy to do and inexpensive) and the inlet concentration. As on-line measurements may be difficult and expensive, a soft-sensor based on high gain techniques can be used to estimate the inlet concentration from some temperature measurements. The soft-sensor has been demonstrated to give correct prediction of inlet concentration and outlet conversion both when the reactor is fully ignited and when conversion is decreasing.

The proposed control system has been validated experimentally both in the case of reaction extinction and in the case of catalyst overheating. In a first run an inlet concentration of methane of 3500 ppmV is fed to the reactor in the time interval 0-10000 s (t_c=990 s) and then the inlet concentration decreases to 3050 ppmV (without changing the switching time). When no control action is implemented on the device the outlet methane concentration starts increasing and the reaction moves towards extinction (Figure 4.19).
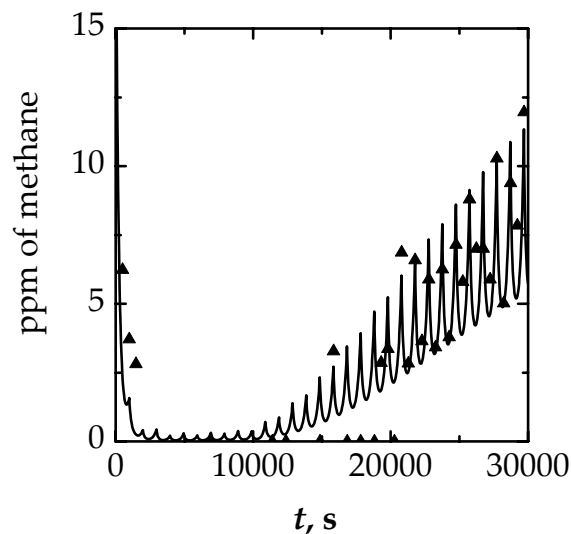

Figure 4.19: Comparison between the predicted (continuous line) and the experimental values (symbols) of the outlet methane concentration in the RFR (t_c = 990s, metal oxide-based catalyst).

According to the previous simulation results (assuming a maximum outlet concentration of methane of 1 ppmV and a maximum temperature of the solid of 650 °C), when the inlet concentration decreases, the switching time

should be reduced to 150 s. Figure 4.20 shows that this control action is able to maintain complete conversion in the reactor; moreover the temperature in the reactor remains below the maximum value required by the catalyst used (Figure 4.21 shows the comparison between the predicted and the measured values of the solid temperatures in the seven sections of the reactor).
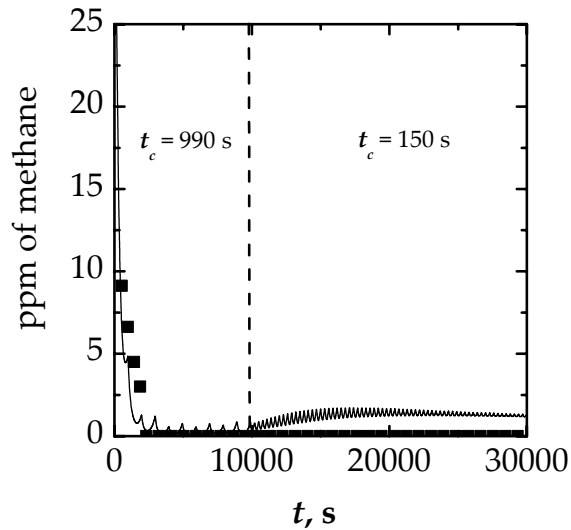

Figure 4.20: Comparison between the predicted (continuous line) and the experimental values (symbols) of the outlet methane concentration in the RFR (t_c = 990s up to 10000s, t_c = 150s after, metal oxide-based catalyst).
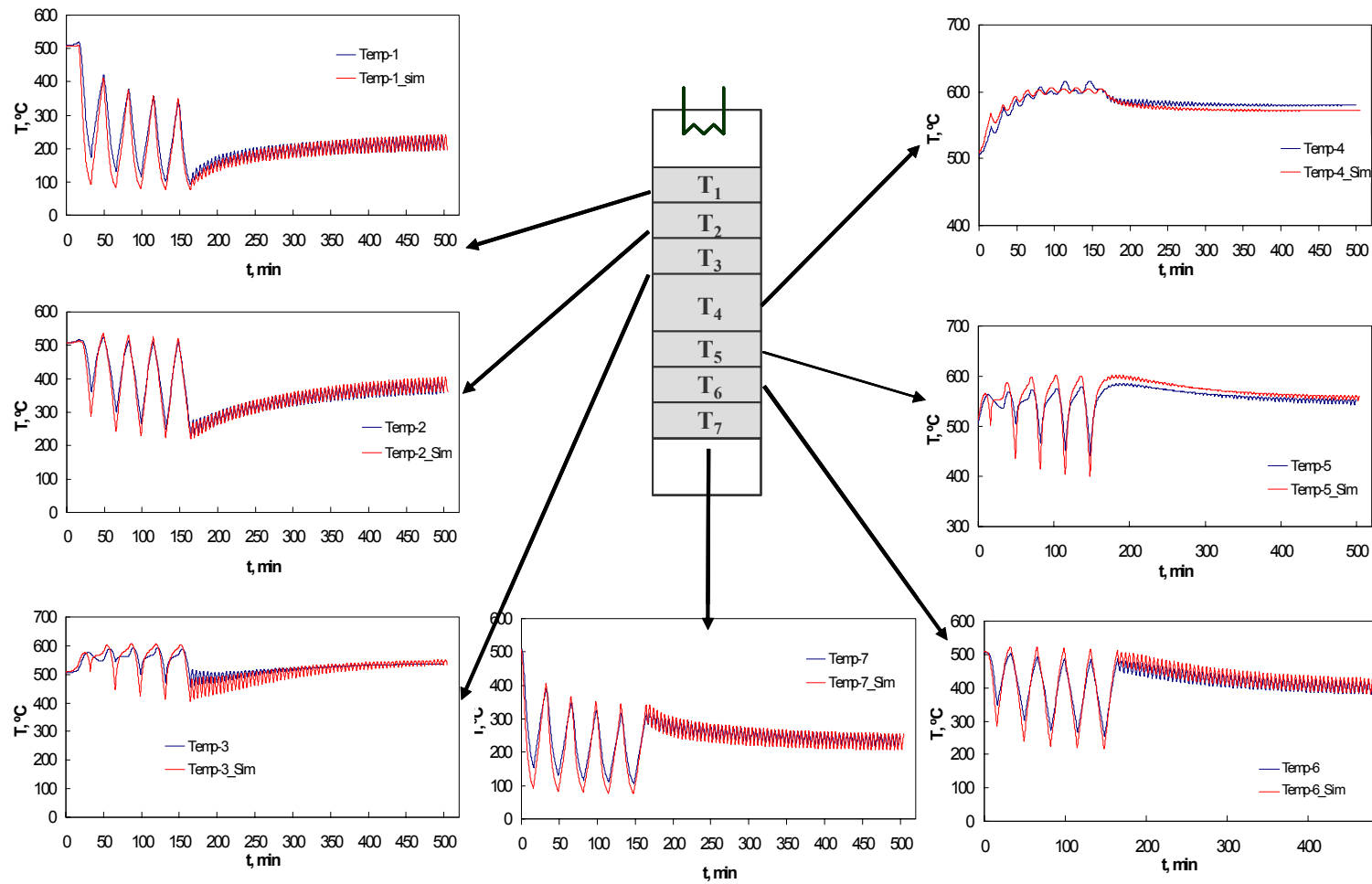
Figure 4.21: Comparison between the simulated and the experimental values of the solid temperature when the inlet concentration changes at 10000s from 3500 ppmV to 3050 ppmV and the switching time is changed from 990 s to 150 s. The values of the temperatures in the seven sections of the reactor are shown.

In a second run an inlet concentration of methane of 3500 ppmV is fed to the reactor in the time interval 0-4440 s (t_c =150 s) and then the inlet concentration increases to 3950 ppmV (without changing the switching time). When no control action is implemented on the devices the solid maximum temperature stars increasing, rapidly moving towards the maximum allowable value for the catalyst used (see for example the temperatures in the sections 3, 4 and 5 in Figure 4.22). According to the simulation results, when the inlet concentration changes the value of the switching time is changes to 990 s and the maximum value of the solid temperature remains below the limit for the catalyst (Figure 4.23).
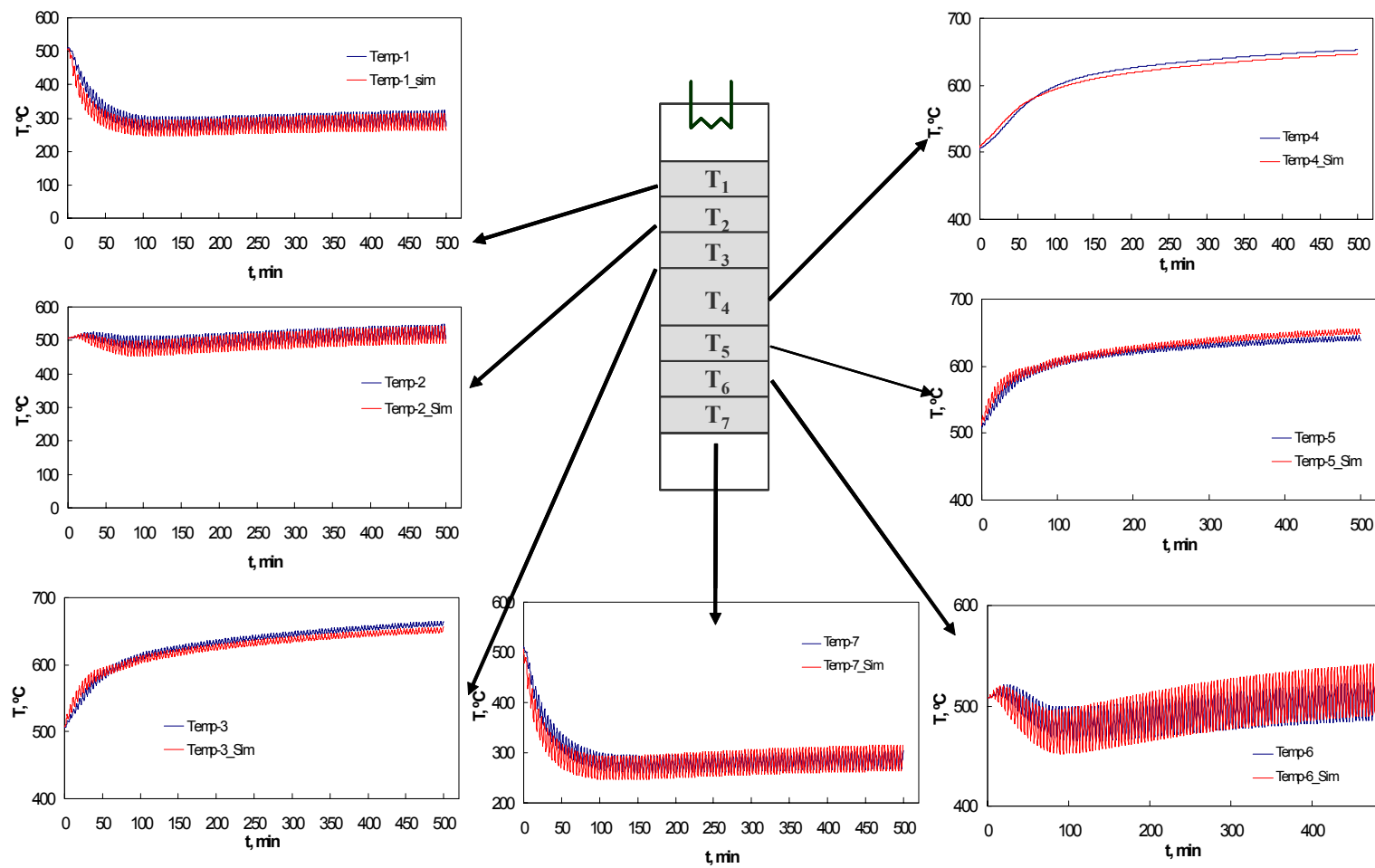
Figure 4.22: Comparison between the simulated and the experimental values of the solid temperature when the inlet concentration changes at 4440s from 3500 ppmV to 3950 ppmV (t_c = 150 s) . The values of the temperatures in the seven sections of the reactor are shown..
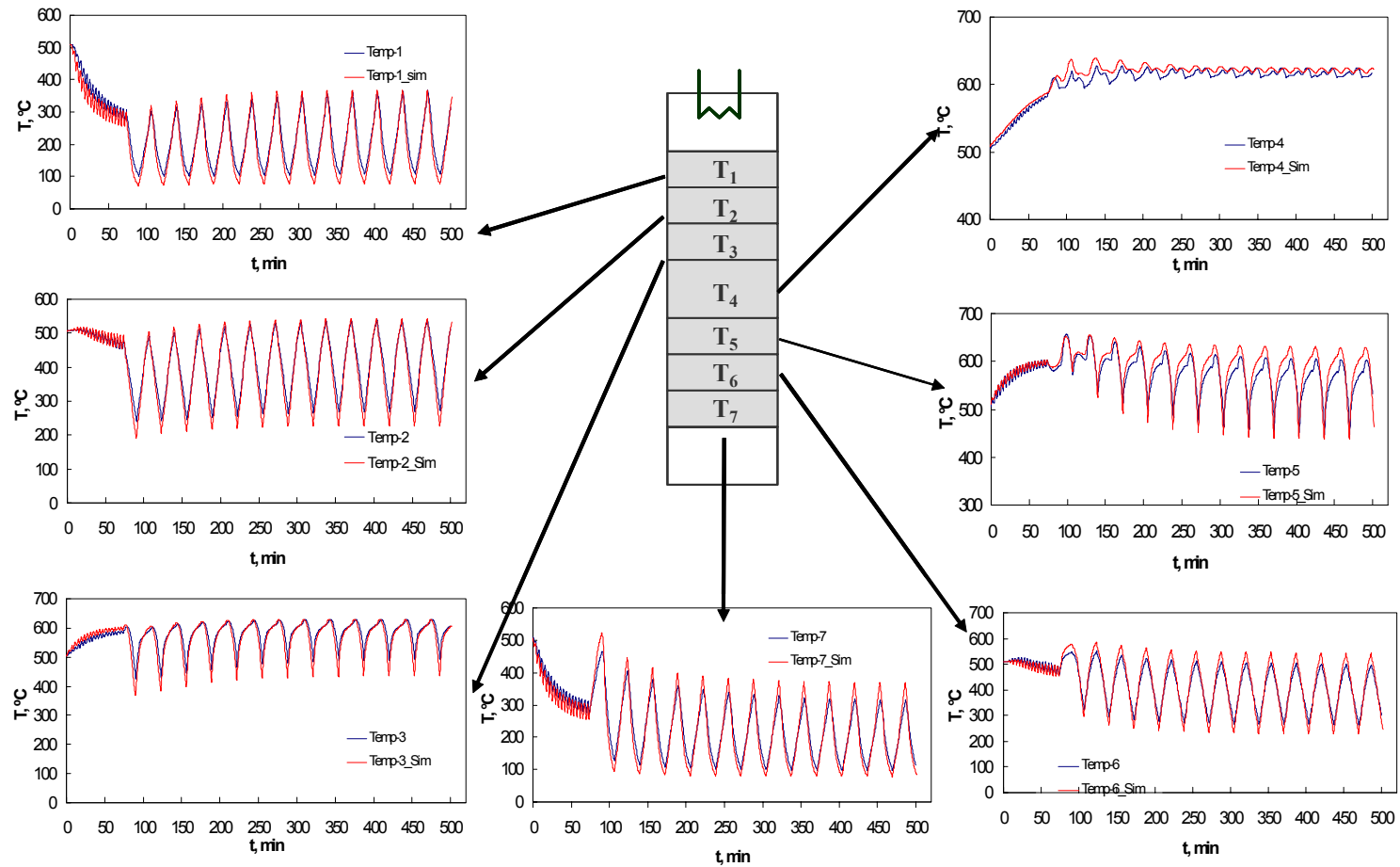
Figure 4.23: Comparison between the simulated and the experimental values of the solid temperature when the inlet concentration changes at 4440s from 3500 ppmV to 3950 ppmV; the switching time is changed from a value of 150 s to 990 s when the inlet concentration increases. The values of the temperatures in the seven sections of the reactor are shown.

112

Chapter 5

Exothermic equilibrium-limited reactions in forced unsteady-state reactors

Beside the possibility of exploiting the thermal storage capacity of a catalytic bed, the forced operation mode may give rise to optimum temperature distribution, which makes possible the creation of favourable thermodynamic conditions for exothermic equilibrium-limited reactions and endothermic processes, as it has been pointed out in (§1).

In the 1990s attempts were made to use unsteady-state reactors to produce synthesis gas by partial oxidation of methane (POM), followed by adiabatic catalytic steam reforming. Gosiewski *et al.* (1999, 2000, 2001) considered a reactor with forced composition cycling: firstly methane and oxygen are supplied and the strongly exothermal complete combustion reaction takes place, then the components for endothermic reforming reactions are introduced (methane and water); the results showed that higher conversion and selectivity can be obtained in comparison to a reactor operating at a constant (averaged) composition of the reacting mixture.

Despite the strongly exothermal methane combustion reaction, the whole process is only weakly exothermal, due to the simultaneous occurring of endothermic reactions; as a consequence the feasibility of this process in a RFR has been considered (Blanks *et al.*, 1990). The catalyst bed is pre-heated to a uniform temperature and the reactant mixture is fed at considerably lower temperature: the cold feed is progressively heated by the catalyst bed

and at a certain depth the exothermic combustion reaction takes place, leading to a temperature rise in the bed. Before reaction front reaches the end of the catalyst bed, the flow direction of the gas is reversed, so that the heat front starts moving in the opposite direction: the catalyst bed is used simultaneously as chemical reactor and heat exchanger (De Groote and Froment, 1995).

In this thesis the syngas production in a RN has been investigated as an alternative to the well investigated RFR and the influence of the main operating parameters will be pointed out by means of numerical simulations. Vanden Bussche *et al.* (1993) showed that methanol synthesis in a RFR can lead to higher conversion and selectivity in comparison with steady-state operation; nevertheless, RFR presents the problem of wash-out, i.e. the drop in product concentration upon flow reversal, due to the removal of unconverted gas immediately after the change of the inlet section. Velardi and Barresi (2002) investigated application of the RN to methanol synthesis showing that this device allows for higher conversion than the RFR and it is not significantly affected by wash-out at the beginning of the cycle. Furthermore, a proper choice of the switching time allows for slight variation of the outlet gas temperature along the cycle, differently from the RFR, thus reducing potential disturbances of the equipment downward. In this thesis the feasibility of carrying out methanol synthesis in the RN will be addressed, with the aim to maximise conversion and selectivity.

5.1 Synthesis gas production in the RN

The feasibility of the production of synthesis gas in a RN as an alternative to the well investigated RFR has been investigated by means of numerical simulations (Fissore *et al.* 2002, 2003a, 2004).

A one-dimensional two-phase model has been used for the simulation of the adiabatic network of three reactors. Mass and energy dispersive transport has been taken into account as well as the transient terms in the gas phase equation and in the energy balance for the solid, while the solid catalytic surface is considered in quasi steady-state condition. The pressure loss inside the reactor is neglected. The effect of the intraparticle mass transport has been taken into account by including in the model the effectiveness factors, which have been estimated following the linearization method proposed by

Gosiewski *et al.* (1999). Conventional Danckwerts boundary conditions are assumed at the inlet section of the network; the continuity of gas temperature and concentration profiles are imposed between the reactors of the network. In addition spatial derivatives should vanish at the outlet section. Initially, gas phase and solid temperature are considered equal and constant along the reactors; the initial reactants concentration is null. More details about the model can be found in (§3.1).

The process is considered to take place on a Pt/MgO catalyst; the reactions are the followings:

(A) $CH_4 + 2O_2 \rightarrow CO_2 + 2H_2O$ (5.1)

(B) $CH_4 + H_2O \rightarrow CO + 3H_2$ (5.2)

(C) $CH_4 + CO_2 \rightarrow 2CO + 2H_2$ (5.3)

(D) $CO + H_2O \rightarrow CO_2 + H_2$ (5.4)

and the reaction rates are given by the following equations (the kinetic parameter can be found in Gosiewski *et al.*, 1999):

$$R'_A = k'_{ps,A} c_{CH_4} c_{O_2}$$ (5.5)

$$R'_B = k'_{ps,B} c_{CH_4} c_{H_2O} \left(1 - \frac{p_{H_2}^3 p_{CO}}{K_{p,B} p_{CH_4} p_{H_2O}} \right)$$ (5.6)

$$R'_C = k'_{ps,C} c_{CH_4} c_{CO_2} \left(1 - \frac{p_{H_2}^2 p_{CO}^2}{K_{p,C} p_{CH_4} p_{CO_2}} \right)$$ (5.7)

$$R'_D = k'_{ps,D} c_{CO} c_{H_2O} \left(1 - \frac{p_{H_2} p_{CO_2}}{K_{p,D} p_{CO} p_{H_2O}} \right)$$ (5.8)

The conditions adopted in the simulations for the base case are given in Table 5.1.

The influence of the feed composition on the partial oxidation of methane for production of synthesis gas has been discussed in detail by De Groote and Froment (1996b); in this work only the influence of the H_2O/CH_4 and CH_4/O_2 ratio has been investigated. Small amounts of CO and CO_2 have been considered in the feed to avoid problems with initial reaction rates, as these compounds appear in the denominator of the kinetic rates adopted. Some hydrogen in the feed can avoid methane cracking in the front part of the reactor, even if it cannot avoid carbon deposition in the reactor; its molar

fraction is reduced to about 2% in the tests with variable H_2O/CH_4 and CH_4/O_2 ratios, to balance the variation of the other species. Relatively large amounts of water have been considered to avoid coking.

The influence of inlet temperature and gas velocity has also been investigated; a single reactor length has been considered here, but it must be pointed out that length, gas velocity and switching time are closely related and a proper range of suitable switching time can be found for any reasonable choice of the first two parameters (Barresi and Vanni, 2002; Fissore and Barresi, 2002).

Table 5.1: Main parameters used in the simulations (base case).

Total length	L	0.5	m
Void fraction	ε	0.43	
Catalyst density	ρ_S	1500	kg m^{-3}
Catalyst void fraction		0.53	
Pellet diameter	d_P	0.005	m
Inlet temperature	$T_{G,0}$	473	K
Total pressure		10^5	Pa
Surface velocity	u_0	2	m s^{-1}

Feed composition		
CH_4	26	% mol
O_2	13	% mol
H_2O	52	% mol
H_2	7	% mol
CO	1	% mol
CO_2	1	% mol

Kinetic constants	
$k'_{ps,A}$	$15.07 \cdot 10^3 \cdot \exp\left[-100320/(RT)\right]$
$k'_{ps,B}$	$48.82 \cdot 10^3 \cdot \exp\left[-114120/(RT)\right]$
$k'_{ps,C}$	$6.804 \cdot 10^3 \cdot \exp\left[-142510/(RT)\right]$
$k'_{ps,D}$	$0.264 \cdot 10^3 \cdot \exp\left[-38130/(RT)\right]$

The PDE system has been solved by discretising the domain of the spatial variable on a grid of evenly spaced points ensuring a grid-independent solution; for the algebraic part, given by the mass balances for the solid phase, the non-linear equations solver HYBRID1 from FORTRAN package MINPACK (Moré *et al.*, 1981) has been used, while the routine LSODE from ODEPACK library has been implemented in order to solve the differential part of the system (Hindmarsh, 1983).

5.1.1 *Temperature and composition profiles*

Figure 5.1 shows an example of the temperature profiles of the catalyst along the reactors, taken at various times between two consecutive switches after cyclic steady state has been reached. The reacting mixture is fed to the network at $T_{G,0}$ = 200°C, while the catalytic beds are uniformly pre-heated at T_{ph} = 600 °C well above the ignition temperature in order to have a safe start-up; the CH_4/O_2 ratio has been set equal to the stoichiometric value. The cold feed extracts heat from the catalyst which gradually cools down; at the ignition temperature the exothermic methane oxidation starts with heat generation. The maximum temperature of the catalyst that is obtained can lead to catalyst sintering or melting; as a consequence a large amount of steam is required in the feed to avoid excessive temperature increase. Methane is then reformed by carbon dioxide and water and finally the composition of the syngas is governed by the water-gas shift reaction. After a certain number of switches of the inlet position, a cyclic steady state is reached, in which the same temperature and concentration profiles along the reactors are obtained in subsequent cycles; particularly important are the intermediate coolings in order to shift the syngas conversion towards higher values. The change of the feed position makes possible to get autothermal processing, thus avoiding any pre-heating of the inlet gases, as a consequence of the storage of the heat of reaction inside the bed.
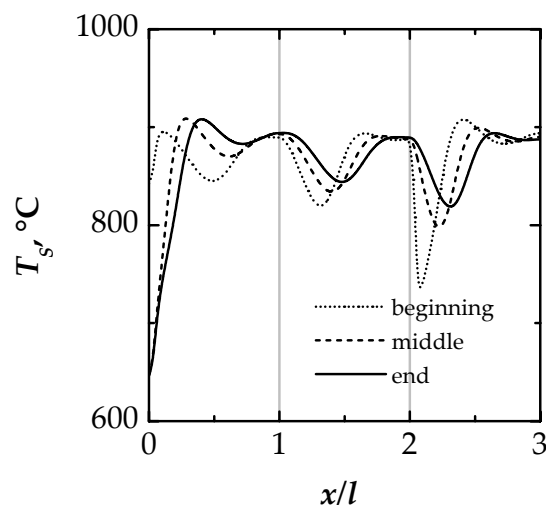

Figure 5.1: Temperature profile of the catalyst at the beginning, in the middle and at the end of the cycle after cyclic steady state has been reached. Operating conditions in Table 5.1, t_c = 50 s (3 beds).

5.1.2 *Influence of the inlet velocity and temperature*

The performances of the network versus the switching time t_c are plotted in Figure 5.2 for various values of the inlet velocity and in Figure 5.3 for various values of the inlet temperature; Figure 5.4 shows the maximum switching time that allows stable operation as a function of both inlet velocity and inlet gas phase temperature.
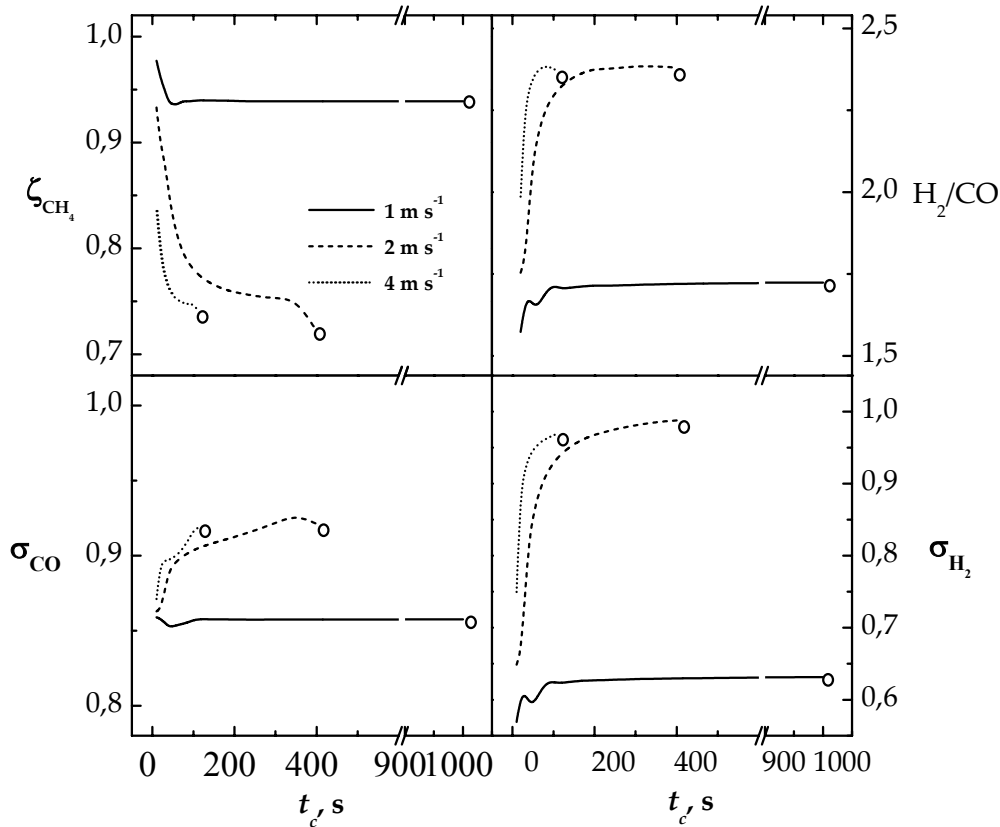

Figure 5.2: Influence of the switching time t_c on CH_4 conversion, CO and H_2 selectivity and H_2/CO ratio for various values of surface velocity. $T_{G,0} = 473$ K, $CH_4/O_2 = 2$, $H_2O/CH_4 = 2$. The circle corresponds to extinction.

It appears that the switching time strongly affects the stability of the network: a maximum value of t_c exists above which methane conversion drops to zero. The reason is that in the network the proper switching period, which ensures stable operation, is closely related to the velocity of the heat front (for a fixed length of the reactor): if the period is too long, the heat wave becomes progressively narrow, while the extension of the non-ignited sections of the network is increased. When the cold zone reaches the second

118

bed, the maximum temperature decreases and the reaction rapidly extinguishes as the amount of heat trapped in the bed does not allow for the ignition of the feed. In the network of afterburners a lower limit exists for t_c because if the switching period is too short, there is no time to accumulate enough heat in the network (Brinkman *et al.* 1999; Fissore and Barresi, 2002); in the case of syngas production such a lower limit has not been found because the total methane oxidation, and subsequent heat generation, takes place immediately after the entrance section (the pre-heating temperature has been chosen in order to guarantee the light off of the feed).
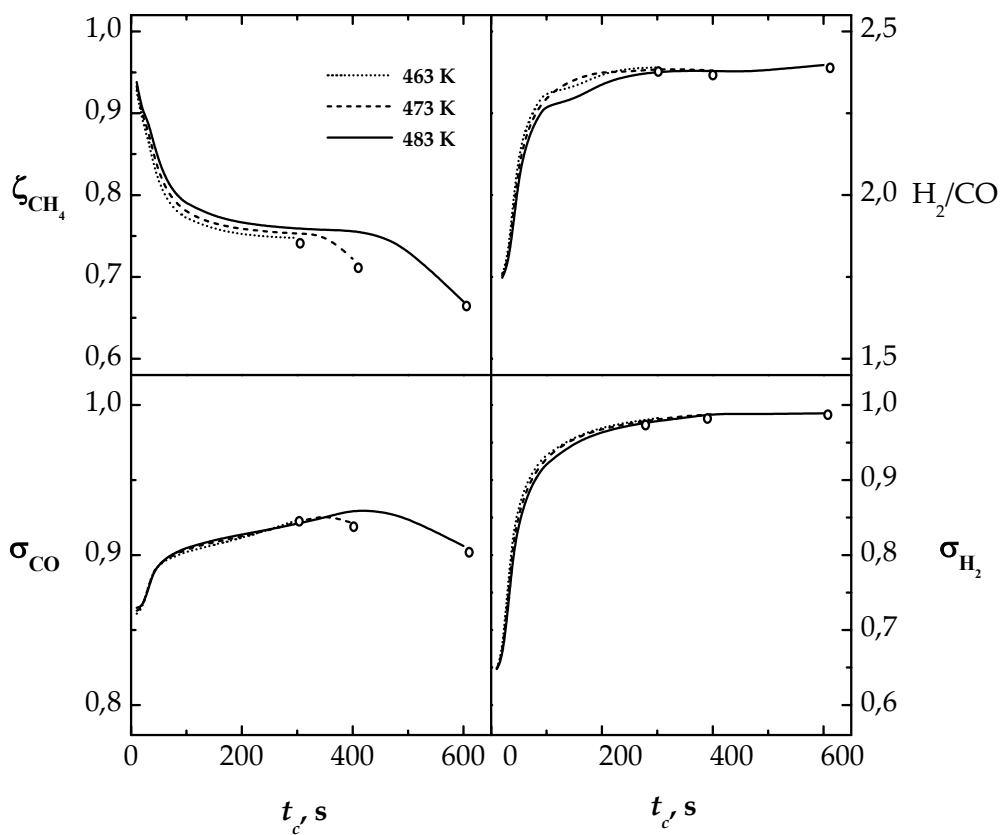

Figure 5.3: Influence of the switching time t_c on CH_4 conversion, CO and H_2 selectivity and H_2/CO ratio for various values of inlet gas temperature. $u_0 = 2$ m s^{-1}, $CH_4/O_2 = 2$, $H_2O/CH_4 = 2$.

The inlet velocity strongly affects both the stability and the performances (conversion/selectivity) of the network; when the inlet flow rate increases, the velocity of the heat front increases too, as a consequence of the more effective heat transfer, so that a lower t_c is required to keep the thermal wave inside the catalytic bed, ensuring stable operation. Methane conversion is increased by operating at low inlet flow rate, but leading to low H_2 and CO selectivity

(not higher than 65% and 85% respectively), while higher inlet flow rates may lead to H_2 selectivity near to 100% and H_2/CO larger than 2, even if methane conversion is considerably decreased.
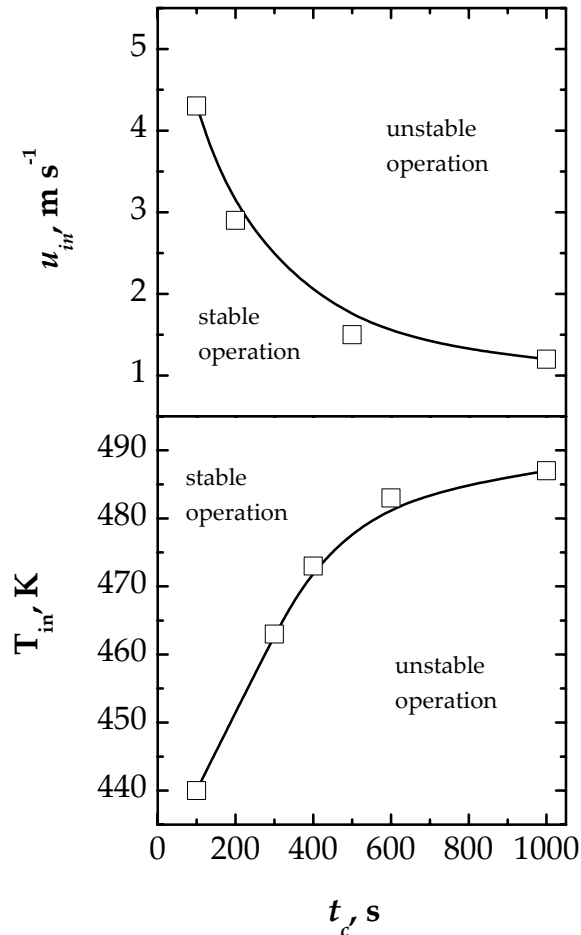

Figure 5.4: Maximum switching time that allows stable operation as a function of surface velocity ($T_{G,0}$ = 473 K) and inlet gas phase temperature (u_0 = 2 m s^{-1}). CH_4/O_2 = 2, H_2O/CH_4 = 2.

The influence of the inlet temperature on reactants conversion and product selectivity is negligible, as it is shown in Figure 5.3; but $T_{G,0}$ strongly influences the extension of the operating range, which can be increased by higher $T_{G,0}$ as a consequence of the larger amount of heat which is introduced by convection.

5.1.3 *Influence of the inlet composition*

The influence of the inlet composition on the conversion and selectivity of the device has been studied by varying the H_2O/CH_4 and CH_4/O_2 ratios, keeping constants all the other parameters (inlet temperature and velocity);

the actual composition of the feed mixture for these cases is given in Table 5.2. The results are shown in Figures 5.5 and 5.6.

Table 5.2: Feed composition (% mol) in the runs with variable H_2O/CH_4 and CH_4/O_2 ratios.

H_2O/CH_4	2	2	1.5	2.5
CH_4/O_2	1.5	2.5	2	2
CH_4	25.5	27.5	32	24
O_2	17	11	16	12
H_2O	51	55	48	60
H_2	2.5	2.5	2	2
CO	2	2	1	1
CO_2	2	2	1	1

Steam is required to reduce the peak temperature via the endothermic steam reforming reaction (B) occurring in parallel with the combustion reaction (A), as it has been shown by De Groote and Froment (1995) and Gosiewski *et al.* (1999) in the case of the RFR.
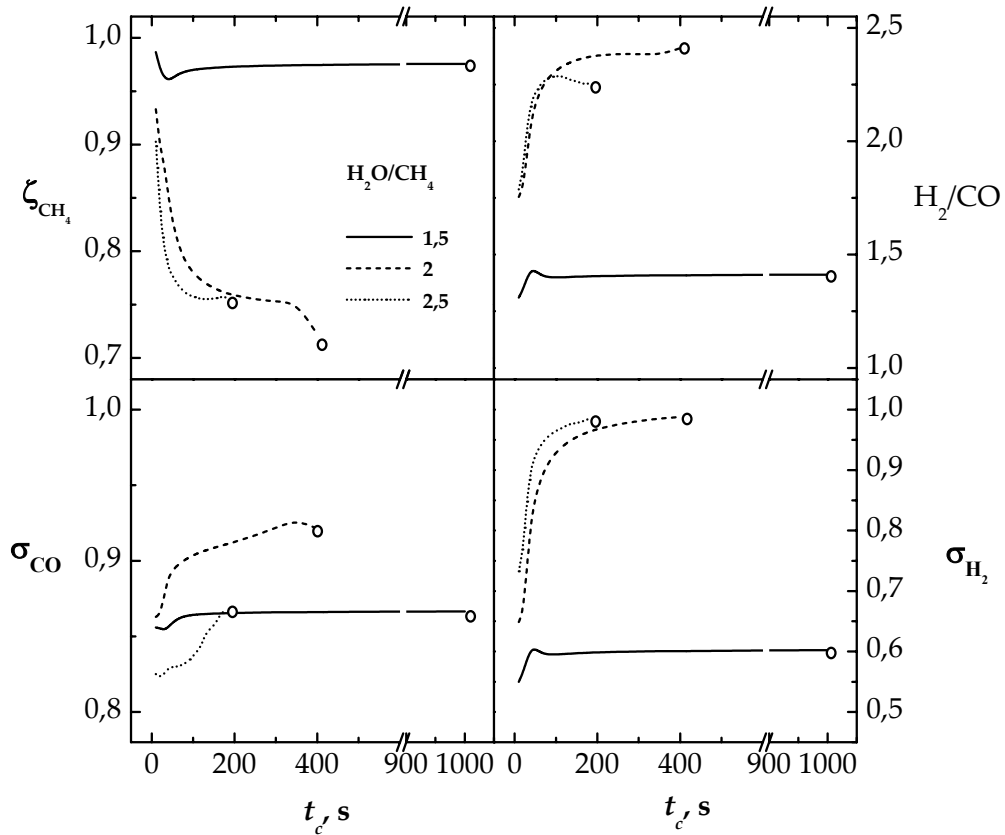

Figure 5.5: Influence of the switching time t_c and H_2O/CH_4 ratio on CH_4 conversion, CO and H_2 selectivity and H_2/CO ratio. $u_0 = 2$ m s^{-1}, $T_{G,0} = 473$ K, $CH_4/O_2 = 2$.
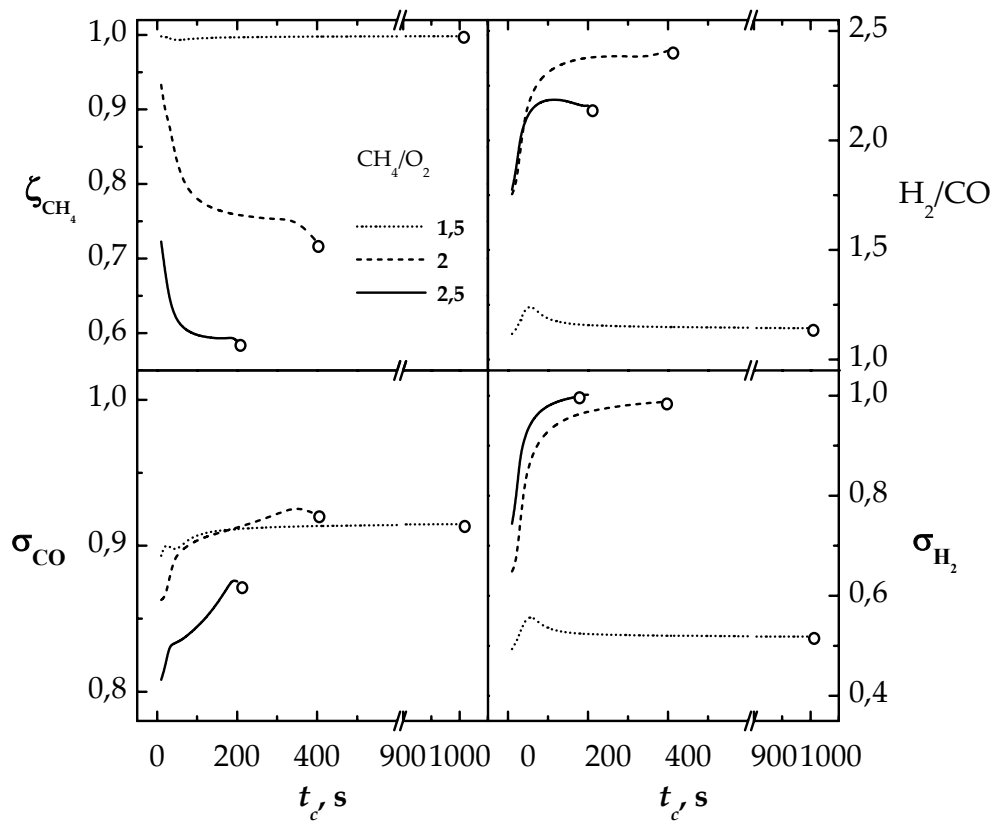
Figure 5.6: Influence of the switching time t_c and CH_4/O_2 ratio on CH_4 conversion, CO and H_2 selectivity and H_2/CO ratio. $u_0 = 2$ m s^{-1}, $T_{G,0} = 473$ K, $H_2O/CH_4 = 2$.

The behaviour of the RN to this respect is similar to that of the RFR, as it is shown in Figure 5.7 (upper graph): increasing H_2O/CH_4 from 1.5 to 2.5 it is possible to lower the maximum temperature of the catalyst by more than 200°C. The higher the water content in the feed, the smaller the heat effect of the process; the range of switching times that allows stable operation becomes smaller as a consequence of the fact that the heat produced by the exothermal combustion reaction is not stored by the catalytic bed, but is immediately used by the endothermic reforming reactions. In the cases considered the process is slightly exothermic, but when the H_2O/CH_4 ratio is very large the overall process can become endothermic and no unsteady-state reactor could work without additional heating. Hydrogen selectivity increases with the H_2O/CH_4 ratio as a consequence of the higher reaction rate of methane steam reforming (reaction B), while CO selectivity at first increases with the H_2O/CH_4 ratio and then decreases when $H_2O/CH_4 = 2.5$.

The influence of the CH_4/O_2 ratio on the maximum temperature of the solid is shown in Figure 5.7 (lower graph): the higher the CH_4/O_2 ratio, the lower the maximum temperature on the solid because of the lower methane conversion via total oxidation. Figure 5.6 shows that if the CH_4/O_2 ratio is increased hydrogen selectivity is enhanced, as a consequence of higher amount of methane available for reforming reactions (B and C), while the range of switching times that allows stable operation is reduced because of the lower heat production by total methane oxidation.
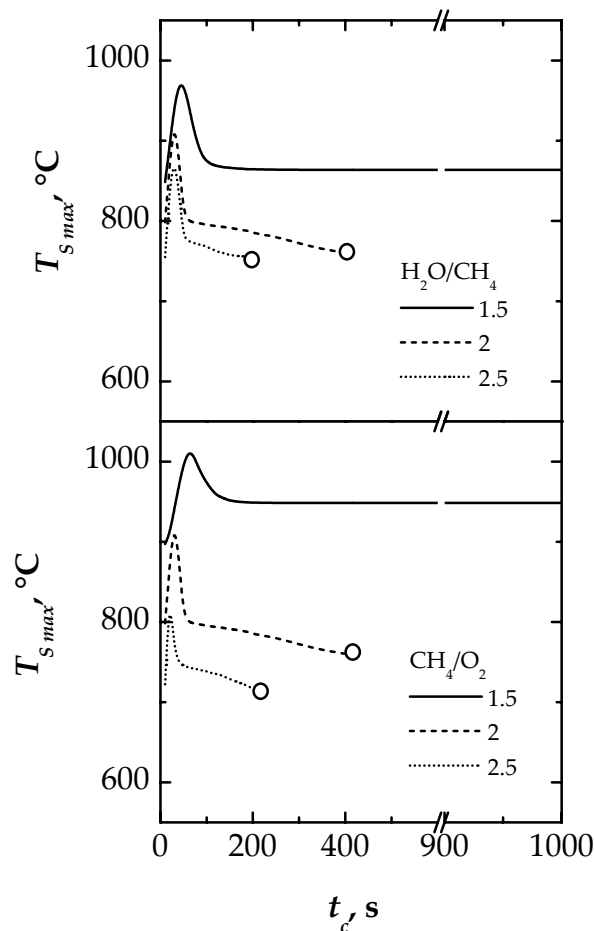

Figure 5.7: Influence of the switching time t_c on the maximum temperature of the catalyst for various values of the H_2O/CH_4 ratio (upper graph, $CH_4/O_2 = 2$) and the CH_4/O_2 ratio (lower graph, $H_2O/CH_4 = 2$). $u_0 = 2$ m s^{-1}, $T_{G,0} = 473$ K.

5.1.4 *Comparison with the RFR*

Figure 5.8 shows a comparison between the RN and the RFR. The composition of the inlet mixture and the feed flow rate are the same for both devices (see Table 5.1); the comparison is carried out for a constant total

length of the reactor system. Stable operation with high methane conversion can be obtained both in the RN and in the RFR but for both devices a maximum value of the switching period is found in order to get autothermal behaviour. This is a consequence of the movement of the heat wave along the reactor during the period of operation; if the flow direction (in the RFR) or the feed position (in the RN) is not changed before a maximum value is reached, the reactors gradually cools down and the conversion falls to zero.
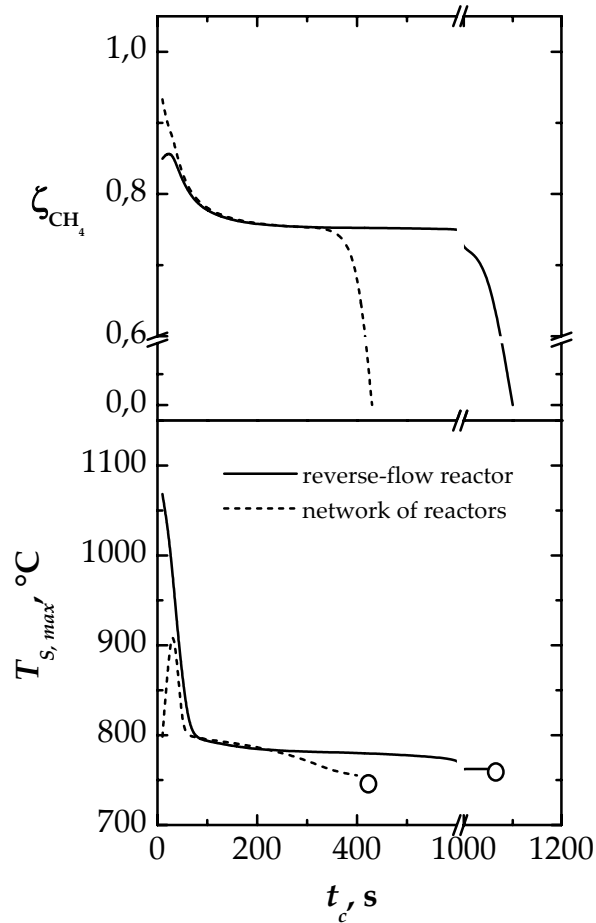

Figure 5.8: Comparison between methane conversion (upper graph) and maximum temperature of the solid (lower graph) in the RFR and in the RN; operating conditions in Table 5.1.

The operating range of the RFR is much larger than that of the network; the same behaviour has been observed when the combustion of lean mixtures takes place in this devices (Fissore and Barresi, 2002). At low t_c higher methane conversion may be obtained in the RN with respect to the RFR; in this range of switching frequency the maximum temperature of the solid in the network is also lower by more than 200 °C than in the RFR. At higher t_c,

124

when stable operation is possible in both devices, the reactant conversion and product selectivity are almost the same.

5.1.5 *Coke deposition in the RN*

Coke deposition can be the critical parameter in defining the performance of a reactor for synthesis gas production. A large amount of water in the feed allows negligible deposition even if low temperature can promote coking by Boudouard reaction.

In the case of the RFR this problem has been addressed by De Groote *et al.* (1996a, b) taking into account coking and gasification kinetics and by Gosiewski (2000, 2001) by means of a simplified thermodynamic approach evaluating the danger of coke deposition. The results indicate that, at the location of the temperature peak, coke can be deposited through the endothermic methane cracking; while at the downstream end of the temperature plateau, a significant amount of deposited carbon is burnt off by oxygen, leading to a net coke gasification; at the decreasing end of the temperature front, carbon is gasified by hydrogen. In any case the movement of the high temperature zones along the reactor may lead to the burning out of soot deposited on the catalyst (Gosiewski, 2000, 2001; De Groote *et al.* 1996a, b); Blanks *et al.* (1990) have also verified experimentally in a RFR that such a system can operate without significant coking problems.

In this work the simplified approach of Gosiewski *et al.* (1999) has been used to analyse the formation of permanent carbon deposits over the catalyst (Fissore *et al.*, 2001b). This is a consequence of the parallel occurrence of methane cracking (M), Boudouard reaction (B), CO reduction (R) and CO_2 decomposition (C). If the chemical affinity of the carbon-producing reactions is negative we can conclude that the reactions proceed towards the consumption of carbon. A series of index parameters V_i can be defined; a value lower than 1, indicate when coking can occur.

$$V_M = \frac{P\dfrac{y_{H_2}^2}{y_{CH_4}}}{K_{p,M}} \quad V_B = \frac{P^{-1}\dfrac{y_{CO_2}}{y_{CO}^2}}{K_{p,B}} \quad V_R = \frac{P^{-1}\dfrac{y_{H_2O}}{y_{CO}y_{H_2}}}{K_{p,R}} \quad V_C = \frac{\dfrac{y_{O_2}}{y_{CO_2}}}{K_{p,C}} \tag{5.9}$$

The functions $F_i = (1-V_i)$ are a dimensionless measure of the distance between the individual reactions and their respective equilibrium. As the carbon formed in any of the carbon-producing reactions can be gasified in the

others, if $F_{glob} = \Sigma_i\, F_i$ is positive for a given section of the bed, it can be assumed that there is a danger of coke deposition.
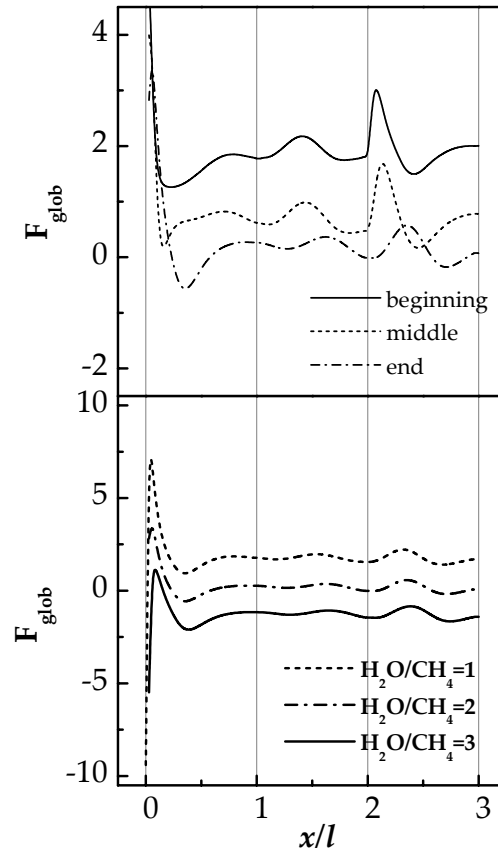

Figure 5.9: Time evolution of F_{glob} in the three RN during each cycle (upper graph) and for different H_2O/CH_4 ratios at the end of the cycle (lower graph); $t_c = 100$ s, $u_0 = 0.1$ m s^{-1}.

The application of this approach to the RFR confirmed the conclusion of Gosiewski (2000): at the location of the temperature peak, coke is deposited through the endothermic methane cracking; at the downstream end of the temperature plateau, a significant amount of carbon is burnt off by oxygen, leading to a net coke gasification. At the decreasing end of the temperature front, carbon is gasified by hydrogen.

Similar results can be obtained in the network of reactors: Figure 5.9 shows that the formation of carbon deposits is more relevant at the beginning of the cycle, but this carbon is gasified since the methane cracking progresses towards gasification, as a consequence of the lower maximum temperature in the reactor and the high hydrogen partial pressure. If we increase the H_2O/CH_4 ratio we strongly reduce the possibility of coking as part of the deposited carbon can be gasified by steam.

126

5.2 Methanol synthesis in the RN

The feasibility of methanol synthesis in a RN from CO, CO_2 and H_2 over a commercial Cu-Zn-Al has been investigated as an alternative to the RFR. A one-dimensional two-phase model has been used for the simulation of the adiabatic network of two and three reactors (§3.1). The kinetic model by Graaf *et al.* (1988), has been used, corresponding to a dual-site Langmuir-Hinshelwood mechanism, based on three independent reactions: methanol formation from CO, water-gas-shift reaction and methanol formation from CO_2:

(A) $\quad CO + H_2 \rightleftharpoons CH_3OH$ $\hfill$ (5.10)

(B) $\quad CO_2 + H_2 \rightleftharpoons CO + H_2O$ $\hfill$ (5.11)

(C) $\quad CO_2 + 3H_2 \rightleftharpoons CH_3OH + H_2O$ $\hfill$ (5.12)

The reaction rates for methanol and water from reactions (A), (B) and (C) are given by the following equations, according to Graaf *et al.* (1988), where partial pressure are used instead of partial fugacity assuming ideal gas behaviour:

$$R'_{CH_3OH,\,A} = \frac{k'_{ps,A} K_{CO} \left[p_{CO} p_{H_2}^{3/2} - p_{CH_3OH} \big/ \left(p_{H_2}^{1/2} K_{p,A} \right) \right]}{\left(1 + K_{CO} p_{CO} + K_{CO_2} p_{CO_2} \right) \left[p_{H_2}^{1/2} + \left(K_{H_2O} / K_{H_2}^{1/2} \right) p_{H_2O} \right]} \tag{5.13}$$

$$R'_{H_2O,\,B} = \frac{k'_{ps,B} K_{CO_2} \left(p_{CO_2} p_{H_2} - p_{H_2O} p_{CO} / K_{p,B} \right)}{\left(1 + K_{CO} p_{CO} + K_{CO_2} p_{CO_2} \right) \left[p_{H_2}^{1/2} + \left(K_{H_2O} / K_{H_2}^{1/2} \right) p_{H_2O} \right]} \tag{5.14}$$

$$R'_{CH_3OH,\,C} = R'_{H_2O,\,C} = \frac{k'_{ps,C} K_{CO_2} \left[p_{CO_2} p_{H_2}^{3/2} - p_{CH_3OH} p_{H_2O} \big/ \left(p_{H_2}^{3/2} K_{p,C} \right) \right]}{\left(1 + K_{CO} p_{CO} + K_{CO_2} p_{CO_2} \right) \left[p_{H_2}^{1/2} + \left(K_{H_2O} / K_{H_2}^{1/2} \right) p_{H_2O} \right]} \tag{5.15}$$

The conditions adopted in the simulations are given in Table 5.3; they are the same previously considered for the reverse flow operation of methanol synthesis by Vanden Bussche *et al.* (1993).

Table 5.3: Main parameters used in the simulation of methanol synthesis in the RN.

Total length	L	0.5	m
Void fraction	ε	0.4	
Catalyst density	ρ_S	1750	kg m^{-3}
Catalyst void fraction		0.5	
Pellet diameter	d_P	0.0054	M
Total pressure		5	MPa
Superficial inlet flow rate	F_{in}	32.65	mol m^{-2} s^{-1}
Feed composition			
CO		4.5	% mol
CO_2		2.0	% mol
CH_3OH		0.0	% mol
H_2O		0.0	% mol
H_2		93.5	% mol
Kinetic and equilibrium constants			
$k'_{ps,A}$	$2.69 \cdot 10^7 \cdot \exp\left[-109900/(RT)\right]$		
$k'_{ps,B}$	$7.31 \cdot 10^8 \cdot \exp\left[-123400/(RT)\right]$		
$k'_{ps,C}$	$4.36 \cdot 10^2 \cdot \exp\left[-65200/(RT)\right]$		
K_{CO}	$7.99 \cdot 10^{-7} \cdot \exp\left[58100/(RT)\right]$		
K_{CO_2}	$1.02 \cdot 10^{-7} \cdot \exp\left[67400/(RT)\right]$		
$K_{H_2O}/K_{H_2}^{1/2}$	$4.13 \cdot 10^{-11} \cdot \exp\left[104500/(RT)\right]$		
$\log_{10} K_{p,A}$	$5139/T - 12.621$		
$\log_{10} K_{p,B}$	$-2073/T - 2.029$		
$\log_{10} K_{p,C}$	$3066/T - 14.650$		

5.2.1 *Temperature and concentration profiles*

Figure 5.10 shows an example of the temperature profiles of the catalyst along the reactors, taken at various times between two consecutive switches. The synthesis gas mixture is fed to the network at $T_{G,0}$=100°C while the catalytic beds are uniformly pre-heated at T_{ph}=220°C, well above the ignition temperature ($\cong$180°C), in order to have a safe start-up. The required feeding temperature is related to switching time, as will be shown in the following; this low $T_{G,0}$ value has been selected according to the results of Vanden Bussche *et al*. (1993) and in order to show the possibility to operate with low feeding temperatures. The cold syngas progressively extracts heat from the

catalyst which gradually cools down; at the ignition temperature the exothermic synthesis reaction starts with heat generation. After a certain number of switches of the inlet position, a cyclic steady state is reached, in which the same temperature profiles are obtained in subsequent cycles. In this way auto-thermal processing is realised because no energy supply is needed except the moderate feed preheating at $T_{G,0}$=100°C, required in order to prevent the possible condensation of the products.
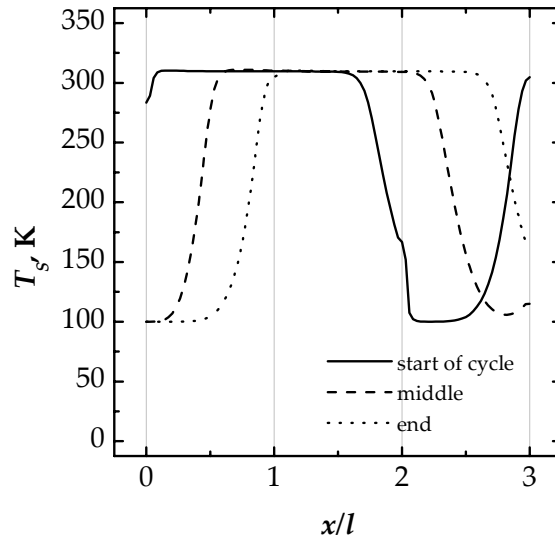

Figure 5.10: Temperature profiles of the catalyst at the beginning, in the middle and at the end of the cycle after cyclic steady state has been reached; t_c=170 s. $T_{G,0}$=100°C.

Curves 2 and 3 are very similar to those observed in the RFR, while profile 1, concerning the first instants after the switch, presents a positive slope in the terminal part of the heat wave. This behaviour can be understood if we consider that the first reactor of the sequence takes the place of the last one when the inlet position is changed. Since in the first reactor, before the switch (curve 3, 0<x/ℓ<1), the temperature profile has a positive slope, this behaviour will be also maintained after the switch (curve 1, 2<x/ℓ<3) for a short time.

The presence of a positive slope at the end of the heat wave gives some advantages, as showed in Figure 5.11. In the third reactor, immediately after the switch, there is the unconverted syngas which was fed to the system when this reactor was the first of the sequence. While the concentration profile moves along the third bed, the high-temperature "tail" of the heat wave (2.5<x/ℓ<3) brings the gases above the ignition temperature, thus allowing the partial conversion of the fresh reactants that otherwise would leave the network unconverted. Thus, the waste related to wash-out in the

first instants after the switching can be strongly limited (the wash-out time is about 4 s).
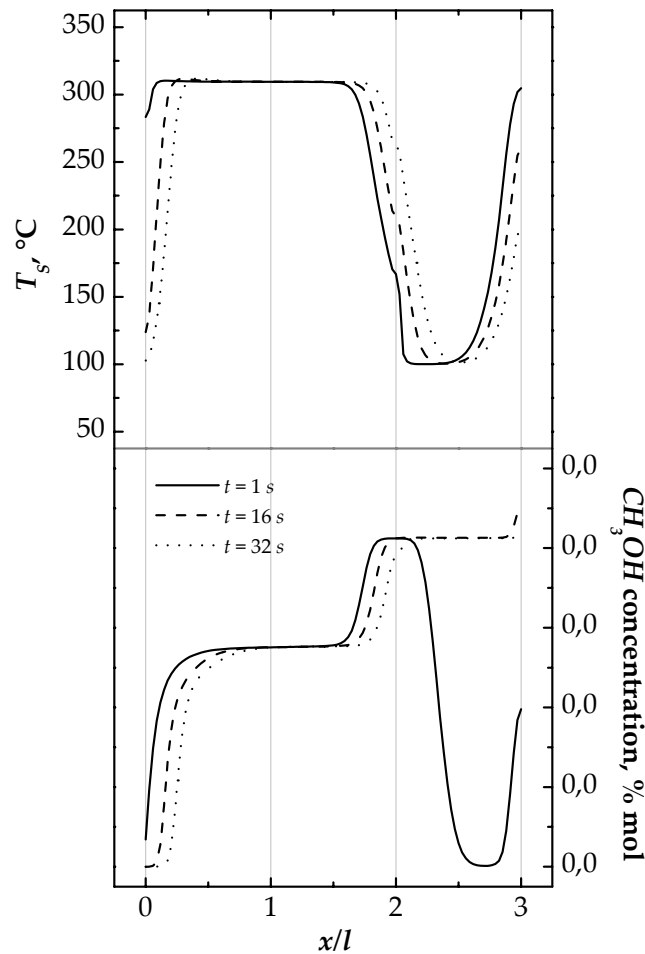

Figure 5.11: Methanol concentration and solid temperature profiles at various times in the first part of the cycle; t_c=170 s. $T_{G,0}$=100°C.

Curves 2b and 3b of Figure 5.11 clearly shows two plateau: in the first one methanol concentration reaches the equilibrium value, corresponding to the maximum temperature. When the temperature decreases, methanol equilibrium concentration is shifted towards higher values, but it remains constant once the temperature falls below the ignition value. Therefore, the first plateau corresponds to an equilibrium limitation, while the second one to a kinetic constraint because reaction rate is negligible below 180°C. Nevertheless, final conversion in the network can be higher than the second plateau limit (curve 2b, x/ℓ=3), because the high-temperature "tail" of the heat wave can re-ignite the partially converted gases coming from the first two beds at a concentration below the equilibrium value, thus giving an extra

push in conversion.

When the high-temperature end of the heat front is driven out of the system and the temperature of the "tail" falls below the ignition value (curve 3a), the outlet conversion decreases returning to a value equal to that of the second plateau. As a consequence, the time evolution of the exit concentration of methanol exhibits a maximum in the first part of every cycle (Figure 5.12), followed by a drop when the high-temperature end of the heat wave leaves the third bed.
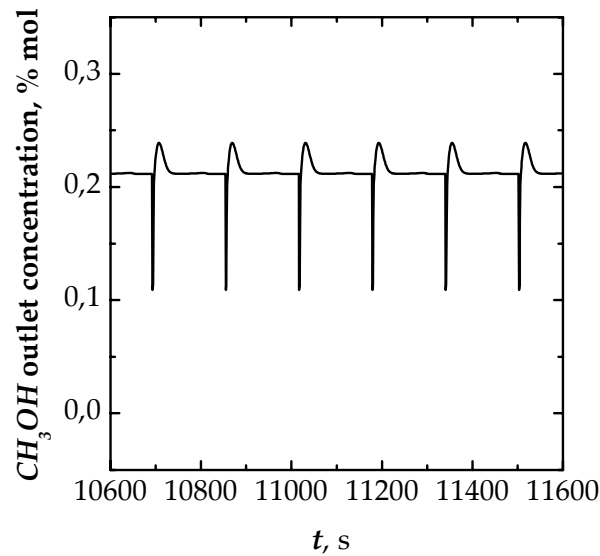

Figure 5.12: Periodic evolution of methanol outlet concentration; t_c=162 s. $T_{G,0}$=100°C.

5.2.2 *Influence of the switching time*

The performances of the network versus the switching time t_c are plotted in Figure 5.13. It appears that two relatively limited ranges of t_c exist in which the system can operate adiabatically and a cyclic steady state of period t_c is obtained; it can be observed that the effect of an increase in t_c is opposite in the two ranges. In these ranges the solutions of the problem are given by periodic functions of period t_c.
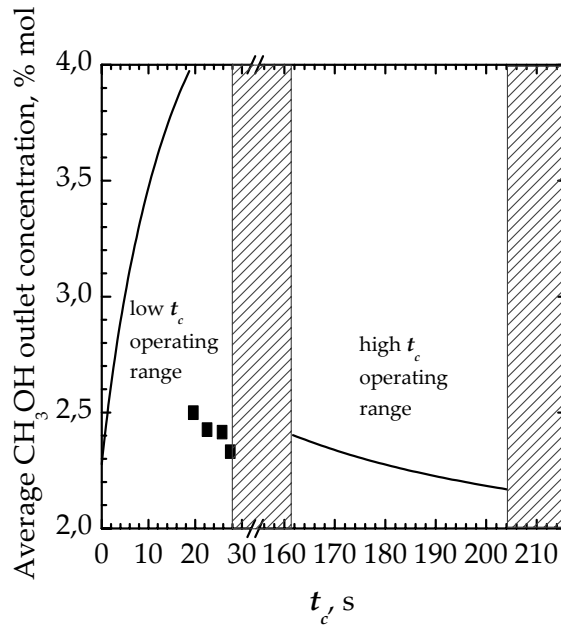
Figure 5.13: Influence of the switching time t_c on the average methanol outlet concentration. Dashed zones correspond to extinction. $T_{G,0}$=100°C.

Figure 5.13 shows that in the high t_c operating region better performances correspond to lower switching times. This is due to an optimal exploitation of the decreasing temperature profile in the third reactor, as it can be seen in Figure 5.14: if t_c is high (curve 4a) the end of the heat wave leaves the system and the increment in conversion due to the final diminution of temperature is very small (curve 4b); on the contrary, if t_c is low (curve 1a and 1b) higher conversion can be obtained thanks to the final decrease in the temperature profile, as the heat front has not yet abandoned the system at the end of the cycle.

Better performances compared to the high t_c range can be obtained at low t_c; in this case the conversion increases with t_c. This is related to the particular morphology of the temperature profiles along the reactors, showed in Figure 5.15 for various t_c values. In the second and third reactor of the sequence the heat waves initially have a negative slope; so the result of the switching strategy realised in the network is analogous to an intermediate cooling, which allows for a further increase of conversion by shifting the reaction far from equilibrium. For very low switching times (curve 1a and 1b) the cooling effect is small and it is vanished by the subsequent increase of temperature. For higher t_c values (curve 3a and 3b) the initial sections of the second and third beds show a deeper temperature drop which allows for a continuously increasing conversion inside the system.
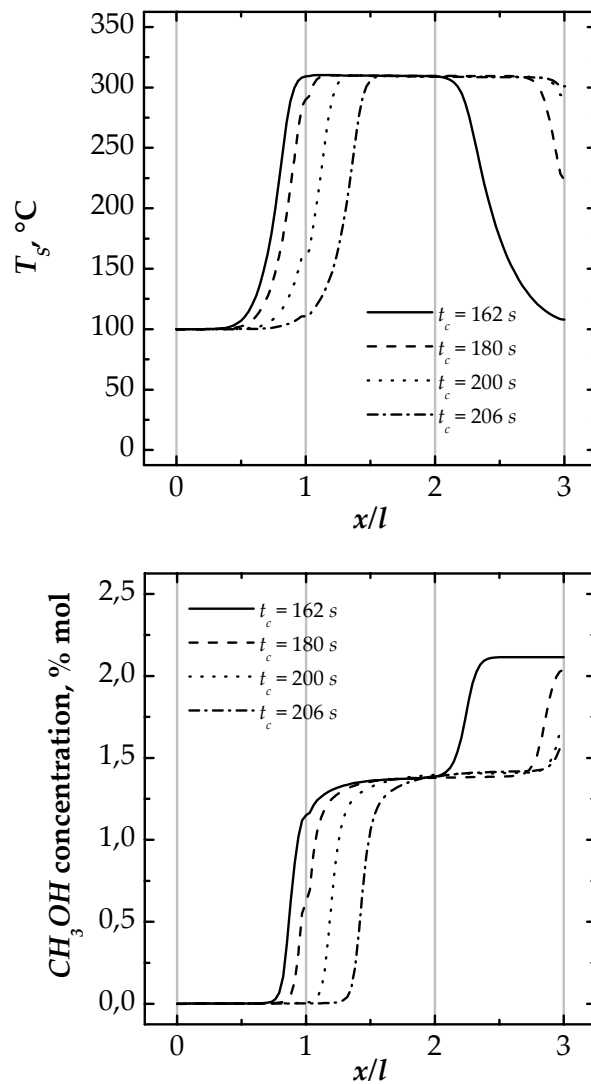
132

Figure 5.14: Influence of the switching time t_c on the temperature profiles of the catalyst and on methanol concentration profiles along the network. High t_c operating range. Profiles are taken at the end of the cycle. $T_{G,0}$=100°C.

A narrow range also exists, close to the zone of maximum conversion, in which complex behaviours (cyclic steady-state of high periodicity) are observed of limited practical interest because the average conversion is lower. The triangles plotted in Figure 5.13 show some values of the conversion that can be obtained in this region (see §5.3.3).

In the range between the high t_c and low t_c operating region ($25 < t_c < 162$ in Figure 5.13) the reaction is led to extinction, as auto-thermal behaviour is not possible for a wide intermediate range of cycle times.
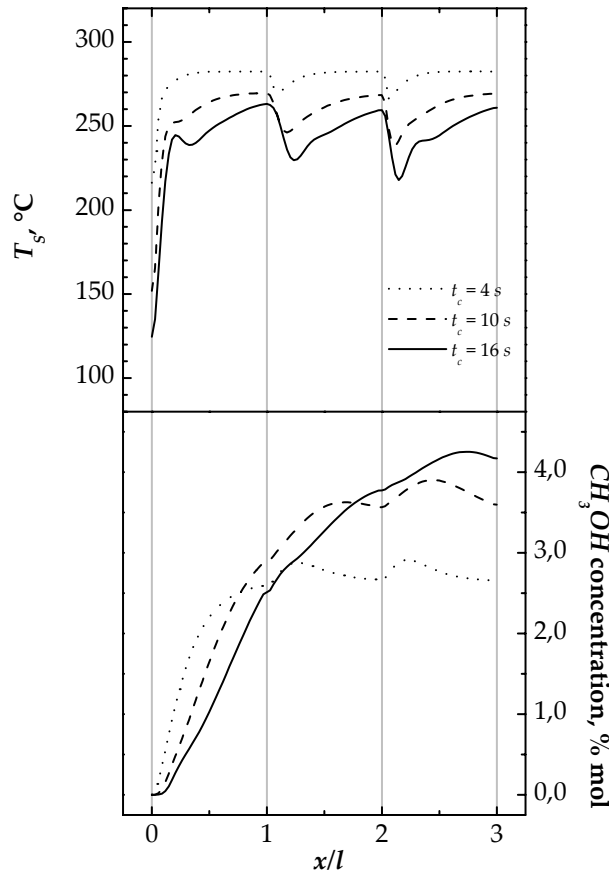
Figure 5.15: Influence of the switching time t_c on the temperature profiles of the catalyst and on methanol concentration profiles along the network. Low t_c operating range. Profiles are taken at the end of the cycle. $T_{G,0}$=100°C.

When the switching frequency is high the heat and mass transfer evaluated according to eq. (3.26) may not be adequate to describe the transport process as the correlation has been proposed for steady-state conditions, which are not obtained when t_c is low. As it is extremely difficult to have reliable estimations of the heat and mass transfer coefficients in these conditions, the sensitivity of the model to these parameters has been evaluated, by changing the value of the heat transfer coefficient (and also the mass transfer coefficient according to Chilton-Colburn's analogy). Figure 5.16 shows the carbon to methanol conversion when these coefficients are 2 and 10 times higher than in the base case (eq. 3.26): the range of t_c in which the operation is feasible is the same, even if the conversion slightly decreases when the value of the coefficients is increased; if the heat and mass transfer coefficients are further increased, no further decrease in the conversion is noticed, as when they are reduced with respect to the base case. The same analysis has been

repeated in the high t_c range, leading to analogous results: the value of the heat and mass trasfer coefficient slightly affects the carbon to methanol conversion, but it does not affect the dynamic behaviour and the range of t_c where stable operation can be obtained. As a consequence, in the followings, the values of heat and mass transfer coefficients are evaluated according to eq. (3.26).
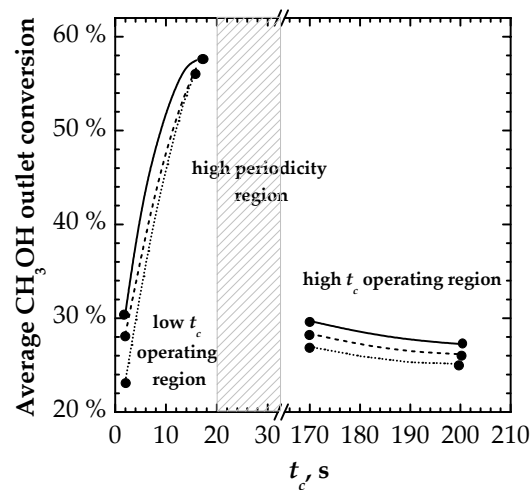

Figure 5.16: Influence of the switching time on the average carbon to methanol conversion when the heat and mass transfer coefficient are evaluated according to eq. 3.26 (solid line) and when their value is multiplied by 2 (dashed line) and by 10 (dotted line); $T_{G,0} = 100°C$.

5.2.3 *Complex behaviour region*

If the switching time belongs to the high t_c operating range, transition from stable periodic operation to a non-ignited state occurs at a precise value of t_c; while operating at low switching time, transition to extinction is not well defined, but it takes place through a region where highly periodic solutions are obtained with lower conversion. Even if permanent pseudo-steady-state conditions have been reached, the profiles in a generic cycle are different from the others since the material and energy balances have a solution of period greater than the cycle time (Fissore *et al*. 2002, 2004; Velardi *et al.*, 2004). For example, Figure 5.17 shows the temperature and concentration profiles in three subsequent cycles for a switching time of 20 s.
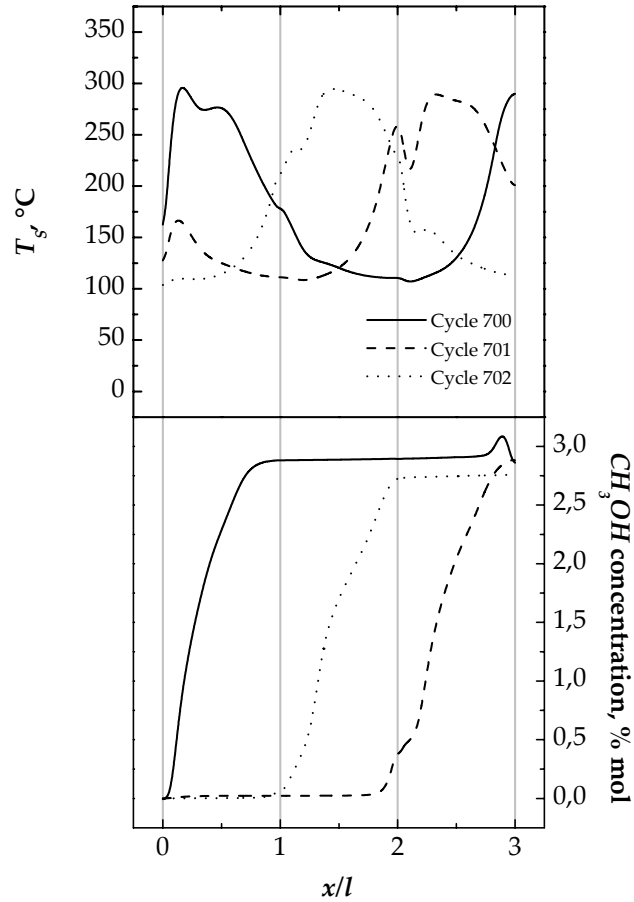
Figure 5.17: Solid temperature (upper graph) and methanol concentration profiles (lower graph) in three subsequent cycles in the complex behaviour region; t_c = 20 s, $T_{G,0}$ = 100°C.

An example of high periodicity of the solution is shown in Figure 5.18, where, for t_c = 20 s, the evolution of the average methanol conversion is plotted vs. the number of operating cycles.
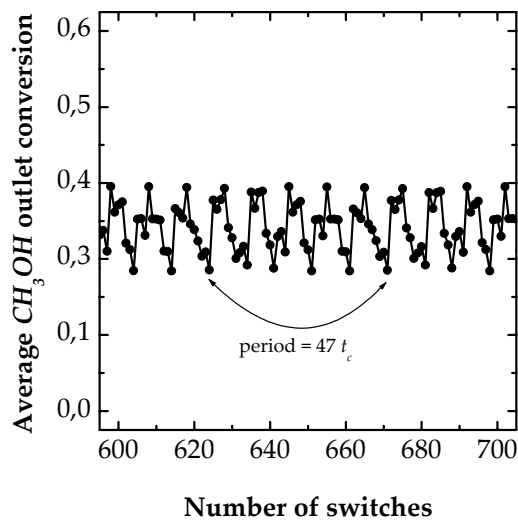

Figure 5.18: Periodic evolution of the average methanol outlet conversion in the complex behaviour region; t_c = 20 s, $T_{G,0}$ = 100°C.

If we choose two representative variables (e.g. outlet gas temperature and methanol conversion) the status of the reactor during a cycle can be defined by a unique couple of values, both operating in the high and in the low switching time range. Conversely, in the complex behaviour region, the status of the system can be represented by a stroboscopic map, given by a number of points equal to the number of cycles corresponding to the periodicity of the solution. The stroboscopic map of Figure 5.19 (left hand side) shows that 47 combinations of outlet gas temperature and methanol conversion are possible when t_c = 20 s, each one corresponding to one of the 47 cycles of the period. If we change t_c also the period of the solution changes. As we move away from the stability operation range the period of the solution increases up to a value of 332 t_c (right hand side), which corresponds to the observed upper limit of this high periodicity range.
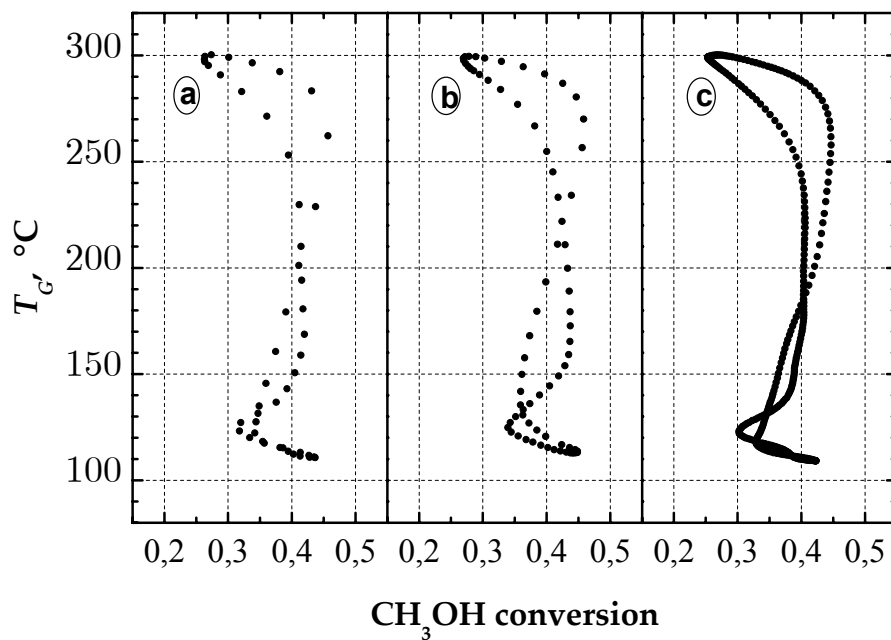
Figure 5.19: Correlation between methanol conversion and the outlet gas temperature for different switching times. a) period = 47 t_c, t_c = 20 s; b) period = 72 t_c, t_c = 22 s; c) period = 332 t_c, t_c = 24 s. Points are taken in the middle of each cycle.

5.2.4 *Influence of the inlet gas temperature*

Figure 5.20 (on the left) summarise the influence of the inlet gas temperature on the outlet methanol conversion. At high switching time, the average methanol concentration increases with the inlet temperature before a maximum is reached. This is a consequence of the influence of the "tail" in

the heat wave which oscillates around the temperature profiles which gives maximum methanol production in the third bed, as it is evidenced in Figure 5.20 (on the right). When operating at low t_c values the performances of the network become worse when increasing the inlet temperature: the larger is $T_{G,0}$, the smaller is the effect of intermediate cooling and the higher is the temperature level of the catalytic bed.
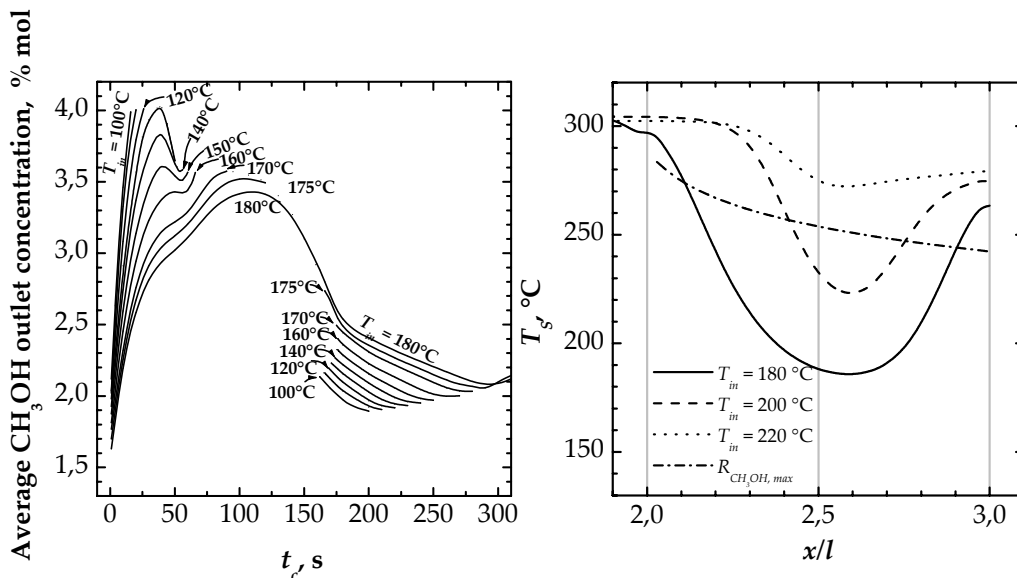

Figure 5.20: Influence of the switching time t_c on the average methanol outlet concentration for various values of the inlet temperature $T_{G,0}$ (on the left). Temperature profiles in the third reactor of the network for different inlet temperatures (t_c=176 s); comparison with the temperature profile which gives maximum CH_3OH generation (on the right)

In order to maximise methanol production, the best choice of operating parameters corresponds to t_c=40 s and $T_{G,0}$=130°C and leads to an average carbon conversion z_{CH_3OH}=58%. As it is evident from Figure 5.21 (left hand side) the temperature profile in the case of optimal conversion approximates the curve corresponding to the maximum methanol generation. On the right hand side, Figure 5.21 shows the temperature-conversion phase plane in the case of maximum methanol generation compared to the network optimal configuration. The curves show that the temperature-conversion trajectory followed in the network is always close to the ideal trajectory which ensures maximum generation of methanol along the reactors.
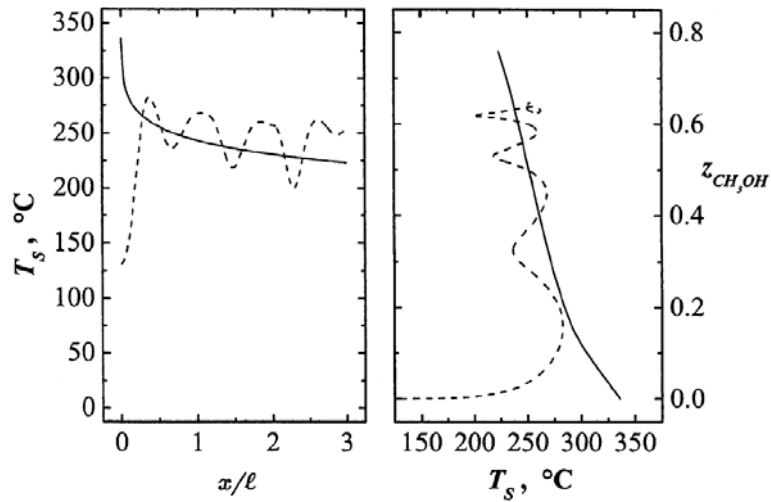
138

Figure 5.21: On the left: comparison between the solid temperature profile in the case of maximum CH₃OH generation (continuous line) and in the optimal network configuration corresponding to t_c=40 s and $T_{G,0}$=130 °C (dashed line). On the right: phase plane comparing the temperature-conversion trajectory in the case of maximum CH₃OH generation (continuous line) and in the optimal network configuration (dashed line). Optimal profiles are taken at the end of the cycle.

5.2.5 *Influence of the number of reactors in the network*

The behaviour of a network of two reactors is shown in Figure 5.22 for different values of the inlet temperature and switching time; if we decrease the number of reactors in the network similar results are obtained even if the stability range is reduced and the conversion is slightly lower (Fissore *et al.*, 2002; Fissore and Barresi, 2004). For inlet temperature lower than 100°C no stable operation can be obtained; for higher temperatures two stability windows are obtained, corresponding to high and low t_c: in the first region methanol conversion increases with the switching time, while in the second the behaviour is the opposite. If the inlet temperature is further increased the two regions join and the average methanol outlet concentration shows a maximum as a function of t_c. This is related to the particular shape of the temperature profiles along the reactors that are obtained for different switching times and inlet gas temperatures.
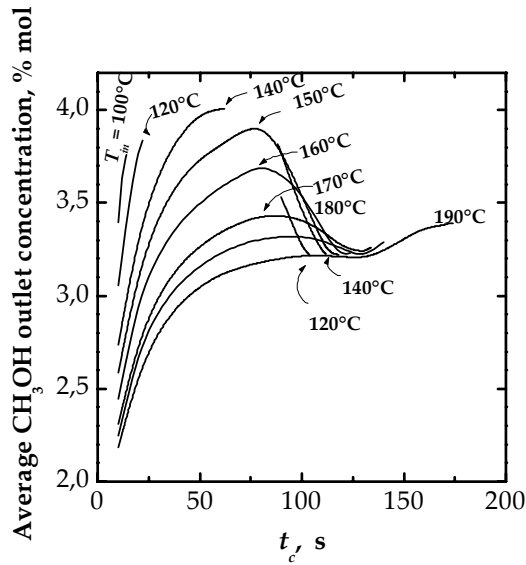
Figure 5.22: Influence of the switching time t_c on the average methanol outlet concentration in the network of two reactors for different values of the inlet temperature.

Figure 5.23 shows the profiles of the solid temperature and of the methanol molar fraction along the reactor for different values of t_c. As in the case of the three RN, the change of the feed position leads to the formation of some temperature drops: these intermediate coolings allows for a continuous increase of methanol conversion along the reactor. If we increase t_c higher methanol conversion is obtained, as a consequence of the more pronounced temperature drops, but when t_c is further increased, the influence of the more relevant cold zone at the inlet of the reactor and of the reduction of the central hot zone (as a consequence of the fact that the thermal wave exits from the reactor) diminishes and the methanol conversion starts decreasing.
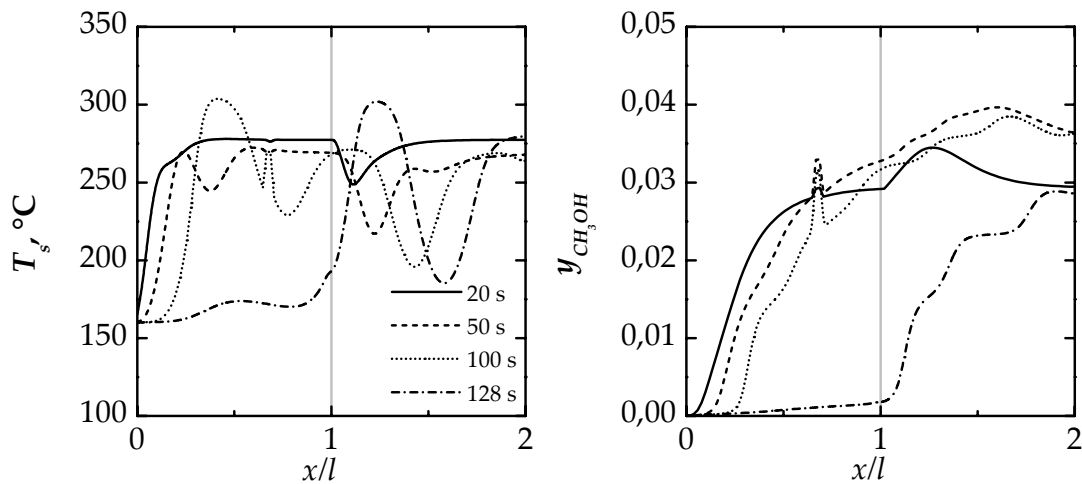

Figure 5.23: Solid temperature profiles (on the left) and methanol concentration profiles (on the right) in the network of two reactors as a function of the switching period; $T_{G,0} = 160°C$.

Figure 5.24 shows the influence of the inlet gas temperature for a fixed value of the switching time. It is evident that the higher the inlet gas temperature the higher the temperature that is reached in the first reactor of the sequence, thus leading to higher methanol concentration as a consequence of the higher reaction rate, but the influence of the intermediate coolings becomes less relevant, thus leading to a reduction of the methanol conversion in the second reactor.
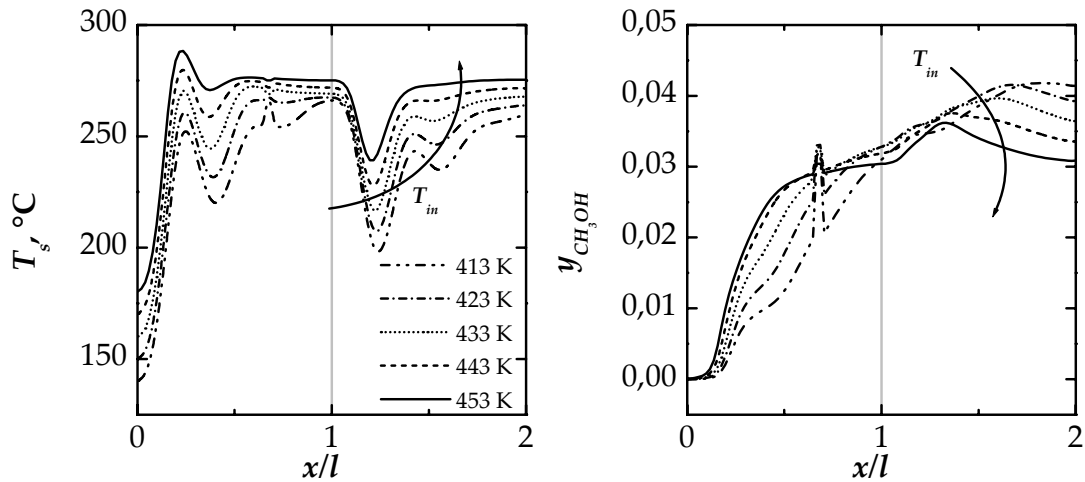

Figure 5.24: Solid temperature profiles (upper graph) and methanol concentration profiles (lower graph) in the network of two reactors as a function of the inlet temperature; t_c = 50 s.

If we compare these results to those obtained for the three RN it is possible to conclude that the behaviour of these devices is similar: the two RN may give rise to similar temperature profiles and the same final conversion is obtained with a lower number of reactors, but the stability range is reduced.

5.2.6 *Comparison with the RFR*

Figure 5.25 shows the time evolution of the average methanol outlet concentration for the RFR and for the RN. During the start-up, curves 2 and 3 exhibit a maximum because the initial solid bed temperature (T_{ph} =220°C) leads to a high conversion in the initial cycles of operation. At low t_c values (curve 1) simulations have been carried out with a higher solid bed pre-heating temperature (T_{ph}=290°C) in order to prevent the extinction in the start-up phase, even if in this way methanol generation is not favoured in the first cycles of operation. When a PSS is reached the performances of the high t_c network are only slightly better than the RFR at the same feeding

temperature; conversely, the network operating at low t_c values shows much higher conversion, but a cyclic steady state regime is obtained after a larger number of cycles.
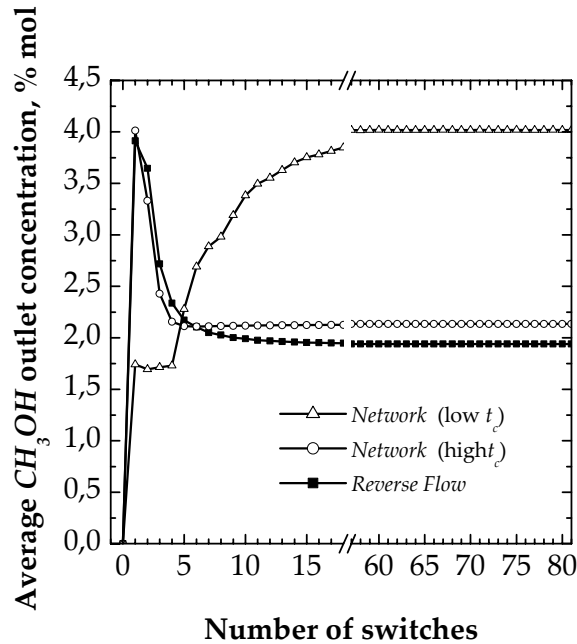
Figure 5.25: Comparison between the RFR and the RN: evolution of the average methanol outlet concentration from start-up to PSS condition. RFR: t_c=114 s, $T_{G,0}$=100°C. RN (high t_c): t_c=162 s, $T_{G,0}$=100°C. RN (low t_c): t_c=40 s, $T_{G,0}$=130°C.

Another comparison between the RFR and the RN is shown in Figure 5.26. At the beginning of the cycle in the RFR methanol conversion drops to zero because of wash-out. The switching strategy realised in the network of three reactors allows for a strong reduction of wash-out, as it is evident from the curve related to high and low t_c values. Furthermore, both for the RFR and the RN operating at high switching times, the outlet gas temperature exhibits a wide variation (about 200°C) between the beginning and the end of the cycle; such a variation could disturb the operation of downward equipment. On the contrary, the network shows a quite smaller ΔT_G at the exit, of the order of 10°C, while operating at low t_c values.

142
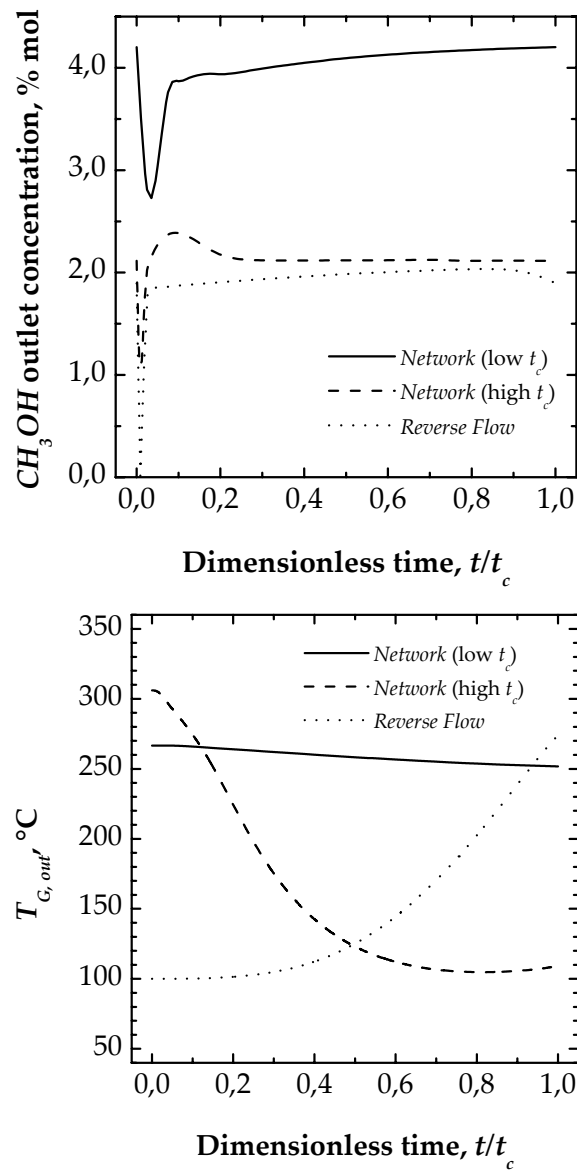
Figure 5.26: Comparison between the RFR and the RN: time evolution of the methanol outlet concentration (above) and of the outlet gas temperature $T_{G,out}$ (below) during a cycle. RFR: t_c=114 s, T_{in}=100°C. RN (high t_c): t_c=162 s, $T_{G,0}$=100°C. RN (low t_c): t_c=40 s, $T_{G,0}$=130°C.

List of symbols

c	molar concentration, mol m^{-3}
d_P	particle diameter, m
F_{in}	superficial inlet flow rate, mol m^{-2}s^{-1}
F_j	dimensionless measure of distance between j-th carbon producing reaction and their respective equilibria
F_{glob}	global measure of the equilibrium distance of carbon producing reaction
K_p	chemical equilibrium constant based on partial pressure
k'_{ps}	reaction rate constant
L	total length, m
l	single reactor length, m
p	partial pressure, Pa
R	ideal gas phase constant, J K^{-1}mol^{-1}
R'	reaction rate, mol s^{-1}kg^{-1}
t	time, s
T	temperature, K
t_c	switching time, s
u	surface velocity, m s^{-1}
V_j	catalyst coking index
x	axial reactor coordinate, m
y	molar fraction

Greeks

ε	void fraction of the catalytic bed
ζ	conversion
ρ	density, kg m^{-3}
σ	selectivity

Subscripts and superscripts

0	initial condition
A, B, C, D	indicates the reaction
G	gas phase
S	solid phase or solid surface

max	maximum value
ph	pre-heating value
out	outlet value

Abbreviations

PSS	Pseudo-steady state
RFR	Reverse-flow reactor
RN	Reactors network

Chapter 6

Control of methanol synthesis in a three reactors network

The forced unsteady-state RN, as well as the RFR, have been demonstrated to give some specific advantages with respect to the traditional steady-state processes; nevertheless the unsteady-state processes may make the total investment increase and operation complex because of the cyclic operation mode and the requirement of advanced process control as, in addition to the intrinsecally dynamic behaviour, one must deal with unexpected external perturbations both in the inlet temperature and in the flow rate. The problem of the control of unsetady-state reactors used for exothermic equilibrium-limited reactions has never been addressed up to this moment. In this thesis the control of a RN for methanol synthesis will be investigated.

6.1 Open loop responses to disturbances

Numerical simulations reveal that high conversion can be obtained in a network of three reactors operating in unsteady-state conditions, but care must be paid to the existence of unstable regions of operation, which separate stable zones where profile along the reactor are completely different. In order to attain and maintain stable periodic operations a simple open-loop control strategy was adopted, which consists of the periodic alternations of the inlet sections at fixed time interval t_c.

The knowledge of the dynamic behaviour of the reactor is quite important for the control of such a system, because the condition of maximum yield is very close to the zones of complex periodic behaviour. Furthermore, the useful operating ranges have a narrow extension, so even small disturbances may drive the reactor out of optimum. For example, for a -10°C step disturbance in the inlet temperature the reactor falls outside the operating range at low t_c values. The slow transition to a complex periodic steady-state can be observed in Figure 6.1. The system exhibits an inverse response, because initially the average carbon to methanol conversion oscillates around 0.59, which improves of about 5% the performance of the optimal network configuration. Nevertheless, the oscillations become larger and the outlet conversion falls down after 150 switches from the disturbance. Finally, a pseudo-steady condition is approached, in which a solution of 48 t_c is obtained.
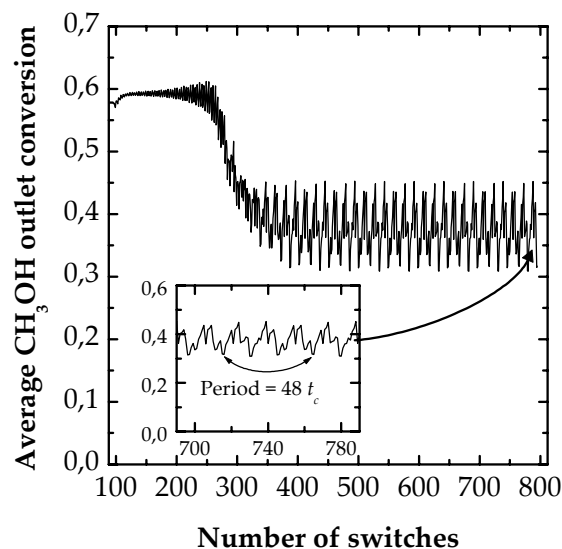

Figure 6.1: Open loop response to a step disturbance $\Delta T_{G,0}$ = -10°C and transition to a multi-periodic steady-state; t_c = 40 s, $T_{G,0}$ = 130°C.
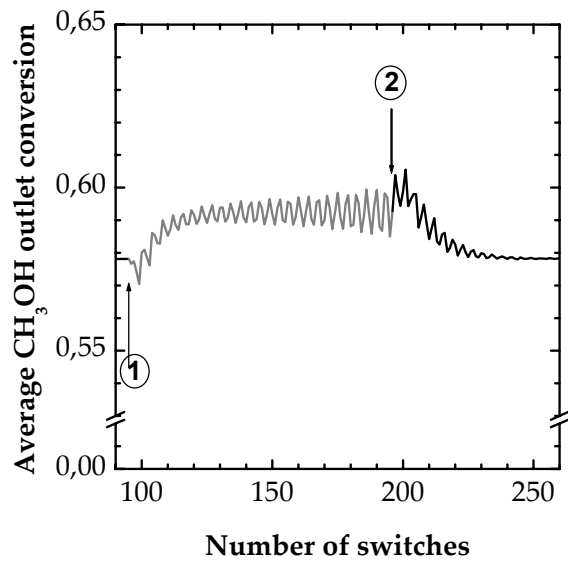
Figure 6.2: Open loop response to a step disturbance $\Delta T_{G,\,0} = $ -10°C (point 1) and restoration of the previous steady-state after the disturbance (point 2); t_c = 40 s, $T_{G,0}$ = 130°C.

If the disturbance has a relatively short length and the switching time is not changed, the system is able to take the average conversion back to its original value. This is shown in Figure 6.2, which shows the evolution of the mean conversion when the disturbance of -10°C on the inlet temperature stops after 195 cycles, before the new cyclic steady-state has been reached.
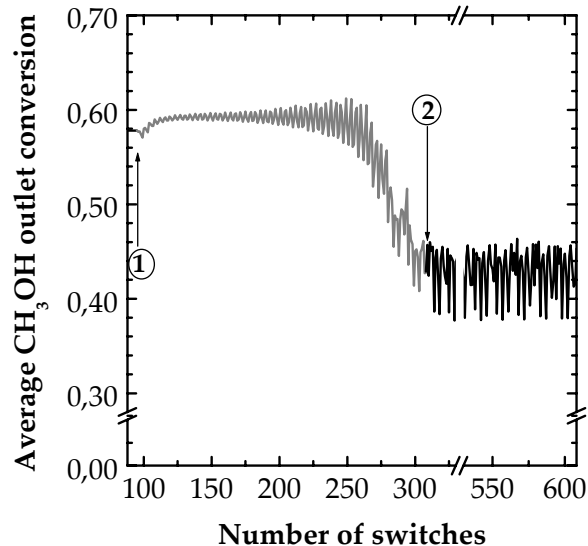

Figure 6.3: Open loop response to a step disturbance $\Delta T_{G,0} = $ -10°C (point 1) and new complex steady-state obtained when the conditions before the disturbance are restored (point 2); t_c = 40 s, $T_{G,0}$ = 130°C.

After a long time disturbance the system is not able to return to the original state without changing the switching time. Figure 6.3 shows the performance of the network when the disturbance $\Delta T_{G,0}$ = -10°C stops after 200 cycles. It can be seen that the reactor does not return to the optimal conditions, but it falls in a new highly periodic steady-state.

As a consequence of these results, a control scheme for this device has to face any disturbances both in the inlet temperature and in the flow rate, as also when the inlet velocity changes the reactor may exhibit similar complex behaviours. This may be accomplished for example by any commercial PID controller. If a tighter control on the outlet methanol conversion is needed a model predictive control (MPC) scheme should be used, varying the switching time to maximise the selectivity of the reactor; the on-line optimisation requires the use of a simplified model and in this thesis an Artificial Neural Network (ANN) based model will be firstly developed to identify the system and then used in the framework of a MPC alghorithm.

6.2 Fundamentals on ANN

ANNs are nowadays extensively employed in different branches of science and technology in such diverse fields as modelling, time series analysis, pattern recognition, signal processing, and control by way of an important property: an ANN may be thought of as a black box that can accept a series of input data and produce one or more outputs. The transformation of the data is performed by several basic processing units, called artificial neurons or simply neurons, which perform identical tasks. The neurons are connected into networks by synapses. The problems handled by ANNs may be quite assorted. One of the most important is modelling, i.e. the search for an analytical function or a procedure that gives a specified n-variable output for any m-variable input. Standard modelling techniques require the mathematical function to be known in advance. Conversely, the ANN does not require the knowledge of such a function: the nonlinearity of a single unit transformation and a sufficiently large number of variable parameters (weights) ensure enough "freedom" to adapt the neural network to any relation between input and output data (see for example Haykin, 1999; Zupan and Gasteiger, 1999).

150

To create a conventional model of a chemical process all phenomena present in the process have to be identified and properly described. Mathematical description of the process - usually containing conservation laws, chemical, physical and chemical-physical processes – is expressed by a set of deterministic (algebraic, differential or integral) equations. In a neural model, the ANN replaces some portions of conventional model and two general methods can be distinguished: a global neural model (GNM), in which the whole model is represented with a single ANN, and a hybrid neural model (HNM), in which only the unknown part of the model is replaced by the ANN. The first approach (GNM), since its introduction in the early nineties (Bhat and McAvoy, 1990), is commonly used mainly for control and regulation purposes. This approach makes possible the modelling of the reactor based on the chosen input-output signals only, without any fundamental knowledge about the system being modelled. Nevertheless, in most practical cases a lot of information is known about the modelled system and only some elements are not sufficiently recognised. From this observation, an idea of neural hybrid model has been derived by Psichogios and Ungar (1992), in which the ANN is used to approximate those unknown elements. In the present work a GNM was used as this approach is more convenient for fast modelling of the reactor. The main disadvantage is the poor ability to generalise the results of modelling, which will be valid in the range of input values used in the training.

The aim of this chapter is to develop an ANN based model to simulate the dynamic behaviour of the three reactors network when low-pressure methanol synthesis takes place. The real process behaviour is dynamically simulated by using a detailed non-linear time domain model. The History Stack Adaptation algorithm (Tadé *et al.*, 1996) was used for the training phase and the influence of the main parameters of the algorithm were discussed.

The architecture of the ANN is variable depending on the complexity of each individual process and the objectives for using them. In this work a feedforward multilayer network will be used (Figure 6.4); 4 layers are present: the first (input) layer contains n_1 nodes corresponding to the actual net inputs; two hidden layers contain respectively n_2 and n_3 nodes and the fourth (output) layer contains n_4 nodes which correspond to the number of monitored state variables. Cybenko (1989) showed that neural networks implementing one, sufficiently large, hidden layer can uniformly approximate any continuous function of n real variables to any desired

accuracy; in this work two hidden layers have been used with the aim to improve the performance of the ANN. The number of input and output nodes is governed by the functional requirements of the ANN. No general guideline is available for the number of hidden nodes on each layer: as a consequence the training process was repeated for different number of hidden nodes and little, if any, improvement in ANN performance was observed. This ANN is fully connected as every node in each layer of the network is connected to every other node in the adjacent forward layer. No back connections or recycles were implemented.
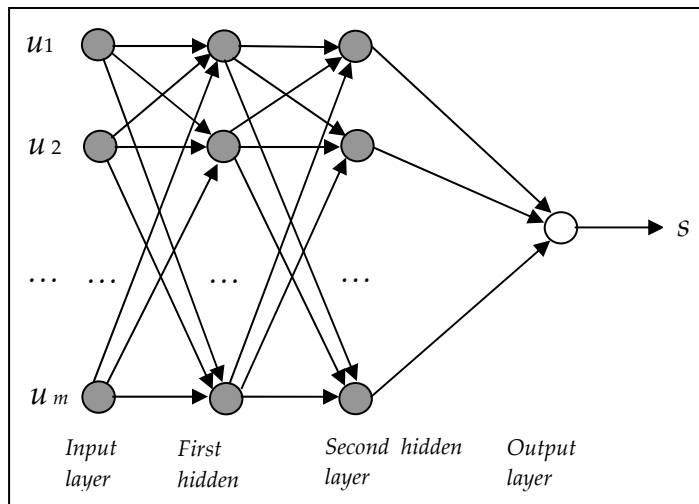
Figure 6.4: Feedforward multilayer neural network architecture.

Figure 6.5 shows the model of a neuron, which forms the basis for designing ANNs. It is possible to identify three basic elements of the neuronal model:

1. a set of synapses or connecting links, each characterised by a weight. Specifically, a signal u_j at the input of the synapse j connected to a neuron k is multiplied by the synaptic weight w_{kj}, which may lie in a range that includes negative as well as positive values;

2. an element for summing the input signals, weighted by the respective synapses of the neuron;

3. an activation function for defining the amplitude of the output of a neuron.

152

Figure 6.5: Nonlinear model of a neuron.

The neuronal model of Figure 6.5 also includes an externally applied bias, denoted by b_k which has the effect of increasing or lowering the net input of the activation function, depending on whether it is positive or negative, respectively. The use of a bias has the effect of applying an affine transformation to the output of the linear combiner in the model of Figure 6.5:

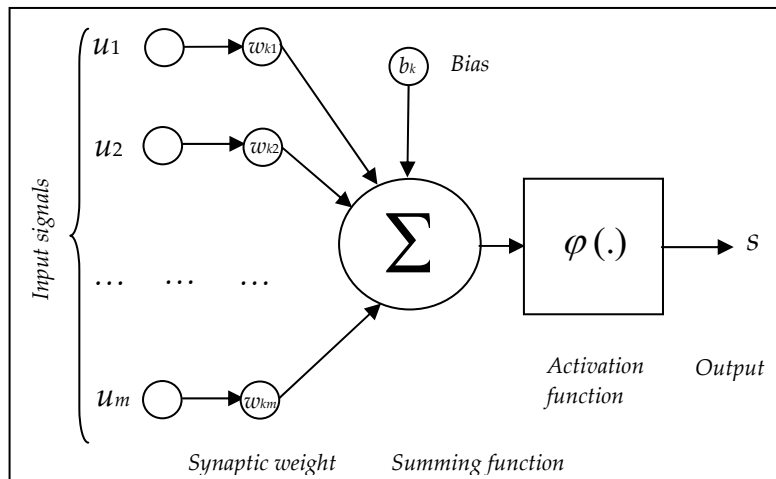$$q_k = u_k + b_k \tag{6.1}$$

The activation function defines the output of a neuron in terms of q_k and can take several forms. In this study, according to Tadé *et al.* (1996) two different activation functions, sigmoid and linear, were used for the hidden and output layers respectively:

$$\varphi(q) = \begin{cases} \mu q & \text{output layer} \\ \dfrac{1}{1+e^{-q}} & \text{hidden layers} \end{cases} \tag{6.2}$$

Learning of the input-output mapping is accomplished by repeated presentations of a sequence of patterns consisting of the input and corresponding target or desired output belonging to a fixed training set. A robust learning heuristic for multilayered feedforward ANNs is the generalised delta rule (GDR) or backpropagation: this method is a supervised learning method as the weights are corrected so as to produce prespecified target values for as many inputs as possible (Zurada, 1992). This algorithm was used because of its simplicity and ease of use. The weights and bias of each node are initialised to small random values at the start of the

learning procedure. The correction of weights and biases is made after each new input is proposed to the ANN.

During learning, the input vector U is presented to the neural network and the output vector s is immediately compared with the target vector $\overline{S}$ $(\overline{s}_1, \overline{s}_2, ..., \overline{s}_m)$ that is the correct output for U. Once the actual error produced by the network is evaluated, this is used to correct the weights and biases throughout the entire ANN:

$$\Delta w_{ji}^l = \alpha \delta_j^l s_i^{l-1} + \beta \Delta w_{ji}^{l(previous)}$$
$$\Delta b_j^l = \alpha \delta_j^l s_i^{l-1} + \beta \Delta b_j^{l(previous)}$$

(6.3)

where l is the index of the current layer, j identifies the current neuron and i is the input source, i.e. the index of the neuron in the upper layer. In this equation δ_j^l, the error introduced by the corresponding neuron, is calculated in two ways, depending on whether the last (output) layer or one of the hidden layers is under consideration:

$$\delta_j^{last} = \left(\overline{s}_j - s_j^{last} \right) s_j^{last} \left(1 - s_j^{last} \right)$$

(6.4)

$$\delta_j^l = \left(\sum_{k=1}^{r} \delta_k^{l+i} w_{kj}^{l+1} \right) s_j^l \left(1 - s_j^l \right)$$

(6.5)

According to eq. (6.3) the correction of the weights in the l-th layer comprises two terms that pull in opposite directions: the first one tends towards a fast "steepest-descent" convergence, while the second is a longer-range function that prevents the solution from getting trapped in shallow local minima. The learning rate is α, whilst β is the momentum factor. By taking into account the correction made on the previous cycle, β can prevent sudden changes in the direction in which corrections are made: this is particularly useful for damping oscillations. The value of the learning rate and momentum constant is generally obtained by trial and error. Some guidelines can be found in the literature (Tadé *et al.*, 1996; Haikin, 1999). The expressions (6.4) and (6.5) can be derived from the delta rule (see for example Zupan and Gasteiger, 1999) and correspond to a discrete-time gradient descent rule that minimises a function of the error between target output and network output for each output element and pattern in the training set. The procedure is then repeated with the other input-output pairs.

The convergence of the ANN may be strongly improved by using the history-stack adaptation (HSA) method instead of the single pattern

presentation (SPP) described above. When each pattern is presented to the ANN the weights and biases are updated in order to minimise the error for that individual pattern. The variation is determined by the learning rate, α, which is generally set to a small value. Consequently, the information contained in a single pattern cannot be assimilated completely in a single presentation and part of the information value is discarded and not absorbed by the learning procedure. Since the patterns are not fully learned in one presentation, this suggests that a method using several replications of each pattern is most appropriate. The HSA method operates by means of a First-In-First-Out stack (containing n_p patterns), which, at each time step, accepts a new pattern from the process and discards the oldest pattern from the stack. The elements of the stack are each used in n_c cycles to update the weights and biases at each time-step. Consequently, each pattern is used $n_p n_c$ times before it is discarded, thereby improving the potential adaptation performance achieved at each time-step. Tadé *et al.* (1996) suggested a few design guidelines for the parameters n_p and n_c of the stack procedure.

6.3 Neural Network identification of the methanol synthesis in a RN

It was pointed out (§5) that in the three reactors network a maximum value of carbon to methanol conversion of 58% may be obtained when $t_c = 40$ s, $T_{G, in}$ = 130°C, with $v_G = 0.021$ m s^{-1}. This value is higher than the conversion of 30-40% that may be achieved in the traditional multi-bed adiabatic reactors. Nevertheless, changes in the inlet gas flow rate and temperature may lead either to lower conversions or to reaction extinction or pseudo-periodic behaviours. Moreover, a tighter control on the outlet methanol conversion is needed to maximise methanol conversion. Because of these requirements as well as the complexity of the dynamics of the process, a Model Predictive Control (MPC) scheme should be adopted. Dufour *et al.* (2003) designed a MPC algorithm to control a catalytic reverse-flow reactor where the combustion of lean mixtures of volatile organic compounds is carried out: the analogy with the countercurrent reactor when the switching frequency approaches infinity was used to obtain a simple model to be solved on-line. As a consequence, the switching time could not be used as a manipulated variable and it was replaced by an external heating device to prevent reaction extinction. Contrarily to this approach, in the case of methanol synthesis the

control algorithm has to vary the switching time to maximise the selectivity of the reactor. Actually, it was shown that such a parameter is effective in controlling the process.

As far as the output variables of the ANN are concerned, they are chosen as the system variables to be controlled, i.e. methanol outlet molar fraction. Since the GNM approach was adopted, the input variables are both the process disturbances (gas temperature and flow rate) and the manipulated variable (switching time). Application of the feedforward neural network (which is a static structure) to describe a dynamic behaviour of the reactor, is possible due to the introduction of a pseudo-dynamic structure (Levin and Narendra, 1995):

$$S(t+1) = f\left(S(t), S(t-1), ..., S(t-t_1), U(t), U(t-1), ..., U(t-t_2)\right) \qquad (6.6)$$

where S and U are respectively the output and input vectors, t_1 and t_2 are the appropriate time delays and the unknown nonlinear function f is approximated by the ANN. In this work the output at time t is given by the input at time t-1, t-2 and t-3 as it is sketched in Figure 6.6; each pattern is made up of the input variables (switching time, inlet flow rate and temperature) evaluated at t, t-1 and t-2, while the output variable is evaluated at t-1, t-2 and t-3 to keep into consideration the time delay of the input on the system response.
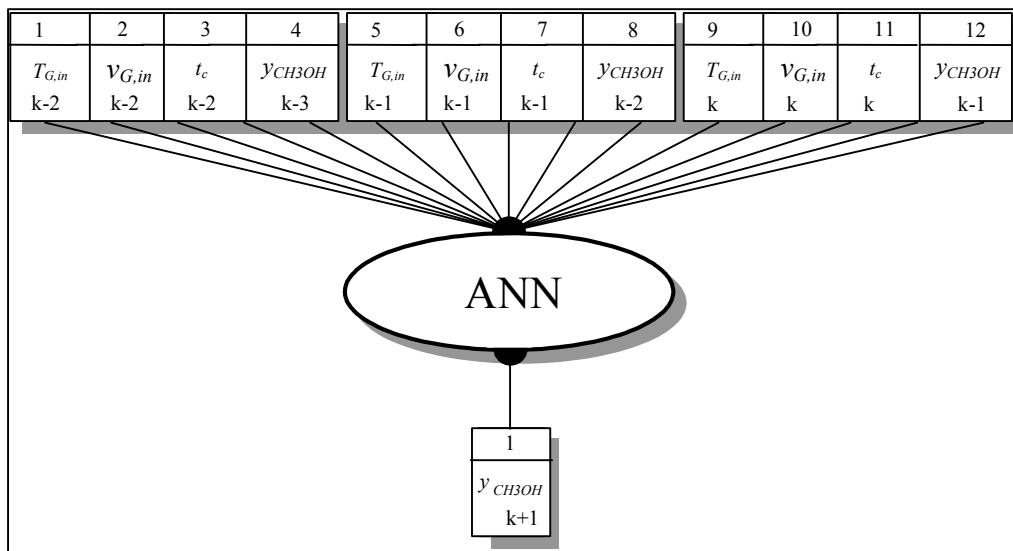

Figure 6.6: Structure of the ANN used for the identification of the RN.

The conditions adopted in the simulations are given in Table 5.3; they are the same previously considered for the unsteady state operation of methanol synthesis in a reverse-flow reactor by Vanden Bussche *et al.* (1993) and in the three reactors network by Velardi and Barresi (2002).

The disturbances in the inlet gas temperature are assumed to be in the range ±30 K and in the inlet gas flow rate in the range ±20% around the values corresponding to the optimal configuration. Finally, the switching time may assume values in the interval 40 ± 15 s. The input patterns were generated according to a Generalised Random Sequence: randomly changing values of T_{in}, $v_{G,in}$ and t_c in the above indicated intervals were produced. Such data were partitioned into two sets, used for both training and testing. The patterns were organised into a stack according to the HSA algorithm. A value of n_p=100 for the patterns in the stack and n_c=10 for the number of repetitions of the stack were implemented, according to Tadé *et al.* (1996), due to the complexity and variety of the dynamics of the reactor.

Since the ANN is intended for control purposes, the sampling time corresponds to the control time, i. e. the time interval between two subsequent control actions. Working with the MPC technique it is necessary to check if an exhaustive search of the optimum of the control objective function can be performed within such interval. The sampling time has also to be lower than 15 s, which is the lower limit of the switching time: a value of 10 s was chosen as an initial guess. The influence of the parameters α, β and μ and of the number of patterns used during the training was firstly investigated. The results are summarised in Figure 6.7, where the mean square error between the prediction of the model and that of the ANN (E_{RMS}) are plotted versus the number of patterns used for the learning: it is immediately evident that few hundreds of patterns are sufficient to have low values of the E_{RMS}, while with the traditional approach of the single pattern presentation hundreds of thousands values are needed.
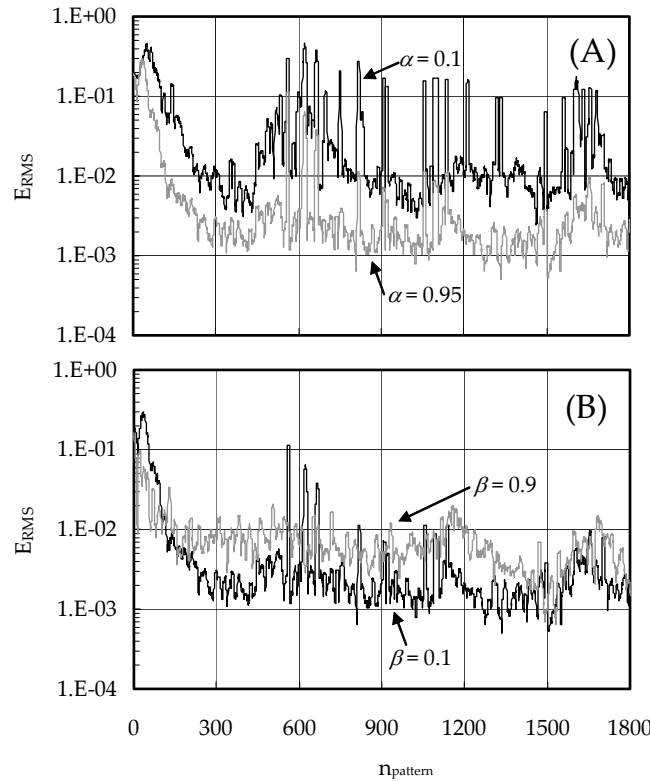
Figure 6.7: E_{RMS} vs. the number of pattern used in the learning phase as a function of the learning parameters: graph (A) shows the influence of the learning rate ($\beta = 0.1$, $\mu = 0.1$); graph (B) shows the influence of the momentum factor rate ($\alpha = 0.95$, $\mu = 0.1$).

Concerning the influence of the parameters the higher is α, the lower is E_{RMS} (graph A); the useful range of values of β is often poorly understood, despite its apparent simplicity: even if in the literature values of β in the range 0.7-0.99 are suggested, in this process the lower is β the lower is E_{RMS}. The choice of the gain μ has clearly an influence on the effective learning rate of the weights of the output node (see eq. (6.2)). Even if a value of $\mu = 1$ is generally suggested as a starting guess, this parameter can be more rigorously optimised: the gain of the sigmoid function is a quadratic function of the activation φ:

$$\frac{\partial \varphi}{\partial q} = \frac{e^{-q}}{\left(1 + e^{-q}\right)^2} = \varphi\left(1 - \varphi\right) \tag{6.7}$$

and this function has a maximum at:

$$\frac{\partial^2 \varphi}{\partial q^2} = 0 = -2\varphi + 1 \quad \Rightarrow \quad \varphi = 0.5 \tag{6.8}$$

158

The aim is to have a similar gain for the linear node. Obviously it is impossible to have the two gains matching for all α, however, approximately, similar gains over the useful range may improve learning. As a consequence, given the range of the input values to the sigmoid function in a trained network, it is possible to calculate the (integral) average gain over this interval and assuming μ equal to this value. For the process considered an optimal value of μ of 0.1 is obtained from this calculus, even if lower values may lead to better performance. In conclusion the "best" choice of the network parameters is $\alpha = 0.95$, $\beta = 0.1$ and $\mu = 0.1$.

Beyond the set of patterns generated for testing the performance of the ANN, further tests have been accomplished, comparing the predictions of the ANN and those of the model in presence of different disturbances of the inlet parameters of the RN. Figure 6.8 shows the results of this comparison when the inlet gas temperature is increased ($\Delta T_{G,0} = + 30°C$, upper graph) and decreased ($\Delta T_{G,0} = -20°C$, lower graph): different dynamic behaviours may occur, but in both cases considered the agreement between the model and the ANN is excellent, and the percentage error is always less than 1%.

Figure 6.8: Comparison between the methanol outlet molar fraction predicted by the model (solid line) and by the ANN (dashed line, with $\alpha = 0.95$, $\beta = 0.1$ and $\mu = 0.1$) when the inlet gas temperature is increased ($\Delta T_{G,in} = + 30°C$, upper graph) and decreased ($\Delta T_{G,in} = -20°C$, lower graph).

Predictions and actual values are even closer when variations in the flow rate are considered as it is shown in Figure 6.9 ($\Delta v_{G,0}$ = + 10%, upper graph; $\Delta v_{G,0}$ = - 10%, lower graph).

Figure 6.9: Comparison between the methanol outlet molar fraction predicted by the model (solid line) and by the ANN (dashed line, with α = 0.95, β = 0.1 and μ = 0.1) when the inlet flow rate is increased ($\Delta v_{G,in}$ = + 10%, upper graph) and decreased ($\Delta v_{G,in}$ = - 10%, lower graph).

The predictions of the ANN and that of the model have also been compared when the switching time is changed, as this is the parameters used by the MPC algorithm for control purposes: Figure 6.10 shows the result of this comparison when the switching time is increased (Δt_c = + 10s, upper graph) and decreased (Δt_c = - 10s, lower graph).
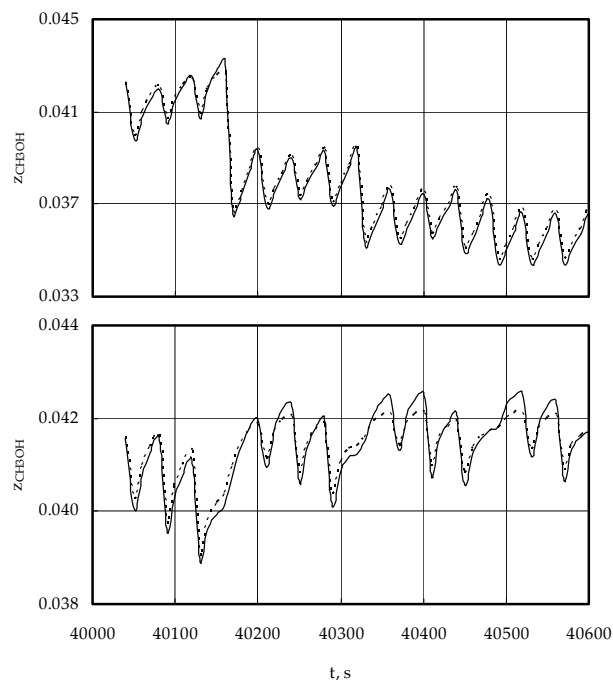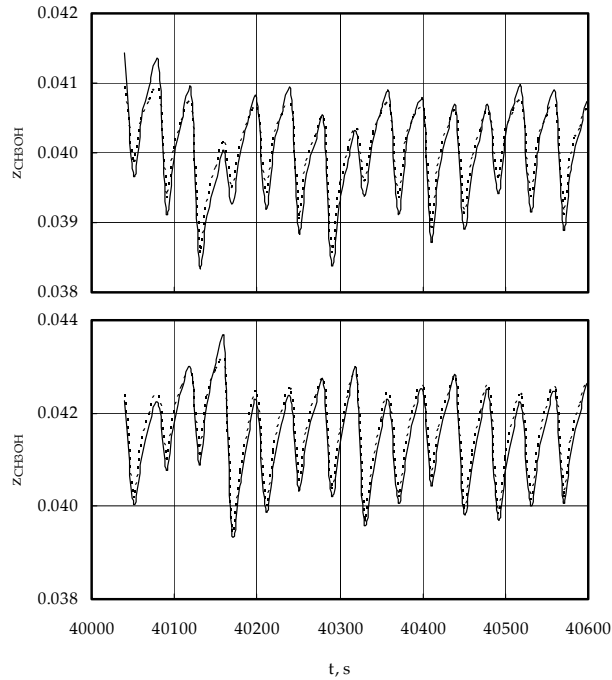
Figure 6.10: Comparison between the methanol outlet molar fraction predicted by the model (solid line) and by the ANN (dashed line, with $\alpha = 0.95$, $\beta = 0.1$ and $\mu = 0.1$) when the switching time is increased ($\Delta t_c = + 10s$, upper graph) and decreased ($\Delta t_c = - 10s$, lower graph).

From these results it is evident that the ANN is able to correctly predict the dynamic of the system even when pseudo-periodic state and complex dynamics are present with a total CPU time of some millisecond. This is the keynote that makes ANN so appealing for advanced control purposes. Evidently the performance of the ANN worsen when the change of the input parameters falls outside the range used for the learning; in this case it is necessary to repeat the learning, but the choice of the parameters (α, β, n_p, n_c and number of patterns used during the learning) remains the same; only μ should be changed according to the previous discussion.

List of symbols

b	bias
n_c	number of cycles of the patterns stack
n_p	number of patterns of each stack
q	input of a neuron (with bias)
s	output of a neuron
T	temperature, K
t	clock time, s
t_c	switching time, s
v	interstitial velocity, m s^{-1}
u	unbiased input signal of a neuron
y	molar fraction
w	synaptic weight

Greeks

α	learning rate
β	momentum constant
δ	error between the prediction of the ANN and the target value
Δ	variation
μ	gain of the linear activation function
ϕ	activation function of a neuron

Subscripts and superscripts

G	gas phase
S	solid phase or solid surface
in	inlet condition
out	outlet value

6.4 Fundamentals on Model Predictive Control

Model Predictive Control is an appropriately descriptive name for a class of computer control schemes that utilise a process model for two central tasks:

1. explicit prediction of future plant behaviour;

2. computation of appropriate corrective control actions $\hat{u}$ required to drive the predicted output as close as possible to the desired target value, i.e. to minimise the difference between the set point and the real value of the controlled variables over a time interval known as prediction horizon:

$$\min_{\hat{u}} \left(\sum_{i=1}^{h_p} \left(y(i) - y_{set}(i) \right)^2 \right) \tag{6.9}$$

where $y(i)$ il the model prediction at the time instant i, $y_{set}(i)$ is the set point value for the variable y at the time instant i and h_p is the prediction horizon.

Originally developed to meet the specialised control needs of power plants and petroleum refineries, MPC technology can now be found in a wide variety of application area, including chemicals, food processing, automotive, aerospace, metallurgy, and pulp and paper. Several authors have published excellent reviews of MPC theoretical issues, including the papers of Garcia *et al.* (1989), Ricker (1981), Morari and Lee (1991, 1999), Eaton and Rawlings (1992), Muske and Rawlings (1993), Rawlings *et al.* (1994), Mayne (1996) and Lee (1996).

A typical industrial process has associated with it the following control problems:

1. it is almost always multivariable (several process variables to be controlled, several manipulated variables available for control, several disturbance variables, some measurable, some not), typically with significant interactions between the process variables;

2. difficult dynamic behaviour (time delays, inverse-response behaviour, occasional open-loop instability);

3. inherent nonlinearities;

4. constraints of all kinds (constraints on the absolute values of the input and output variables, constraints on the rate of change of the inputs, other equality and inequality constraints).

The MPC is able to fulfil all the requirements noted above:

1. it is particularly easy to use for multivariable systems and handle process interactions with ease;

2. it handles time delays, inverse response, as well as other difficult process dynamics with ease;

3. it is posed as an optimisation problem and is therefore capable of meeting the control objectives by optimising the control effort (if the problem is so posed), and at the same time is capable of handling constraints of all kinds.

Beside this, it is important to notice that chemical processes often have slow dynamics so that it may takes a substantial amount of time for the full effect of each single control action to be completely manifested in the observable process output. The immediate implication is that it is not possible to obtain the full picture of the consequences of previously applied control actions from only the current process output measurement. In deciding what control action to take at the current time instant therefore it is useful:

1. to consider first how the process output will behave in the future if no further control action is taken;

2. to target control action towards rectifying what remains to be corrected after the full effects of the previously implemented control action have been completely manifested.

As a consequence the fundamental framework of MPC consists of four elements (Figure 6.11):

1. *Reference trajectory specification*

The first element of MPC is the definition of a desired target trajectory for the process output $y^*(k)$. This can simply be a step to the new set-point value or, more commonly, it can be a desired reference trajectory that is less abrupt that a step.

2. *Process output prediction*

Some appropriate model, *M*, is used to predict the process output over a predetermined, extended time horizon (with the current time as the prediction origin) in the absence of further control action. For discrete-time models this means prediction $\hat{y}(k+1)$, $\hat{y}(k+2)$,..., $\hat{y}(k+i)$ for *i* sample times into the future based on all actual past control inputs $u(k)$, $u(k-1)$, ..., $u(k-j)$.
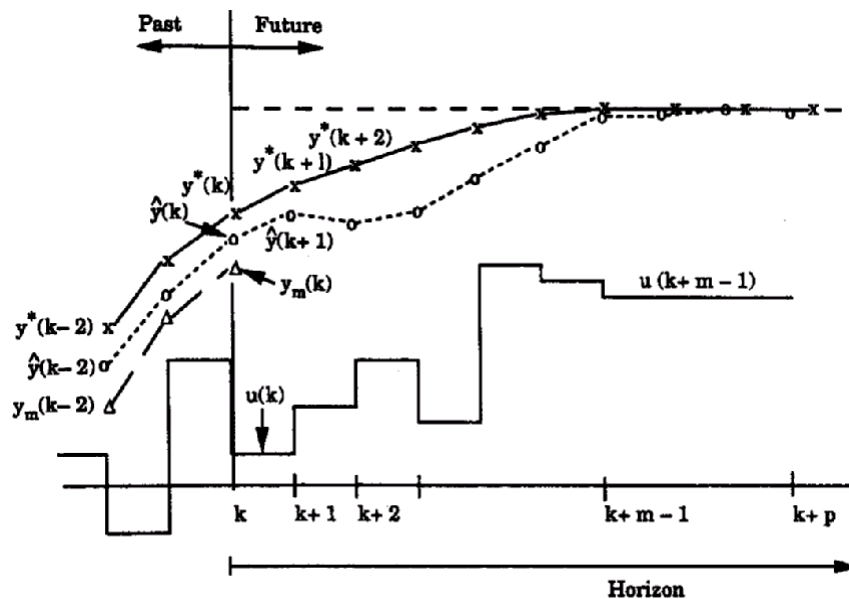

Figure 6.11: Example of elements in model predictive control: x—x: reference trajectory, y^*, o—o: predicted output; $\hat{y}$, Δ—Δ: measured output; y_m, —: control action, u.

3. *Control action sequence computation*

The same model *M* is used to calculate a sequence of control moves that will satisfy some specified optimisation objective, such as

- minimising the predicted deviation of the process output from target over the prediction horizon,

- minimising the expenditure of control effort in driving the process output to target,

subject to prespecified operating constraints.

4. *Error prediction update*

In recognition of the fact that no model can constitute a perfect representation of reality, plant measurements $y_m(k)$ is compared with model prediction $\hat{y}(k)$ and the prediction error $e(k) = y_m(k) - \hat{y}(k)$ is used to update future predictions.

A wide variety of MPC schemes are currently available as commercial computer software packages offered by various vendors; what differentiates one specific scheme from the other is the strategy and philosophy underlying how each element is actually implemented. A good qualitatively review, which is beyond the aim of this thesis, can be found in Ogunnaike and Ray (1994).

In this work an ANN based model has been used for the optimisation procedure; some example of the application of ANN in MPC schemes can be found in Psichogios and Ungar (1991), Nahas *et al.* (1992) and Turner *et al.* (1996). For a generic discrete input-output model

$$\hat{y}(k) = g\left(\hat{u}(k-1), \hat{u}(k-2), ..., \hat{u}(k-n_a), \hat{y}(k-1), \hat{y}(k-2), ..., \hat{y}(k-n_b)\right) \quad (6.10)$$

where $\hat{y}(k)$ is the prediction of the ANN for the manipulated variable at the time instant k, $\hat{u}(k)$ are the manipulated variables at the time instant k, n_a and n_b are the number of time interval where the input and the output respectively are considered, the MPC evaluates the optimal input sequence by minimising the function:

$$\min_{\hat{u}(k),...,\hat{u}(k+h_c-1)} \left\{ \sum_{j=k+1}^{k+h_p} \omega_y \left[\hat{y}(i) - y_{set}(i)\right]^2 + \sum_{j=k}^{k+h_p-1} \omega_u \left[\hat{u}(i) - \hat{u}(i-1)\right]^2 \right\} \quad (6.11)$$

where $y_{set}(i)$ is the assigned set point for the output variable y at the time instant i, h_p is the prediction horizon, i.e. the number of time intervals in the future where the state of the system is predicted, given the initial state and the sequence of control actions $\hat{u}(k),...,\hat{u}(k+h_c-1)$, and h_c is the control horizon, i.e. the number of time intervals in the future where the value of the manipulated variables are calculated.

The prediction horizon may be larger that the control horizon; in this situation for the time instant between h_c and h_p the manipulated variables assume the values they have in the final instant of the control horizon.

Even if in the optimisation $h_c > 1$, and thus the MPC gives the entire sequence of manipulated variables up to h_c, only the first one is implemented and the minimisation is repeated in the subsequent time interval.

The objective function may be formulated in different way to keep into consideration both economical issues and other constraints; for example in eq. (6.11) ω_y may be used to give penalty to offsets, while ω_u gives penalty to large changes between two subsequent control actions.

A feedback contribution is needed to take into consideration modelling mismatch with the process (Henson and Seborg, 1997). In this work the modelling mismatch with the reality $d(k) = y(k) - \hat{y}(k)$ is evaluated at each time instants and this correction term evaluated at the time instant k is added to the predictions of the model along all the prediction horizon, as it is shown in Figure 6.12, thus leading to the following modified objective function (Psichogios and Ungar, 1991):

$$\min_{\hat{u}(k),...,\hat{u}(k+h_c-1)} \left\{ \sum_{j=k+1}^{k+h_p} \omega_y \left[y_{set}(i) - \left(\hat{y}(i) + d(k) \right) \right]^2 + \sum_{j=k}^{k+h_p-1} \omega_u \left[\hat{u}(i) - \hat{u}(i-1) \right]^2 \right\} \quad (6.12)$$

$d(k)$ may be considered as the sum of two contributions:

1. the difference between model predictions and reality due to model approximations and unmodelled disturbances,

2. measurements white noise, which has a null mean value along a certain time interval, but is different from zero at each instants.
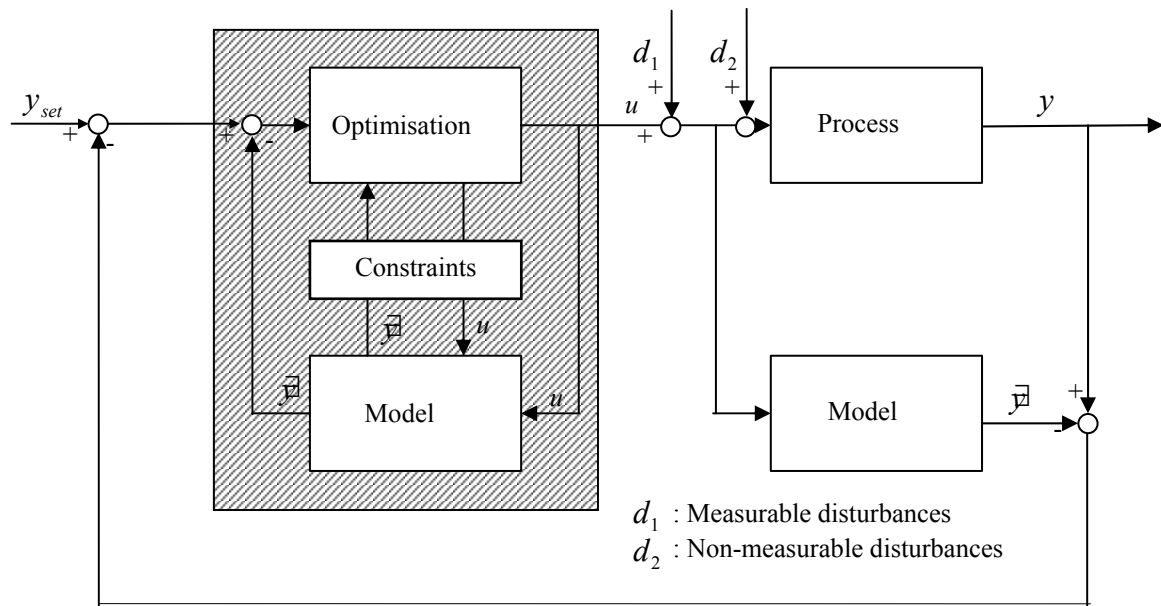
Figure 6.12: Block diagram of the MPC algorithm

In order to render the correction $d(k)$ less dependent from the white noise a moving average filter can be used (Tadé *et al.*, 1996):

$$d(k) = d(k-1)\lambda + d(k)(1-\lambda) \tag{6.13}$$

λ is the forgetting factor and may assume values in the interval [0, 1]; the higher the noise, the higher the value of λ.

6.5 Application of MPC to the three reactors network

For the process considered the control time is equal to the switching time: when the feeding position should be changed, the control system has to decide the new switching time, having as an objective the maximisation of the mean value of methanol molar fraction in the product stream over a period. Disturbances in the feeding temperature and flow rate have been taken into consideration.

The ANN model which has been derived in (§6.3) has been used as a simplified model for the optimisation procedure. The ANN has been trained again in order to have, as output variable, the mean outlet methanol molar fraction for the considered switching time; the sampling time is now equal to the switching time. The ANN designed with the same parameter found in

(§6.3), namely n_c, n_p, α, β, μ, has been used to simulate the process, giving good agreement with the predictions of the detailed model.

The objective function which has been used in the algorithm is the following:

$$F = \sum_{i=k+1}^{k+h_p} \left\{ \sum_{c=1}^{n_c} \omega_c \left[\frac{y_c(i) - y_{c,SET}(i)}{y_{c,SET}(i)} \right]^2 \right\} + \sum_{l=k}^{k+h_c-1} \left\{ \sum_{m=1}^{n_m} \omega_m \left[\frac{u_m(l) - u_m(l-1)}{u_m(l-1)} \right]^2 \right\} \qquad (6.14)$$

where:

   n_c = number of controlled variables

   n_m = number of manipulated variables

   y_c = controlled variable (mean methanol outlet molar fraction)

   $y_{c,SET}$ = set point for the controlled variable

   u_m = manipulated variable (switching time)

The optimisation has been carried out using a robust Simplex method (Buzzi Ferraris, 1998). The controller parameters (h_p, h_c and ω_m) have to be tuned with the aim to obtain a robust and stable controlled system. Garcia and Morari (1982) and Muske and Rawlings (1993) give some general guidelines for designing linear MPC algorithm; in the case of non linear system no general rules can be found in the literature and trial and error techniques have to be used for the best selection of the parameters. Thus the influence of the main parameter of the MPC algorithm has been addressed; a step of amplitude -20°C in the feed temperature has been used as a test disturbance.

1. *Prediction horizon*

The prediction horizon is the number of future intervals when the value of the function that has to be optimised is evaluated; for a constant value of the control horizon, the higher h_p, the higher should be the possibility for the control system to predict the future behaviour of the process, this allowing for lower changes in the manipulated variables. The main drawback of using high values of the prediction horizon is that the same values of the disturbance is considered, thus forcing the control system to work on a problem which may differ substantially from the reality.

Figure 6.13 shows the results obtained when the value of the control horizon is $h_c = 3$ and $\omega_m = 0.01$ for various values of the prediction horizon;

both the predicted outlet methanol molar fractions (upper chart) and the calculated switching time (lower chart) are shown.
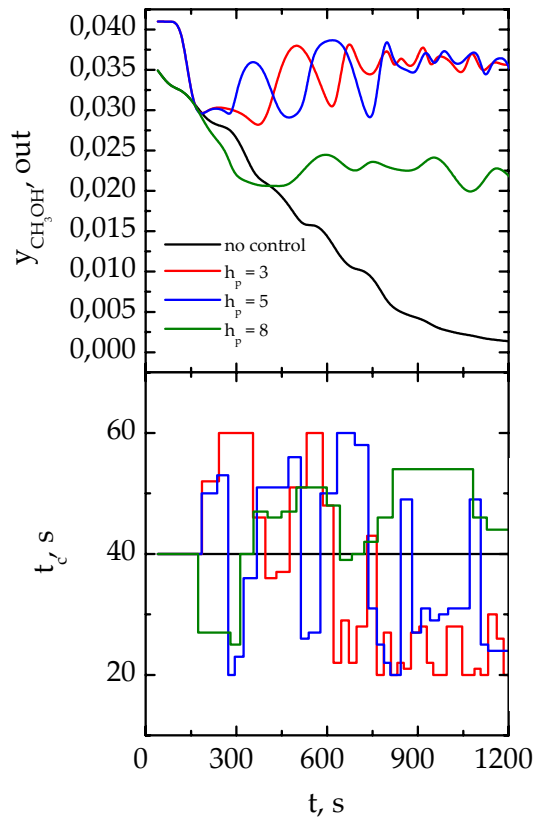

Figure 6.13: Time evolution of the switching time (lower graph) and of the outlet mean molar fraction (upper graph) as predicted when the MPC algorithm is used ($h_c = 5$, $\omega_m = 0.01$) with various values of the prediction horizon (h_p).

When no control actions are undertaken the system moves rapidly towards extinction; when the MPC algorithm is working, the switching time is changed in order to maximise the objective function, in this case the methanol outlet molar fraction. As expected, when the prediction horizon is increased the control system may predict the future behaviour of the process in a larger time interval, thus allowing for lower changes in the manipulated variables, but when the prediction horizon has a value of 8 time intervals the control system is compelled to work on a problem which starts differing substantially from the reality as the same value of the disturbance is considered, thus resulting in a significant reduction of the methanol yield.

2. *Control horizon*

The control horizon is the number of future intervals when the value of the manipulated variables is evaluated; for a constant value of the prediction horizon, the higher h_c, the higher the number of degrees of freedom of the controller, which becomes more aggressive and allows for higher methanol conversion. When the value of h_c is lower than the prediction horizon, a constant value of the manipulated variables is used for the time interval between h_p and h_c, thus limiting the possibility of the control system of proposing a more articulated time profile of the manipulated variable. The main drawback of using high values of the control horizon (and thus of the prediction horizon) is that the same values of the disturbance is considered, thus forcing the control system to work on a problem which may differ substantially from the reality.
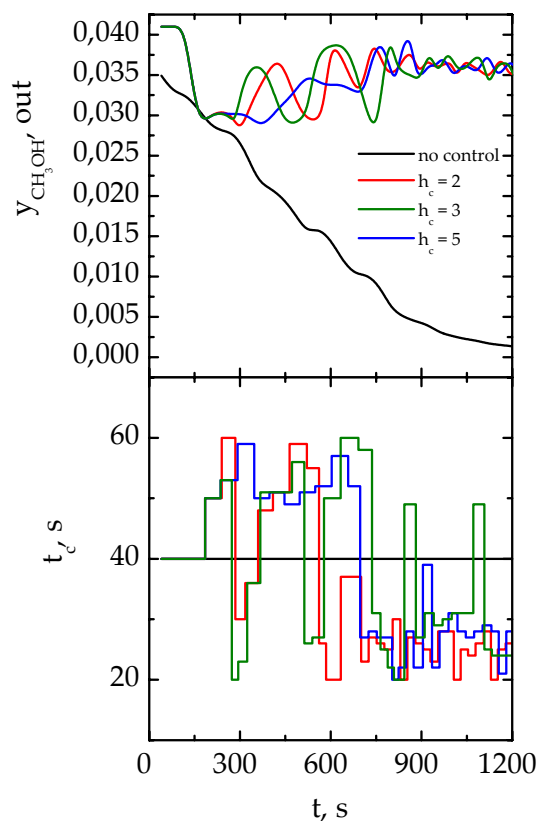

Figure 6.14: Time evolution of the switching time (lower graph) and of the outlet mean molar fraction (upper graph) as predicted when the MPC algorithm is used ($h_p = 5$, $\omega_m = 0.01$) with various values of the control horizon (h_c).

Figure 6.14 shows the results obtained when the value of the control horizon is h_p = 5 and ω_m = 0.01 for various values of the prediction horizon; both the predicted outlet methanol molar fractions (upper chart) and the calculated switching time (lower chart) are shown. When no control actions are undertaken the system moves rapidly towards extinction; when the MPC algorithm is working, the switching time is changed in order to maximise the objective function, in this case the methanol outlet molar fraction. As expected, when the control horizon is increased the control system becomes more aggressive but the final methanol outlet molar fraction results unchanged, due to the steady-state value in presence of the new inlet parameters. As a consequence the response of the system with a value of h_p = 5 and h_c = 3 may be considered adequate.

3. *Weight on the controlled variable*

The higher the value of the weight on the manipulated variable (ω_m), the higher the importance of the second term of eq. (6.14), thus reducing the amplitude of the variation of the manipulated variables and lowering the efficiency of the control system; Figure 6.15 evidences this behaviour when the value of ω_m is varied from 0.1 to 1.0: the value of the switching time is changed too slowly and even if the final value of the outlet molar fraction results unchanged, the performance of the system during the transient results worst. Moreover even small values of ω_m allows to stabilise the system, thus a value of ω_m = 0.01 is considered adequate.
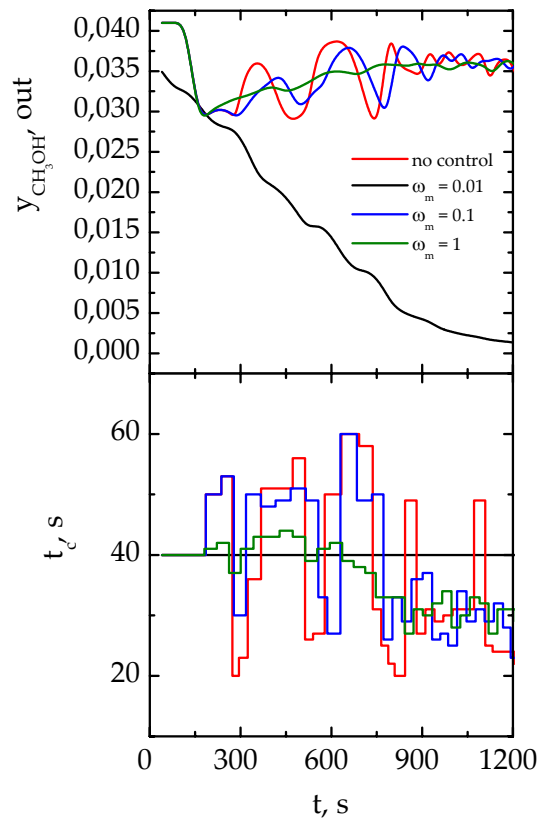
172

Figure 6.15: Time evolution of the switching time (lower graph) and of the outlet mean molar fraction (upper graph) as predicted when the MPC algorithm is used (h_c = 3, h_p = 5) with various values of the weight ω_m.

The set of parameters of the MPC algorithm has been tested also with other disturbances, evidencing that a good disturbance rejection may be obtained. Figure 6.16 shows for example the time evolution of the switching time (as predicted by the MPC controller) and of the mean outlet molar fraction when the inlet gas temperature is increased of 20°C. Despite the change in the inlet conditions, the control system is able to maximise the mean outlet methanol molar fraction, with respect to the process constraints on the manipulated variable; fast responses with small oscillations are obtained.
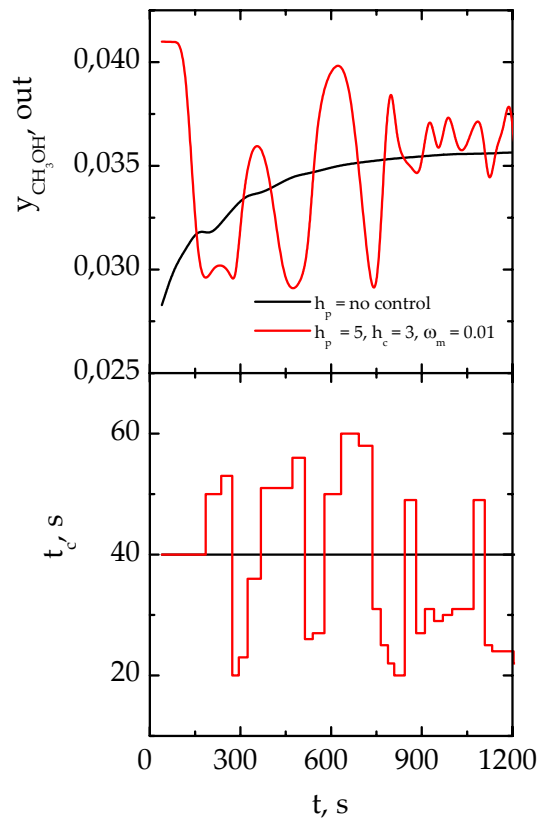
Figure 6.16: Time evolution of the switching time (lower graph) and of the outlet mean molar fraction (upper graph) as predicted when the inlet temperature is increased of 20°C. (h_c = 3, h_p = 5, $\omega_{m,}$ = 0.01)

Figure 6.16 shows also the results that are obtained when the switching time is not changed, i.e. the control system is not working. In this case the results are similar, even if when the control system is active a slightly higher methanol molar fraction may be obtained, particularly at the beginning of the transient and when the new pseudo-steady-state is reached.

Chapter 7

Conclusions

Forced unsteady-state catalytic reactors have been addressed in this thesis; two applications have been investigated in details, namely the autothermal combustion of lean VOC mixtures and exothermic equilibrium limited reactions.

As concerns the autothermal treatment of lean VOC mixtures the three main features of this research are the following:

- the assessment of the reverse-flow reactor as a device which allows for the combustion of lean mixtures without auxiliary fuel; the two and the three reactors network with variable feeding position has also been investigated as an alternative to the reverse-flow reactor. The dynamics of the two devices has been investigated by means of simulations, pointing out that the reverse-flow reactor exhibits a higher range of operating parameters (inlet flow rate and concentration) which allows for autothermal operation, thus ensuring stable operation without emissions of unburned compounds even in presence of strongly variable feeding characteristics. On the contrary, the reactors network can operate autothermally only in a narrow range of parameters; thus its application is advisable only in presence of constant feeding conditions. Moreover, in the reactors network the flow direction is never changed, thus avoiding the emissions of unconverted reactants which occurs in the reverse-flow reactors immediately after the change of the flow direction (wash out effect).

- the optimisation of the reverse-flow reactor for the combustion of lean methane mixtures, with particular respect to the role played by the catalyst physical and chemical properties.

- the experimental validation of the model used for the study of the dynamics of the device; both detailed and simplified models have been stated. With this respect, a bench scale reactor has been used, with a peculiar temperature control assessment to ensure adiabatic operation (as in large-scale industrial equipments). The role of the wall reactor on the stability of the process has also been addressed.

- a Model Based control system has been proposed and tested experimentally in order to avoid catalyst overheating, when the inlet concentration increases, or reactor extinction when the inlet concentration decreases. The key feature of the control system is the estimation of the inlet concentration and outlet conversion from some temperature measurements. A high gain observer has been designed to this purpose and validated experimentally.

As concerns the possibility of using unsteady-state reactors for exothermic equilibrium-limited reactions, two processes have been considered, namely the synthesis gas production and the low pressure methanol synthesis. The main features of this research are the followings:

- the reactors network has been proposed as an alternative technology for the production of the synthesis gas by means of partial oxidation of methane followed by autothermal steam reforming; the influence of the main operating parameters has been investigated by means of simulations, having as an objective the optimisation of this device. The results evidenced that the values of methane conversion are almost the same that can be achieved in the reverse-flow reactor, even if the reactors network is particularly interesting with respect to the control of the formation of carbon deposits on the catalyst.

- the reactors network has been proposed as an alternative technology for the low pressure methanol synthesis, evidencing that substantial improvements in reactant conversion and product selectivity, with respect

both to traditional steady-state process and to the reverse-flow reactor, may be obtained. Nevertheless, in addition to the intrinsecally dynamic behaviour, one must deal with unexpected external perturbations both in the inlet temperature and in the flow rate.

- the problem of the control of the low pressure methanol sinthesys in the three reactors network has been addressed. A model predictive control strategy has been investigated because of the complex dynamic behaviour showed by the process in correspondence of the optimal operation point. A simplified model, based on arficial neural networks has been developed to satisfy the requirements of the on-line optimisation of the model predictive control algorithm.

References

Abdul-Kareem K. H., Silveston P. L., Hudgins R. R., 1980, Behaviour of catalytic oxidation of carbon monoxide under cycling conditions, *Chem. Eng. Sci.* 35, 2077.

Adesina A. A., Hudgins R. R., Silveston P. L., 1986, A comparison of forced feed cycling of the Fisher-Tropsch synthesis over iron and cobalt catalysts, *Can. J. Chem. Eng.* 64, 447.

Al-Taie A. S., Kershenbaum L. S., 1978, Effect of periodic operation on the selectivity of catalytic reactions, *ACS Symp. Ser.* 65, 512.

Baiker A., Richarz W., 1976, Pressure in flow pulsed catalytic reactors, *Chem. Ing. Tech.* 48, 1203.

Balakotaiah V., Dommeti S. M. S., 1999, Effective models for packed-bed catalytic reactors, *Chem. Eng. Sci.* 54, 1621.

Barresi A. A., Vanni M., 2002, Dynamics and control of forced-unsteady-state catalytic combustors, in *Nonlinear dynamics and control in process engineering. Recent advances* (G. Continillo, S. Crescitelli, M. Giona Eds.), Springer-Verlag, Milano, 73.

Barresi A. A., Vanni M., Brinkmann M., Baldi G., 1997, Nonstationary catalytic destruction of lean waste gases in a network of burners and a reverse-flow reactor under non-adiabatic conditions, *Proc. 1st European Congress on Chemical Engineering, ECCE1,* Florence, Italy, 4-7 May 1997, Vol. 1, 587.

Barresi A. A., Vanni M., Brinkmann, M., Baldi G., 1999a, Control of an autothermal network of nonstationary catalytic reactors, *AIChE J.* 45, 1597.

Barresi A. A., Vanni M., Brinkmann M., Baldi G., 1999b, Influence of the wall heat losses on the performance of a network of nonstationary catalytic burners, *Chem. Eng. Technol.* 22, 237.

Barresi A. A., Fissore D., Baldi G., Vanni M., 2001a, Abatement of gaseous pollutants from iron-making processes using forced un steady-state catalytic combustors, in: "Combustion and the Environment: Proceedings XXIV Event of the Italian section of the Combustion Institute", September 16-19, Santa Margherita Ligure (Genova), Italy, VII-3. The Combustion Institute.

Barresi A. A., Fissore D., Vanni M., Baldi G., 2001b, Enhancement of selectivity of oxidative reactions in forced unsteady-state reactors, in: "Proceedings of 4th World Congress on Oxidation Catalysis", September 16-21, Berlin, Germany.

Barresi A. A., Fissore D., Delmon B., 2001c, Influence of the physical and chemical properties of the catalyst on the combustion of the fugitive emissions from coke ovens, in "Proceedings 3rd International Conference on Environmental Catalysis", December 10-13, Tokyo, Japan, 161.

Bestele D., Zeitz M., 1981, Canonical design for nonlinear observers with linearizable error dynamics, *Int. J. of Control* 23, 419.

Bhat N., McAvoy T. J., 1990, Use of neural nets for dynamic modelling and control of chemical process systems, *Comput. Chem. Eng.* 14, 573.

Bilimoria M. R., Bailey J. E., 1978, Dynamic studies of acetylene hydrogenation on nickel catalysts, *ACS Symp. Ser.* 65, 526.

Blanks R. F., Wittring T. S., Peterson D. A., 1990, Bidirectional adiabatic synthesis gas reactor, *Chem. Eng. Sci.* 45, 2407.

Bonard G., Hammouri H., 1991, A high gain observer for a class of uniformly observable systems, in *Proc. Of the 30th C.D.C.*, Brighton, England, 1494.

Boreskov G. K., Matros J. S., 1983, Unsteady-state performance of heterogeneous catalytic reactions, *Catal. Rev.-Sci. Eng.* 25, 551.

Briggs J. P., Hudgins R. R., Silveston P. L., 1977, Composition cycling of an SO_2 oxidation reactor, *Chem. Eng. Sci.* 32, 1087.

Brinkmann M., Barresi A. A., Vanni M., Baldi G., 1999, Unsteady state treatment of very lean waste gases in a network of catalytic burners. *Catal. Today* 47, 263.

Budman H., Kzyonsek M., Silveston P., 1996, Control of nonadiabatic packed bed reactor under periodic flow reversal, *Canad. J. Chem. Eng.* 74, 751.

Bunimovich G. A., Vernikovskaia N. V., Strots V. O., Balzhinimaev B. S., Matros Y. S., 1995, SO_2 oxidation in a reverse-flow reactor: influence of a vanadium catalyst dynamic properties, *Chem. Eng. Sci.* 50, 565.

Buntebarth G., Schopper J. R., 1997, Experimental and theoretical investigations on the influence of fluids, solids and interactions between them on thermal properties of porous rocks, *Phys. Chem. Earth* 23, 1141.

Buzzi Ferraris, G, 1998, Metodi numerici e software in C++, Addison-Wesley.

Chanchlani K. G., Hudgins R. R., Silveston P. L., 1994, Methanol synthesis under periodic operation: an experimental investigation, *Can. J. Chem. Eng.* 72, 657.

Chaouki J., Gui G., Sapundzhiev C., Kusohorsky D., Klvana D., 1994, Combustion of methane in a cyclic catalytic reactor, *Ind. Eng. Chem. Res.* 33, 2957.

Cittadini M., Vanni M., Barresi A. A., Baldi G., 1999, Efficient design and scale-up of reverse flow catalytic combustors, *Proceedings* of *ICheaP-4: The Fourth Italian Conference on Chemical and Process Engineering*, Firenze, Italy (May 2-5), 631.

Cittadini M., Vanni M., Barresi A. A., Baldi G., 2000, Development and design of a forced unsteady-state reactor through numerical simulation, 10*th European Symposium on Computer Aided Process Engineering; Computer-Aided Chemical Engineering Series,* Vol. 8, Elsevier, Amsterdam, 697.

Cittadini M., Vanni M., Barresi A. A., Baldi G., 2001, Simplified procedure for design of catalytic combustors with periodic flow reversal, *Chem. Eng. Proc.* 40, 255.

Cittadini M., Vanni M., Barresi A. A., 2002, Transient behaviour and start-up of periodic flow reversal reactors for catalytic decontamination of waste gases, *Chem. Eng. Proc.* 41, 437.

Crone G., Renken A., 1979, Effect of periodic process execution on radical polymerizations, *Ger. Chem. Eng.* 2, 337.

Cunill F., Van de Beld L., Westerterp K. R., 1997, Catalytic combustion of very lean mixtures in a reverse flow reactor using an internal electrical heater, *Ind. Eng. Chem. Res.* 36, 4198.

Cutlip M. B., 1979, Concentration forcing of catalytic surface rate process. Part I. Isothermal carbon monoxide oxidation over supported platinum, *AIChE J.* 25, 502.

Cybenko, G, (1989). Approximation by superpositions of sigmoidal function. *Mathematics of control, Signals and Systems*, vol. 2, 303-314.

Dautzenberg F. M., Helle J. N., Van Santen R. A., Verbeek H., 1977, Pulse technique analysis of the kinetics of the Fisher-Tropsch reaction, *J. Catal.* 50, 8.

De Groote A. M., Froment G. F., 1995, Reactor modeling and simulations in synthesis gas production, *Rev. Chem. Eng.* 11, 145.

De Groote A. M., Froment G. F., 1996, Simulation of the catalytic partial oxidation of methane to synthesis gas, *Appl. Catal. A: General* 138, 245.

De Groote A. M., Froment G. F., Kobylinski T. H., 1996, Synthesis gas production from natural gas in a fixed bed reactor with reversed flow, *Canad. J. Chem. Eng.* 74, 735.

Denis G. H., Kabel R. L., 1970, Effect of temperature changes on a tubular heterogeneous catalytic reactor , *Chem. Eng. Sci.* 25, 1057.

Deza F., Busvelle E., Gauthier J. P., 1992, High gain estimation for nonlinear systems, *Syst. Control Lett.* 18, 295.

Dixon A., Cresswell D. L., 1979, Theoretical prediction of effective heat transfer parameters in packed beds, *AIChE J.* 25, 663.

Dufour P., Couenne F., Touré Y., 2003, Model predictive control of a catalytic reverse flow reactor, *IEEE T. Contr. Syst. T.* 11, 705.

Eaton J. W., Rawlings J. B., 1992, Model predictive control of chemical processes, *Chem. Eng. Sci.* 47, 705.

Edouard D., Hammouri H., Schweich D., 2003, Observer design for reverse flow reactor, *AIChE J.,* submitted.

Edwards M. F., Richardson J. F., 1968, Gas dispersion in packed beds, *Chem. Eng. Sci.* 23, 109.

Eigenberger G., Nieken U., 1988, Catalytic combustion with periodical flow reversal, *Chem. Eng. Sci.* 43, 2109.

Eigenberger G., Nieken U., 1994, Catalytic cleaning of polluted air: reaction engineering problems and new solution, *Int. Chem. Eng.*, 34, 4.

El-Masry H. A., 1985, The Claus reaction: effect of forced feed concentration cycling, *Appl. Catal.* 16, 301.

Farza M., Hammouri H., Busavon K., 1998, A simple observer for a class of nonlinear systems, *Appl. Math. Lett.* 11, 27.

Fissore D., Barresi A. A., Ordóñez S., Díez F. V., 2001a, Comparison between the Pd/Al$_2$O$_3$ and a perovskite-type catalyst performances for the catalytic combustion of the fugitive emissions from a coke oven plant, in: "Proceedings 3rd International Conference on Environmental Catalysis", December 10-13, Tokyo, Japan, 159.

Fissore D., Barresi A. A., Baldi G., 2001b, On the reduction of the formation of carbon deposits in forced unsteady-state catalytic reactors for the production of syngas, in: "Nuovi orientamenti dell'Industria Chimica. Atti XVI Congresso Nazionale della Divisione di Chimica Industriale", October 2-4, Milano, Italy, 211.

Fissore D., Velardi S., Manca D., 2001c, Conversion enhancement of exothermic reversible reactions in forced un steady-state catalytic reactors, in: "Nuovi orientamenti dell'Industria Chimica. Atti XVI Congresso Nazionale della Divisione di Chimica Industriale", October 2-4, Milano, Italy, 67.

Fissore D., Barresi A. A., 2002, Comparison between the reverse-flow reactor and a network of reactors for the oxidation of lean VOC mixtures, *Chem. Eng. Technol.* 25, 421.

Fissore D., Barresi A. A., Velardi S., Vanni M., 2002, Conversion enhancement of exothermic reactions in unsteady-state ring reactor network. *17th International Symposium on Chemical Reaction Engineering (ISCRE 17)*, Hong Kong, China, 25-28 August 2002, paper #0508.

Fissore D., Barresi A. A., 2003, On the influence of the catalyst physical properties on the stability of forced unsteady-state after-burners. *Chem. Eng. Res. Des., Trans. IChemE. part A*, 81,611.

Fissore D., Barresi A. A., Velardi S., Vanni M., 2004, On the properties of the forced unsteady-state ring reactor network. *Chin. J. Chem. Eng.*, in press.

Fissore D., Barresi A. A., Baldi G., 2003a, Synthesis gas production in a forced unsteady-state reactor network, *Ind. Eng. Chem. Res. (Levenspiel issue)*, 42, 2489.

Fissore D., Hevia M. G. H., Barresi A. A., Ordóñez S., 2003b, Design and control of a bench-scale reverse-flow reactor for VOC combustion, in: "Proceedings 4th European Congress of Chemical Engineering (ECCE4)", September 21-25, Granada, Spain, Vol. 14, 17.

Fissore D., Edouard D., Hammouri H., Barresi A. A., 2003c, Soft-sensors design for unsteady-state VOC afterburners, in: "Combustion and the Environment: Proceedings Joint Meeting of The Scandinavian-Nordic and Italian Sections of The Combustion Institute - XXVI Event of the Italian section of the Combustion Institute", September 18-21, Ischia (Napoli), Italy, 6.8.1. The Combustion Institute.

Friedland N., 1996, Observers, in *The control handbook* (W. S. Levine ed.), CRC Press.

Froment G. F., 1990, in *Unsteady state processes in catalysis*, Matros Y. S. ed., VPS BV, Utrecht, The Netherlands.

Garcia C. E., Prett D. M., Morari M., 1989, Model predictive control: Theory and practice - a survey, *Automatica* 25, 335.

Gauthier J. P., Hammouri H., Othman S., 1992, A simple observer for nonlinear systems, application to bioreactors, *IEEE Trans. Autom. Control* 37, 875.

Gauthier J. P., Kupka A. K., 1994, Observability and observers for nonlinear systems, *Siam J. Control Optim.* 32, 975.

Gawdzik A., Rakowsky L., 1988, Dynamic properties of the adiabatic tubular reactor with switch flow, *Chem. Eng. Sci.* 43, 3023.

Gerasev A. P., Matros Y. S., 1991, Nonstationary method for ammonia synthesis, *Theoret. Foundation Chem. Engng.* 25, 680.

Gosiewski K., 2000, Mathematical simulation of reactors for catalytic conversion of methane to syngas with forced concentration cycling, *Chem. Eng. Proc.* 39, 459.

Gosiewski K., 2001, Simulations of non-stationary reactors for the catalytic conversion of methane to synthesis gas, *Chem. Eng. Sci.* 56, 1501.

Gosiewski K., Stzaba R., 1990, A simplified design of reverse flow nonstationary reactor for low reactant concentration, in *Unsteady State Processes in Catalysis* (Matros Y.S. ed.), VSP, Urecht, The Netherlands.

Gosiewski K., Bartmann U., Moszczynski M., Mleczko L., 1999, Effect of the intraparticle mass transport limitations on temperature profiles and catalytic performance of the reverse-flow reactor for the partial oxidation of methane to synthesis gas, *Chem. Eng. Sci.* 54, 4589.

Graaf G. H., Stamhuis E. J., Beenackers A. A. C. M., 1988, Kinetics of low-pressure methanol synthesis, *Chem. Eng. Sci.* 43, 3185.

Grozev G. G., Sapundzhiev C. G., 1997, Modelling of reversed flow fixed bed reactor for catalytic decontamination of waste gases, *Chem. Eng. Technol.* 20, 378.

Gupta V. K., Bhatia S. K., 1991, Solution of cyclic profiles in catalytic reactor operation with periodic flow reversal, *Comput. Chem. Eng.* 15, 229.

Hammouri H., Farza M., 2003, Nonlinear observers for local uniform observable systems, *ESAIM Contr. Op. Ca. Va.* 9, 353.

Haure P. M., Hudgins R. R., Silveston P. L., 1989, Periodic operation of a trickle-bed reactor, *AIChE J.* 35, 1437.

Haykin S., 1999, *Neural networks – A comprehensive foundation*, Prentice Hall, London.

Haynes T. N., Caram H. S., 1994, The simulated moving bed chemical reactor, *Chem. Eng. Sci.* 49, 5465.

Haynes T. N., Georgakis C., Caram H. S., 1992, The application of reverse flow reactors to endothermic reactions, *Chem. Eng. Sci.* 47, 2927.

Haynes T. N., Georgakis C., Caram H. S., 1995, The design of reverse flow reactors for catalytic combustion system, *Chem. Eng. Sci.* 50, 401.

Helmrich H., Renken A., Schuegerl K., 1974, Beeinflussung der effektiven gerschwindigkeit heterogen-katalytischer reaktionen durch aufgezuungene konzantrationsschwankungen, *Chem. Ing. Tech.* 46, 647.

Henson M. A., Seborg D. E., 1997, Nonlinear process control, Prentice Hall College Div.

Hevia M. A. G., Fissore D., Ordonez S., Diez F. V., Barresi, A. A., 2002, Importance of the wall effects in reverse flow reactors for catalytic combustion of methane lean mixtures, in: *Proceedings 15th International Congress of Chemical and Process Engineering (CHISA 2002)*, 25-29 August 2002, Praha, Czech Republic. Process Engineering Publisher, Praha; CD-

ROM Edition, Magic Ware, paper P1.158 [#1447].

Hevia M. A. G., Vega A., Ordóñez S., Fissore D., 2003a, Catalytic combustion of methane lean mixtures in a reverse flow reactor, in "Chemical Industry and Environment IV" (A. Macias-Machin and J. Umbria Eds.). Grupo Energia y Medio Ambiente, EMA. Universidad de Las Palmas de Gran Canaria, Spain, Vol. 2, 175.

Hevia M. G. H., Fissore D., Ordóñez S., Díez F. V., Barresi A. A., Baldi G., 2003b, Design and testing of a bench-scale reverse-flow combustor with reduced influence of the wall effects, Proceedings of the Fourth International Conference on Unsteady-State Processes in Catalysis (USPC4), Sapoundjiev H. ed., Natural Resources Canada, October 26-29, 2003, Montreal, Quebec Canada, 59.

Hindmarsh A. C., 1983, *ODEPACK, a systematized collection of ODE solvers*. Stepleman R. S. et al. Eds., Amsterdam.

Jain A., Hudgins R. R., Silveston P. L., 1983, Influence of forced feed composition cycling on the rate of ammonia synthesis over an industrial iron catalyst. Part I: effect of cycling parameters and mean composition, *Can. J. Chem. Eng.* 61, 824.

Khinast J., Jeong Y.O., Luss D., 1999, Dependence of cooled reverse-flow reactor dynamic on reactor model, *AIChE J.* 45, 299.

Kolios G., Eigenberger G., 1999, Styrene synthesis in a reverse flow reactor, *Chem. Eng. Sci.* 54, 2637.

Kunii D., Smith J. M., 1960, Heat transfer characteristics of porous rocks, *AIChE J.* 6, 71.

Lee C. K., Leung S. Y. S., Bailey J. E., 1980, Experimental studies of a consecutive-competitive reaction in steady state and forced periodic CSTRs, *Can. J. Chem. Eng.* 58, 212.

Lee J. H., 1996, Recent advances in model predictive control and other related areas, in *Chemical Process Control - CPC V*, Fifth International Congress on Chemical Process Control, Kantor J. C., Garcia C. E. and Carnahan B. eds., AIChE Symposium Series 316, Tahoe City, California, 201.

Lehr C. G., Yurchak S., Kabel R. L, 1968, Response of a tubular catalytic heterogeneous reactor to a step increase in flow rate, *AIChE J.* 14, 627.

Leupold E. I., Renken A., 1977, A new non-stationary process for the production of ethyl-acetate, *Chem. Ing. Tech.* 49, 667.

Levin A. U., Nerendra K. S., 1995, Identification using feedforward networks. *Neural Computat.* 7, 349.

Mayne D. Q., 1996, Nonlinear model predictive control: An assesment, in *Chemical Process Control - CPC V*, Fifth International Congress on Chemical Process Control, Kantor J. C., Garcia C. E. and Carnahan B. eds., AIChE Symposium Series 316, Tahoe City, California, 301.

Matros Y. S., 1985, *Unsteady processes in catalytic reactor*, Elsevier, Amsterdam.

Matros Y. S., 1989, *Catalytic processes under unsteady-state conditions*, Elsevier, Amsterdam.

Matros Y. S., 1990, Performances of catalytic processes under unsteady conditions, in *Unsteady state processes in catalysis* (Matros Y. S. ed.), VPS BV, Utrecht, The Netherlands.

Matros Y. S., Bunimovich G. A., 1995, Control of volatile organic compounds by the catalytic reverse process, *Ind. Eng. Chem. Res*. 34, 1630.

Matros Y. S., Bunimovich G. A., 1996, Reverse-flow operation in catalytic reactors, *Cat. Rev.-Sci. Eng.* 38, 1.

Matros Y. S., Noskov A. S., Chumachenko V. A., 1993a, Progress in reverse-process application to catalytic incineration problems, *Chem. Eng. Process.* 32, 89.

Matros Y. S., Bunimovich G. A., Noskov A. S., 1993b, The decontamination of gases by unsteady-state catalytic method. Theory and practice, *Catal. Today*, 17, 261.

Morari M., Lee J. H., 1991, Model predictive control: The good, the bad, and the ugly, in *Chemical Process Control - CPC IV*, Fourth International Congress on Chemical Process Control, Arkun Y. and Ray W. H. eds., Elsevier, Amsterdam, 419.

Morari M., Lee J. H., 1999, Model predictive control: past, present and future, *Comput. Chem. Eng.* 23, 667.

Moré J. J., Garbow B. S., Hillstrom K. E., 1980, *User guide for MINPACK*; ANL-80-74, Argonne National Laboratory.

Mueller-Erlwein E., Guba J., 1988, Experimentelle untersuchung zum periodischen reaktorbetrieb bei der heterogen katalysierten oxidehydrierung von isobutyraldehyd zu methacrolein, *Chem. Eng. Tech.* 60, 1072.

Muske K. R., Rawlings J. B., 1993, Model predictive control with linear models, *AIChE J.* 39, 262.

Nahas E. P., Henson M. A., Seborg D. E., 1992, Nonlinear internal model control strategy for neural network models, *Comput. Chem. Eng.* 16, 1039.

Nappi A., Fabbricino L., Hudgins R. R., Silveston P. L., 1985, Influence of forced feed composition cycling on catalytic methanol synthesis, *Can. J. Chem. Eng.* 63, 963.

Neophydes S. G., Froment G. F., 1992, A bench scale study of reversed flow methanol synthesis, *Ind. Eng. Chem. Res.* 31, 1583.

Nieken U., Kolios G., Eigenberger G. A., 1994a, Fixed-bed reactors with periodic flow reversal: experimental results for catalytic combustion, *Catal. Today* 20, 335.

Nieken U., Kolios G., Eigenberger G. A., 1994b, Control of the ignited steady state in autothermal fixed-bed reactors for catalytic combustion, *Chem. Eng. Sci.* 49, 5507.

Nieken U., Kolios G., Eigenberger G., 1995, Limiting cases and approximate solutions for fixed-bed reactors with periodic flow reversal, *AIChE J.* 41, 1915.

Ogunnaike, B. A., Ray, W. H., 1994, *Process dynamics, modelling and control.* Oxford University Press, New York.

Psichogios D. C., Ungar L. H., 1991, Direct and indirect model based control using artificial neural networks, *Ind. Eng. Chem. Res.* 30, 2564.

Purwono S., Budman H., Hudgins R. R., Silveston P. L., Matros Y. S., 1994, Runaway in packed bed reactors operating with periodic flow reversal, *Chem. Eng. Sci.* 49, 5473.

Rambeau G., Amariglio H., 1981, Ammonia synthesis on ruthenium powder from 100 to 500°C and hydrogenation of pre-adsorbed nitrogen down to –70°C, *Appl. Catal.* 1, 291.

Ramdani K., 2001, Le réacteur à inversion de flux pour la destruction de Composés organiques volatils. Modèles, expériences et dynamique. Ph.D. thesis, University "Claude Bernard", Lyon, France.

Ramdani K., Pontier R., Schweich D., 2001, Reverse flow reactor at short switching periods for VOC combustion, *Chem. Eng. Sci.* 56, 1531.

Rawlings J. B., Meadows E. S., Muske K. R., 1994, Nonlinear model predictive control: A tutorial and survey, *ADCHEM '94 Proceedings,* Kyoto, Japan.

Reacek J., Kubicek M., Marek M., 1992, Modelling of a tubular reactor with flow reversal, *Chem. Eng. Sci.* 47, 2897.

Renken A., 1974, Improving selectivity and yield by conducting processes in a periodic fashion, *Chem. Eng. Tech.* 46, 113.

Renken A., 1990, Application: of unsteady state processes in modelling heterogeneous catalytic kinetics, in *Unsteady State Processes in Catalysis* (Matros Y.S. ed.), VSP VP, Urecht, The Netherlands.

Renken A., 1993, Transient operation for the purpose of modelling heterogeneous catalytic reactions, *Int. Chem. Eng.* 33, 61.

Renken A., Mueller M., Wandrey C., 1976, Experimental studies of the improvement of fixed-bed reactors by periodic operation – the catalytic oxidation of ethylene, *Proc. 4th Int. Symp., Heidelberg* 1, III-107.

Ricker N. L., 1981, Model predictive control: State of the art, in *Chemical Process Control - CPC IV,* Fourth International Congress on Chemical Process Control, Arkun Y. and Ray W. H. eds., Elsevier, Amsterdam, 271.

Saleh-Alhamed Y. A., 1992, Periodic operation studies on the partial oxidation of propilene to acrolein and acrylic acid, *Chem. Eng. Sci.* 9, 2885.

Salomons S., Hayes R. E., Poirier M., Sapoundjiev H., 2003, Flow reversal reactor for the catalytic combustion of lean methane mixtures, *Catal. Today* 83, 59.

Sapundziev C., Chaouki J., Guy C., Klvana D., 1993, Catalytic combustion of natural gas in a fixed bed reactor with flow reversal, *Chem. Eng. Comm.* 125, 171.

Silveston P. L., Hudgins R. R., 1981, Reduction of sulfur dioxide emissions from a sulfuric acid plant by means of feed modulation, *Env. Sci. Tech.* 15, 419.

Silveston P. L., Forrissier M., 1985, Influence of composition modulation and product yield and selectivity in the partial oxidation of propylene over an antimony-tin oxide catalyst, *Ind. Eng. Chem. Prod. Res. Dev.* 24, 320.

Snyder J. D., Subramanian S., 1993, Numerical simulation of a periodic flow reversal reactor for sulfur dioxide oxidation, *Chem. Eng. Sci.* 48, 4051.

Snyder J. D., Subramanian S., 1994, A novel reverse flow strategy for ethylbenzene dehydrogenation in a packed bed reactor, *Chem. Eng. Sci.* 49, 5585.

Sun Q., Young B., Williams D. F., Glasser D., Hildebrandt D., 1996, A periodic flow reversal reactor: an infinitely fast switching model and a practical proposal for its implementation, *Can. J. Chem. Eng.* 74, 760.

Tadé M. O., Mills P. M., Zomaya A. Y., 1996, *Neuro-adaptive process control: a practical approach*, John Wiley & Sons.

Thullie J., Burghadt A., 1995, Simplified procedure for estimating maximum cycling time of flow-reversal reactors, *Chem. Eng. Sci.* 50, 2299.

Turner P., Montague G., Morris J., 1996, Dynamic neural networks in non-linear predictive control (an industrial application), *Comput. Chem. Eng.* 20, S937.

Van de Beld L., 1995, *Air purification by catalytic oxidation in an adiabatic packed bed reactor with periodic flow reversal*. Ph.D. thesis, University of Twente, Enschede, the Netherlands.

Van de Beld L., Westerterp K. R., 1996, Air purification in a reverse-flow reactor: Model simulations vs. experiments, *AIChE J.* 42, 1139.

Van de Beld L., Westerterp K. R., 1997, Operation of a catalytic reverse flow reactor for the purification of air contaminated with volatile organic compounds, *Canad. J. Chem. Eng.* 75, 975.

Vanden Bussche K. M., Froment G. F., 1996. The STAR configuration for methanol synthesis in reversed flow reactors, *Canad. J. Chem. Eng.* 74, 729.

Vanden Bussche K. M., Neophydes S. G., Zolotarskii I. A., Froment G. F., 1993, Modeling and simulation of the reversed flow operation of fixed bed reactor for methanol synthesis, *Chem. Eng. Sci.* 48, 3335.

Wandrey C., Renken A., 1973, Zur beeinflussung der produktverteilung durch periodiche konzentrationsschwankungen ber der oxidation von kohlenwasserstoffen, *Chem. Ing. Tech.* 45, 854.

Velardi S. A., Barresi A. A., 2002, Methanol synthesis in a forced unsteady-state reactor network, *Chem. Eng. Sci.* 57, 2995.

Velardi S., Barresi A. A., Fissore D., Baldi G., 2003, Forced unsteady state methanol synthesis in a reactor network, Proceedings of the Fourth International Conference on Unsteady-State Processes in Catalysis (USPC4), Sapoundjiev H. ed., Natural Resources Canada, October 26-29, 2003, Montreal, Quebec Canada, 46.

Velardi S., Barresi A. A., Manca D., Fissore D., 2004, Complex dynamic behaviour of methanol synthesis in the ring reactor network, *Chem. Eng. J.*, in press.

Vortmeyer D., Schafer R. J., 1974, Equivalence of one- and two-dimensional models for heat transfer processes in packed beds: one dimensional theory, *Chem. Eng. Sci.* 29, 485.

Wicke E., Vortmeyer D., 1959, Zündzonen heterogener Reaktionen in gasdurchströmten Körnerschichten, *Ber. Bunsenges. Phys Chem.* 63, 145.

Wilson D. H., Renken R. G., 1982, Concentration forcing in ammonia synthesis. I. Controlled cycling operation, *Chem. Eng. Sci.*, 37, 343.

Xiao W. D., Yuan W. K., 1994, Modelling and simulation for adiabatic fixed bed reactor with flow reversal, *Chem. Eng. Sci.* 21, 3631.

Young B., Hildebrandt D., Glasser D., 1992, Analysis of an exothermic reversible reaction in a catalytic reactor with periodic flow reversal, *Chem. Eng. Sci.* 47, 1825.

Zagoruiko A. N., Matros Y. S., Ravi Kumar V., Kulkarni B. D., 1992, Reactor performance with periodic flow reversal for a multi-step complex reaction, *Chem. Eng. Sci.* 47, 4315.

Zufle H., Turek T., 1997a, Catalytic combustion in a reactor with periodic flow reversal: 1. experimental results, *Chem. Eng. Proc.* 36, 327.

Zufle H., Turek T., 1997b, Catalytic combustion in a reactor with periodic flow reversal: 2. steady state reactor model, *Chem. Eng. Proc.* 36, 341.

Zupan J., Gasteiger J., 1999, *Neural networks in chemistry and drug design*, Wiley-VCH, Weinheim.

Acknowledgements

Publications of Davide Fissore in international journals

Fissore D., Barresi A. A., 2002, Comparison between the reverse-flow reactor and a network of reactors for the oxidation of lean VOC mixtures, *Chem. Eng. Technol.* 25(4), pp. 421-426.

Fissore D., Barresi A. A., 2003, On the influence of the physical properties of the catalyst on the performances of forced unsteady-state after-burners, *Chem. Eng. Res. Des., Trans. IchemE. part A*, 81, pp. 611-617.

Fissore D., Barresi A. A., Baldi G., 2003, Synthesis gas production in a forced unsteady-state reactor network, *Ind. Eng. Chem. Res. (Levenspiel Issue)* 42(12), pp. 2489-2495.

Velardi S., Barresi A. A., Manca D., Fissore D., 2004, Complex dynamic behaviour of methanol synthesis in the ring reactor Network, *Chem. Eng. J.*, in press.

Fissore D., Barresi A. A., Velardi S., Vanni M., 2004, On the properties of the forced unsteady-state ring reactor network, *Chinese J. Chem. Eng.*, in press.

Fissore D., Manca D., Barresi A.A., 2004, Modelling of methanol synthesis in forced unsteady-state ring reactors networks by Artificial Neural Networks for control purposes. *Chem. Eng. Sci. (special issue on USPC4)*, submitted.

Publications of Davide Fissore in proceedings of conferences

Barresi A. A., Fissore D., Baldi G., Vanni M., 2001, Abatement of gaseous pollutants from iron-making processes using forced unsteady-state catalytic combustors, in: "Combustion and the Environment: Proceedings XXIV Event of the Italian section of the Combustion Institute", September 16-19, Santa Margherita Ligure (Genova), Italy, pp. VII-3 – VII-6. The Combustion Institute [ISBN 88-88104-01-1].

Barresi A. A., Fissore D., Vanni M., Baldi G., 2001, Enhancement of selectivity of oxidative reactions in forced unsteady-state reactors, in: "Proceedings of 4th World Congress on Oxidation Catalysis", September 16-21, Berlin, Germany [SELOX-0-7-92].

Fissore D., Velardi S., Manca D., 2001, Conversion enhancement of exothermic reversible reactions in forced unsteady-state catalytic reactors, in: "Nuovi orientamenti dell'Industria Chimica. Atti XVI Congresso Nazionale della Divisione di Chimica Industriale", October 2-4, Milano, Italy, pp. 67-68.

Fissore D., Barresi A. A., Baldi G., 2001, On the reduction of the formation of carbon deposits in forced unsteady-state catalytic reactors for the production of syngas, in: "Nuovi orientamenti dell'Industria Chimica. Atti XVI Congresso Nazionale della Divisione di Chimica Industriale", October 2-4, Milano, Italy, pp. 211-212.

Díez F., Sastre H., Vega A., Ordóñez S., Hurtado P., Delmon B., Alifanti M., Blangenois N., Thyrion F., Auer R., Vulpescu G., Baldi G., Barresi A., Vanni M., Cittadini M., Fissore D., Alvarez J., Alvarez F., Rubín L., 2001, Integrated laboratory development of catalyst and reactor for abatement of fugitive emissions. In: "Proceedings 3rd International Conference on Environmental Catalysis", December 10-13, Tokyo, Japan, pp. 149-150 [PP-32].

Fissore D., Barresi A. A., Ordóñez S., Díez F. V., 2001, Comparison between the Pd/Al_2O_3 and a perovskite-type catalyst performances for the catalytic combustion of the fugitive emissions from a coke oven plant, in: "Proceedings 3rd International Conference on Environmental Catalysis", December 10-13, Tokyo, Japan, pp. 159-160 [PP-37].

Barresi A. A., Fissore D., Delmon B., 2001, Influence of the physical and chemical properties of the catalyst on the combustion of the fugitive emissions from coke ovens, in "Proceedings 3rd International Conference on Environmental Catalysis", December 10-13, Tokyo, Japan, pp. 161-162 [PP-38].

Fissore D., Barresi A. A., Velardi S., Vanni M., 2002, Conversion enhancement of exothermic reversible reactions in unsteady-state ring reactor, 17th International Symposium on Chemical Reaction Engineering, August 25-28, Hong Kong, China, Paper #0508.

Hevia M. A. G., Fissore D., Ordóñez S., Díez F. V., Barresi A. A., 2002, Importance of the wall effects in reverse flow reactors for catalytic combustion of methane lean mixtures, in "Proceedings 15th International Congress of Chemical and Process Engineering (CHISA 2002)", August 25-29, Praha, Czech Republic, Paper P1.158. Process Engineering Publisher, Praha; CD-ROM Edition, Magic Ware, [ISBN 80-86059-33-2].

Hevia M. A. G., Vega A., Ordóñez S., Fissore D., 2003, Catalytic combustion of methane lean mixtures in a reverse flow reactor, in "Chemical Industry and Environment IV" (A. Macias-Machin and J. Umbria Eds.). Grupo Energia y Medio Ambiente, EMA. Universidad de Las Palmas de Gran Canaria, Spain, Vol. 2, pp. 175-184 [ISBN 84-89528-61-6].

Fissore D., Edouard D., Hammouri H., Barresi A. A., 2003, Soft-sensors design for unsteady-state VOC afterburners, in: "Combustion and the Environment: Proceedings Joint Meeting of The Scandinavian-Nordic and Italian Sections of The Combustion Institute - XXVI Event of the Italian section of the Combustion Institute", September 18-21, Ischia (Napoli), Italy, pp.6.8.1-6.8.4. The Combustion Institute [ISBN 88-88104-04-6].

Fissore D., Hevia M. G. H., Barresi A. A., Ordóñez S., 2003, Design and control of a bench-scale reverse-flow reactor for VOC combustion, in: "Proceedings 4th European Congress of Chemical Engineering (ECCE4)", September 21-25, Granada, Spain, Vol. 14, pp. 17-19.

Velardi S., Barresi A. A., Fissore D., Baldi G., 2003, Forced unsteady state methanol synthesis in a reactor network, Proceedings of the Fourth International Conference on Unsteady-State Processes in Catalysis (USPC4), Sapoundjiev H. ed., Natural Resources Canada, October 26-29, 2003, Montreal, Quebec Canada, pp. 46-47.

Hevia M. G. H., Fissore D., Ordóñez S., Díez F. V., Barresi A. A., Baldi G., 2003, Design and testing of a bench-scale reverse-flow combustor with reduced influence of the wall effects, Proceedings of the Fourth International Conference on Unsteady-State Processes in Catalysis (USPC4), Sapoundjiev H. ed., Natural Resources Canada, October 26-29, 2003, Montreal, Quebec Canada, pp. 59-60.